UNIVERSITE BIOLOGIE BRETAGNE SANTE LOIRE

UNIVERSITÉ DE NANTES

Thèse de doctorat de

L'UNIVERSITE DE NANTES
Comue Université Bretagne Loire
ECOLE DOCTORALE N° 605
Biologie Santé
Spécialité : « *Cancérologie* »

Par

Kathryn Jacobs

« Exploring the Role of Intercellular and Intracellular Signaling in the Sustenance of Glioblastoma Stem-like Cells »

Thèse présentée et soutenue à Nantes, le 21 février 2020.
Unité de recherche : UMR1232
Thèse N° :

Rapporteurs avant soutenance :

Pr. Marja Jäättelä	Professeur d'Université, Université de Copenhagen
Dr. Servane Tauszig-Delamasure	Directrice de Recherche, Université de Lyon 1

Composition du Jury :

Président :	Dr. Eric Chevet	Directeur de Recherche, Université de Rennes
Examinateurs :	Dr. Stéphane Manenti	Directeur de Recherche, Université Toulouse III
	Pr. Margot Thome-Miazza	Professeur d'Université, Université de Lausanne
Dir. de thèse :	Dr. Julie Gavard	Directrice de Recherche, Université de Nantes

TABLE OF CONTENTS

LIST OF FIGURES

LIST OF TABLES

Abbreviations

ALG2 : Apoptosis-linked Gene 2
AMBRA : activating molecule in Beclin-1 regulated autophagy protein 1
AMP ; adenosine monophosphate
AMPK : AMP-activated Protein Kinase
APLNR : Apelin receptor
AP1 : Activator Protein 1
ASM : Acid Sphingomyelinase
ATCC : American Type Culture Collection
ATG : Autophagy Related Protein
BBB : Blood Brain Barrier
BCL-2 : B- cell Lymphoma 2
BCL-10 : B-cell CLL/lymphoma 10
BDNF : brain-derived neurotrophic factor
βGC : β-glucocerebrosidase
BMP : Bone Morphogenetic Protein
BORC : BLOC-1 related complex
BRD4 : Bromodomain Containing Protein 4
BRUCE : Baculovirus IAP repeat repeat-containing ubiquitin-conjugating enzyme
CAD : Cationic Amphiphilic Drugs
CARD11: caspase recruitment domain family member 11
CAR-T-Cell : Chimeric Anfigen Receptor T-Cell
CASTOR : cellular arginine sensor for mTORC1
CHO : Chinese hamster ovary cells
CIMP : CpG Island Methylator Phenotype
CLEAR : Coordinated Lysosomal Expression and Regulation
Co-IP : Co-immunoprecipitation
CSF-1R : Colony Stimulating Growth Factor-1 Receptor
CTS : Cathepsin
DEPTOR : DEP Domain Containing mTOR Interacting Protein
DFCP1 : Double FYVE-containing protein1
DLBCL : Diffuse Large B- cell Lymphoma
DRAM-1 : DNA damage regulated autophagy modulator 1
DYRK3 : dual specificity tyrosine-phosphorylation-regulated kinase 3
EC : Endothelial Cells
EGFR : Epidermal Growth Factor Receptor
ER : Endoplasmic Reticulum
ESCRT : endosomal sorting complex required for transport
EV : Extracellular Vesicle
FAT : FRAP, ATM, and TRRAP
FDA : Food and Drug Association
FIP200 : FAK family kinase-interacting protein of 200kDa
FKBP12 : FK506-binding protein 12
FYCO1 : FYVE and coiled-coil domain-containing protein 1
GABARAP : γ-aminobutyric Acid Receptor-associated Proteins
GAP : GTPase Activating Protein
GBM : Glioblastoma
GEF : Guanine Exchange Factor
GEMM : Genetic Engineered Mouse Model
GF : Growth Factor
GGA : Goligi-localized γ-ear-containing ADP ribosylation factor binding proteins
gp130 : Glycoprotein 130
GPCR: G-protein coupled receptor
GSC : Glioblastoma Stem-like Cells
GSEA : Gene Set Enrichment Analysis
HCAM : Homing Cell Adhesion Molecule
HEAT : Huntington, elongation factor 3, protein phosphatase 2A, and TOR1
HeLa : Human Leukemia-60 cells
HIF-1 : Hypoxia inducible Factor 1
HOPs : Homotypic fusion and protein sorting
HUVEC : Human Umbilical Vein Endothelial Cells
IDH : Isocitrate Dehydrogenase
IGF-1R : Insulin Growth Factor Receptor
IL6 : Interleukin 6

JAK : Janus Kinase
KO : Knock Out

LAMP : Lysosomal Associated Membrane Proteins
LAPTM5 : lysosomal-associated protein transmembrane 5
LARP1 : La-related protein 1
LCD : Lysosomal Cell Death
LC3 : Light Chain 3
LDA : Limited dilution assay
LIF : Leukemia Inhibitory Factor
LIMP2 : Lysosomal Integral Membrane Protein 2
LIR : LC3 Interacting Region
LMP : Lysosomal Membrane Permeabilization
LPS: Lipopolysaccharides
MALT1 : Mucosa-associated Lymphoid tissue 1
MCOLN1 : Mucolipin 1
MEF: Mouse Embryonic Fibroblasts
MGMT : Methylguanine Methyltransferase
mLST8 :mammalian Lethal with SEC13 protein
MPZ : Mepazine
mTOR : Mechanistic Target of Rapamycin
mTORC : Mechanistic Target of Rapamycin Complex
M6PR : Mannose-6-phosphate Receptor
NICD : Notch Intracellular Domain
NOD-SCID : Non-obese Diabetic Severe Combined Immunodeficient
NOS : Not Otherwise Specified
NSC : Neural Stem Cells
ORP1L : Oxysterol Binding Protein Related Protein 1
PAS : Phagophore Assembly Site
PDCD4 : Programmed cell death protein 4
PDGF : Platelet Derived Growth Factor
PD-L1 : Programmed Cell Death Ligand 1
PDOX : Patient Derived Orthotopic Xenograft
PE : Phosphatidylethanolamine
PFK : Phospho-fructo Kinase
PKC : Protein Kinase C
PLA : Proximity ligation assay
PLEKHM1 : Pleckstrin homology domain containing protein family member 1
PM : Plasma Membrane
PRAS40 : Proline-rich AKT Substrate of 40 kDa
PTEN : Phosphatase and Tensin Homologue
QKI : Quaking
RAPTOR : Regulatory Protein Associated with mTOR
RCAS-TVA : Replication-competent Avian Sarcoma-leukosis Virus-Tumor Virus A
REDD1 : regulated in DNA damage and development 1
Rheb : Ras homolog enriched in brain
RICTOR : Rapamycin Insensitive Companion of mTOR
RILP : Rab7-interacting Lysosomal Protein
ROS : Reactive Oxygen Species
RTK : Receptor Tyrosine Kinase
SCID : Severe Combined Immunodeficient
SGK1 : serine/threonine-protein kinase 1
SHH : Sonic Hedgehog
SNAP29 : Synaptosomal-associated Protein 29
SNARE : sensitive factor attachment protein
SOX: Sry-related HMG box
SQSTM1 : Sequestosome 1
SREBPs : sterol responsive element binding protein
STAT3 : signal transducer and activator of transcription 3
STK11 : serine threonine kinase 11
STX17 : syntaxin-17
SVZ : Subventricular Zone
S1P : Sphingosine 1-phosphate
S1P1 :Sphingosine1-phosphate receptor 1
TCGA : The Cancer Genome Atlas
TGF : Transforming Growth Factor
TGN : Trans-Golgi Network
TMZ : Temolzolomide
TOP : Terminal Oligopyrimidine
TOS : TOR signaling motif

TSC : Tuberous Sclerosis Complex
TTF : Tumor Treating Fields
ULK1 : Unc-51-like Kinase 1
UVRAG : UV-radiation resistance-associated gene
VASN : Vasorin
VAMP7 : vesicle-associated membrane protein 7
v-ATPase : Vacuolar H+ ATPase
VEGF : Vascular Endothelial Growth Factor
VHL : von Hippel-Lindau
VPS : vacuolar protein sorting
VTI1B : Vps10 tail interactor-1B
WAC : WW-domain containing adaptor with coiled coil
WIPI : WD-repeat-domain phosphoinositide-interacting
WT : Wildtype

Abstract

Glioblastoma multiforme, GBM, is the deadliest adult primary brain tumor with a median survival time of approximately 12 to 15 months. Within these heterogeneous tumors exists a subpopulation of cells with stem-like properties termed glioblastoma stem-like cells, GSCs. As they are suspected to be involved in initiation, expansion, and relapse, they represent a promising strategy for treating these tumors. *In situ*, GSCs reside in part in a protective vascular niche in close interaction with endothelial cells, however these cells have also been found in more hostile areas of the tumor, away from their privileged microenvironment. Therefore, uncovering intrinsic cell signaling regulating autocrine and paracrine survival mechanisms can produce novel targets for therapy.

Here, we approach the analysis of signaling mechanisms employed by GSCs in their survival, in order to identify potential targets for therapy. On one hand, we report that the glycoprotein gp130 has an important role in endothelial cell communication with GSCs. In fact, the endothelial secretome is able to sustain GSC stemness in the absence of other mitogens. However, pharmacological blockade of gp130 abrogates this effect. On the other hand, in the absence of signals emanating from endothelial cells, we uncover that the paracaspase MALT1 is important to maintain GSC survival and expansion, as knockdown or inhibition of this protease is lethal to these cells. From a molecular standpoint, we found that inhibition of MALT1 disrupts endo-lysosomal homeostasis, resulting in a lysosomal cell death concomitant with mTOR inactivation. Therefore, we identified two signaling axes within GSCs with the potential for therapeutic targeting.

Résumé

Le Glioblastome Multiforme, GBM, est une tumeur cérébrale parmi les plus agressives de l'adulte, avec une médiane de survie s'échelonnant autour de 12 à 15 mois. Au sein de ces tumeurs hétérogènes réside une sous-population de cellules aux propriétés souches appelées GSC pour cellules de type souche du glioblastome, Une stratégie potentielle pour le traitement de ces tumeurs consisterait à cibler ces GSCs, suspectées d'être impliquées dans l'initiation, l'expansion et la récurrence des tumeurs. Au sein des tumeurs, ces GSCs résident à la fois dans une niche vasculaire protectrice en interaction étroite avec les cellules endothéliales et dans des zones non vascularisées, plus hostiles. Dans ce contexte, il est crucial de mieux caractériser la signalisation cellulaire intrinsèque régulant les mécanismes de survie autocrine et paracrine des GSCs.

Ma thèse s'est concentrée sur l'analyse des mécanismes de signalisation régissant les décisions de vie/mort des GSCs, dans le but d'offrir de nouvelles perspectives thérapeutiques. D'une part, mes résultats montrent que la glycoprotéine gp130 joue un rôle important dans la communication entre les GSCs et les cellules endothéliales. Le sécrétome endothélial est en effet capable de maintenir le caractère souche des GSCs, en l'absence d'autres mitogènes externes. Le blocage pharmacologique de gp130 annule cet effet. Par ailleurs, en l'absence de signaux émanant des cellules endothéliales, j'ai mis en évidence le rôle instrumental de la paracaspase MALT1 dans la survie et l'expansion des GSCs. La suppression ou l'inhibition de cette protéase s'avère toxique pour ces cellules. D'un point de vue mécanistique, j'ai trouvé que l'inhibition de MALT1 perturbe l'homéostasie endo-lysosomale, entraînant une mort cellulaire lysosomale concomitante à l'inactivation de mTOR. J'ai donc identifié deux axes de signalisation au sein des GSCs avec un potentiel de ciblage thérapeutique.

Introduction

1. Brain Tumors

1.1 Glioblastoma

Gliomas represent approximately 80% of all diagnosed adult malignant brain tumors. They are classified in three types depending on the cell of origin: astrocytes, oligodendrocytes, and ependymal cells; and spread into four grades (I, II, III, IV). Grade II tumors have the characteristics of being well differentiated with an increased cell concentration amid some abnormalities, but mostly resembling noncancerous cells. Higher-grade gliomas (Grade III) show exacerbated vessel concentration, increased cell density and cellular anomalies. Cells can become anaplastic with excessive mitosis. Common histo-pathological features of Grade IV include elevated cell frequency and atypia, extensive, but abnormal vascularization and areas of necrosis (Westphal and Lamszus, 2011). Grade IV can permeate the normal parenchyma through varied growth patterns. Although uncommon, some may spread to the ventricles. This infiltrative capacity leads to incomplete tumor removal, causing new masses to form at the border of the original lesion (Gaspar et al., 1992).

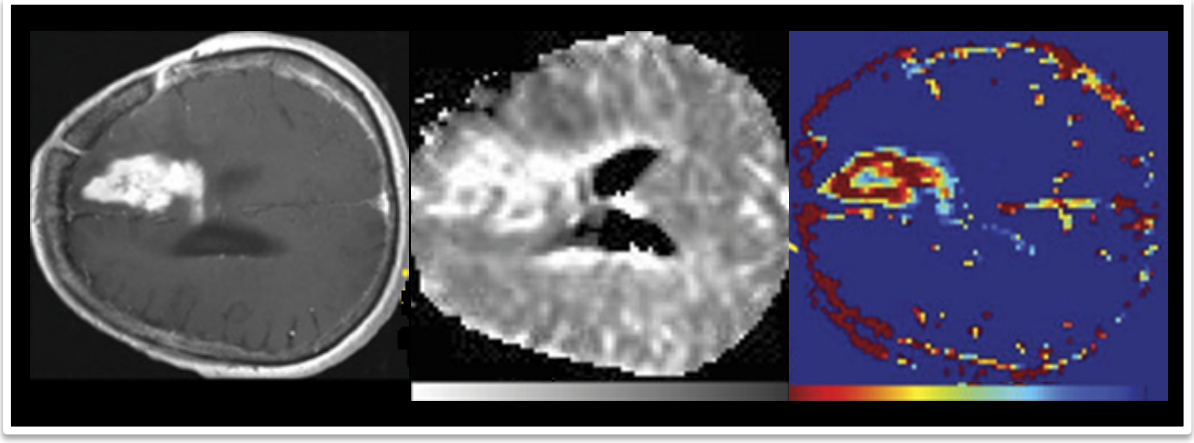

Figure 1: Clinical Imaging of GBM.

(left) MRI with contrast; (center) Map of microvessel size; (right) Map of blood brain barrier permeability (Batchelor et al., 2007).

The 2016 world health organization (WHO) classification of tumors of the central nervous system allocates Grade IV astrocytoma for glioblastoma multiform (GBM). GBM is the most frequently occurring type of glioma (about 50%) with an incidence of 3.3/100,000 in North America (Baldi et al., 2010; Ostrom et al., 2014). In France, about 3000 new cases of GBM are diagnosed each year (Zouaoui et al., 2012). Median survival ranges from 12 to 15 months following diagnosis, with a 5

year-survival of only 5% (Ostrom et al., 2014; Yan et al., 2013). GBM subdivides into three categories. The first type, IDH[1]-wild-type, represents nearly 90% of these tumors which are clinically defined as primary GBM and mostly occur in patients over the age of 55 (Louis et al., 2016; Ohgaki and Kleihues, 2013). The second type, termed IDH-mutant, represent the other 10% of cases, arising primarily in younger patients, and are classified as secondary GBM, as these patients often have previously developed lower grade diffuse gliomas (Louis et al., 2016; Ohgaki and Kleihues, 2013). The third category, NOS (not otherwise specified), is reserved for tumors where the IDH status cannot be evaluated. These tumors still maintain astrocytic features, vascular proliferation and necrosis. Most of these tumors are likely IDH wild-type, however, due to unavailable IDH status they are given a separate denotation (Louis et al., 2016). Other common changes in Grade IV tumors include amplifications in the EGFR[2] gene in 57% of primary GBM, as compared to 8% of secondary GBM (Brennan et al., 2013). Moreover, the tumor suppressor PTEN[3] is frequently altered in GBM, with mutations in up to 40% of patients, in addition to a loss of heterozygosity in 60 to 80% of all GBM (Kwon et al., 2008).

GBM are most frequently localized into cerebral hemispheres; 95% of tumors are found in the supratentorial region, while, in contrast, very few tumors arise in brainstem, spinal cord or cerebellum (Nakada et al., 2011). The only established risk factor for developing a GBM is exposure of the central nervous system to ionizing radiation (Elsamadicy et al., 2015; Taylor et al., 2010), although GBM incidence may change between ethnicity, gender, age, and exposure to specific xenobiotics. Clinical presentation includes neural deficit, which vary depending on tumor localization, in 40-60% of patients. These can range from hearing and vision impairment in temporal lobe tumors, to personality changes in some patients who present with frontal lobe tumors. Hemiparesis can also occur. Other symptoms include unilaterally localized headaches in 30-50% of clinical cases, and seizures in 20-40% of them (Hanif et al., 2017).

[1] Isocitrate Dehydrogenase
[2] Epidermal Growth Factor Receptor
[3] Phosphatase and Tensin Homologue

1.2 Molecular Subtypes

In 2010, seminal work by Verhaak and colleagues identified four molecular subtypes of GBM: Classical, Mesynchymal, Proneural, and Neural (Verhaak et al., 2010). Proneural subtype has an oligodendrocytic signature, while Classical tumors express an astrocytic gene repertoire. Mesenchymal tumors are highly correlated with a cultured astroglial profile and the Neural molecular category is associated with oligodendrocytic and astrocytic differentiation, in addition to encompassing genes expressed in neurons (Verhaak et al., 2010). Those molecular subtypes are canonically characterized as follows:

- Proneural: The major features of Proneural GBM include *IDH1* mutations and *PDGFRA* alterations. Frequent loss or mutation of *TP53,* and expression of oligodendrocytic markers *OLIG2* and *NKX2-2* similarly occur (Verhaak et al., 2010). Conversely, protein abundance of the tumor supressor *p21* is reduced and negatively correlated with *OLIG2* levels (Ligon et al., 2007). Proneural tumors are also characterized with higher expression of proneural development genes encoding transcription factors, such as *SOX* (Sry-related HMG box), *DCX, ASCL1,* and *TCF4* genes. More recent analysis further subdivides the Proneural subtype by CpG island methylation status. CpG island methylator phenotype (CIMP+) Proneural subtype represents the tumors resulting from secondary GBM, they have IDH mutations and ensure the best prognosis of any GBM subtype. By contrast, CIMP- Proneural tumors contain *PDGFRA* amplification, and have a worse prognosis than CIMP+ counterparts (Nakano, 2015).
- Classical: Classical GBM retain a chromosome 7 amplification accompanied by a chromosome 10 loss. Most Classical tumors (*ie* 97%) also acquire an *EGFR* amplification, but lack *TP53* mutation. Neural precursor and stem cell marker *NES*, in addition to *NOTCH* and Sonic hedgehog, *SHH,* signaling pathways are highly expressed (Verhaak et al., 2010).
- Mesenchymal: The majority of Mesenchymal tumors possess a low *NF1* expression. *NF1* is a tumor supressor gene which primarily regulates RAS. Loss of this gene leads to increased MAP kinase activity, a pro-tumorigenic pathway (Carroll, 2012). Mesenchymal tumors also present with frequent co-mutation of *NF1* and

PTEN. They display mesenchymal markers such as *CHI3L1* and *MET*, as well as *CD44* and *MERTK*, genes well-known to associate with the epithelial-to-mesenchymal transition. They likewise exhibit higher levels of tumor necrosis factor (TNF) and NF-κB pathways including *TRADD, RELB*, and *TNFRSF1A* (Verhaak et al.,2010).

- Neural: The Neural subtype is defined by the expression of neuron markers such as *NEFL*, *GABRA1*, *SYT1* and *SLC12A5* (Verhaak et al., 2010).

The most relevant clinical associations with subtype in this study was age, with younger patients predominantly falling in the Proneural category and having a significant survival advantage. A more recent study by Verhaak's group determined that the Neural phenotype may not hold tumor specific features as these samples came from tumor margins where more non-tumoral neural tissue is likely to be detectable. Therefore the Neural subtype may actually correspond to a normal neural lineage contamination in the original study (Gill et al., 2014; Wang et al., 2017b), as such it has been excluded from Table 1. Subtype features are summarized in Table 1.

Subtype	CIMP+ Proneural	CIMP- Proneural	Mesenchymal	Classical
Frequence	10%	12%	30%	35%
Average Age	44.5	50.6	53.4	57.7
Prognostic	Relatively benign	Benign or poor	Poor	Poor
Response to Therapy	Not Resistant	Not Resistant	Resistant	Resistant
Mutations	IDH1, TP53, ATRX	PDGFRA, TP53, CDKN2A, CDK4	NF1	EGFRVIII or mut, CDKN2A
Methylation	Global	Low	Low	Low

Table 1: Summary of GBM subtype characteristics. These include frequence, average age, prognostic, response to therapy, mutations, and methylation status.

Characterization of molecular subtype implicates associations with the tumor microenvironment. Analysis of Mesenchymal alterations showed that increased macrophage/microglia infiltration was due to aberrations in *NF1.* Further, the poor prognosis correlated with the Mesenchymal subtype and with a higher frequency of macrophages/microglia, which might contribute to a sub-optimal response to radiotherapy (Wang et al., 2017).

More recent studies have emphasized that tumors contain cells with differing subtype specific gene expression. Indeed, single cell analysis of five patient tumors showed that all tumors contain a heterogeneous mixture of cells belonging to different GBM subtypes (Patel et al., 2014). One way this can occur is a Proneural to Mesenchymal transition after radiation treatment (Halliday et al., 2014). However, tumor cells grown *ex vivo* under stem cell conditions maintain features of the dominant subtype of the tumor from which they were derived, implying that changes in environment are the key drivers for subtype variations. Correspondingly, transcriptomic analysis from multi-region sampling of several patient biopsies unmasked that tumor cells from the enhancing region had a Proneural signature; tumor cells from the necrotic region a Mesenchymal signature, and cells from an intermediate region (enhanced margin) contain features of both Classical and Proneural subtypes (Jin et al., 2017). Therefore, developing subtype specific therapies may be less effective than previously thought.

1.3 Treatments

1.3.1 Standard of Care

When possible, the most effective treatment in GBM involves surgical resection of the primary tumor. This can provide patients with immediate relief from tumor mass related effects and symptoms. Brown et al. showed that more extensive resection of the tumor resulted in increased 1 and 2 year survival rates in addition to an improvement in progression free survival (Brown et al., 2016). The use of fluorescent dyes to identify tumor tissue has further enhanced the accuracy of this process. A phase III clinical trial, using 5-aminolevulinic acid to visualize tumor tissue as compared to conventional microsurgery, showed a better rate of complete tumor

resection (65% versus 36%) and superior 6 month progression free survival (41% versus 21%), however there was no impact on overall survival (Stummer et al., 2006). Additionally, it has recently been established that subcortical electro-stimulation mapping during an awake craniotomy can improve resection margins and patient quality of life in low-grade gliomas (Ghinda and Duffau, 2017), thus this protocol might be applied to higher grade tumors as well.

Post-surgery, patients undergo radiation therapy, which focally targets MRI-evident tumor and surrounding margins to a cumulative dose of 60 Gy. Daily doses of 1.8 to 2.0 Gy fractions for approximately 6 weeks is usually applied, three to four weeks postoperative procedure (Han et al., 2015a, 2015b). Increased radiation dosage up to 76 Gy did not appear to extend patient survival (Kirkpatrick et al., 2017). Moreover, shorter courses of augmented doses of radiotherapy, known as hypofractionation, have been evaluated in elderly patients. In a randomized trial comparing 6 weeks (30 fractions of 60 Gy) to 3 weeks (15 fractions of 40 Gy) in patients over 60 years-old, there was neither a difference in median patient survival, nor in quality of life. However, patients in the hypofractionation group required less post-treatment corticosteroids. Therefore, it was concluded that hypofractionation was a viable treatment option for elderly patients (Roa et al., 2004). Proton therapy uses particles rather than photons to deliver radiation, allowing for enhanced focalization of the treatment. This lessens the radiation exposure of non-target tissues, reducing patient fatigue and neurocognitive dysfunction associated with brain irradiation. In addition, proton therapy offers a dosimetric advantage over conventional radiotherapy in glioma. A retroactive study comparing photon and proton therapy illustrated an improved overall survival for proton-treated patients. Randomized trials still need to be performed to confirm these findings (Harrabi et al., 2016; Jhaveri et al., 2018).

Temozolomide (TMZ) is a DNA-alkylating agent for chemotherapy, which efficiently crosses the blood brain barrier (please see section 1.4) to deliver relevant concentrations in the brain. TMZ is, in fact, a prodrug with aqueous chemistry typical of imidazotetrazine compounds with bicyclic aromatic heterocycles. Under neutral or alkaline conditions, structural changes allow the hydrolytic ring to open and dispense an intermediate active compound. Thus, the acidic pH of the GBM tumor

microenvironment stabilizes the prodrug form of TMZ. Once inside cells, intermediates then release methyl diazonium ions to interact with nucleophilic sites in DNA and methylate it (Moody and Wheelhouse, 2014). TMZ acts by supplying a methyl group to purines in DNA to form O^6-methylguanine which causes DNA changes and leads to cell cycle arrest at G2/M phase, during consequent replication cycles (Nanegrungsunk et al., 2015). However, methylguanine methyltransferase (MGMT) can remove this methylation, and therefore tumors with wild-type MGMT are

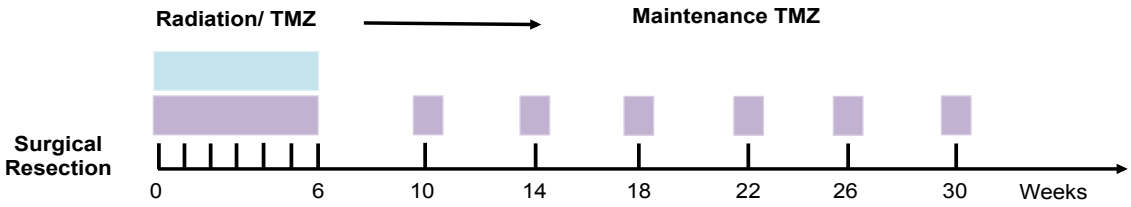

Figure 2: Timeline of standard of care. Following surgical resection patients receive both radiotherapy and TMZ for 6 weeks followed by a maintenance dose of TMZ (5 times in 28 days) for 6 months after.

most likely resistant to TMZ treatment. Plus, DNA mismatch repair may fail in GBM and cause the O^6-methylguanine to be ineffective (Zhang et al., 2012). Therefore, knowing a patient's MGMT status and capacity to mismatch repair can inform their response to TMZ.

A 2005 phase III trial showed that daily TMZ given in parallel to radiotherapy (75 mg/m^2) for 40-49 days and followed by 6 maintenance cycles of TMZ (150-200 mg/m^2), 5 times over a 28 day period, prolonged patient survival (Stupp et al., 2005, 2009, 2015). Based on these results, this became the standard of care procedure, named the Stupp protocol for newly diagnosed GBM: combined radiation and TMZ followed by a continuation of TMZ (Figure 2). Different dosing schedules of TMZ have been investigated; an intensified maintenance dose of TMZ (75 mg/m^2), 21 times over a 28 day-period, was compared to the standard dose, doubling the cumulative administration of TMZ. There was no noted outcome difference, however patients had higher incidence of grade 3 and 4 toxicities (Gilbert et al., 2013).

1.3.2 Anti-angiogenic Therapy

Angiogenesis is the process by which new blood vessels grow from existing ones. In tumors, angiogenesis is hijacked to provide nutrients and oxygen to the

rapidly expanding cancer cells. Vascular Endothelial Growth Factor (VEGF) is the prototype of angiogenic factors and belongs to the family of heparin binding proteins, operating through tyrosine kinase receptors (VEGFRs). Upon receptor binding, VEGF promotes angiogenesis and stimulates endothelial cell proliferation and migration. VEGF expression can be induced by growth factors like epidermal growth factor (EGF), transforming growth factor (TGFα/β), fibroblast growth factor (FGF) and platelet derived growth factor (PDGF) (Yadav et al., 2015).

Bevacizumab is an antibody that targets the pro-angiogenic factor VEGF. It was developed by Genentech and approved by the food and drug administration (FDA) in 2009 (Cohen et al., 2009). Bevacizumab is a specific antibody, which binds to all isoforms of human VEGF-A. Tyrosine kinase inhibitors sunitinib, sorafenib, and pazopanib, in contrast, inactivate VEGF signaling by targeting VEGFRs, with off-target inhibition of PDGFR and c-KIT (Meadows and Hurwitz, 2012). The group of Jeremy Rich demonstrated that bevacizumab abolished the GSC-driven pro-angiogenic effects, including tube formation and vessel migration, on human umbilical vein endothelial cells (HUVEC). This antibody-based treatment also reduced the growth of ectopic and orthotopic xenografts from primary tumor cells (Bao et al., 2006a; Calabrese et al., 2007). Combining bevacizumab with TMZ and radiation was explored in 3 phase III randomized trials with two focused on newly diagnosed GBM and the third one devoted to recurrent GBM. All three clinical studies showed increased progression free survival and baseline quality of life; however, this was accompanied by an augmentation in grade 3 or higher toxicities. Moreover, there was no improvement in overall survival, though it was expected based on imaging analysis (Chinot et al., 2014; Gilbert et al., 2014; Wick et al., 2017). In contrast, some studies claim that bevacizumab and other VEGF pathway inhibitors do benefit patients by reducing peritumoral edema, which lessens the need for corticosteroid prescription and can in turn significantly improve patient quality of life (Batchelor et al., 2007; Nagpal et al., 2011). However, as all three phase-III clinical trials report amplification of severe toxicities for bevacizumab-treated patients, its uses for such purposes should be cautioned.

Why do anti-angiogenic therapies fail? John de Groot's group showed that xenografts resistant to anti-VEGF treatment contained an invasive mesenchymal

signature, as illustrated by the expression of STAT3, c-MET, and TGFβ (Piao et al., 2013). Moreover, it has also been demonstrated that one potential mechanism of resistance in GBM involves the recruitment of pro-angiogenic inflammatory cells, as a source of angiogenic chemokines and cytokines, to restore tumor vascularization (Gabrusiewicz et al., 2014; Piao et al., 2013; Rivera et al., 2015). A recent study by Gabriele Bergers's laboratory suggests a role for the tumor immune microenvironment in resistance to anti-angiogenic therapy. Their work elucidated that tumor cells resistant to anti-angiogenic therapy had increased programmed cell death ligand 1, PD-L1, expression, allowing them to escape immune detection (Allen et al., 2017).

1.3.3 Immunotherapy

Immunotherapy has vastly improved patient outcome in clinical trials of metastatic melanoma (Albertini, 2018). As such, it may represent a viable option for the treatment of other cancers with poor prognosis. Indeed, in the recent issue of Nature reviews cancer, focusing on brain tumors, an Peter Fecci and colleagues devoted their review to the prospect of immunotherapy for the treatment of brain tumors (Sampson et al., 2020).

The programmed cell death receptor, PD-1, is expressed on the surface of activated T-cells, and acts as an immune checkpoint to prevent autoimmunity. Cells expressing a ligand for the receptor, such as PD-L1, can inactivate these T-cells via PD-1/PD-L1 interaction. Many cancer cells overexpress PD-L1 to escape immune responses. Therefore this immune checkpoint is an attractive target for anti-cancer therapy (Chen et al., 2012b). In fact, a phase I clinical trial of pembrolizumab, in patients with recurrent, but resectable tumors, showed a statistically significant survival rate for those receiving immunotherapy. Pembrolizumab is a monoclonal antibody that binds the PD-1 receptor in lymphocytes to prevent PD-L1 interaction. This was combined with bevacizumab, as a second line therapy, for most of the patients in the trial after immunotherapy was removed. Overall survival improved from 7.5 months to 13.7 months in the pembrolizumab treated group (Cloughesy et al., 2019). Therefore, combining immunotherapy with anti-angiogenic therapy remains an open axis to explore for the treatment of GBM.

Another promising immunotherapy for GBM includes the formation of chimeric antigen receptor T-cells, CAR-T-cells. Several clinical trials explore the efficacy of targeting the EGFRvIII receptor, a common mutation of EGFR in GBM, using rindopepimut (Del Vecchio et al., 2012; Swartz et al., 2014). Phase I and II trials have shown significant improvement in overall survival for vaccinated patients, however some drawbacks to this approach exist. Not all GBM express EGFRvIII, and its expression has been shown to fluctuate throughout disease progression (van den Bent et al., 2015). Further, CAR-T therapy can promote immunosuppressive response including up-regulation of PD-L1. Hence, a current trial, seeks to ameliorate patient outcome by combining pembrolizumab with EGFRvIII-CAR-T therapy to reduce immunosuppressive side effects (Akhavan et al., 2019). Together, this evidence shows that there are many hurdles to overcome in developing novel and effective treatments.

Moreover, a recent study by Peter Fecci's group demonstrated that naïve T-cells accumulate in the bone marrow in preclinical models of GBM, as well as in GBM patients, prior to treatment. Circulating lymphocyte rate, in GBM patients, borders on the ones found in immunosuppressed patients, such as AIDS (Chongsathidkiet et al., 2018). This sequestering was occurring due to loss of S1P1 (sphingosine 1-phosphate receptor 1) on the surface of these T-cells (Chongsathidkiet et al., 2018). Sphingosine 1-phosphate (S1P) is a bioactive lipid that acts as the ligand for several G protein coupled S1P receptors. This signaling axis also promotes the development of type 1 helper T-cells (Blaho et al., 2015). When Fecci's group prevented S1P1 internalization, T-cell sequestration was abolished and enhances the efficacy of immune checkpoint-based therapy in animal models (Chongsathidkiet et al., 2018). Additionally, in order to target tumor-associated macrophages, colony stimulating growth factor-1 receptor (CSF-1R) inhibitors have been employed. These inhibitors were shown to block gliomagenesis and debulk the tumor by a glioma-cell independent mechanism. Instead, they alter macrophage polarization to promote phagocytosis of tumor cells (Pyonteck et al., 2013; Quail et al., 2016). Therefore, enhancing the immune response may improve patient outcome.

1.3.4 Other Alternatives

One alternative method of treating GBM, proposes the use of virotherapy, *ie* live attenuated virus, to target the tumor cells. As early as 1991, Martuza and colleagues showed that the herpes simplex virus mutant could kill GBM immortalized cells *in vitro* and *in vivo* (Martuza et al., 1991). Moreover, it was later revealed that an attenuated adenovirus could exert similar effects, and that cell death in this case was likely due to autophagy (Alonso et al., 2008, 2012; Fueyo et al., 2000; Ito et al., 2006). With recent outbreaks bringing the Zika virus to the global health conversation, Zhu and colleagues showed that this oncolytic virus effectively targets Glioblastoma Stem-like Cells, GSCs (please see section 1.6). Furthermore, the virus was found selective for these cells, as it infected them at a much higher rate than normal neural stem cells. Attenuated Zika virus maintained its efficacy against GSCs, and had an additive effect when combined with TMZ treatment (Zhu et al., 2017). A study by Chen-Feng Qin's laboratory confirmed this effect using intracranial injection of the Zika-LAV vaccine, which is currently undergoing testing as a potential vaccine against the Zika virus (Chen et al., 2018). Similarly, a trial of inactivated poliovirus in patients with recurrent GBM demonstrated an increased overall survival in virus treated group (Desjardins et al., 2018).

Carmustine, or Gliadel, wafers are biodegradable polymers, which contain 3.85% carmustine, an alkylating agent. They are implanted upon surgical resection of the tumor and deliver a controlled release of 7.7 mg carmustine for approximately 5 days. The efficacy of these wafers in clinical trials remains inconclusive. While some trials report survival benefits, they are not statistically significant (Affronti et al., 2009; Brem et al., 1995; Westphal et al., 2003). Also, at least one study shows no significant improvement and drastically higher toxicity in patients who received carmustine (De Bonis et al., 2012).

Other studies have introduced the idea of a cancer cell trap for GBM therapy. These traps are designed with both chemoattractant, to target the tumor cells to the cage, and chemotherapy to kill the sequestered cells (Van Der Sanden et al., 2013). A recent report demonstrated that bacterial cellulose could be used as the polymer for such a trap in rats (Autier et al., 2019). However, much research remains to be done on these therapies before determining their true efficacy in patients.

Tumor treating fields (TTF), which involves low intensity (100-300 kHz) alternating electric fields delivered via insulated electrodes, operate as antimitotic physical treatment (Kirson et al., 2004). The first phase III trial compared TTF alone to chemotherapy alone in recurrent GBM. GBM patients undergoing this treatment wear transducers, placed on the shaved scalp, for more than 18 hours a day. Due to this inconvenience, not all patients in the trial complied with the guidelines of therapy. When analyzing patients that followed the therapy at least 75% of the time, an overall improvement in patient survival and no significant adverse effects was observed (Stupp et al., 2012). In 2009, Roger Stupp initiated a phase III trial for newly diagnosed GBM. Patients either received TTF in addition to maintenance TMZ or maintenance TMZ alone following standard of care surgery and chemo/radiotherapy. In 2015, preliminary findings detailed progression free survival of 7.1 months in patients treated with TTFs compared to 4 months for those treated with TMZ alone (Fabian et al., 2019). The final study, published in 2017, revealed that treatment with TTFs leads to a superior median overall survival of 20.9 months compared to 16. Of note, half the patients undergoing TTF therapy experienced mild to moderate skin toxicity (Stupp et al., 2017). The FDA approved TTFs for use on newly diagnosed GBM in 2015, representing a rare therapy to pass clinical trials for GBM. Subsequent trials combining TTF with other therapies are currently underway.

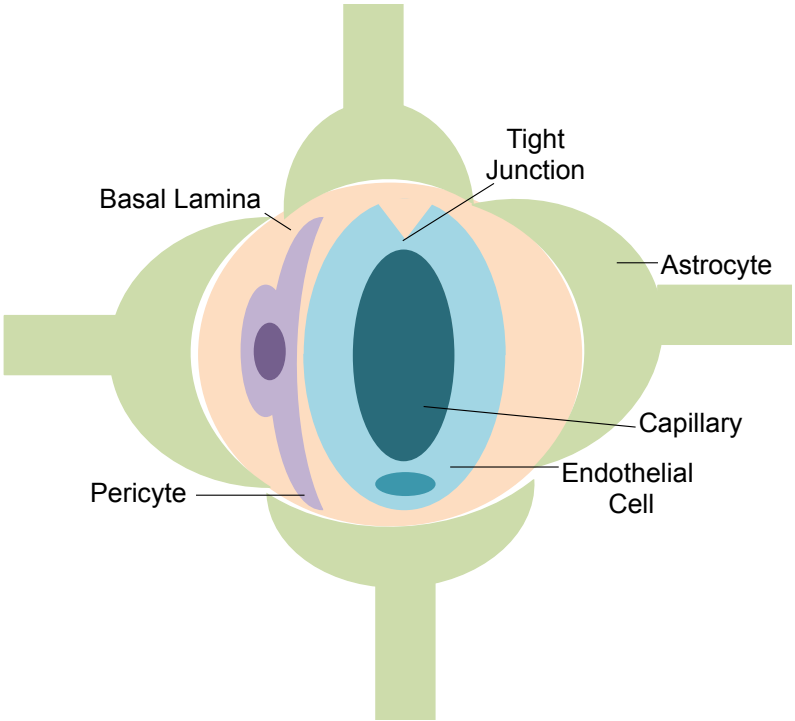

Figure 3: Schematic of Blood Brain Barrier (BBB) cellular organization. At the BBB, endothelial cells are covered with pericytes and surrounded by astrocyte end-feet.

1.4 Blood Brain Barrier

The vasculature of the brain delivers blood through bilateral sets of arteries, namely, internal carotid arteries and vertebral arteries, which branch to reach all areas of the brain. The cerebral vasculature

serves several functions including supplying the brain with nutrients, ridding the brain of waste products, restricting ion and fluidic movement, and aiding in overall brain homeostasis. The restriction of ions and fluids allows for optimal neuronal functions, as fluctuations in ions which can occur after eating or exercising would disrupt synaptic and axonal signaling (Abbott et al., 2006).

The blood brain barrier (BBB) acts as a discriminatory hurdle to molecules, infectious agents and toxins seeking to enter the brain through the bloodstream. The BBB relies on endothelial cells, which form tight junctions with each other along cerebral microvessels, in order to shield the brain from infection and regulate its microenvironment. Astrocytes and pericytes also participate in the organization of the BBB; pericytes and microglia support the rigidity by associating with the basal lamina of endothelial cells. Astrocytes line the perivascular space to form endfeet (Abbott et al., 2006; Obermeier et al., 2013). Pericytes cover about 20% of endothelial cells in the BBB, and can regulate blood flow through the brain capillaries via contracting and relaxing (Armulik et al., 2005; Jespersen and Østergaard, 2012) (Figure 3). Meanwhile, astrocytes connect the brain capillaries to neurons providing them with nutrients and preventing oxidative stress (Hirrlinger and Dringen, 2010). In addition, the extracellular matrix of the basal lamina contains laminin, collagen, proteoglycans and other extracellular matrix proteins. Alterations of these protein compositions can increase BBB permeability (Aumailley and Smyth, 1998; Tanjore and Kalluri, 2006; Zhou et al., 2018). Gases, like oxygen and carbon dioxide passively diffuse through the endothelial barrier, as do lipophilic agents like barbiturates and ethanol, however hydrophilic molecules are excluded (Abbott et al., 2006). In order to prevent transport of molecules across the BBB, endothelial cells express efflux pumps like p-glycoproteins to expulse molecules back to the bloodstream. Because many drugs, including anti-cancer therapies, have a high brain efflux index, attaining relevant concentrations for clinical efficacy in the brain is challenging (Kakee et al., 1996).

While many vessels within tumors are leaky and disorganized, the invasive region of the tumor maintains an intact BBB in GBM. One would expect the abnormal vessels of the tumor core to allow for increased passage route to drugs; however, the migrating and invasive cells of the tumor margin are surrounded by a normal brain vasculature, preventing such treatments from reaching them (van Tellingen et al.,

2015). Also, permeability increase usually led to uncontrolled fluid movement, elevated interstitial fluid pressure (IFP), and edema, which collectively oppose the crossing of vascular walls.

Various strategies have been adopted to deliver drugs to the brain including modification of drugs and prodrugs, disruption of tight junctions, local delivery through neurosurgery, and nanoparticles. These methods exhibit these main drawbacks: i) disturbing junctions increases the risk of toxins entering with the drugs, ii) altering chemical structure of drugs can be costly and long to develop, and iii) neurosurgery should be avoided when possible to increase the patient's quality of life. However, nanoparticles are non-invasive, cost efficient, and easy to synthesize, therefore, they represent a potential solution to distributing anticancer drugs across the BBB (Zhou et al., 2018). Moreover, a recent clinical trial suggests that low intensity pulsed ultrasound can safely disrupt the BBB for chemotherapy delivery (Carpentier et al., 2016; Idbaih et al., 2019). In order to develop and deliver novel therapies to GBM patients, delivery strategies must be adopted to account for and overcome the BBB.

1.5 Experimental Models

1.5.1 In Vitro

The most widely used established cell lines to study GBM, including U87 (established from a 44 year old female patient with highly malignant astrocytoma), U251 (derived from a male patient with malignant grade IV astrocytoma) and T98G (originated from human glioblastoma multiforme tumor of a 61

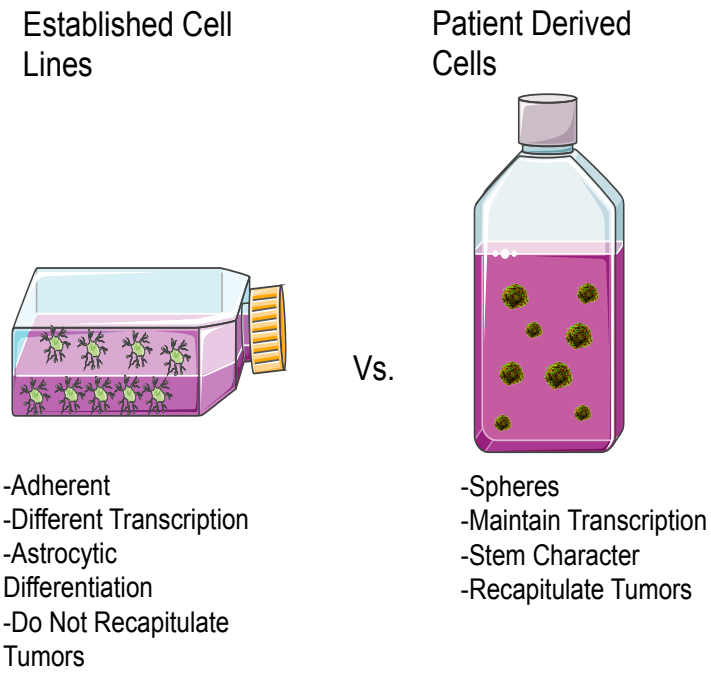

Figure 4: Comparison of established cell lines and patient derived cells.

year old male), are grown in milieu containing serum, which promotes astrocytic differentiation (Pontén and Macintyre, 1968; Stein, 1979; Westermark et al., 1973). Therefore transcriptional and epigenetic programs in these cells do not reflect the neural stem cell pathways, which are activated in Glioblastoma Stem-like Cells (Lee et al., 2006). Further, xenografts resulting from these established cell lines do not resemble human GBM histopathological characteristics (Lee et al., 2006). Analysis of U87 from the American Type Culture Collection (ATCC) suggests that it was likely switched with another cell line as it does not match original Uppsala stocks (Allen et al., 2016). This calls into question the results of numerous GBM studies performed using U87, and together, this information cautions the use of established cell lines, as they do not recapitulate human disease.

In order to long-term culture mouse neural stem cells, a protocol was established by which these cells were grown in suspension as neurospheres. To achieve this, their milieu lacked serum but rather contained defined composition and concentration of growth factors, such as EGF, FGF and insulin, to sustain stemness self-renewal (Reynolds and Weiss, 1992; Robertson et al., 2019). Patient-derived primary GBM cells can also be maintained under similar settings (Galli et al., 2004; Singh et al., 2003). Under spheroid culture conditions, they uphold transcriptional status of parental tumors and can reiterate features of the primary tumor upon xenotransplantation (Robertson et al., 2019). These cells are well characterized and easily shared between laboratories. However, upon extended culture, tumor heterogeneity is lost and subclone populations emerge, which often lose IDH status of the original tumor. Still, the use of patient-derived cells as an *in vitro* model better recapitulates the primary tumor than classical cell models (Figure 4).

Recently, Lancaster et al developed a method to establish neural tissue with similar organization to a developing cortex from human pluripotent stem cells (Lancaster et al., 2013). These developed tissues are termed organoids as they have features of the original organ. This procedure has been adapted to grow primary GBM samples (Hubert et al., 2016). Recent work by Howard Fine's laboratory demonstrated a novel 3D co-culture system using brain organoids and GSCs. They established organoids, or "mini-brains" from human embryonic stem cells. Upon creation of organoids, co-culture experiments with GSCs obtained a 100% tumor

formation rate. These “tumors” carry the infiltrative behavior and resistance to standard of care therapies, launching a system to study classic characteristics of GBM under highly controlled and readily alterable conditions (Linkous et al., 2019). One benefit of both types of organoid models is that they allow for the study of hypoxic and necrotic tumor features. Major drawbacks include high variability in both the shape of the organoid and the cell type produced, as well as time consuming formation (Robertson et al., 2019). Additionally, they lack tumor vasculature and immunological landscape, so they do not fully recapitulate *in vivo* tumor organization. Therefore, while organoids present many advantages, factors such as time limitations and availability of patient material presently limit their widespread use in GBM studies.

1.5.2 *In Vivo*

Mice are the most cost effective and accessible model organism to study GBM. Models include genetically engineered disease models or transplanted tumor cells. Both allografts and xenografts are implanted either orthotopically in the brain or subcutaneously. Additionally, growing evidence points to the potential use of canine glioma to model human disease. In dogs, gliomas occur spontaneously, and therefore there is a coevolution of the tumor and its microenvironment, as well as relevant tumor heterogeneity, and an intact immune system (Koehler et al., 2018). A potential drawback is that their use would require coordination with veterinarians and owner consent, which can make cohorts difficult to establish.

Allograft transplantation allows tumors to develop in immune-competent mice. This permits investigators to study the role of the immune system in the tumor’s initiation, progression, and response to therapy. The most common model of this uses the GL261 cell line established from carcinogen-induced glioma (Robertson et al., 2019). GL261 has nonetheless developed genetic drift by accumulating mutations, such as KRAS, which are not associated with GBM. This has led to *in vivo* models that do not accurately reflect a GBM tumor (Szatmári et al., 2006). CRISPR technology offers a solution to this problem; models are being created altering genes in mouse NSCs to promote tumorigenicity. This should favor the study of GBM in an intact immune system, should greatly improve modeling of the disease, and may allow access to early steps of gliomagenesis (Robertson et al., 2019).

Subcutaneous models are technically simple and can be adopted for pilot studies to verify a molecule's efficacy on tumor cells *in vivo*. Additionally, these systems endorse the study of a cell tumor initiating capacities through visible tracking of tumor growth over time. This serves a purpose for newly isolated GSCs or cells undergoing gene silencing. These models are also useful for testing molecules that do not efficiently cross the blood brain barrier, before setting up costly experiments, which involve, for instance the implantation of mini-pumps directly to the brain or pharmaco-kinetic manipulation of the lead compound to improve its delivery to the brain. Subcutaneous tumors occur in a different environment that lacked central nervous system specificity. Indeed, these models lack the infiltrative behavior of GBM in the brain, the signs of neurological defects, and the tumor microenvironment, all of which are important factors in selecting therapies (Liu et al., 2015a). Therefore, whenever possible, subcutaneous studies should be supplemented using orthotopic models.

Xenograft models of GBM involve the transplantation of either established human cell lines, such as U87, or patient-derived primary cells in immune compromised mice. The disadvantage of established cell lines remains the same as *in vitro*; they do not precisely recapitulate human disease, and especially the early stage of tumor development. Often, the patient-derived cells used for xenografts are GSCs, which have been expanded by *in vitro* cell culture prior to implantation. These GSCs are fully able to recreate tumors, and have the advantage of being characterized, archived and distributed by researchers (Robertson et al., 2019). However, these cells lose tumor heterogeneity, and these models cannot evaluate the influence of the immune system. Patient-derived orthotopic xenografts (PDOX) involve the direct implantation of tumor tissue from patients without an intermediate cell culture step. These systems more fully capture genetic diversity and maintain some of the tumor microenvironment, such as vessels, extracellular matrix, and some immune regulators. Nevertheless, PDOX are costly, labor intensive, and involve close partnership with surgeons and thus are not readily available to all researchers (Robertson et al., 2019). Unfortunately, selection also inevitably occurs in these models, through *in vivo* passage. Work by Ben-David et al. showed high rates of copy number alteration in PDOX (Ben-David et al., 2017). Therefore, with the exception of first implantations, fresh from patients, *in vivo* culture of tumor cells

through PDOX may actually be no better than *in vitro* expanded GSC models (deCarvalho et al., 2018).

Introducing defined genetic alterations in oncogenes and tumor suppressor genes to generate spontaneous tumors creates genetic engineered mouse models, GEMMs. A common model, used in GBM, and developed by Luis Parada's group, combines loss of *Trp53* and conditional knockout of *Nf1* (Zhu et al., 2005). For the formation of IDH mutant tumors, IDH1R132H is conditionally expressed in the subventricular zone (SVZ) of adult mice, which nicely models the early events in gliomagenesis (Bardella et al., 2016). Viral delivery through a replication-competent avian sarcoma-leukosis virus-tumor virus A, RCAS-TVA, system can also be used to deliver oncogenes *in vivo*. Expression of TVA, the receptor of subgroup A avian leucosis viruses, renders cells vulnerable to infection with RCAS viruses (Robertson et al., 2019). HRAS and AKT overexpression through viral delivery is able to transform NSCs to tumorigenic cells (Marumoto et al., 2009). Eric Holland's work also used this technology to establish *Nes*-TVA Cdkn2A-/- mice, very susceptible to tumor formation (Holland et al., 2000). A limitation of this system is the need to breed TVA-expressing mouse strains. Likewise, the viral cargo cannot contain large genes like EGFRvIII, which constrains possible genetic mutations. GEMMs have the

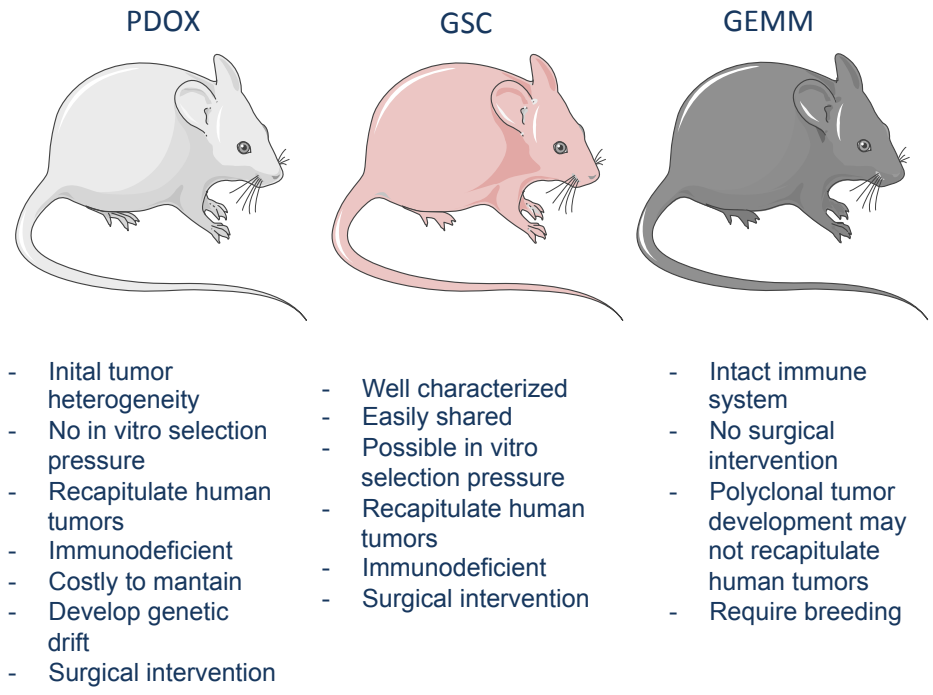

Figure 5: Advantages and disadvantages of common mouse models of GBM.

advantage of not requiring surgery to achieve orthotopic models. These mice also have intact immune systems, so its effect on potential therapies can be evaluated.

However, GEMMs undergo a polyclonal tumor initiation, which does not reflect human disease. CRISPR-based approaches that do not require cargo limited viral delivery or mouse breeding may likely replace in the future currently used GEMMs (Robertson et al., 2019).

There are advantages and disadvantages to all established mouse models of GBM, and none of them fully recapitulate human disease (Figure 5). This may account for the large number of proposed treatments, which work in pre-clinical models but fail to prolong patient survival in clinics. With the advent of CRISPR technology and an improved understanding of GBM, there will hopefully soon be better models to study the tumor and its microenvironment *in vivo*.

Recently, other model organisms have been used to study various aspects of GBM. Zebrafish represent an attractive model for the use in high-throughput drug screening as they are small, inexpensive to maintain, and do not develop an immune system until embryonic day 21, making xenotransplantation possible. Several groups have reported the use of orthotopic xenograft models in zebrafish, demonstrating their ability to recapitulate human disease (Lal et al., 2012; Pudelko et al., 2018; Welker et al., 2016). *Drosophila* models of GBM can be useful in genetic screening for those genes important to the cancer phenotype, as it is rather handy to generate tissue specific genetic alterations in this system. One such model uses overexpression of tyrosine kinase receptors (EGFR or PI3K) in the glia of *Drosophila* (Witte et al., 2009). Hence, alternative model organisms can be useful in identifying novel treatments and targets to be confirmed with cellular and mouse systems.

1.6 Glioblastoma Stem-like Cells

Cancer stem cells were first identified in acute myeloid leukemia in 1994, with the discovery of a proportion of cells able to initiate human leukemia in severe combined immunodeficient mice (SCID) (Lapidot et al., 1994), and later characterized for their capacity to differentiate and self-renew in a similar manner to that of hematopoietic stem cells (Bonnet and Dick, 1997). This led to the

establishment of the cancer stem cell hypothesis whereby it was proposed that tumor heterogeneity emanated from a subpopulation of cancer cells that possess tumorigenic properties (Pardal et al., 2003; Reya et al., 2001). A decade after initial observations in leukemia, this concept was expanded to solid tumors with the identification of a subpopulation of tumorigenic cells in breast cancer (Al-Hajj et al., 2003).

In 1992, Brent Reynolds and Samuel Weiss published their discovery that certain brain-derived cells held self-renewal and multipotency properties *in vitro* (Reynolds and Weiss, 1992). Around the same time, it was uncovered that new neurons continually develop throughout adulthood, with the discovery that brain-derived cells from the SVZ of adult mice could differentiate into new neurons *in vitro* (Lois and Alvarez-Buylla, 1993). However, direct evidence of cells with these stem properties *in vivo* did not emerge until 2007 with the pivotal findings of Fred Gage's laboratory conclusively elucidating the existence of SOX2+ adult neural stem cells (NSCs) in the hippocampus (Suh et al., 2007). Following the breakthrough of adult NSCs came the hypothesis that cancer stem cells could also be present in brain cancers. In line with this, Peter Dirks's laboratory determined that a proportion of brain tumor cells were positive for CD133 (Prominin) and able to self-renew. These cells could also initiate tumors in immunodeficient mice (NOD-SCID[4]), which resembled original patient tumors (Singh et al., 2003, 2004). This was also concurrently confirmed by Angelo Vescovi's group (Galli et al., 2004). These cells have been termed Glioblastoma Stem-like Cells or GSCs. Jeremy Rich's team then showed that these cells could promote tumor angiogenesis in xenografts due to an elevated expression of VEGF (Bao et al., 2006a). This discovery was followed by influential findings from the same laboratory claiming that the CD133+ tumor cells were enriched in cell cultures and xenografts following ionized radiation, and that this resistance was accompanied by increased activation of the DNA damage checkpoint CHK1/CHK2 (Bao et al., 2006b). Likewise, Liu et al. demonstrated that CD133+ tumor cells had higher expression of MGMT mRNA and were resistant to chemotherapy (Liu et al., 2006).

[4] Non-obese diabetic severe combined immunodeficient mice

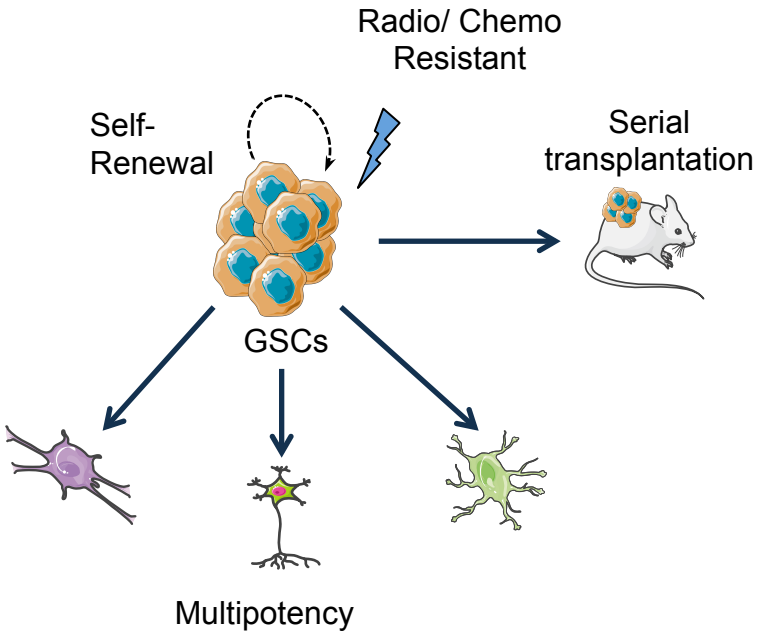

Figure 6: Graphical representation of GSC properties. These include self renewal, multipotency, radio and chemo resistance, and the capacity for serial transplantation.

Eric Holland's group later reported that GSCs also overexpress ATP-binding cassette transporter ABCG2, which allows GSCs to export TMZ via a PTEN/PI3K/AKT dependent mechanism (Bleau et al., 2009). It was subsequently confirmed that TMZ targets the proliferative, but not quiescent GSC population of tumors and that these GSCs are responsible for tumor recurrence (Chen et al., 2012c). Together these data demonstrated that GBM contain cancer stem cells with the properties of self-renewal, tumor initiation, and radio and chemo-resistance, and that GSCs are responsible for tumor recurrence (Chen et al., 2012d; Yan et al., 2013) (Figure 6).

Several cell surface markers, including CD15, CD44, and CD133, which mediate interactions with the microenvironment have been proposed (Lathia et al., 2015). CD133, also known as prominin-1 (PROM1), as already mentioned, was used to distinguish cells with higher self-renewal and differentiation capacity in the initial identification of GSCs (Singh et al., 2003, 2004). However, this marker is not universally informative and can lead to false-negative identification of cancer stem cells (Beier et al., 2007). Further, CD133 is less expressed in cells that are in G_0/G_1, which is often the case for relatively quiescent GSCs (Sun et al., 2009). CD15, or Lewis x, and CD44, also referred to as homing cell adhesion molecule (HCAM) have also been suggested as potential GSC markers with subtype specific association, Proneural and Mesenchymal, respectively (Bhat et al., 2013). However, they may also have large false-positive rates (Lathia et al., 2015). Many other cancer stem cell markers in GSCs have been identified through their characteristic as markers of

normal stem cells, including SOX2 (Hemmati et al., 2003), NESTIN (Tunici et al., 2004), NANOG (Ben-Porath et al., 2008), and OLIG2 (Ligon et al., 2007). However, these markers are intracellular and therefore have little utility in cell sorting isolation methods, but are largely employed for *in situ* identification. Therefore, there are no universal markers of GSCs; rather GSCs are defined by the expression of multiple stem markers, in addition to their properties of self-renewal, therapeutic resistance, ability to differentiate, and tumor initiation.

1.7 Cell of Origin

Before the conclusive proof of adult neural stem cells, it was believed that astrocytes were the cell of origin for GBM initiation (Chen et al., 2012d). For this process to occur, it would require cells to undergo de-differentiation to recapture immature glia and progenitor aspects, as was done to create induced pluripotent stem cells (Takahashi and Yamanaka, 2006). Supporting this hypothesis, work done by Bachoo et al. showed that *in vitro* neonatal cortical astrocytes could regain neural progenitor properties after prolonged culture with growth factors, and that they could generate gliomas via transformation of these astrocytes (Bachoo et al., 2002). However, there is a lack of evidence to support that mature astrocytes can undergo this process.

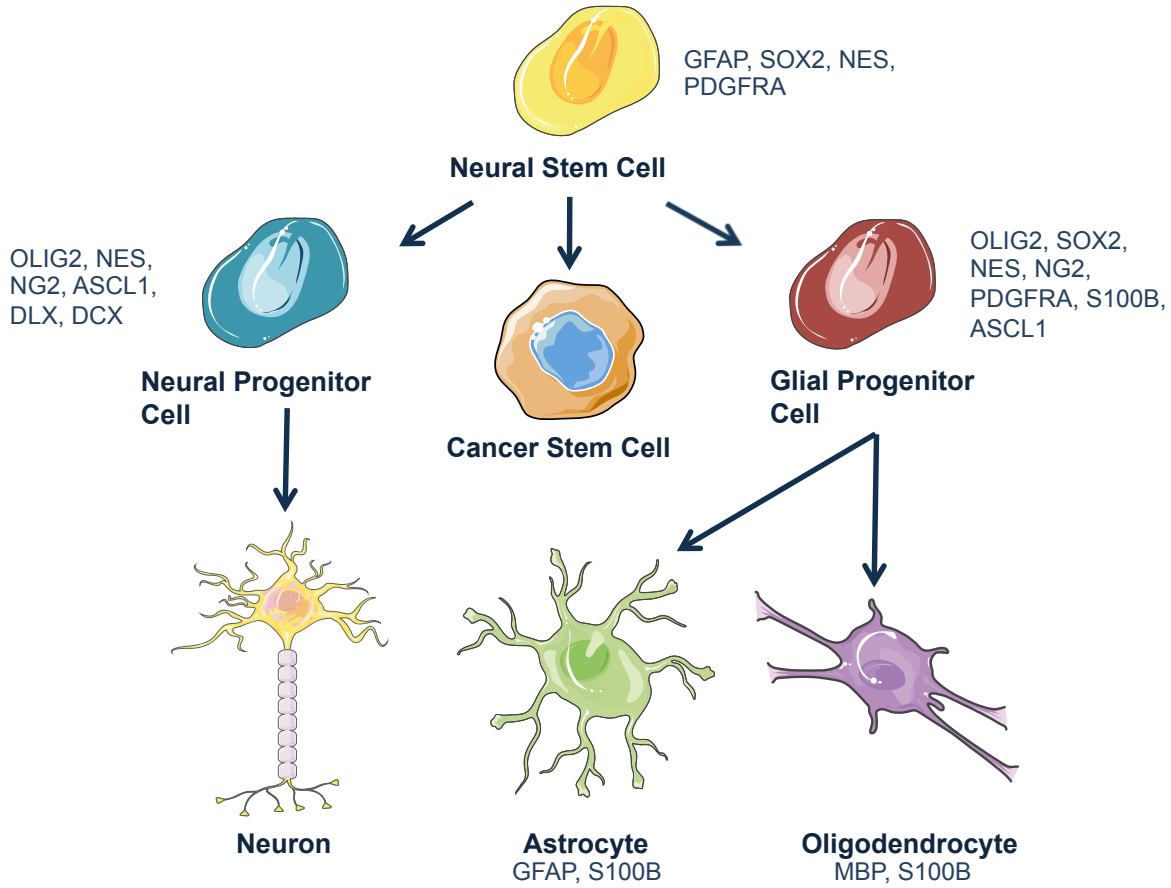

Figure 7: Graphical representation of neural stem cell differentiation. Markers of cell types are included.

With the discovery of adult NSCs, the hypothesis shifted away from astrocyte de-differentiation. As NSCs feature self-renewal capabilities, they were natural candidate for the glioma cell of origin. Indeed, abnormalities occur in cells of the NSC niche of GEMMs (Kwon et al., 2008; Zhu et al., 2005). Further, inducible deletion of *Tp53*, *Nf1* and *Pten* specifically in mouse NSCs produced gliomas in 100% of the mice (Alcantara Llaguno et al., 2009). IDH mutation or HRAS and AKT overexpression in NSCs also leads to the development of GBM in GEMMs (Bardella et al., 2016; Holland et al., 2000). In 2018, Lee and colleagues used a method of deep sequencing to provide evidence that astrocyte-like NSCs, in the SVZ of GBM patients, contain driver mutations of GBM, and thus are likely the cell of origin (Lee et al., 2018) (Figure 7). Recent data from Luis Parada's group showed that mutations in NSCs and neural progenitor cells, but not differentiated neurons induce gliomagenesis in mice (Llaguno et al., 2019). Therefore, mutations in neural progenitor cells may also initiate GBM, independent of NSCs. Certainly; GBM

remains a diverse disease with tumors occurring in varied locations. It is thus plausible that these tumors result from multiple, highly plastic cell types.

1.8 Stem Cell Niche

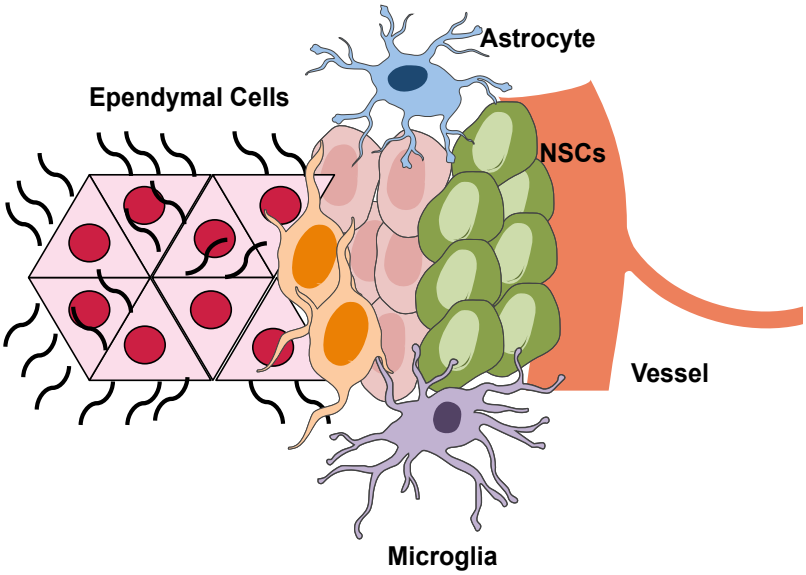

Figure 8: Graphical depiction of NSC niche. This represents NSCs in close contact with vessels. NSCs reside on ependymal cells, which form pinwheel structures. Neural progenitor cells, astrocytes, and microglia are also present in this microenvironment.

The major function of the stem cell niche is to regulate self-renewal and fate. Adult NSCs, also referred to as GFAP+-astrocyte type B cells, reside in a niche in close contact to capillaries in the SVZ and hippocampus (Riquelme et al., 2008; Tavazoie et al., 2008). In adult neurogenesis, these NSCs ultimately give rise to neuroblasts, which travel the length of the SVZ to eventually reach the olfactory bulb and differentiate into neurons (Tavazoie et al., 2008). Neurogenesis has been linked to angiogenesis in mammals where new neurons are found in close contact with vessels in the hippocampus (Palmer et al., 2000). Correspondingly, endothelial cells were able to promote the self-renewal of NSCs *in vitro* (Shen et al., 2004). Tavazoie and colleagues confirmed that the vasculature is an integral part of the NSC niche and that NSCs directly interact with blood vessels in regions that lack pericyte coverage (Tavazoie et al., 2008).

The adult NSC niche includes ependymal cells, the vasculature, astrocytes, microglia and immature and mature NSCs (Ma et al., 2005a) (Figure 8). Ependymal cells form a pinwheel structure on which NSCs reside. They secrete factors like NOGGIN, which inhibits bone morphogenetic proteins (BMPs), to prevent NSC

differentiation (Mirzadeh et al., 2008). The ECs secrete VEGF to promote self-renewal of NSCs, in addition to NEUROTROPHIN-3 which induces quiescence (Bond et al., 2015; Delgado et al., 2014). NSCs themselves also supply factors for both paracrine and autocrine signaling. Neurotransmitter GABA and NOTCH ligand DELTA-LIKE 1 (DLL1) released by neural progenitor cells also regulate quiescence in NSCs through feedback mechanisms (Bond et al., 2015).

Likewise, GSCs reside, at least in part, in a perivascular niche in close contact with endothelial cells (Calabrese et al., 2007; Lathia et al., 2015). Further supporting the existence of a similar niche for NSCs and GSCs, Piccirillo *et al* demonstrated that BMPs have a similar effect on GSCs as they do on NSCs. In normal adult stem cells, the introduction of BMP4 causes cells to differentiate towards an astroglial fate (Bonaguidi et al., 2005). Likewise, the addition of BMP4 to GBM culture reduced proliferation and promoted differentiation (Piccirillo et al., 2006).

1.9 A Vascular Niche for GSCs

1.9.1 Endothelial Secretome

The vasculature of GBM is characterized by irregular angiogenesis, producing leaky and dysfunctional blood vessels. Bao and colleagues showed that GSCs can affect tumor angiogenesis through the secretion of VEGF (Bao et al., 2006a) Seminal work by Calabrese and colleagues showed that NESTIN positive cells in brain tumors are found near ECs. They further showed that CD133+ brain tumor cells can specifically interact with ECs and that ECs can maintain these cancer stem cells in an undifferentiated state by secreting soluble factors (Calabrese et al., 2007). Confirming this study, Ricci-Vitiani and colleagues further showed that GSCs

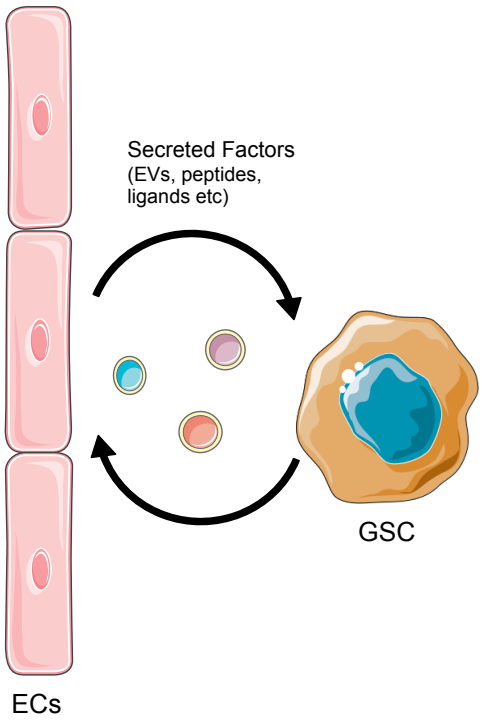

Figure 9: GSCs and ECs reciprocity. Endothelial cells and GSCs both secrete factors into the microenvironment, which affect self-renewal, angiogenesis, differentiation etc.

themselves can differentiate into endothelial cells *in vitro* and possibly *in vivo* (Ricci-Vitiani et al., 2010), therefore adding another axis by which GSCs contribute to tumor angiogenesis. Also, GSCs can transdifferentiate into pericytes to support vessel integrity and promote tumor growth, highlighting a reciprocal interaction between GSCs and the vasculature (Cheng et al., 2013).

Krusche and colleagues identified that GSCs up-regulate expression of the Ephrin-B2 ligand to desensitize cells from vascular confinement and promote invasion. Ephrin-B2 is expressed by ECs; it is a receptor tyrosine kinase of the Eph family known to effect migration, proliferation, and stemness. The augmentation of Ephrin-B2 ligand in GSCs saturated signaling with its receptor on ECs to prevent EC sequestering of GSCs. Also, overexpression of Ephrin-B2 in NSCs leads to gliomagenesis. Conversely, knockdown of Ephrin-B2 in GSCs delayed tumorigenesis (Krusche et al., 2016). Moreover, WNT7a/b expression in tumor cells was necessary for single cell vessel co-option, the process by which tumor cells employ preexisting blood vessels for growth and survival. WNT7a/b levels were also correlated with oligodendrocyte precursor-like (OPC) markers in glioma. Inhibition of WNT signaling improved response to TMZ, while anti-VEGF therapy increased expression of WNT7 and OPC marker OLIG2 (Griveau et al., 2018). These studies emphasize the coordinated signaling between GSCs and ECs (Figure 9).

Moreover, endothelial cell-secreted factors promote mechanistic (formerly mammalian) target of rapamycin (mTOR), a central regulator of cellular growth and metabolism, activation in GSCs. Previous work by our laboratory demonstrated that the endothelial secretome can maintain mTOR signaling in GSCs *in vitro* in the absence of other mitogens (Galan-Moya et al., 2011). In fact, conditioned medium from endothelial cells prevents apoptosis and autophagy induced by mitogen deprivation (Galan-Moya et al., 2014). Eric Holland's group showed that the mTOR pathway is activated in radio-resistant medulloblastoma, which allows them to bypass cell cycle arrest (Bleau et al., 2009). Together, these data illustrate the importance of the endothelial secretome on GSC maintenance.

Endothelial cells contribute to GSC maintenance by secreting a variety of factors, including Notch ligands. They can also secrete nitric oxide to activate the Notch pathway in GSCs (Charles et al., 2010; Fan et al., 2010). Notch signaling occurs when ligands bind Notch receptors causing gamma secretase to process the receptor and release the Notch intracellular domain (NICD). Consequently, NICD translocates to the nucleus with co-factors to activate target genes of the pathway (Figure 10). There is an observed reduction in CD133+ glioma cells in the absence of Notch ligands (Zhu et al., 2011). Notch signaling has also been shown to be important in the development of normal brain cells including glia and neurons (Morrison et al., 2000). Activation of the Notch pathway in GSCs by ECs maintains the GSC stem state.

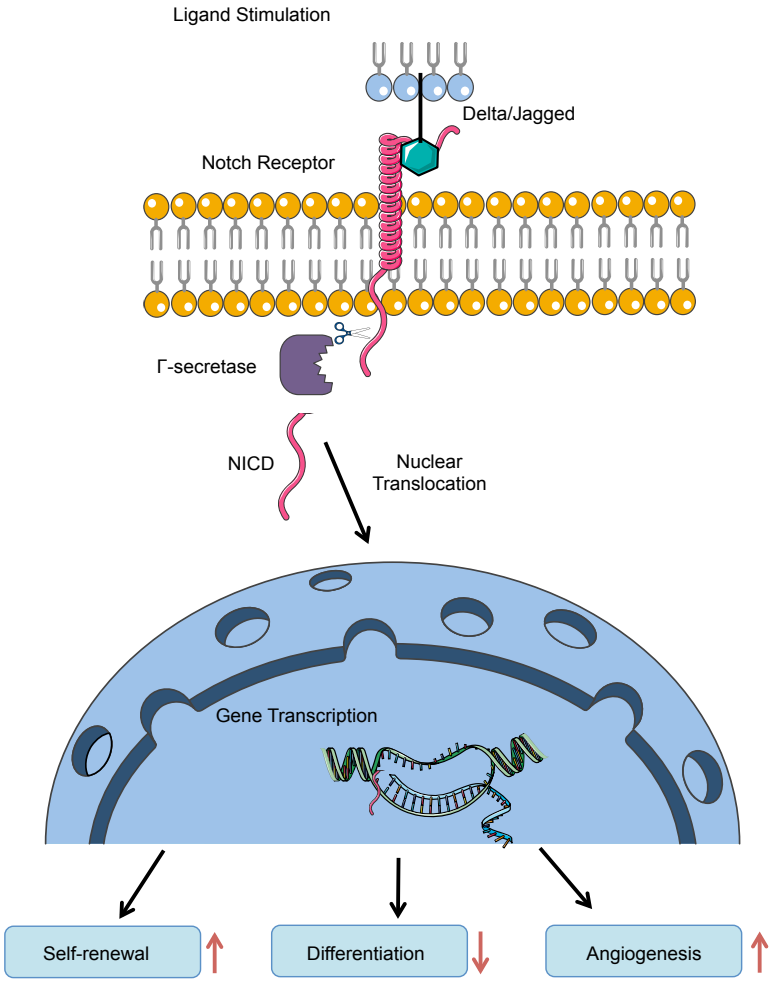

Figure 10: Overview of Notch pathway signaling. Upon binding of the notch ligand, gamma secretase cleaves the intracellular portion (NICD) of the Notch receptor, freeing it to translocate to the nucleus and bind its targets.

Comparatively, ECs secrete Sonic hedgehog (SHH) into the perivascular niche, which can also sustain GSC self-renewal (Clement et al., 2007). Moreover, EC-derived Angiopoietin1, a ligand involved in angiogenic remodeling, activates its tyrosine-kinase receptor Tie2 in GSCs to promote expression of adhesion molecules, N-cadherin and integrin β1, which expedites invasion (Liu et al., 2010).

1.9.2 Cytokines and Growth Factors

The interleukin 6 (IL6) cytokine is highly expressed in GBM and has been linked to poor patient prognosis (Choi et al., 2002; Tchirkov et al., 2007). Work by Jeremy Rich's laboratory demonstrated that GSCs express the IL6 receptor, and targeting either the receptor or ligand reduces cell viability *in vitro* and tumor growth in orthotopic xenografts. IL6 promotes survival in these cells by activating the JAK/STAT3 signaling pathway (Wang et al., 2009). One study suggests that IL6 in the niche is produced, at least in part, by Glioma-associated Mesenchymal Stem Cells, a component of the stroma (Hossain et al., 2015). More recent analysis by the same group established that CD9 stabilizes the IL6 receptor and its co-receptor glycoprotein130 (gp130) to prevent receptor recycling by the lysosome, and maintain STAT3 signaling in GSCs (Shi et al., 2017). Accordingly, blocking STAT3 signaling downstream of IL6 stimulation reduced tumor growth in mice (Shi et al., 2018).

Recent mass spectrometry analysis of the brain endothelial secretome by our laboratory identified the vasoactive peptide, apelin, as critical for GSC maintenance and growth (Harford-Wright et al., 2017). Apelin is expressed in endothelial cells, and has been shown to induce proliferation and vessel sprouting in ECs (Kidoya et al., 2008). Our findings demonstrate that apelin could sustain GSC expansion in the absence of all other mitogens. Also, pharmacological blockade of the apelin receptor drastically reduced tumor growth in preclinical models of GBM and sensitized GSCs to TMZ treatment *in vitro* (Harford-Wright et al., 2017). The importance of apelin in the glioblastoma niche was later confirmed in a study by Ronald Kalin's group where it as found that apelin can effect both vessel formation and tumor cell invasion, and that its blockade enhances anti-angiogenic therapy (Mastrella et al., 2019a). A recent study in hematopoietic stem cells emphasizes the significance of both these aspects of apelin signaling. In mouse models of radiation, EC-derived apelin maintained the hematopoietic stem cells which in turn supported vessel integrity (Chen et al., 2019a).

1.9.3 Extracellular Vesicle Communication

There is now a large body of evidence that GSCs can influence the vasculature through the secretion of small extracellular vesicles (EVs). Small EVs are membrane bound vesicles, which are derived from endosomes, and released by cells for intercellular communication. Small EVs can contain varying molecules including proteins, lipids, and nucleic acids (André-Grégoire and Gavard, 2016). GBM-originating EVs were shown to promote tumor angiogenesis by affecting tubulogenesis and permeability (Giusti et al., 2016; Ricklefs et al., 2016; Treps et al., 2017). In fact, the pivotal findings of Skog et al. first demonstrated that GSC-originated EVs could transfer mRNAs to endothelial cells (Skog et al., 2008). Correspondingly, one study illustrated that GSC-derived EVs delivered microRNA-1 to stromal cells to alter endothelial tube formation and glioma cell invasion (Bronisz et al., 2014). In keeping with this, our group has discovered that semaphorin 3A, a molecule that promotes permeability, released in EVs by GSCs, enhanced vascular permeability in GBM xenografts, and therefore corrupts brain vasculature (Treps et al., 2016). Indeed, our laboratory later clarified that EVs from GSCs also contain pro-angiogenic VEGF-A (Treps et al., 2017). Further, upon treatment with TMZ, there was increased release of GSC-derived EVs, which contained more cell adhesion-related proteins than EVs derived from vehicle treated cells (André-Grégoire et al., 2018). GSC-derived EVs can also affect other cells of the niche, including microglia/macrophages (van der Vos et al., 2016). GSCs are not the only cells of the tumor microenvironment to release exosomes. Recently, it was reported that stromal-derived exosomes enhance tumorigenicity of GSCs in xenografts (Figueroa et al., 2017).

Therefore, reciprocal signaling cues from ECs and GSCs affect tumor cell response to therapies, which highlights the importance of the tumor microenvironment in the development of novel therapies.

1.10 Hypoxia

While GBM are highly vascularized, these tumors also contain hypoxic zones. Hypoxia is defined as the decrease in oxygen availability in cells, and can affect cell proliferation, viability and differentiation (Hamanaka and Chandel, 2009). This

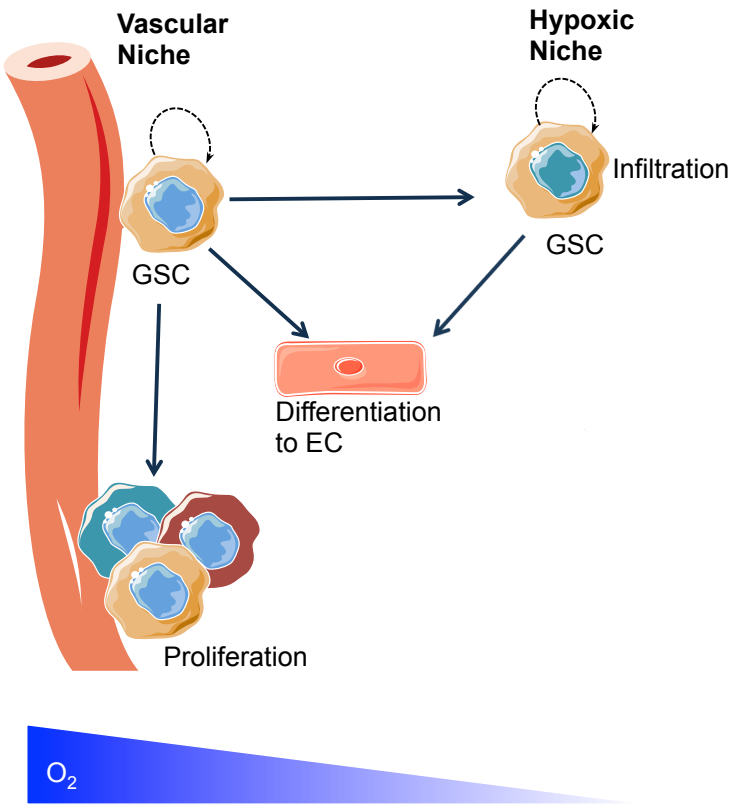

Figure 11: Vascular and hypoxic niche of GSCs. GSCs can reside and self-renew in both vascular and hypoxic niches.

process can be associated with inflammation, ischemia, and most notably cancer. The importance of this concept was highlighted in 2019 with the awarding of the Nobel Prize in physiology or medicine to William Kaelin, Peter Ratcliffe, and Gregg Semenza for their work on how oxygen rate affects cellular functions. Most solid tumors contain hypoxic zones with low oxygen. This is exemplified in GBM, in which the altered vasculature leads to inconsistent oxygen delivery. Local regions of hypoxia can create necrotic zones within the tumor. Cancer cells adapt to these unfavorable conditions by promoting tumor angiogenesis and switching from oxidative respiration to glycolysis to fulfill metabolic requirements. Hypoxia-Inducible Factors, HIF-1 and HIF-2, are transcription factors which have been identified to regulate this process (Nakayama, 2009; Semenza, 2010). HIFs can activate pro-survival genes and counteract apoptosis induction under hypoxia. Under normoxia, HIF-1α subunit is ubiquitinated by von Hippel-Lindau (VHL) and further degraded by the proteasome (Tanimoto et al., 2000). By contrast, HIF-1α is stabilized under low oxygen, and subsequently translocated to the nucleus, where it can complex with the HIF-1β subunit to form an active transcription complex, able to bind target genes (Loor and Schumacker, 2008).

Microscopic analysis of GBM biopsies shows multiple hypoxic zones, due to irregular tumor neo-vascularization (Monteiro et al., 2017). GBM vessels are disorganized and extremely permeable with abnormal endothelial walls partially due

to lack of pericyte coverage (Monteiro et al., 2017; Plate and Mennel, 1995; Yuan et al., 1994). HIF-1α can be upregulated in GBM due to EGFR mutation/amplification and/or PTEN deletion. These mutations are responsible for constitutive activation of PI3K/AKT/mTOR signaling, that in turn increases HIF-1α expression (Clarke et al., 2001; Sansal and Sellers, 2004). Additionally, *TRP53* deletion can augment HIF-1α expression by preventing MDM2-mediated ubiquitination for proteosomal degradation (Ravi et al., 2000).

Hypoxia is a known regulator of the so called “angiogenic switch” in addition to being an orchestrator of stem cell fate (Li et al., 2009). Under low oxygen conditions, embryonic stem cells maintain pluripotent state and block differentiation (Ezashi et al., 2005) (Figure 11). In line with this, in *in vitro* cultures of glioma cells, a higher proportion of cells express stem cell marker, CD133, under hypoxia (Platet et al., 2007). Therefore, hypoxia appears as an essential factor in the cancer stem cell niche (Gilbertson and Rich, 2007). Accordingly, work by the laboratory of Jeremy Rich demonstrates that while all GBM cells up-regulate HIF-1α under hypoxia, GSCs specifically express HIF-2α, which is required for VEGF expression, as well as known HIF-2 target genes like OCT4 and GLUT1. They also show that expression of HIFs in these cells promotes survival and prevents apoptosis (Li et al., 2009).

In order for tumor cells to propagate, they need access to oxygen and nutrients, and they adapt their metabolism to their rapid expansion, thus hypoxia might be deleterious to their growth. GSCs circumvent this by lengthening growth factor signaling to survive under hostile conditions.

1.11 Mechanisms to resist hypoxia and hostile environment

In normal cells, upon ligand stimulation, receptor-ligand complexes are internalized and degraded by the lysosome to prevent saturation of signaling pathways (Mellman, 1996). Mutations in cancer cells have been shown to pervert this pathway either by mutating receptors to no longer require ligand stimulus (such as an EGFRvIII mutation) or to prevent downstream endocytosis. GSCs have adapted to reduce receptor recycling in an unfavorable tumor environment such as hypoxia (Shingu et al., 2016).

Recent findings by Man and colleagues demonstrate that under hypoxic conditions, GSCs maintain Notch signaling by preventing endo-lysosomal degradation of receptors through Vasorin (VASN)-mediated stabilization (Man et al., 2018). Previous findings demonstrated that VASN expression is induced under hypoxic conditions and that it is overexpressed in human GBM (Choksi et al., 2011). VASN is an inhibitor of TGFβ signaling, with a role in angiogenesis, as well as the capacity to block TNF-mediated apoptosis (Choksi et al., 2011; Ikeda et al., 2004). It was lately confirmed to promote tumor angiogenesis in GBM (Liang et al., 2019). In the context of Notch signaling, VASN acts as a competitive inhibitor of Numb, the Notch receptor inhibitor, stabilizing Notch1 at the plasma membrane and preventing recycling. This increases Notch signaling and allows GSC survival under harsh hypoxic conditions (Man et al., 2018).

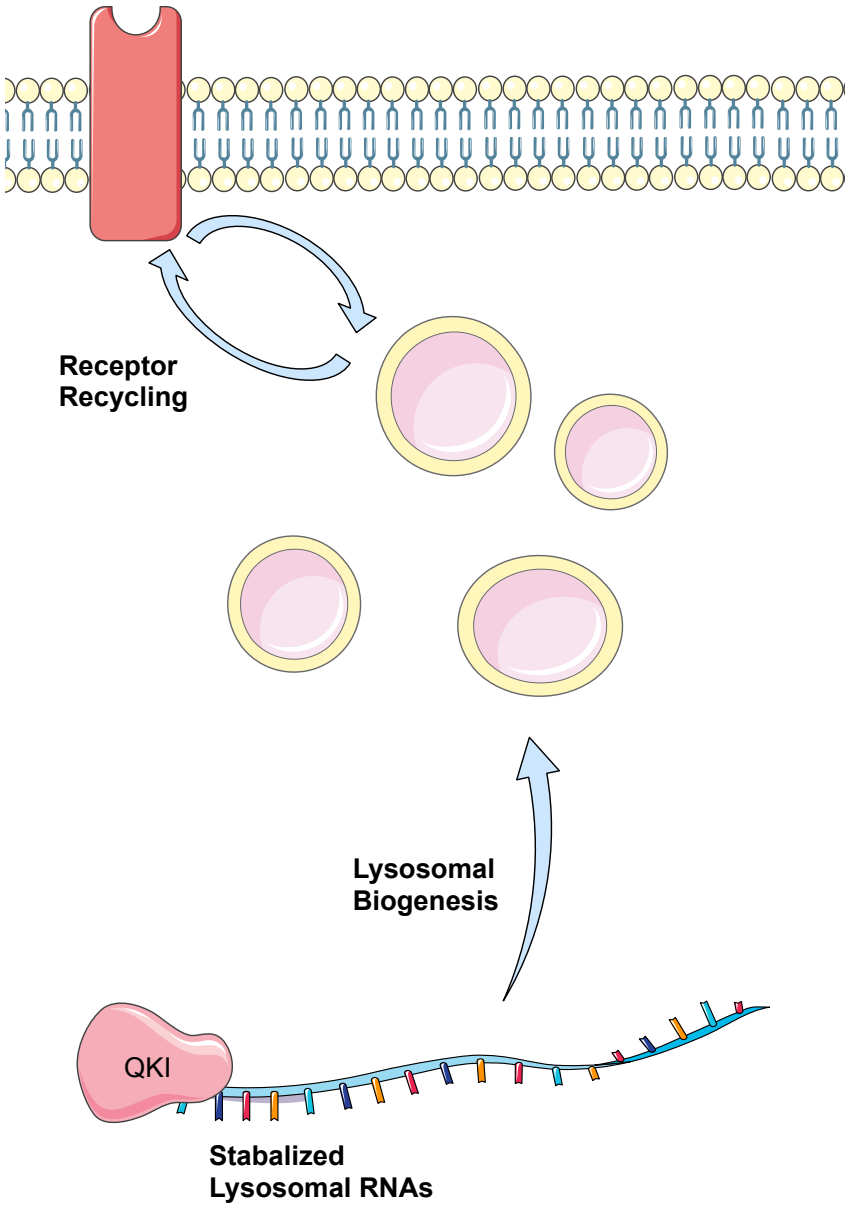

Figure 12: The role of QKI in GSC biology. QKI binds directly to mRNA of lysosomal genes to stabilize them in GSCs. This promotes lysosomal biogenesis and can ultimately affect receptor recycling.

In parallel, Quaking (QKI) is an RNA binding protein critical for oligodendrocyte differentiation and myelin formation as

well as the development of monocytes, endothelial cells, and smooth muscle (Darbelli and Richard, 2016). It regulates RNA homeostasis by influencing stability, splicing, and translation. QKI has also been established as a tumor suppressor in gastric, colon, and prostate cancers (Darbelli and Richard, 2016). In GBM, analysis of the cancer genome atlas, TCGA, showed methylation of the *QKI* locus in 20% of GBM samples (Chen et al., 2012a). Pivotal work by Shingu and colleagues demonstrated that GSCs survive in suboptimal tumor environment by downregulating endo-lysosomes. Deletion of QKI in transformed NSC maintained stemness outside the SVZ in mice. QKI binds directly to lysosomal RNAs in transformed NSCs and acts as a regulator of lysosomal biogenesis. Indeed, when *Qki* was deleted, there were lower levels of endo-lysosomes resulting in reduced receptor recycling. Further, QKI expression was inversely correlated with self-renewal receptor (EGFR, Notch1, Frizzled, SOX2) protein levels. The proposed mechanism of GSC survival in harsh tumor environments was to decreasing endo-lysosomes and thus prolonging receptor signaling (Figure 12)(Shingu et al., 2016). Altering receptor recycling, by limiting endo-lysosomal degradation, is therefore one mechanism by which GSCs survive in the hostile tumor microenvironment. Hence, modifying the endo-lysosomal architecture of GSCs may represent a novel way to target them.

2. Lysosomes

2.1 Discovery and Overview

Christian de Duve was awarded with the Nobel Prize in 1974 for having discovered lysosomes. They were named so as it means “digestive body” in Greek. While performing centrifugal tissue fractionations to study glucose 6-phosphatase in the function of insulin, the group unveiled that acid phosphatase, another liver phosphatase, was inactive in their homogenate in 1955. This phosphatase resides in a sac-like particle separated from the rest of the cell (de Duve, 2005). Subsequently, they uncovered other enzymes residing in the same particles: cathepsin (now cathepsin D), ribonuclease, deoxyribonuclease, and β-glucuronidase (de Duve, 2005; de Duve et al., 1955). The presence of these hydrolases in the same compartment leads to the hypothesis that these particles exerted collective digestive function, which resulted in the naming “lysosome”. The structure of this organelle was confirmed with morphological studies using electron microscopy in 1956, in collaboration with Alex Novikoff (Figure 13)(de Duve, 2005; Novikoff et al., 1956).

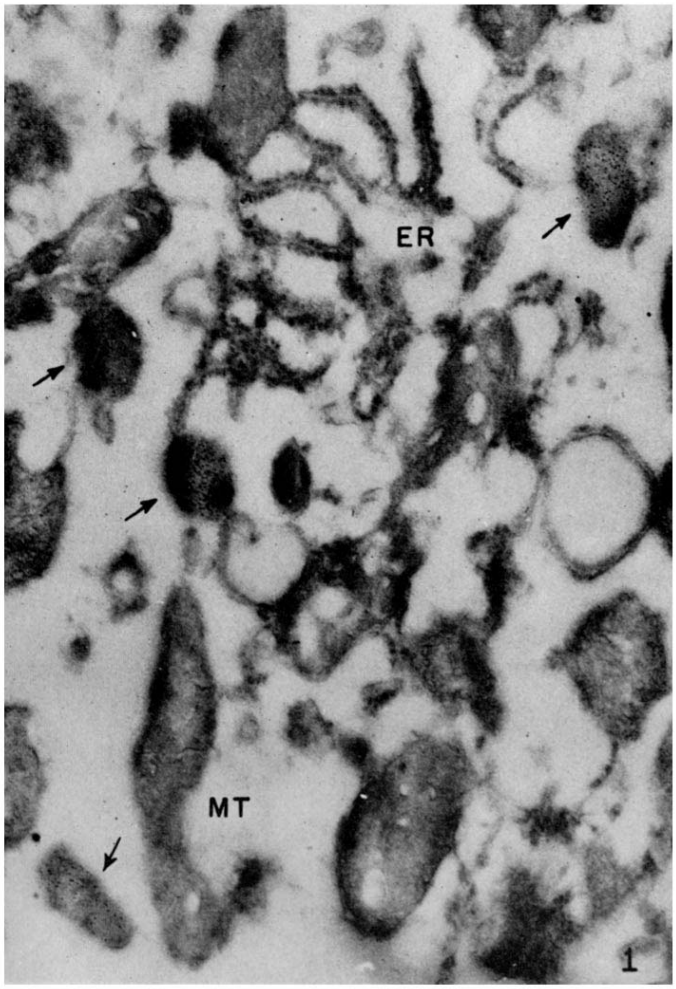

Figure 13: First electron microscopy of lysosomes. Arrows denote dense bodies (lysosomes). From Novikoff et al., 1956.

One of the most notable characteristics of the lysosome is its acidic pH (between 4.5-5.5), established by the vacuolar H+ ATPase (v-ATPase) which sits on the lysosomal membrane and pumps protons across the membrane, in addition to

the counterflux of ions (K+, Na+, and Cl-) (Forgac, 2007; Perera and Zoncu, 2016). This low pH is optimal for the functioning of hydrolases in the degradation of the lysosomal cargos (Perera and Zoncu, 2016). Lysosomes receive their substrates through a variety of trafficking functions including endocytosis, phagocytosis, and autophagy (please see the following sections). Physiological involvement comprises cholesterol homeostasis, plasma membrane repair, pathogen defense, bone and tissue remodeling, cell signaling, and cell death (Saftig and Klumperman, 2009). Therefore, lysosomes are diverse, dynamic organelles with complex functions that are still being uncovered.

2.2 Lysosomal Composition and Biogenesis

The lysosome is composed of an outer membrane comprising a single phospholipid bilayer of approximately 10 nanometers thickness, which contains many transmembrane proteins. In fact, there exist two major classes of proteins, which constitute this compartment: lysosomal membrane proteins and hydrolases.

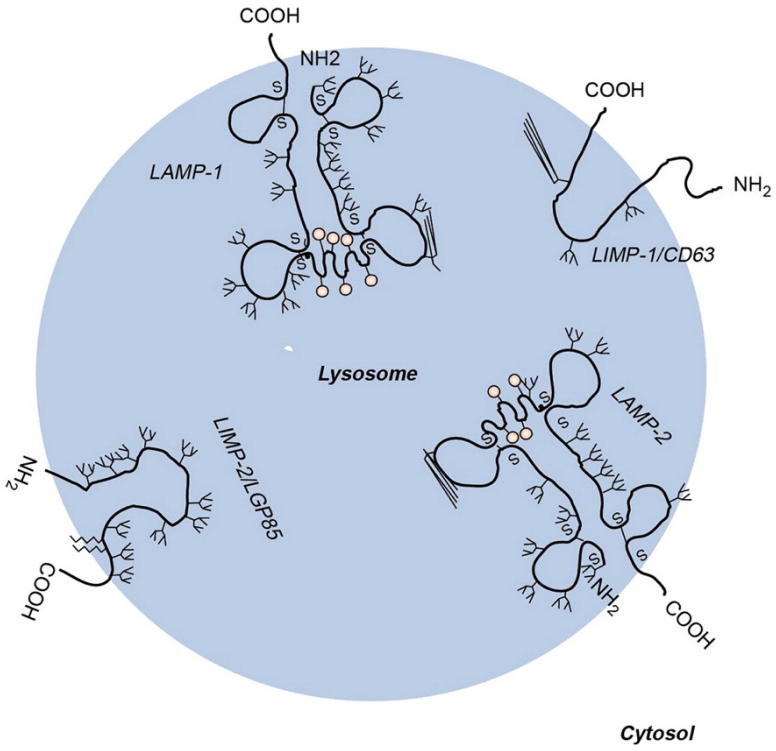

Figure 14: Lysosomal membrane proteins.
From Gonzalez et al 2014

Lysosomal membrane proteins, as the name suggests, reside on the limiting lipid bilayer of the lysosome. They harbor varied functions including: acidification, protein import and export, and membrane fusion (Eskelinen et al., 2003). The most abundant lysosomal membrane proteins are the lysosomal associated membrane proteins LAMP1 and LAMP2, the lysosomal integral membrane protein 2 (LIMP2), and the tetraspanin CD63 (Gonzalez et al., 2014;

Saftig and Klumperman, 2009). These proteins are heavily glycosylated to prevent auto-digestion within the lysosome (Kornfeld and Mellman, 1989; Saftig and Klumperman, 2009). Hydrolases each have a specific set of cargos, which they target for degradation and are the principle proteins responsible for the lysosome's capacity for catabolism. These proteases also process antigens and pro-proteins, degrade the extracellular matrix, and can initiate apoptosis (Conus and Simon, 2008).

Pivotal findings by Andrea Ballabio's group identified a consensus sequence, GTCACGTGAC, in the promoter of many lysosomal genes which became known as the coordinated lysosomal expression and regulation, or CLEAR, element (Sardiello et al., 2009). This constitutes a type of E-box that is recognized by basic helix-loop-helix MiTF/TFE family transcription factors, namely: TFEB, TFE3, MITF, and TFEC. Of these transcription factors, TFE3 and TFEB have both been shown to regulate lysosomal biogenesis. In fact, TFEB is considered a master regulator of lysosomal biogenesis. Overexpression of TFEB provoked the transcription of numerous lysosomal protein encoding genes in HeLa cells (Sardiello et al., 2009). TFEB was also shown to bind to the promoters of genes involved in autophagy, underlining a

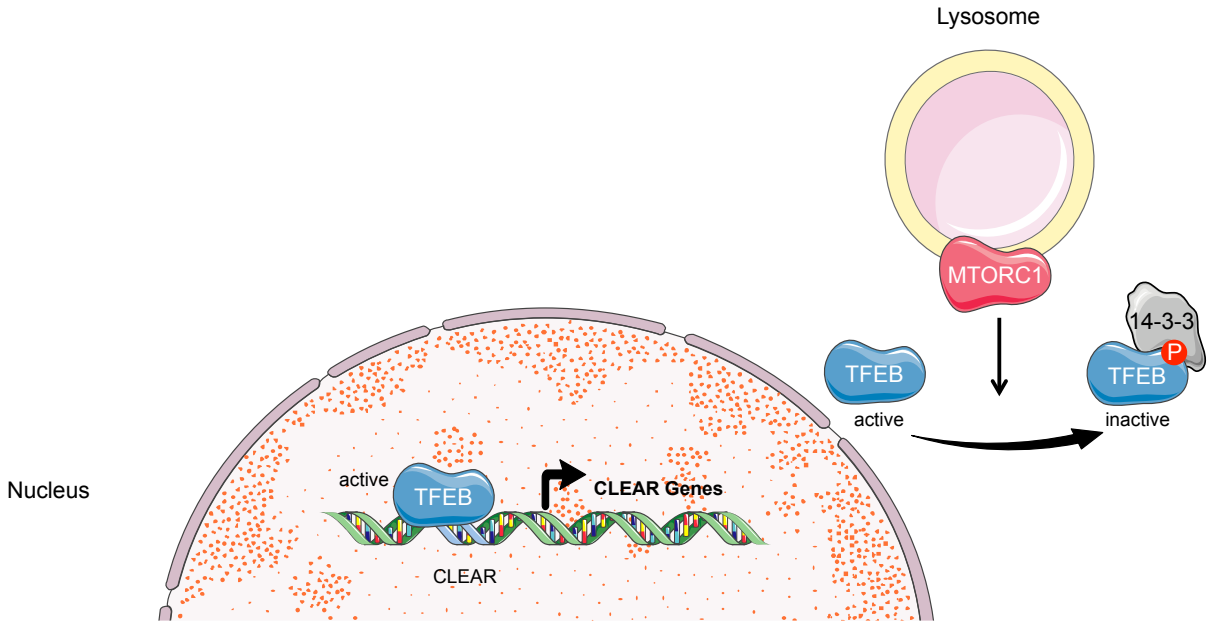

Figure 15: overview of TFEB action. Under nutrient rich conditions, mTORC1 phosphorylates TFEB to promote recruitment of the chaperone 14-3-3. This causes TFEB to remain cytosolic and inactive. Upon nutrient depletion, TFEB translocates to the nucleus to bind targets.

clear co-regulation between lysosome and autophagosome formation (Settembre and Ballabio, 2011). TFEB is regulated via post-translational modification, namely by phosphorylation at serine 142 and 211. When TFEB is phosphorylated at both of these residues, it remains cytosolic and inactive. However, under conditions of lysosomal dysfunction or starvation, TFEB is dephosphorylated and translocates to the nucleus to activate target genes (Napolitano and Ballabio, 2016a). Phosphorylation at serine 211 recruits the chaperone 14-3-3 to dock on TFEB and mask nuclear localization signal, therefore preventing it from nuclear shuttling (Figure 15). Both ERK2 and the mTORC1 complex have been shown to phosphorylate TFEB under nutrient rich conditions (Martina et al., 2012; Roczniak-Ferguson et al., 2012). As mTORC1 has also been implicated in autophagy regulation, its action on TFEB serves as another layer of control on these interconnected processes.

In addition to this established 'canonical' TFEB action, a recent report implicated bromodomain containing protein 4 (BRD4) as a transcriptional repressor of the CLEAR network, acting independently of TFEB (Sakamaki et al., 2017). Likewise, in glioma, the RNA binding protein QKI was shown to interact specifically with lysosomal RNAs regulating their stability, again in a TFEB-independent fashion (Shingu et al., 2016). Therefore, there may be other TFEB-independent processes regulating lysosome biogenesis yet to be uncovered.

2.2.1 Formation of Lysosomes

During lysosomal biogenesis, many newly synthesized lysosomal proteins are trafficked through the trans-golgi network (TGN) to the endosomal system. For hydrolases, this occurs via the mannose-6-phosphate receptor (M6PR) mediated transport system. In the golgi, lysosomal enzyme precursors acquire 6-phosphomannosyl moieties, which act as M6P recognition markers (Reitman and Kornfeld, 1981a, 1981b; Waheed et al., 1981). There are two types of M6PR: cation-independent (300 kDa) or cation-dependent (46 kDa). These two receptors are type I transmembrane glycoproteins, and compose the p-type lectin family. In the TGN, M6PRs bind AP[5] or GGA[6] proteins. This causes clathrin-coated vesicles to form and

[5] Activator Protein 1
[6] Goligi-localized γ-ear-containing ADP ribosylation factor binding proteins

traffic to early endosomes. M6PRs orient with the lysosomal enzyme binding site toward the vesicle lumen, and the C-terminus toward the vesicle exterior (Sahagian and Steer, 1985). Deficiencies in this pathway can lead to the secretion of lysosomal enzymes, altering its function and resulting in lysosomal storage disorders (Ludwig et al., 1995). Lysosomal storage disorders arise from an inability of lysosomes to degrade one or more substrate due to genetic mutations. This results in accumulation of lysosomal substrates and cell death. Symptoms and severity of lysosomal storage disorders depend on the tissues affected and the extent of mutations. In fact, a potential treatment for this kind of malfunctions involves enzyme replacement therapy for M6P derivatives (Gary-Bobo et al., 2007; Solomon and Muro, 2017; Zhu et al., 2004).

Vesicles containing lysosomal hydrolases bud from the TGN and arrive at the endosome. Endosome maturation causes the formation of the late endosome, which has a pH around 6. Lysosomal enzymes bind M6PR at a pH of about 6.5, so acidification of the “pre-lysosomal compartment” leads to their release from M6PRs, which can then recycle back to the golgi. In addition to its localization at the golgi, the cation-independent M6PR is also found at cell surface, allowing it to shuttle extracellular content to the lysosome (Dahms, 1996; Gary-Bobo et al., 2007; Kornfeld, 1992; Munier-Lehmann et al., 1996). Therefore, lysosomal components can be transferred after both *de novo* synthesis and endocytosis via the M6PR sorting pathway.

The vacuolar protein sorting (VPS10) domain containing family of proteins is involved in direct transport of hydrolases to the lysosome. In mammalian cells, these proteins include Sortilin, SorLA, SORC1, SORC2 and SORC3. Sortilin is responsible for direct lysosomal shuttling of acid sphingomyelinase (Ni and Morales, 2006; Petersen et al., 1997). Cathepsin D and Cathepsin H, two other lysosomal hydrolases can co-immunoprecipitate with Sortilin (Canuel et al., 2008). Additionally, electron microscopy analysis reveals that Sortilin colocalizes with cation-independent M6PR in the TGN. Thus, although unrelated to M6PRs, Sortilin likely targets hydrolases to the lysosome by the same clathrin-mediated pathway (Saftig and Klumperman, 2009). Unlike M6PR, Sortilin associates with ligands through binding at its β-propeller domain, and therefore does not require glycosylation (Quistgaard et al., 2009).

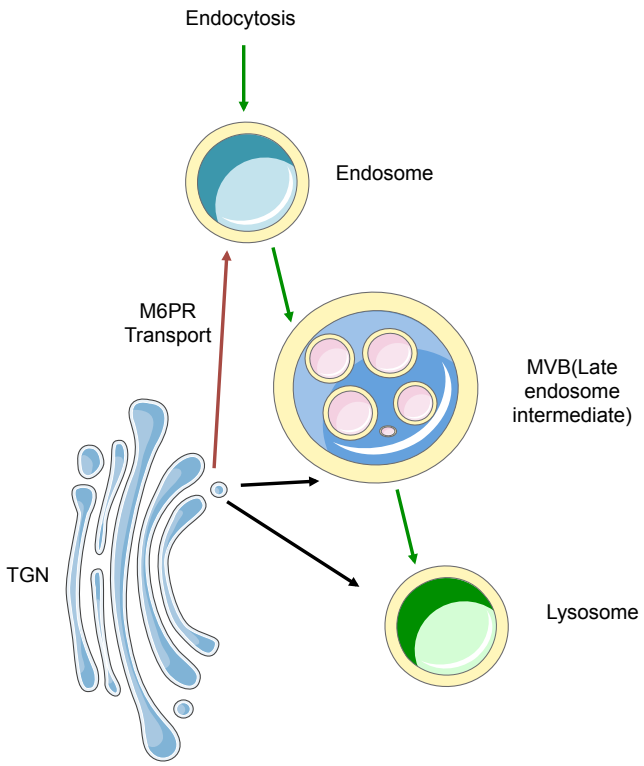

Figure 16: Summary of lysosomal protein transport. After translation, lysosomal proteins are sorted from the golgi either by M6PR dependant translocation to the endosome, or directly to the MVB or lysosome. Lysosomal proteins can also be endocytosed.

β-glucocerebrosidase (βGC) is a lysosomal enzyme that lacks the M6P tag, and therefore is trafficked to the lysosome in a M6PR-independent manner. Mutations in this enzyme produce the most common lysosomal storage disorder, Type I Gaucher disease. So how is it targeted to the lysosome? Strikingly, βGC was found to interact directly with the lysosomal membrane protein LIMP2 (Reczek et al., 2007). LIMP2 is heavily glycosylated, and contains sorting signals at the C-terminus. The binding of these two proteins is dependent of the cellular pH; in the endoplasmic reticulum, βGC and LIMP2 associate, and traffic together to the lysosome. At acidic lysosomal pH, they dissociate and can perform their independent functions. Of note, βGC is no longer sorted to the lysosome in LIMP2 knock-out mice (Gamp et al., 2003). However, deletion of LIMP2 C-terminus does not affect its lysosomal placement (Kuronita et al., 2005). LIMP2-βGC association represents a noteworthy lysosomal targeting method, whereby the transport of lysosomal membrane proteins and hydrolases converge.

Two major routes have been proposed for the transport of lysosomal membrane proteins to their destination. The “direct” pathway refers to passage from the TGN to the early and late endosomes without an intermediate step. By contrast, in the “indirect” pathway, these proteins are first delivered to the plasma membrane

before internalization and sequestering in the early endosome, late endosome, or lysosome. TGN vesicle transport is summarized in figure 16. Work by Juan Bonifacino's group demonstrated that elimination of clathrin or AP complexes caused LAMP proteins to accumulate at the plasma membrane of HeLa cells, suggesting that the "indirect" pathway is likely a major trafficking route for LAMPs to the lysosome (Janvier and Bonifacino, 2005). However, earlier pulse chase studies of LAMP1 in HL-60[7] cells revealed the majority of LAMP1 shuttled via the direct pathway (Carlsson and Fukuda, 1992). Moreover, in CHO[8] cells LAMP1 transport was largely dependent on protein abundance, where LAMP1 was enriched at the plasma membrane alongside increased expression (Harter and Mellman, 1992). Also, particular lysosomal membrane proteins can have sorting motifs for divergent trafficking pathways. Mucolipin 1 (MCOLN1) for example contains two di-leucine type motifs, which promote separate transport events. The N-terminal motif promotes direct TGN to lysosome passage, while the C-terminal signal guides MCOLN1 movement to the plasma membrane where it is thereafter endocytosed (Vergarajauregui and Puertollano, 2006). Hence, the contribution of each pathway may differ between cell type, expression level, and cellular conditions.

Experimental evidence suggests multiple methods of TGN exit for lysosomal membrane proteins. The lysosomal-associated protein transmembrane 5 (LAPTM5), for example, requires GGA3, suggesting a trafficking similar to the M6PR pathway used for hydrolase transport (Pak et al., 2006). Conversely, *in vitro* analysis of vesicles containing LAMP1 and LAMP2 implies that they sort distinctly from the M6PR transport system (Karlsson and Carlsson, 1998). Indeed, knockdown of AP1 in HeLa cells or its depletion in mice did not impede LAMP1 transport to the lysosome (Janvier and Bonifacino, 2005; Meyer et al., 2000). The same was true when clathrin was silenced in HeLa cells (Janvier and Bonifacino, 2005; Meyer et al., 2000).

Together, these data indicate a complex and diverse mechanism by which different proteins reach the lysosome.

[7] Human Leukemia-60 cells
[8] Chinese hamster ovary cells

2.3 Lysosomal Positioning

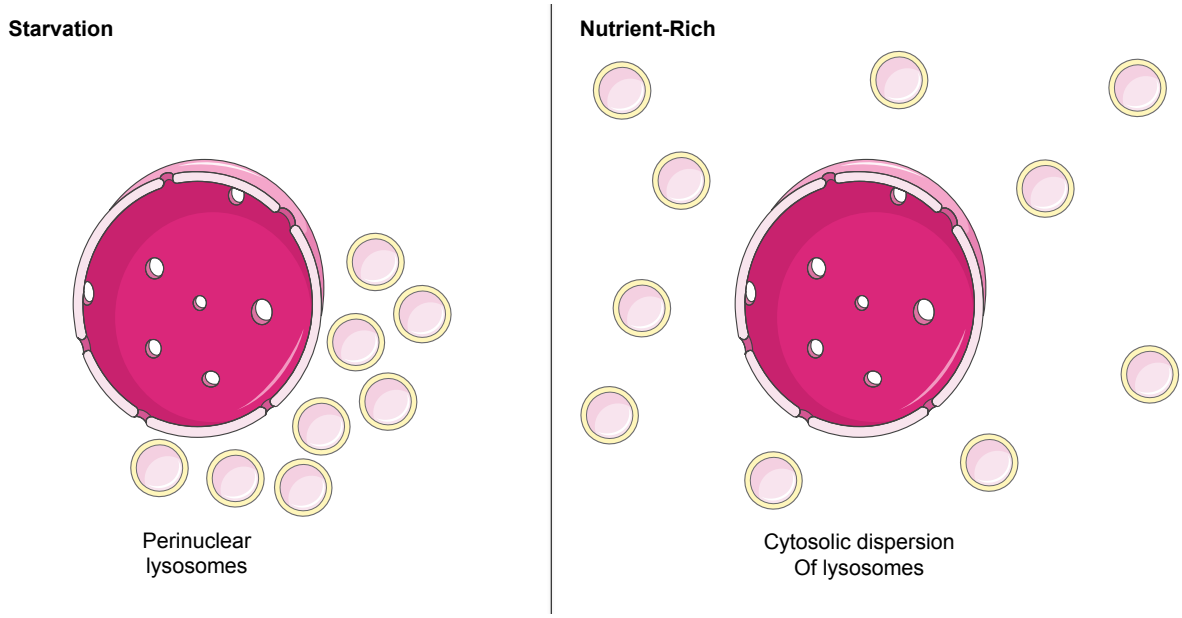

Figure 17: Lysosomal positioning. (Left) Under starvation, lysosomes cluster in a perinuclear fashion. (Right) In nutrient rich conditions, lysosomes can be found dispersed throughout the cytosol.

While it was previously thought that lysosomes were static structures with either perinuclear or uniform cytosolic distribution, recent findings have shown their dynamic, calcium-dependent movement including: exocytosis, fusing with each other and with other organelles (endosome, phagosome, and autophagosome), as well as reformation from hybrid organelles (Lawrence and Zoncu, 2019). This shuttling is dependent on the BLOC-1 related complex (BORC), localized on the lysosomal membrane, which associates with ARL8, a small GTPase, and kinesin-5, to travel along microtubules. Lysosomes traverse microtubules and change direction by switching between plus-end directed kinesin motors and minus-end directed dynein-dynactin motor complexes. Cells lacking BORC do not display lysosomal localization to the cell periphery (Pu et al., 2015). Lysosomal movement is not continuous, rather it appears to stop and start depending on and adaptating to cellular conditions. Acidification of the cytosol disperses perinuclear lysosomes, whereas starvation, aggresome formation or lysosomal storage disorders result in the opposite phenotype (Heuser, 1989; Korolchuk et al., 2011; Li et al., 2016; Zaarur et al., 2014).

Lysosomal positioning is tightly linked with the amino acid sensing response. Interesting findings by Korolchuk et al. showed interdependence between mTOR activation and lysosomal placement. Upon starvation, lysosomes localize in a perinuclear fashion, while nutrient replenishing triggers accumulation of the lysosomes at the cell periphery (Figure 17). Of note, the upstream signaling pathway for mTOR (detailed in chapter 3) is initiated by nutrient receptors at the plasma membrane, so this marginal organization may enhance the activation by bringing its components closer together (Korolchuk et al., 2011). Indeed, upon nutrient deprivation, the Ragulator-LAMTOR complex, involved in mTOR lysosomal localization, inhibits BORC binding. Therefore, lysosomes remain perinuclear, which may favor subsequent autophagy initiation (Filipek et al., 2017).

Furthermore, calcium release from the lysosomal lumen through the MCOLN1 channel improves the association between lysosomes and dynein-dynactin complexes via direct binding of ALG2[9]. This facilitates the perinuclear clustering of lysosomes near the site of autophagosome formation (detailed in section 2.4.3) to enhance autophagy induction. Cholesterol also enables the perinuclear organization of lysosomes, independent of MCOLN1, through RAB7-RILP[10]-ORP1L[11] interaction (Li et al., 2016; Rocha et al., 2009).

Lysosomes tether to target organelles, such as endosomes, via the homotypic fusion and vacuole protein sorting (HOPS) complex, the assembly of which is controlled by the small GTPase Rab7. VAMP7[12] or 8 on the lysosome form contacts with target membranes by binding to syntaxin-7 and 8, and VTI1B[13]. These SNAREs form parallel helix bundles called SNAREpins which bring membranes sufficiently close for fusion to occur (Luzio et al., 2007).

Lysosomes can tubulate by connecting to both kinesins and dynein at once, therefore pulling them in opposite directions. One clear example of this ensues in macrophages treated with LPS[14], these tubular lysosomes are more motile, suggesting that tubulation may play a role in antigen presentation (Li et al., 2016; Mrakovic et al., 2012). Moreover, the movement of lysosomes can create connection

[9] apoptosis-linked gene 2
[10] Rab7-interacting lysosomal protein
[11] oxysterol binding protein related protein 1
[12] vesicle-associated membrane protein
[13] Vps10 tail interactor-1B
[14] lipopolysaccharides

sites with other organelles including ER, TG and peroxisomes. In the TGN, the interaction controls the spatial distribution of the lysosomes (Wang and Hong, 2002). In peroxisomes, these contacts regulate cholesterol transport (Chu et al., 2015). Similarly, ER-lysosome connections have recently been linked to cholesterol sensing and homeostasis (Höglinger et al., 2019; Lim et al., 2019). Furthermore, ER-late endosome contacts also have been implicated in neurite growth and cellular protrusions (Raiborg et al., 2015). Therefore, lysosomal repositioning enables movement in response to specific stimuli and communication with other organelles in order to carry out their varied functions.

2.4 Lysosomal Fusion

Lysosomes act as the terminal delivery site for several degradative processes including endocytosis and autophagy. Moreover, lysosomes can remove unwanted cargos from the cell through exocytosis. These processes involve the fusion of lysosomes with different membranes of the cell including endosomes, the plasma membrane, and autophagosomes.

2.4.1 Endocytosis

Lysosomes act as the endpoint for many molecular cargos that the cell internalizes. During endocytosis, extracellular and membrane components are coopted into vesicles, pass through the endosome, and often are delivered to the lysosome for degradation and recycling. Some cargos, such as transferrin, deliver essential components, eg iron, for lysosomal function (Inpanathan and Botelho, 2019).

Another function of the lysosome is recycling of cell receptors and ligands. For low-density lipoprotein ligands, they dissociate from their receptors in the acidic compartment after endocytosis and are subsequently degraded in the lysosomal lumen by hydrolases. Disengaged receptors can meanwhile be recycled to the cell surface for further signaling. In contrast, EGF remains bound to its cognate receptor as it travels through the late endosome to the lysosome (Kirchhausen et al., 2014). By this method, the lysosome can regulate the length of signaling cascades, upon ligand triggering. Indeed, one mechanism cancer stem cells use to increase the duration of growth factor signaling is to down-regulate their endo-lysosomal

degradation (Man et al., 2018; Shingu et al., 2016). Moreover, endocytosis can remodel the plasma membrane by removing transporters and adhesion molecules in response to stimuli (Ross et al., 2015).

Upon endocytosis, cargos are sorted in the early endosome, a compartment defined by Rab5 and EEA1 expression. Those components marked for degradation are retained in the late endosome. Rab7 and LAMP1 expression, components also present in the lysosome, label late endosomes. These late endosomes then fuse either terminally, or transiently with lysosomes to form endo-lysosomes where they deliver their cargo for degradation (Bissig et al., 2017; Bright et al., 2016).

2.4.2 Lysosomal Exocytosis

Lysosomes can join with the plasma membrane upon increase in cytosolic calcium levels. This process has long been understood to occur in hematopoietic cells, in order to destroy targets through the release of specialized secretory lysosomes (Stinchcombe and Griffiths, 1999). In 2001, a study in fibroblasts revealed that conventional lysosomes can also undergo this shuttling (Reddy et al., 2001). This process is referred to as lysosomal exocytosis, where lysosomes dock at the plasma membrane and release their content into the extracellular space.

As in lysosomal-endosomal merging, SNAREs are essential to this type of fusion. LAMP1 is a major player in the docking step, and is negatively regulated by Neu-1[15] through processing of sialic acids, 9 carbon monosaccharides, in the glycosylated region of LAMP1. Correspondingly, expression of over-sialylated LAMP1 enhances lysosomal exocytosis (Yogalingam et al., 2008). Additionally, TFEB has been implicated in this process, as its overexpression can provoke lysosomal exocytosis *in vitro* and *in vivo* (Spampanato et al., 2013).

Lysosomal exocytosis has emerged as important for the reparation of the plasma membrane and the removal of pathogenic bacteria and viruses from the cell (Huynh et al., 2004; Jaiswal et al., 2002; Reddy et al., 2001; Roy et al., 2004). Moreover, cancer cells can pirate this route to degrade the extracellular matrix and facilitate invasion (Machado et al., 2015).

[15] Neuraminidase-1

2.4.3 Autophagy

Macroautophagy, hereafter referred to as autophagy, is a process for bulk degradation in the cell in response to stress, nutrient or growth factor deprivation, or hypoxia. Upon initiation, autophagy-related proteins, ATGs, are engaged at the phagophore assembly site, PAS, to form a C-shaped structure, or phagophore. This phagophore elongates to engulf the portion of cytosolic material for degradation, eventually sealing into a double membrane vesicle, termed autophagosome. Fully formed autophagosomes travel along microtubules to reach and fuse with the lysosome, allowing for the destruction of cargos (Dikic and Elazar, 2018).

2.4.3i Autophagosome Composition and Induction

There are five complexes of ATGs essential for a functional autophagy pathway. The first is the ULK1[16] complex, or the initiation complex, which consists of ULK1, FIP200[17], ATG13, and ATG101. ULK1 was first identified in HEK293 cells where its knockdown was sufficient to inhibit autophagy. This effect was confirmed in starvation-induced autophagy with ULK1/2 knockout MEFs (Chan et al., 2007; Cheong et al., 2011). Autophagy is ignited thanks to the serine/threonine kinase action of ULK1. Accordingly, autophagic flux is blocked by the expression of the kinase dead version of ULK1 or its chemical inhibition (Chan et al., 2009; Egan et al., 2015; Petherick et al., 2015). Conversely, interaction of ULK1 with ATG13 or FIP200 increases its enzymatic activity (Ganley et al., 2009; Hosokawa et al., 2009; Jung et al., 2009). Additionally, autophosphorylation at threonine 180 in the activation loop of ULK1 may be important for its kinase action (Bach et al., 2011; Lazarus et al., 2015). After stimulation, ULK1 phosphorylates other components within the initiation complex, ATG13 and FIP200 (Hosokawa et al., 2009; Jung et al., 2009). The complex forms puncta under amino acid starvation that colocalize with omegasomes, ie ER structures that support autophagosome biogenesis (Karanasios et al., 2013).

ULK1 complex activity is also regulated by mTOR and AMPK. Upon nutrient detection, mTOR phosphorylates ULK1 at serine 637 and 757 to inactivate it (Ganley et al., 2009; Hosokawa et al., 2009; Jung et al., 2009). mTOR additionally

[16] Unc-51-like Kinase 1
[17] FAK family kinase-interacting protein of 200kDa.

phosphorylates ATG13 to block its translocation to autophagy initiation site (Puente et al., 2016). In contrast, under energy deprivation, there is an increase in cellular adenosine monophosphate, AMP, which activates AMPK[18]. AMPK can inactivate in turn the mTORC1 complex (please see chapter 3 for details), which prevents the inhibitory effects on ULK1. Notably, AMPK can also directly phosphorylate ULK1 at multiple sites to activate it (Egan et al., 2011; Kim et al., 2011).

The second complex contains ATG9 bound phospholipid vesicles. ATG9 is the sole transmembrane ATG; it delivers a lipid membrane source for phagophore formation, and associates with the initiation complex at the PAS (Karanasios et al.,

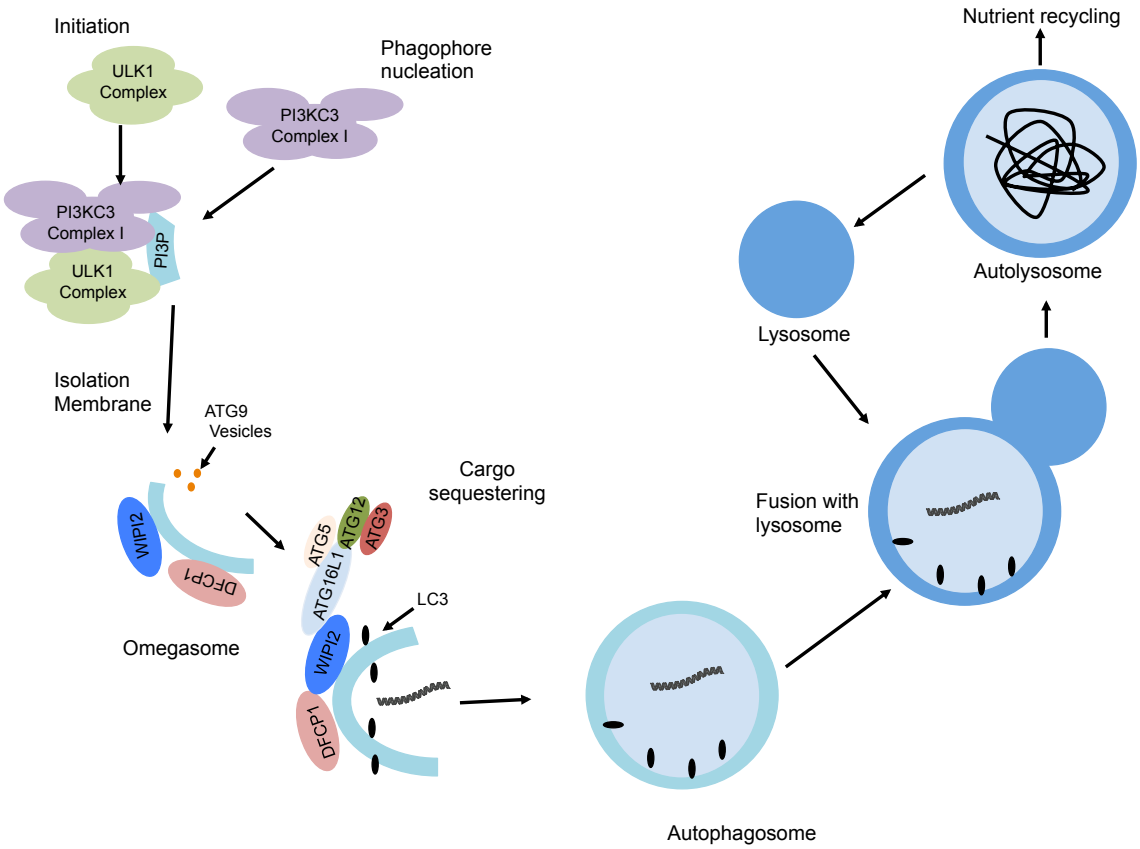

Figure 18: Simplified overview of autophagy. Briefly, upon activation, ULK1 complex and PI3KC3 complex come together with ATG9 vesicles to form the isolation membrane at the PAS. This leads to formation of the phagophore, which matures with association of ATG8s (here LC3). Upon phagophore closure autophagosomes mature and ATGs dissociate from outermembrane. Autophagosomes tether to lysosome for fusion and degradation of internal cargo.

2013; Nishimura et al., 2017). In mammals, ATG9 is not incorporated into

[18] AMP-activated protein kinase

autophagosomes, but transiently associates with omegosome (Orsi et al., 2012). Live cell imaging suggests that autophagosome formation occurs when ATG9 coalesces with the ER (Karanasios et al., 2016). Correspondingly, ATG9 deficient mutants in yeast or mammals fail to form autophagosomes (Orsi et al., 2012; Yamamoto et al., 2012).

The class III PI3K complex, PI3KC3, contains VPS34[19], Beclin1, p115, and ATG14 or UVRAG[20] depending on the context. AMPK can also directly phosphorylate VPS34 and Beclin1 (Kim et al., 2011). The fourth class composes WIPI[21] proteins and ATG2 proteins. Finally, the fifth complex consists of the ubiquitin-like proteins ATG12 and ATG5, which interact with ATG16L and members of the ATG8 protein family. The ATG8 protein family has two subfamilies: light chain 3 (LC3) A, B, and C and γ-aminobutyric acid receptor-associated proteins (GABARAPs), which conjugate with membrane phosphatidylethanolamine (PE) (Dikic and Elazar, 2018).

Phagophore formation occurs at the omegasome, which are enriched in PI3Ps and are marked with PI3P binding protein DFCP[22]. ULK1 and PI3KC3-C1 complexes are activated and recruited to the PAS along with ATG9 vesicles. The mechanism of ULK1 recruitment is still being uncovered. One study found that the positive regulator of autophagy, WAC[23], translocates GABARAP to the centrosome, which can then be transferred to the phagophore. GABARAP could recruit and activate ULK1 (Joachim et al., 2015; McKnight et al., 2012). More is known about PI3KC3-C1. ULK1 phosphorylates ATG14, which interacts with ATG13 under amino acid starvation. This stimulates the kinase activity of PI3KC3 and initiates phagophore formation (Park et al., 2016). ATG9 is regulated in part by ULK1 phosphorylation (Karanasios et al., 2016; Papinski et al., 2014).

2.4.3ii Phagophore Expansion and Maturation

ATG8s are the most important proteins for phagophore expansion. ATG4 processes pro-ATG8s exposing a glycine residue in the C-terminus, which is

[19] Vacuolar protein sorting 34
[20] UV-radiation resistance-associated gene
[21] WD repeat domain phosphoinositide-interacting
[22] Double FYVE-containing protein1
[23] WW-domain containing adaptor with coiled coil

essential for PE conjugation. Processed ATG8s are then activated by ATG7 which is an E1-like enzyme. Consequently, ATG3 fuses ATG8s to PE, converting from the freely diffuse form (for LC3 this is LC3-I) to the lipidated form (LC3-II) (Hamasaki et al., 2013; Slobodkin and Elazar, 2013). For PE attachment to occur, it requires ATG3 to be stimulated by ATG12-ATG5 E3 activity. WIPI2 recruits ATG12-ATG5-ATG16L to the PAS through its interaction with ATG16L (Dooley et al., 2014; Fujioka et al., 2010; Kuma et al., 2002). The lipidation of ATG8s promotes phagophore expansion and can facilitate cargo recruitment in selective autophagy as cargo receptors, like SQSTM1/p62[24], contain an LC3 interacting region (LIR), where ATG8s directly bind (Slobodkin and Elazar, 2013). Of note, recent studies demonstrate that autophagosomes can form without the conjugation machinery or ATG8s (Nguyen et al., 2016; Tsuboyama et al., 2016).

Following the closure of the phagophore, autophagosomes undergo a maturation phase where ATGs dissociate from the outermembrane, and the fusion proteins, syntaxin-17 (STX17), and SNAP29[25], are recruited (Diao et al., 2015; Itakura et al., 2012). ATG8s link autophagosomes to kinesins through the autophagy specific adaptors, including FYCO1[26]. They also drive fusion by recruiting the HOPS complex (McEwan et al., 2015; Olsvik et al., 2015). Interestingly, ATG14 has also been implicated in the maturation of the autophagosome via interaction with STX17 to foster membrane tethering (Itakura et al., 2012).

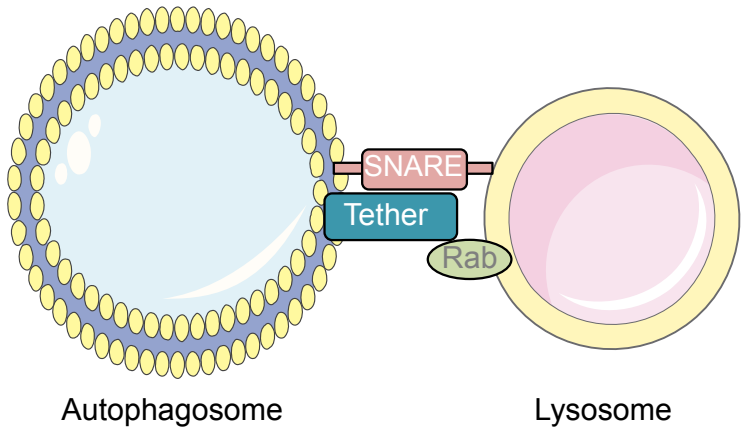

Figure 19: Overview of autophagosome-lysosome fusion. The SNAREpin forms when lysosomal VAMP8 associates with Stx17 and SNAP29 on the autophagosome.

2.4.3iii Lysosomal Fusion

Similar to lysosomal fusion with other organelles, autophagosomes require the formation of the

[24] Sequestosome 1
[25] Synaptosomal-associated protein 29
[26] FYVE and coiled-coil domain-containing protein 1

SNAREpin via VAMP8 on the lysosomal side and SNAP29 and syntaxin-17 (Stx17) on the autophagosome. These SNAREs are translocated from the ER to the autophagosome after formation of the double membrane structure. Knockdown of Stx17 causes accumulation of autophagosomes (Itakura et al., 2012).

ATG14 has a role in tethering and fusion as it was demonstrated to stabilize Stx17 and SNAP29 on autophagosomes (Diao et al., 2015). Likewise, the subfamily of ATG8s, known as GABARAPs, drive fusion of autophagosomes with lysosomes by recruiting PLEKHM1[27], which in turn interacts with the HOPS complex (McEwan et al., 2015; Nguyen et al., 2016). Recently, Fumiyo Ikeda's group identified the inhibitor of apoptosis protein BRUCE[28] as an important factor in autolysosome formation. They found that BRUCE resides on the surface of the lysosome. Upon fusion with the autophagosome, BRUCE interacts with Stx17 and GABARAP/GABARAPL1 to facilitate merging (Ebner et al., 2018).

2.4.3iv Other Autophagy Regulators

Autophagy can also be regulated transcriptionally. In addition to its regulator effects on ATGs, mTOR negatively regulates TFEB, a transcription factor for many autophagy genes. Upon mTOR inhibition, TFEB translocates to the nucleus and promotes the transcription of its target genes (please see also section 2.2). Therefore, TFEB enhances autophagy by inducing the expression of essential components of this metabolic pathway (Settembre et al., 2013). Moreover, TFEB regulates mTOR activity through the expression of RagD (please see chapter 3). Increased RagD facilitates mTORC1 lysosomal localization upon nutrient sensing, hence TFEB action fine tunes mTORC1 signaling (Di Malta et al., 2017). Regulation of autophagy by the transcription factor FOXO3 has been reported in cardiomyocytes (Mammucari et al., 2007; Zhao et al., 2007). Furthermore, Kevin Ryan's group recently demonstrated that BRD4 and methyl-transferase G9A repress CLEAR network transcription, independently of TFEB, therefore regulating autophagy at the transcriptional level (Sakamaki et al., 2017).

Autophagy is further controlled through post-translational modifications of regulators involved in the modification of pathway components. As previously

[27] Pleckstrin homology domain containing protein family member1
[28] Baculovirus IAP repeat repeat-containing ubiquitin-conjugating enzyme

described, mTOR and AMPK modulate autophagy through inhibitory or activating phosphorylation. In addition, BCL-2[29], AKT, and EGFR are all negative regulators of Beclin-1 (Dikic and Elazar, 2018; Pattingre et al., 2005). Also, histone acetyl-transferase p300 acetylates VPS34 to prevent complex formation (Su et al., 2017). In contrast, the PI3KC3 complex1 binds to AMBRA1[30] to promote autophagy through Beclin1 interaction (Fimia et al., 2007). Therefore, the autophagic pathway is tightly regulated by a variety of factors in response to cellular cues, as such, dysfunction of these regulators can lead to defects in autophagic clearance.

2.5 Lysosomal Cell Death

The idea that lysosomes can drive cell death was proposed in the 1970s (Firestone et al., 1979). Indeed, Christian de Duve described lysosomes as "suicide bags," able to rupture cells and tissue upon their lysis. However, it was not extensively explored until recently, potentially due in part to the fact that lysosomal ultrastructure is not always changed during this process (Brunk and Ericsson, 1972). Lysosomal dysfunction includes changes in expression of hydrolases in addition to alterations in their size, number, pH and positioning. Deterioration of these organelles can likewise cause blockade of processes like autophagy, leading to an

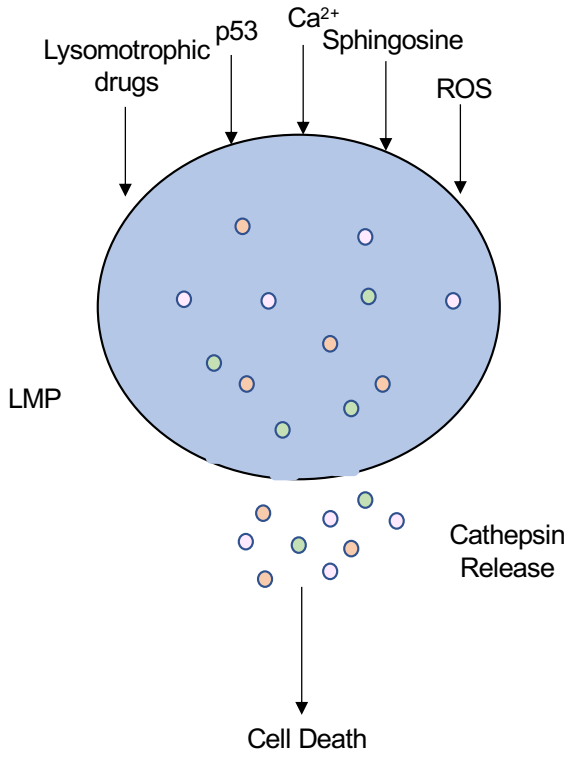

Figure 20: Lysosomal cell death. Different signals can induce lysosomal cell death including lysomotrophic drugs, p53, Ca^{2+}, sphingosine, and ROS. This induces permeabilization of the lysosomal membrane, leading to release of lysosomal cathepsins, and cell death.

[29] B- cell Lymphoma 2
[30] activating molecule in Beclin-1 regulated autophagy protein 1

accumulation of lysosomal substrates (Aits and Jäättelä, 2013).

Lysosomal membrane permeabilization (LMP) is defined as any perturbation in the lysosomal membrane, which leads to lysosomal materials to leak out into the cytosol (Figure 20). This can range from total lysosomal lysis, which lowers the pH of the cytosol and causes cell death by necrosis, to selective cathepsin release, which can induce cell death through signaling cascades. Among cathepsins, the major players in LMP are cathepsins B and D, as well as chromotrypsin B and proteinase 3 (Aits and Jäättelä, 2013; Loison et al., 2014; Zhao et al., 2010). LMP is often accompanied by lysosomal enlargement, however it is unclear whether it is essential for the process to occur. Indeed, Repnik and colleagues suggested that enlargement is not sufficient to trigger membrane dismantlement, while others believe large lysosomes are more prone to breach (Ono et al., 2003; Repnik et al., 2014).

LMP can be induced by a variety of triggers. Lysomotrophic detergents damage the membrane, as they are weak bases, which easily cross the lipid bilayer and can be subsequently trapped to accumulate in the acidic lysosomal lumen. Some known lysomotrophic agents include amines with hydrophobic side chains, such as imidazole and morpholine, cisprofloxacin, sphingosine and siramesine (Boya et al., 2003; Firestone et al., 1979; Kågedal et al., 2001; Ostenfeld et al., 2008). In addition to lysomotrophic drugs, studies have demonstrated that nanoparticles can stimulate LMP, and lead to deleterious accumulation of lysosomes with an autophagic flux defect (Wang et al., 2013, 2018). Moreover, microtubule poisons, like vincristine and paclitaxel, alter lysosomal stability (Castino et al., 2009; Groth-Pedersen et al., 2007).

Reactive oxygen species (ROS) can trigger LMP, as ROS often accumulate in response to certain drugs and ionizing radiation (Kurz et al., 2008a). Oxidative stress causes hydrogen peroxide to diffuse into the lysosome, where it creates hydroxyl radicals by reacting with iron (Kurz et al., 2008b). These radicals can destabilize the lysosomal membrane through lipid peroxidation and damage integral proteins. ROS can also contribute to LMP by activating lysosomal calcium channels (Sumoza-Toledo and Penner, 2011). Accordingly, antioxidants and redox regulators can rescue cells from ROS-induced LMP (Kurz et al., 2008a, 2008b).

Cathepsins mediate the downstream effects of lysosomal cell death, but they can also initiate LMP. Increased cysteine cathepsin activity drives sensitization to LMP in cancer cells (Fehrenbacher et al., 2004, 2008; Groth-Pedersen et al., 2007,

2012; Kreuzaler et al., 2011). Minor lysosomal leakage in these cells could induce LMP through cleavage of cytosolic substrates such as sphingosine kinase 1, which maintains the stability of lysosomes (Mora et al., 2010; Taha et al., 2005). Accordingly, cathepsin inhibitors can partially rescue cells from LCD. Moreover, the calcium activated lysosomal enzymes, calpains, promote LMP by cleaving HSP70 and LAMP2a. HSP70 protects the lysosomal membrane from oxidative stress by recycling damaged proteins (Arnandis et al., 2012; Sahara and Yamashima, 2010).

Alternatively, the integrity of the lysosomal membrane can be altered by changes in sphingolipids. Inactivating mutations of acid sphingomyelinase (ASM) are associated with lysosomal storage disorders, like Niemann-Pick disease. HSP70 supports ASM interaction with its docking lipid BMP[31] (Gabandé-Rodríguez et al., 2014; Kirkegaard et al., 2010). Drugs that target ASM therefore can induce LMP. These range from antidepressants to antihistamines and are collectively known as cationic amphiphilic drugs (CAD). These compounds freely diffuse across the lysosomal membrane and displace ASM from BMP, which leads to the degradation of ASM and an accrual of sphingomyelin (Gulbins and Kolesnick, 2013; Kirkegaard et al., 2010; Petersen et al., 2013).

The most studied CAD is siramesine. The group of Marja Jäättelä demonstrated that this drug is a lysomotrophic detergent, which leads to autophagosome accumulation (Ostenfeld et al., 2008). Moreover, siramesine selectively targets cancer cells and can resensitize these cells to chemotherapy (Groth-Pedersen et al., 2007; Petersen et al., 2013). Likewise, in a study with leukemic cells, siramesine and desipramine, another CAD, preferentially targeted cancer cells compared to B-cells (Dielschneider et al., 2016). In keeping with this, inhibition of HSP70 also disrupts ASM activity and prompts LMP, therefore making it another attractive target in cancer therapy (Granato et al., 2013; Kirkegaard et al., 2010; Nylandsted et al., 2002).

Increased sphingosine in the lysosomal membrane causes LMP. Ceramide is degraded by acid ceramidase to sphingosine, which diffuses out of the lysosome to convert to sphingosine-1 phosphate (S1P) by sphingosine kinase. S1P promotes cell survival, while sphingosine and ceramide encourage cell growth arrest (Shida et al., 2008). Inhibition of sphingosine kinase thus provokes cell death (Mora et al., 2010;

[31] bis monoacylglycerophosphate

Noack et al., 2014; Taha et al., 2005). The sphingosine kinase 2 inhibitor opaganib also shows a potent anti-tumor activity and is being evaluated in clinical trials for liver cancer and multiple myeloma (Britten et al., 2017; Ding et al., 2016; Lewis et al., 2016).

Upon LMP, several endo-lysosomal damage response mechanisms are employed by the cell to escape death. This includes TFEB-induced lysosomal biogenesis, selective autophagy of lysosomes known as lysophagy, repair by the ESCRT[32] machinery, and lysosomal exocytosis. Cells activate the transcription of lysosomal genes via TFEB to compensate for dysfunctional lysosomes (Raben and Puertollano, 2016). Galectins act as lysosomal damage sensors by binding to β-galactosides on damaged lysosomes and recruiting the autophagic machinery for clearance (Chauhan et al., 2016; Hung et al., 2013; Papadopoulos and Meyer, 2017; Thurston et al., 2012). For minor loss of lysosomal membrane integrity, the ESCRT machinery is recruited to the lysosomal membrane to facilitate its healing (Radulovic et al., 2018; Skowyra et al., 2018). Finally, in response to anti-cancer agents, damaged lysosomes may relocate to the plasma membrane and release their cargo into the extracellular space, though this response mechanism is poorly understood (Zhitomirsky and Assaraf, 2017).

Lysosomal dysfunction leads to potent cell death. This can be highly deleterious for patients with lysosomal storage disorders; however, it represents an intriguing axis for anti-cancer therapy.

2.6 Lysosomes and Cancer

Lysosomal recycling is essential for the growth and survival of cancer cells, as these cells require constant nutrient supply and clearance of damaged organelles for their continued propagation. Targeting the lysosome can affect proteostasis and cellular homeostasis on multiple levels, as they play a role in metabolism, protein aggregate clearance, reactive oxygen species and cell death. During oncogenesis, cells exhibit alterations in lysosomal volume and cellular localization (Figure 21). Cancer cells can feature larger lysosomes making them more fragile and susceptible to LMP. In addition, the higher metabolic activity causes iron accumulation in the

[32] endosomal sorting complex required for transport

lysosome, sensitizing them to ROS production. For instance, salinomycin causes iron accumulation in the lysosomes of breast cancer stem cells leading to lysosomal ROS accumulation and cell death (Gyrd-Hansen et al., 2004; Mai et al., 2017; Ono et al., 2003).

Lysosomal hydrolases are involved in tumor growth, invasion, and even angiogenesis. Various studies have demonstrated changes to the trafficking and localization of cathepsins B, D, and L (CTS) (Démoz et al., 1999; Donatien et al., 1996; Joyce and Hanahan, 2004; Nishimura et al., 1998; Rochefort et al., 2000; Sloane et al., 1994). There is a positive correlation between CTSD expression and tumor size, grade and prognosis (Benes et al., 2008; Leto et al., 2004). CTSB expression is also increased in most cancer types, as well as in tumor-associated macrophages (TAM) and cancer-associated fibroblasts (CAF). CTSB is implicated in tumor invasion and can be found on the surface of tumor cells. Accordingly, CTSB deficiency in pancreatic islet tumors and mammary tumors reduced tumor growth (Joyce and Hanahan, 2004; Vasiljeva et al., 2006). In line with this, CTSB inhibitor CA-074 has proven effective at treating preclinical models of breast cancer (Withana et al., 2012). Conversely, increased CTSB activity in lysosomes can cause cleavage of LAMP1 and 2, destabilizing the lysosome and promoting cell death. Therefore CTSB may be a useful biomarker for determining whether or not to use LMP-inducing drugs as a treatment strategy (Fehrenbacher et al., 2008; Ostenfeld et al., 2005).

As demonstrated in the previous section, CADs like siramine and desipramine have potent anti-tumor properties (Dielschneider et al., 2016; Petersen et al., 2013). Additionally, in non-small cell lung cancer, other CADs including loratadine and astemizole were successful (Ellegaard et al., 2016). Likewise, terfenadine induced cell death in prostate cancer cells and astemizole showed efficacy in breast cancer and leukemia cells (Wang et al., 2014). CADs may also be applicable at resensitizing resistant cancer cells to therapy (Ellegaard et al., 2016; Hait et al., 1993; Jaffrézou et al., 1995; Petersen et al., 2013). The usefulness of this class of molecules emphasizes the promise of targeting lysosomes in cancer.

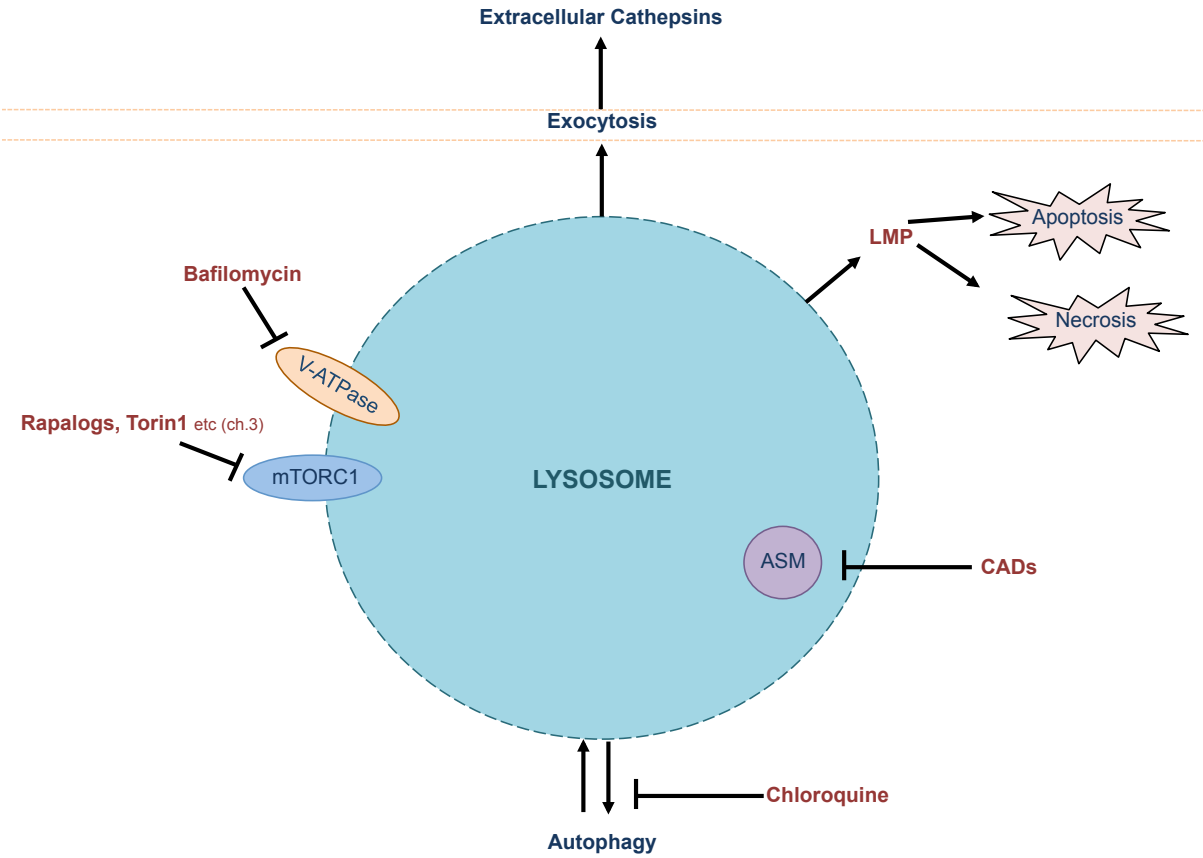

Figure 21: Potential lysosomal vulnerabilities in cancer therapy. These targets include autophagy (via chloroquine), mTORC signaling (via rapalogs and Torin1), lysosomal acidification (via bafilomycin), and LMP induction (which can occur via CAD drugs targeting acid sphingomylenase).

In glioma, several groups have explored induction of lysosomal cell death as a tumor cell elimination strategy. Loss of HSP70 expression eradicated orthotopic xenografts of GBM (Nylandsted et al., 2002). Moreover, Mora et al. showed that in glioma, there is a difference in sphingolipid metabolism, as compared to astrocytes, making them more sensitive to lysosomal cell death upon sphingosine kinase blockade (Mora et al., 2010). Sphingosine kinase inhibitors were additionally shown to be successful in combination with the standard-of-care chemotherapy agent TMZ (Noack et al., 2014). More recently, Le Joncour and colleagues used the lysomotrophic compound clemastine to prompt LMP in *in vitro* and *in vivo* models of GBM. The use of this drug induced cell death *in vitro* and reduced tumor growth *in vivo* emphasizing the potential of targeting the lysosome in GBM (Le Joncour et al., 2019).

As mentioned earlier, mTORC1 docks at the lysosome in order to perform its signaling functions. mTOR signaling is up-regulated in approximately 30% of human

tumors, including GBM (Fine et al., 2009; Saxton and Sabatini, 2017). Therefore, the next chapter explores mTOR activation and its implications in cancer in greater detail.

3. mTOR

3.1 Historical Overview

The mechanistic target of rapamycin, *mTOR*, gene regulates growth and metabolism in a cell, and was identified decades after the drug rapamycin for which it gets its name. Rapamycin was isolated in 1975 from the *Streptomyces hygroscopius* and originally proposed as an anti-fungal agent (Baker et al., 1978; Vézina et al., 1975). Later, this drug was shown to have immunosuppressive and anti-tumor properties. Indeed, clinical trials using rapamycin after organ transplantation demonstrated its potent immunosuppressive functions (Douros and Suffness, 1981; Eng et al., 1984). However, first mechanistic insight into rapamycin's molecular action did not occur until the 1990s with the identification of its complex formation with the immunophilin FKBP12[33], a protein known to interact with the immunosuppressant drug, tacrolimus, and inhibit cell growth and proliferation. These drugs act competitively to associate with FKBP12 and bind their respective target proteins (Dumont et al., 1990; Schreiber, 1991).

Target genes, *TOR1/2,* and *DRR1/2*, of rapamycin were first uncovered in yeast based on their ability to confer resistance to the drug upon their mutation (Cafferkey et al., 1993; Heitman et al., 1991; Kunz et al., 1993). Michael Hall, whose work idenfied TOR genes, received the Lasker prize for this discovery in 2017. The mammalian homologue was identified using screens of FKBP12-rapamycin interactors, and differently named by three groups as rapamycin and FKBP12 target 1 (RAFT1) (Sabatini et al., 1994), FKBP12-rapamycin associated protein (FRAP) (Brown et al., 1994), or rapamycin target 1 (RAPT1) (Chiu et al., 1994). After sequence homology with TOR proteins was confirmed, the gene became known as mTOR (Sabers et al., 1995). In yeast, purification of TOR1 and TOR2 led to the discovery of two separate complexes with distinct functions: TORC1 which is rapamycin sensitive, and TORC2 which is not (Loewith et al., 2002). In Eukaryotes, there is only one *mTOR* gene, however, this gene product partitions in between distinct mTORC1 and mTORC2 complexes (Saxton and Sabatini, 2017).

[33] FK506-binding protein 12

3.2 Complex Composition

mTOR is a protein kinase of the PI3K-related kinase family. It contains several protein-protein interacting domains in the N-terminus including 20 HEAT (**H**untington, **e**longation factor 3, protein phosphatase 2**A**, and **T**OR1) repeats and a FAT (**F**RAP, **A**TM, and **T**RRAP) domain. Each HEAT repeat forms two alpha helices of approximately 40 amino acids. The C-terminus domain comprises the protein kinase domain, with sequence homology to that of PI3K, and a FAT domain at the C-terminus (FATC), which is essential for kinase function (Hay and Sonenberg, 2004; Takahashi et al., 2000). Pivotal findings by David Sabatini's team and Kazuyoshi Yonezawa's group discovered the members of the mTORC1 complex. The mTORC1 consists of three main components: mTOR, RAPTOR (regulatory protein associated with mTOR), and mLST8 (mammalian lethal with Sec13 protein 8) (Hara et al., 2002;

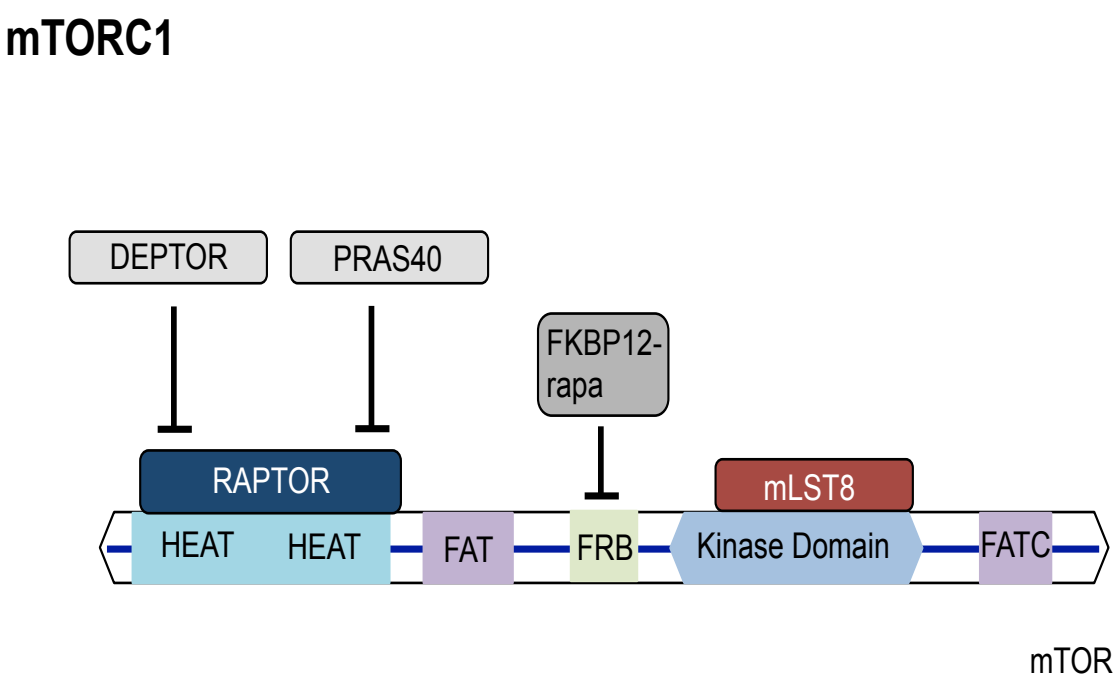

Figure 22: Composition of mTORC1 composed of mTOR, Raptor, and mLST8. Inhibitors include : FKBP12-rapamyycin complex, PRAS40, and DEPTOR
HEAT= Huntington, elongation factor 3, protein phosphatase 2A, and TOR1, FAT= FRAP, ATM, and TRRAP.

Kim et al., 2002, 2003). RAPTOR was simultaneously detected by both groups using crosslinking autoradiography or high salt immunoprecipitation followed by mass spectrometry analysis (Hara et al., 2002; Kim et al., 2002). RAPTOR is responsible for the recruitment of mTOR substrates. It does so by binding a TOR signaling motif, TOS, on mTOR substrates (Nojima et al., 2003; Schalm et al., 2003). RAPTOR also

participates in the subcellular localization of the mTORC1 complex. By deploying mass spectrometry in HEK293T cells, Sabatini's group then identified mLST8 using the mTOR/RAPTOR immunocomplex as a bait (Kim et al., 2003). mLST8 binds at the kinase activation loop and is believed to play a role in its stabilization. However its presence is not essential for a functional mTORC1 complex (Guertin et al., 2006; Yang et al., 2013). In addition to the core components, the mTORC1 complex has two negative regulators PRAS40 (proline-rich AKT substrate of 40 kDa) (Sancak et al., 2007; Vander Haar et al., 2007; Wang et al., 2007) and DEPTOR (DEP domain containing mTOR interacting protein) (Peterson et al., 2009). Cryo-electron microscopy reveals that RAPTOR binds at the heat repeats. Crystal structure of mTOR bound to mLST8 has also uncovered that FKBP12-rapamycin associates with the FRB domain of mTOR to block substrates from the active site (Saxton and Sabatini, 2017) (Figure 22).

mTORC2 similarly contains mTOR and mLST8, but the third component, RICTOR (rapamycin insensitive companion of mTOR) replaces RAPTOR with analogous functions. Inhibitory subunits of mTORC2 include DEPTOR, mSin1 and PROTOR1/2 (Frias et al., 2006; Jacinto et al., 2006; Pearce et al., 2007; Yang et al., 2006) (Figure 23). While FKBP12-rapamycin does not directly bind this complex, mTORC2 signaling is diminished by extended rapamycin treatment, likely due to a lack of free mTOR to incorporate into complexes (Sarbassov et al., 2006).

mTORC2

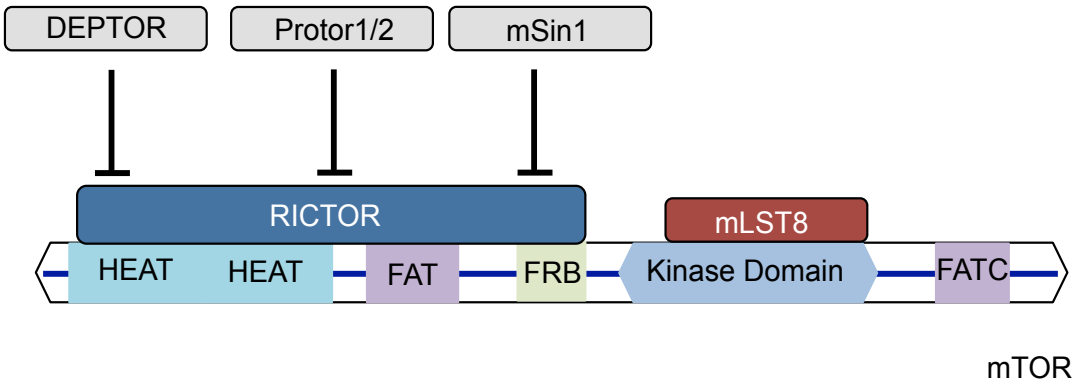

Figure 23: Composition of mTORC2 composed of mTOR, RICTOR, and mLST8. Inhibitors include : mSin1, Proctor1/2, and DEPTOR
HEAT= Huntington, elongation factor 3, protein phosphatase 2A, and TOR1, FAT= FRAP, ATM, and TRRAP.

3.3 Upstream Activation

3.3.1 Growth Factors

Various growth factors and mitogens activate the mTORC1 complex (Figure 24). Interestingly, these diverse pathways converge by inhibiting the negative regulator of mTORC1 tuberous sclerosis complex, TSC. This complex includes TSC1, TSC2, and TBC1D7 to form a hetero-trimer. It acts as a GAP[34] for the small GTPase Rheb[35], which directly associates with mTORC1, and is necessary for mTORC1 activation (Garami et al., 2003; Inoki et al., 2003a; Tee et al., 2003). Upon AKT activation, the TSC is disabled, and Rheb, anchored to the lysosomal membrane, becomes loaded with GTP and able to recruit mTORC1 to the lysosomal surface (Long et al., 2005; Sancak et al., 2007, 2008).

The implicated growth factor pathways include the insulin growth factor

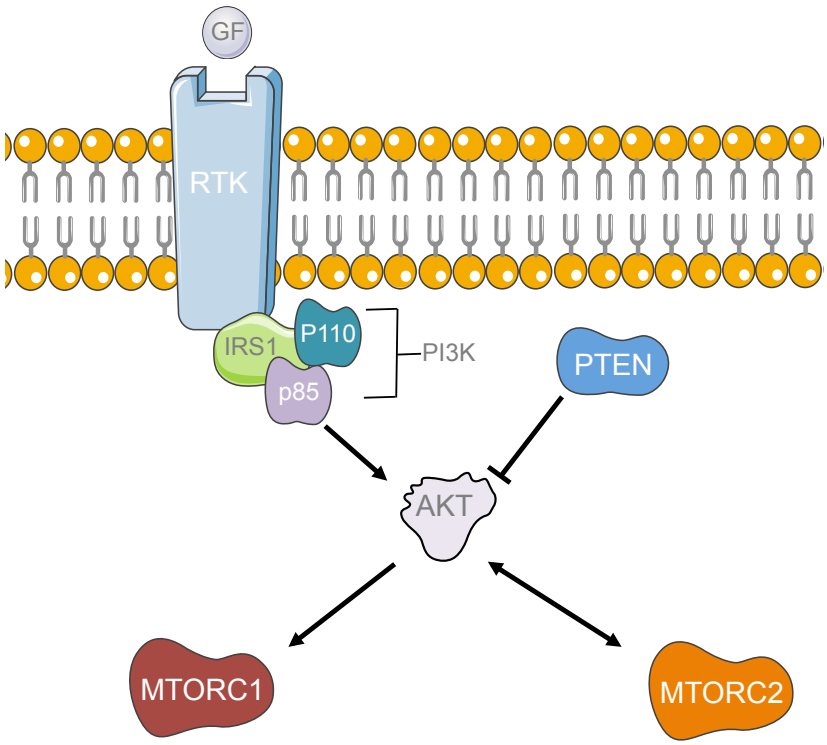

Figure 24: Schematic of growth factor (GF) receptor tyrosine kinase (RTK) signaling. Upon growth factor sensing, PI3K action is incited by RTKs. In turn it stimulates AKT, which will trigger both the mTORC1 and 2 complexes. mTORC2 then further phosphorylates AKT to fully activate it.

[34] GAPs inactivate GTPases by stimulating GTP hydrolysis
[35] Ras homolog enriched in brain

receptor 1 (IGF-1R), which triggers PI3K, eventually resulting in AKT restricting TSC2 (Figure 24)(Inoki et al., 2002; Manning et al., 2002). Once inhibited, the TSC dissociates from the lysosome membrane, liberating Rheb (Menon et al., 2014). Likewise, Ras signaling, downstream of receptor tyrosine kinases, can redundantly initiate mTORC1 via ERK (Ma et al., 2005b; Roux et al., 2004). Other pathways able to trigger downstream mTOR include, but are not limited to: EGF, VEGF, BDNF[36], Wnt pathway, and TNFα. Both Wnt and TNFα pathways inhibit TSC1 to stimulate mTORC1 (Inoki et al., 2006; Lee et al., 2007; Saxton and Sabatini, 2017; Takei et al., 2004). Thus, growth factors and mitogens act as the inciting signal of the mTORC1 cascade.

3.3.2 Environmental Stress

Environmental stress is incompatible with growth functions of mTOR; therefore, there are a variety of mechanisms to shut down signaling under these conditions.

Upon cellular starvation, when glucose becomes scarce, the stress response regulator AMP-activated protein kinase (AMPK) can oppose mTOR signaling at two levels. Not only does its kinase function activate TSC2, but it also inhibitorily phosphorylates RAPTOR (Gwinn et al., 2008; Inoki et al., 2003b; Shaw et al., 2004). Markedly, cells that lack AMPK can still inactivate mTORC1 through a Rag GTPase dependent mechanism, signifying that the glucose sensing function of mTOR has not fully been elucidated (Kalender et al., 2010).

Hypoxia, as discussed in chapter 1, refers to a state of low oxygen availability. Like under glucose deprivation, the stress of hypoxia drives AMPK, which inactivates mTOR. In addition, regulated in DNA damage and development 1 (REDD1), a protein induced in response to stresses like hypoxia and DNA damage, can also hinder mTORC1 via activation of the TSC (Brugarolas et al., 2004). In addition, in response to DNA damage stimuli, mTORC1 activity may be blocked via several p53 target genes, including the regulatory subunit of AMPK (*AMPKβ*), *PTEN*, and *TSC2* (Feng et al., 2007). Moreover, it has been reported that mTORC1 is sequestered in stress granules, cytosolic aggregates of proteins and RNA, through interaction with

[36] brain-derived neurotrophic factor

DYRK3[37] under unfavorable cellular conditions (Wippich et al., 2013). Thedieck et al. then illustrated that the protein Astrin interacts specifically with RAPTOR under oxidative stress to recruit mTORC1 to the stress granules (Thedieck et al., 2013). Together, these findings highlight the impact of cellular stress on mTORC1.

3.3.3 Amino Acid Sensing

mTORC1 activation on a global level can occur in response to feeding. Not only due to increased glucose availability, but also due to digestion of dietary proteins, which liberate amino acids for protein synthesis and metabolism. Simultaneous discoveries in *Drosophila* by the Guan laboratory (Kim et al., 2008) and mammalian cells by Sabatini's group (Sancak et al., 2008) placed Rag GTPases as members of the mTORC1 cascade. Four Rags (A, B, C, D) form heterodimers of Rag A or B with Rag C or D, and cluster at the membrane of the lysosome via binding to the Ragulator complex. This Ragulator complex, again discovered by Sabatini's laboratory, is composed of LAMTOR proteins 1-5 (also known as MP1, p14, p18, HPXIP, and C7ORF59), and acts as a guanine exchange factor (GEF) for the Rag GTPases (Bar-Peled et al., 2012; Sancak et al., 2010). The Ragulator binds Rag A or B more strongly in the absence of amino acids, preventing GDP-GTP exchange. Amino acid signaling serves to weaken this interaction and thus, increases GTP-Rag A/B loading.

At the same time, the Sabatini group also implicated the lysosomal v-ATPase in mTORC1-amino acid pathway. The v-ATPase senses amino acid accumulation in the lysosomal lumen and transmits this to the Ragulator via an "inside-out" signaling method. Accordingly, blockade of the v-ATPase induces the Ragulator to bind RagA/B more strongly, regardless of available amino acids (Bar-Peled et al., 2012; Zoncu et al., 2011). Therefore, the v-ATPase communicates the amino acid stimulus to the Ragulator. This promotes GTP loading on Rag A or B, which links directly to RAPTOR and docks mTORC1 at the lysosomal surface, where it also associates with Rheb (Figure 24). The localization of Rheb at the lysosomal membrane converges amino acid sensing with growth factor stimulus, as mTORC1 is only "on" when both Rags and Rheb are active.

[37] dual specificity tyrosine- phosphorylation-regulated kinase 3

How exactly does mTORC1 detect amino acids? This occurs through two methods, via intra-lysosomal detection, and upstream due to cytosolic complexes.

1- In terms of lysosomal sensing, following the discovery of v-ATPase's role, the amino acid transporter, SLC38A9 was shown to interact with the v-ATPase-Ragulator complex (Jung et al., 2015; Rebsamen et al., 2015; Wang et al., 2015). Wang et al. illustrated that SLC38A9 is required for arginine-specific mTORC1 signaling, as knock-out of SLC38A9 blunted arginine but not leucine dependent activation of the complex (Wang et al., 2015). More recently, a role of SLC38A9 in

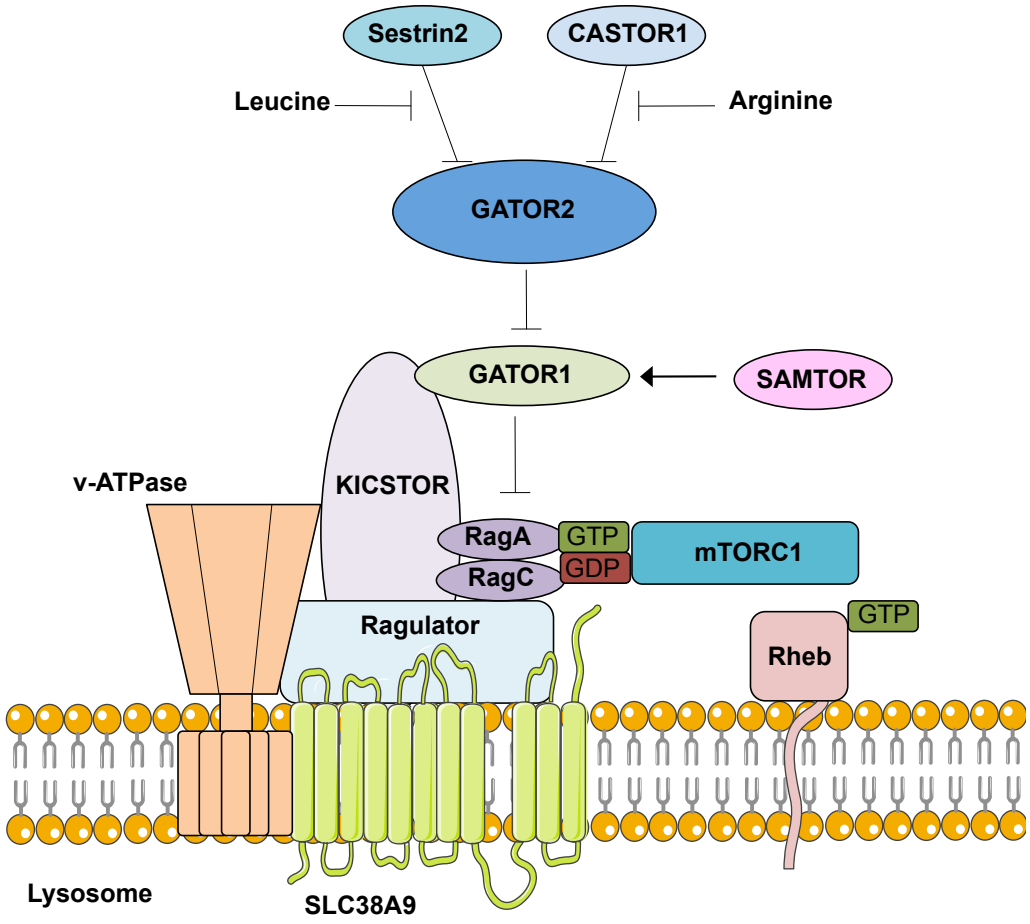

Figure 25: mTORC1 lysosomal docking and amino acid sensing. mTORC1 docks at the lysosome via association with Rags (here shown RagA and RagC), which bind the regulator. For this to occur, Rheb must be in an active (GTP) bound state. GATOR 1/2 complexes sense amino acid levels to fine tune this action.

the outpouring of amino acids from the lysosome to facilitate mTORC1 activation was described (detailed below) (Wyant et al., 2017). Consequently, Kevin Ryan's

group uncovered that DRAM-1[38], a protein previously implicated in autophagy, recruits other amino acid transporters SLC1A5 and SLC7A5 to the lysosomal membrane to invoke a similar amino acid efflux (Beaumatin et al., 2019). In terms of amino acid influx at the lysosome, SLC7A5 is recruited to the lysosome by LAPTM4b[39]. The influx of amino acids via SLC7A5 stimulates mTORC1 through the poorly defined v-ATPase-dependent mechanism (Milkereit et al., 2015). It is important to note that most research regarding amino acid sensing has been done *in vitro* with the withdrawal and refeeding of a mixture of amino acids. Hence, the full list of strategies by which mTORC1 recognizes intra-lysosomal amino acids remains to be elucidated.

2- Cytosolic amino acid recognition occurs via the GATOR1 (DEPDC5, Nprl2, and Nprl3) and GATOR2 (Mios, WDR24, WDR59, Seh1L and Sec13) complexes. GATOR1 acts a GAP for Rag A or B, to inhibit the mTORC1 cascade (Bar-Peled et al., 2013). GATOR1 is recruited to the lysosome by another complex, KICSTOR (Kaptin, ITFG2, C12orf66, and SZT2), upstream of Rags in the activation process. KICSTOR functions as a scaffold to modulate the amino acid sensing response (Peng et al., 2017; Wolfson et al., 2017). Conversely, GATOR2 positively regulates mTORC1 by interacting with GATOR1 at the lysosomal membrane, checking its GAP action through an unknown mechanism (Bar-Peled et al., 2013). Sestrin2, a leucine sensor, associates with GATOR2 in the absence of amino acids. It disperses upon leucine binding, freeing GATOR2 to act (Chantranupong et al., 2014; Parmigiani et al., 2014; Wolfson et al., 2016). Intriguingly, Sestrin2 transcription is up-regulated upon prolonged amino acid starvation (Ye et al., 2015), indicating that it functions in both the acute and prolonged perception of amino acids. Similarly, arginine sensor CASTOR1[40], abolishes GATOR2 activity when amino acids are scarce, and dissociates upon arginine detection (Chantranupong et al., 2016; Saxton et al., 2016). Recently, another negative regulator of mTORC1, SAMTOR[41] (or C7orf60), was uncovered. Unlike CASTOR1 and Sestrin2, which regulate GATOR2, SAMTOR interacts with GATOR1 and KICSTOR in the absence of methionine. Upon, s-adenosylmethionine binding, SAMTOR dissociates. The exact mechanism

[38] DNA damage regulated autophagy modulator 1
[39] Lysosomal protein transmembrane 4 beta
[40] cellular arginine sensor for mTORC1
[41] S-adenosylmethionine sensor upstream of mTORC1

by which SAMTOR enhances GATOR1 function remains to be uncovered (Gu et al., 2017). These mechanisms of amino acid sensing are summarized in Figure 25.

Several other means of activating mTORC1 via amino acids have been reported. The Folliculin-FNIP2 complex acts as a GAP for Rag C or D in response to amino acids, thus driving mTORC1 (Petit et al., 2013; Tsun et al., 2013). Glutamine can also stimulate mTORC1 independent of Rags through Arf GTPases (Jewell et al., 2015). Therefore, the full extent of mTORC1 sensing amino acids remains to be seen.

3.3.4 mTORC2 Activation

mTORC2 is largely initiated by insulin-PI3K signaling (Figure 24). mSin1 contains a domain which obstructs the mTOR catalytic function in the absence of insulin. Upon insulin stimulation, PI3K downstream signaling alleviates inhibition of mSin1, to allow activation of the complex. AKT can also phosphorylate mSin1, implying a positive feedback mechanism where AKT fosters the mTORC2 cascade, which in turn phosphorylates and fully activates AKT (Liu et al., 2015b; Yang et al., 2015). Unlike mTORC1, which docks at the lysosome, mTORC2 localizes in distinct cellular compartments. These include the plasma membrane, the mitochondria, and a portion of endosomal vesicles (Ebner et al., 2017). Further, mTORC2 undergoes a negative feedback loop with mTORC1. Insulin activates mTORC1/2; mTORC1 then phosphorylates GRB10, a negative regulator of IGF-1 signaling (Hsu et al., 2011; Yu et al., 2011). mTORC1 and S6K can also directly inhibitorily phosphorylate the IRS proteins at multiple sites. This prevents downstream, PI3K/AKT signaling and therefore inhibits mTORC2 activation (Harrington et al., 2004; Tanti and Jager, 2009; Tremblay and Marette, 2001).

3.4 Downstream Signaling

mTOR signaling regulates a variety of downstream actions, including protein synthesis and turnover, metabolism, proliferation, and cell survival, detailed as followed.

3.4.1 Protein Synthesis

Once activated, mTORC1 stimulates protein synthesis through the phosphorylation of two downstream effectors, p70S6 kinase 1 (S6K1) and 4EBP, the eIF4E binding protein.

mTOR phosphorylates S6K1 at threonine 389. This activates the kinase and allows it to in turn stimulate PDK1. It also drives substrates that promote mRNA translation such as eIF4B, which is a regulator of the 5'cap binding eIF4F complex (Holz et al., 2005). Furthermore, S6K1 phosphorylates PDCD4[42], an inhibitor of eIF4B, to promote its degradation (Dorrello et al., 2006).

4EBP acts independently of S6K1. It is an inhibitor of translation, which segregates eIF4E from assembling the eIF4F translation complex. When active, mTORC1 phosphorylates to disable 4EBP1 on multiple sites, causing it to dissociate from eIF4E, and initiating 5' cap–dependent mRNA translation (Brunn et al., 1997; Gingras et al., 1998). mTOR inhibition quashes general mRNA translation. However, work by Thoreen and colleagues showed it more severely suppresses mRNAs containing 5' TOP[43] motifs (Thoreen et al., 2012). Recent studies have also implicated the protein LARP1[44] in this process. LARP1 binds directly to the 5' cap of TOP mRNAs and represses their transcription, preventing the recruitment of eIF4F, in an mTOR-dependent manner (Fonseca et al., 2015; Lahr et al., 2017; Philippe et al., 2018). Thus, mTOR inhibition represses translation from multiple axes (figure 26).

3.4.2 Lipid and Glucose Metabolism

In order for cells to grow, they require enough lipids to form and expand their membranes. The mTORC1 complex affects *de novo* lipid synthesis via SREBPs (sterol responsive element binding protein). SREBPs are transcription factors, which regulate the expression of genes involved in the biogenesis of fatty acids and cholesterol (Porstmann et al., 2008). mTORC1 affects SREBP through S6K1-

[42] Programmed cell death protein 4
[43] terminal oligopyrimidine
[44] La-related protein 1

dependent activation and through inactivation of Lipin1, an SREBP inhibitor (Düvel et al., 2010; Peterson et al., 2011). Likewise, mTORC1 has been implicated in nucleic acid synthesis. S6K1 triggers carbamoyl-phosphate synthetase phosphorylation. carbamoyl-phosphate synthetase is an important component of *de novo* pyrimidine synthesis (Ben-Sahra et al., 2013).

Further, mTORC1 plays an essential role in glucose metabolism, by enabling a switch from oxidative phosphorylation to glycolysis. It does so by increasing the expression of HIF1-α, which in turn promotes the expression of glycolytic enzymes including phospho-fructo kinase, PFK. SREBP similarly augments the activity of the oxidative pentose phosphate pathway, to generate NADPH and other metabolites (Düvel et al., 2010).

3.4.3 Protein Turnover

Moreover, mTORC1 can control cell growth by suppressing the catabolism of proteins, particularly via the suppression of autophagy. The ULK1 kinase is activated, early in the initiation of autophagy, to drive autophagosome formation (detailed in chapter 2). Under nutrient rich conditions, mTORC1 facilitates inhibitory

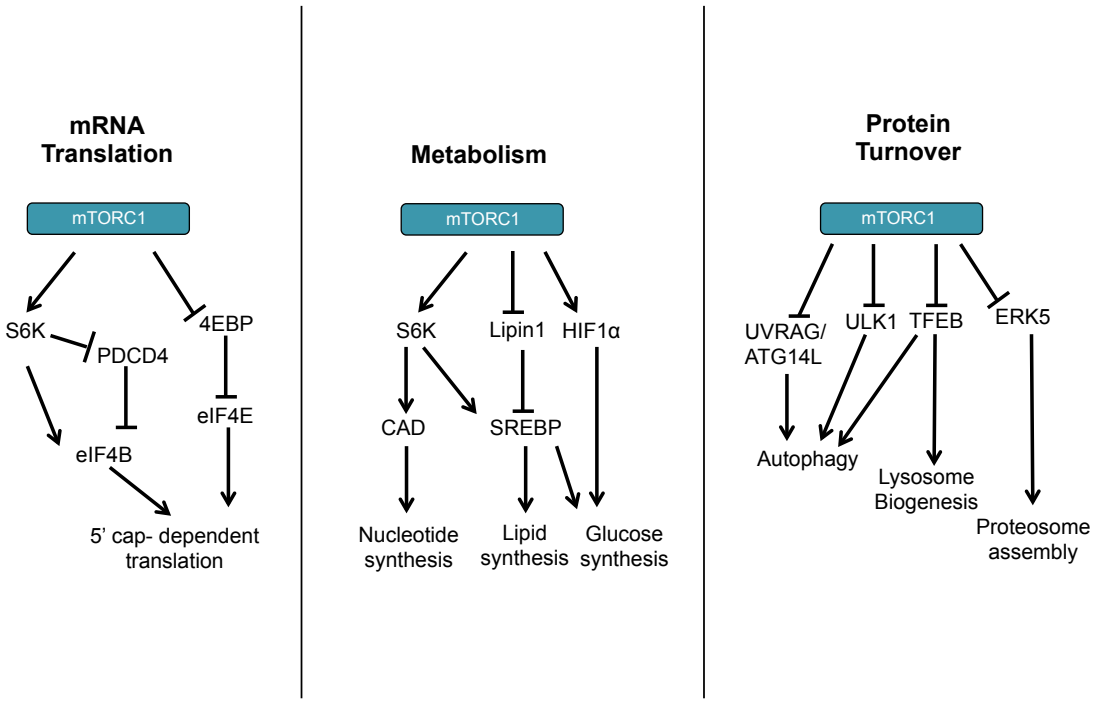

Figure 26: Summary of mTORC1 downstream signaling. (Left) mTORC1 effects translation by two independent methods, activating phosphorylation of S6K and by inhibitory phosphorylation of 4EBP1. (Center) mTORC1 alters metabolism via stimulation of S6K and HIF1α and blockade of Lipin1. (Right) mTORC1 can hinder protein turnover by affecting autophagy (via ATG14/UVRAG and ULK1 inhibition), lysosomal biogenesis (TFEB blockade), or through the less well-understood effect on proteasome assembly (ERK5 inhibition).

phosphorylation at serine 757, which prevents ULK1 stimulation by AMPK, a crucial autophagy initiator (Kim et al., 2011). mTOR also negatively phosphorylates other proteins involved in autophagosome formation, including ATG14L (Yuan et al., 2013) and serine 498 of UVRAG (Kim et al., 2015). mTORC1 can further regulate autophagy by inhibiting the nuclear translocation of TFEB (detailed in chapter 2) and therefore preventing the transcription of autophagy and lysosomal genes (Martina et al., 2012; Settembre et al., 2012).

In addition to autophagy, the ubiquitin proteasome system is another major pathway involved in protein turnover. In this system, proteins are tagged with ubiquitin, which targets them to the 20S proteasome for degradation. Recently, mTORC1 activity has been linked to this process. Two studies illustrated that mTOR blockade led to elevated proteolysis by the proteasome through amplified protein ubiquitination. Inhibition of ERK5 in these conditions lead to increased quantity of proteasomal chaperones (Rousseau and Bertolotti, 2016; Zhao et al., 2015). However, how exactly mTORC1 regulates this activity is still an open conundrum. mTORC1 downstream functions are summarized in Figure 26.

3.4.5 mTORC2 Downstream Signaling

The major function of the mTORC2 complex is to control cell survival and proliferation. It does this by phosphorylating various members of the AGC family of protein kinases, namely different protein kinase Cs (PKCs). The earliest identified substrate of mTORC2 is PKCα, a protein known to regulate the actin cytoskeleton (Jacinto et al., 2004; Sarbassov et al., 2004). mTORC2 also phosphorylates PKCδ, PKCζ, PKCγ, and PKCε, which too are involved in cytoskeleton remodeling and cellular migration (Gan et al., 2012; Li and Gao, 2014; Thomanetz et al., 2013).

Most notably, mTORC2 activates AKT (Sarbassov et al., 2005), the downstream effector of PI3K, to promote proliferation, growth, and survival. This is achieved through inhibition of: the mTORC1 inhibitor TSC2, the metabolic regulator GSK3β, and the FoxO1 and FoxO3a transcription factors. Intriguingly, mTORC2 was required for the phosphorylation of FoxO1/3a *in vivo*, but, was dispensable for TSC2 phosphorylation (Guertin et al., 2006; Jacinto et al., 2006). Furthermore, mTORC2 regulates survival through the phosphorylation of another AGC family member,

serine/threonine-protein kinase 1, SGK1, a kinase also involved in ion transport (García-Martínez and Alessi, 2008).

3.5 mTOR and Brain Function

mTOR plays a role in various neurological processes. Mice with inactivating mutations in *mTOR* lack the telencephalon, the anterior region of the forebrain, highlighting a crucial role in neural development (Hentges et al., 2001). Also, early embryonic activation of mTOR produced microcephaly, and over-activation in post-mitotic neurons created problems in cortical lamination and neurodegeneration (Kassai et al., 2014). Notably, loss of TSC components vastly altered neuronal architecture. TSC deficiency in neurons leads to multiple axon formation. In addition, mice lacking TSC1 in either neurons or astrocytes developed large neurons and dysplastic glial cells (Choi et al., 2008; Meikle et al., 2007; Tavazoie et al., 2005). These studies underline the importance of balanced mTOR signaling in the developing brain.

Tuberous sclerosis complex (TSC) is a rare multisystem genetic disorder due to loss of TSC1 or TSC2, which affects multiple organs including brain, skin, eyes, kidney, heart, and lungs. mTORC1 hyper-activation in TSC leads to epileptic seizures in 90% of patients (Lipton and Sahin, 2014). Mice with loss of neural TSC1 or TSC2 had severe epileptic episodes, which rapamycin could alleviate (Zeng et al., 2008). Further, GATOR1 and KICSTOR mutations have been linked to epilepsy in patients (Basel-Vanagaite et al., 2013; Ricos et al., 2016). In neurodegenerative diseases, such as Alzheimer's disease and Huntington's disease, where autophagy dysfunction has been implicated, there is a corresponding increase in mTOR activation (Li et al., 2005; Ravikumar et al., 2004). As such mTOR inhibitors are among the autophagy stimulatory drugs currently under evaluation to treat these disorders (Nixon, 2013). Hence, over-activation of mTOR can lead to pathological conditions in the brain.

3.6 mTOR and Cancer

As the mTOR pathway regulates cell size, metabolism, proliferation, and survival, it is unsurprising that many cancer cells pirate this signaling cascade.

Several of the upstream activators involved in mTOR activation are commonly mutated in cancer. This results in the hyper-activation of the cascade across approximately 30% of human tumors. There are three major routes to alter mTOR in cancer: through upstream regulators, through its binding partners, or through mTOR itself (Saxton and Sabatini, 2017).

1- Upstream. The most common method that cancer cells alter mTOR signaling is through upstream oncogenes and tumor suppressors. The PI3K pathway converges on mTORC1 and mTORC2, and can be mutated in a variety of ways, including amplification of AKT, PIK3CA, EGFR or IGFR (insulin growth factor receptor). As Ras acts in parallel to PI3K, amplification upstream of either signal can result in aberrant activation of both mTORCs (Tian et al., 2019). Moreover, silencing mutations in tumor suppressors PTEN, p53, TSC1/2, and serine threonine kinase 11 (STK11) contribute to undisciplined mTOR activation in cancer. One example of this is that PTEN-loss induces prostate tumor formation via mTORC2 complex signaling (Guertin et al., 2009).

2- Binding Partners. Genetic abnormality of mTORC components can also trigger the pathway. The mTORC2 component, RICTOR, is genetically amplified in breast cancer, non-small cell lung cancer, and glioma (Tian et al., 2019). In glioma, the overexpression of RICTOR was associated with hyper-activation of AKT and tumor aggressiveness (Masri et al., 2007). Another mTORC complex component susceptible to mutation is Rheb. One study showed that mutations in Rheb (Y35N or E139K) increased phosphorylation of the S6 Kinase 1 compared to wild-type Rheb (Grabiner et al., 2014). Indeed, in a large scale genomic analysis study, Rheb Y35N was identified as a novel cancer-associated mutation (Lawrence et al., 2014). Thus, defects in mTOR binding partners can also be utilized by cancer cells to stimulate the pathway.

3- mTOR itself. There are 33 known mutations in the mTOR protein that can lead to aberrant mTOR signaling in various cancers (Grabiner et al., 2014). This was discovered through public database analysis by David Sabatini's laboratory. They found that these mutations cluster in 6 different regions of the mTOR gene, the most highly recurrent mutations included the following encoding amino acid substitutions C1483, E1799, T1977, S2215, L2427, and R2505. Cancers with the largest changes in mTOR were found to be colorectal, endometrial and lung. However, this might be a bias as these cancers have the highest general mutation rates and are the most

represented in public databases. Mutated mTOR associates less with DEPTOR, the mTOR inhibitor, which may partially explain how it is overactivated. Interestingly, mTOR alteration had no effect on pathway sensitivity to rapamycin (Grabiner et al., 2014). In fact multiple studies demonstrate increased rapamycin sensitivity upon PTEN deletion (Meric-Bernstam et al., 2012; Neshat et al., 2001).

Most GBM have atypical stimulation of mTOR signaling, with 90% showing hyper-activation of PI3K signaling. This is due to common PTEN deletion and EGFR amplification or mutation (constitutively active EGFRvIII) (Cancer Genome Atlas Research Network, 2008; Fine et al., 2009). Confirming genetic analyses, a study by Chakravarti and colleagues tested 92 glioma samples and found increased phosphorylation of PI3K, AKT and S6K proteins in GBM as compared to non-GBM tumors. They further correlated activation of the pathway with radio-resistance in GBM patients (Chakravarti et al., 2004). Along these lines, work by Tanaka et al. showed that EGFRvIII promotes mTORC2 activation in GBM and this activation conferred resistance to chemotherapy (Tanaka et al., 2011). The direct involvement of mTORC2 in GBM biology was elucidated through a Drosophila model of GBM, which overexpresses EGFR, RAS, and PI3K. In this model, knockdown of RICTOR or mSIN1, components of the mTORC2 complex, prevented tumor growth (Read et al., 2009). Further, mice overexpressing RICTOR in astroglial cells develop oligodendroglial tumors in the SVZ (Bashir et al., 2012). Moreover, subunits of the GATOR complex are mutated at a low frequency in GBM (Bar-Peled et al., 2013), which may also contribute to aberrant mTOR activation in these tumors.

In spite of a potential role for mTOR in GBM biology, first generation inhibitors (rapalogs) failed in clinical trials. It is believed that one major reason they were unsuccessful is their inability to block mTORC2 (Mecca et al., 2018a). Several studies confirmed the efficacy of ATP-competitive mTOR kinase inhibitors at targeting GBM in preclinical models (Gini et al., 2013; Lin et al., 2017; Mecca et al., 2018b). Unlike rapalogs, these compounds inhibit mTOR's catalytic activity and can therefore suppress both complexes. Consequently, a phase I clinical trial of one such inhibitor, AZD8055 (NCT01316809) in recurrent GBM is ongoing.

mTOR activation thus represents an interesting axis to explore in the context of GSC biology. As demonstrated in the above chapters, the identification of novel targets within GSCs may improve treatment response in GBM. My thesis aims to

evaluate both internal and external signaling cues in GSCs, as detailed in the following section.

Project Goals

GBM is the most commonly occurring adult primary brain tumor with a 5 year survival rate of only 5% (Ostrom et al., 2014; Yan et al., 2013). Standard of care therapy comprises a surgical resection of the tumor, when possible, followed by chemotherapy (TMZ) and radiation, known as the Stupp protocol (Stupp et al., 2005, 2009, 2015). While these therapies may provide patients with some benefit, it is essentially for pain and symptoms relief, as tumors habitually recur and fatal. Growing evidence points to this relapse being due to a subpopulation of tumor cells, GSCs, with the stem properties of self-renewal and multipotency, and transformed features such as tumor initiating capabilities and resistance to therapies (Lathia et al, 2015). Therefore, new targets within the GSCs must be identified to eliminate these cells and improve patient outcome.

The interaction between GSCs and their environment is essential for their survival. GSCs are present in both perivascular and hypoxic tumor regions. In the perivascular region, these cells receive positive signals from endothelial cells and pericytes, which allow them to retain their undifferentiated state. By contrast, under unfavorable conditions, they resist deleterious effects of hypoxia and nutrient deprivation by down-regulating endo-lysosomes to decrease recycling and enhance receptor signaling (Man et al, 2017; Shingu et al, 2016). Hence, to target GSCs one must consider their diverse microenvironments.

The primary goal of this PhD project was to identify novel therapeutic targets within the signaling pathways involved in sustaining GSCs. This was achieved by studying two separate axes of signaling.

1. Paracrine Signaling between GSCs and Endothelial Cells

Previous work by our lab exemplified that the endothelial secretome was able to maintain stemness properties in patient-derived GSCs *in vitro*. I further evaluated the importance of the transmembrane glycoprotein 130 (gp130) in GSCs, known to be

essential in signal transduction following cytokine stimulation, here assessed in response to endothelial cues.

2. Non-oncogenic Addiction via Intrinsic Signaling

The NF-κB transcription factor marshalls cell proliferation and viability, as well as the paracrine action of cytokines. As this pathway is implicated in many cancers, we evaluated the TCGA for mediators of NF-κB signaling and identified that the paracaspase MALT1 was highly correlated with patient probability of survival. We thus explored the role of MALT1 activity in GSC maintenance.

Results

First Article

Neutralizing gp130 interferes with Endothelial-mediated Effects on Glioblastoma Stem-like Cells

The tumorigenic nature of GSCs is dependent on their interaction with the tumor microenvironment. Within GBM there exist both vascularized and hypoxic zones fostering tumor heterogeneity. As such, GSCs can confront a variety of different extracellular signaling cues, which affect their maintenance. Numerous studies report a privileged interaction between a portion of GSCs and endothelial cells within the tumor (Calabrese et al., 2007; Galan-Moya et al., 2011; Harford-Wright et al., 2017). This close contact favors reciprocal communication between the tumor vasculature and GSCs. Previous work by our lab demonstrated that endothelial secreted factors were able to sustain GSC self-renewal in the absence of other exogenous mitogens (Galan-Moya et al., 2011, 2014). Therefore, elucidating the composition of the endothelial secretome could produce novel therapeutic targets to interrupt paracrine signaling.

In order to achieve this goal, our group employed mass spectrometry analysis of the brain endothelial cell secretome to identify factors that may be important in GSC signaling. The vasoactive peptide apelin was identified. Exogenous apelin was able to maintain GSC stemness properties *in vitro* and recapitulated endothelial secretome action. Moreover, pharmacological blockade with the MM54 inhibitor of the apelin receptor, APLNR, obliterated self-renewal of GSCs *in vitro* and tumor growth in ectopic and orthotopic xenograft models of GBM. Likewise, MM54 had a synergistic effect with TMZ at suboptimal doses *in vitro*. Hence, targeting factors of the endothelial secretome is a potentially attractive strategy for the treatment of GBM (Annex 2) (Harford-Wright et al., 2017).

With this in mind, we revisited other receptors on GSCs that might be involved in endothelial communication. Among the pathway reported to operate in non-oncogene addiction, the IL6-mediated activation of the JAK/STAT pathway is of importance in GSCs (Shi et al., 2017, 2018). IL6 family cytokines trigger a JAK phosphorylation cascade ultimately activating the transcription factor STAT3, which regulates pathways involved in survival, stemness and angiogenesis (Kim et al., 2014). Moreover, IL6 is a cytokine abundantly present in the tumor microenvironment of GSCs (Hossain et al., 2015). The glycoprotein gp130 acts as a co-receptor in

several signal transduction pathways including IL6, and has the potential for pharmacological inhibition. A recent report suggests a potent effect of gp130 knockdown on GSC viability. In contrast to these findings, our data demonstrate that

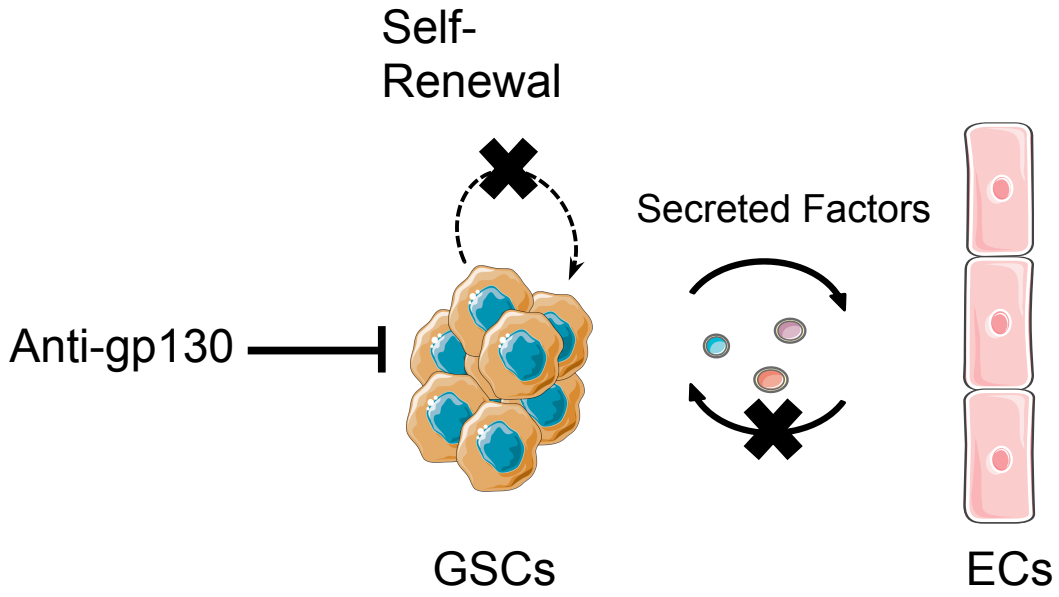

Figure 27: overview of gp130 action. Blocking gp130 reduces EC induced self-renewal in GSCs.

the use of a blocking antibody against gp130 has no impact on cell viability, but rather it abrogates the protective effect of endothelial-secreted factors on GSC expansion. This suggests a more complex role for gp130 in GSCs requiring further investigation.

- Endothelial secreted factors maintain GSCs *in vitro*.
- Pharmacological blockade of gp130 abolishes this effect.
- gp130 inhibition has no effect on overall viability.

Cell Death and Differentiation (2017) 24, 384

www.nature.com/cdd

Correspondence

Neutralizing gp130 interferes with endothelial-mediated effects on glioblastoma stem-like cells

Cell Death and Differentiation (2017) **24,** 384; doi:10.1038/cdd.2016.163; published online 6 January 2017

Dear Editor,

Glioblastoma (GBM) is the most common and lethal primary brain tumor in adults. The aggressiveness of the disease partly relies on a subpopulation of tumor cells, termed as glioblastoma stem-like cells (GSCs) with a phenotype similar to that of normal neural stem cells such as multipotency and the ability to self-renewal.[1,2] GSCs have been implicated in tumor initiation and growth, resistance to therapies, and recurrence.[1–3] Additionally, it has been reported that GSCs reside in vascular niches in close contact with brain endothelial cells. These niches may regulate GSC self-renewal, determine cell fate, and protect these cells from chemo- and radiation therapies.[3,4] Accordingly, the localization of GSCs in close proximity to endothelial cells facilitates reciprocal communication, allowing notably the vascular niche to provide paracrine factors essential to maintain GSCs.[4,5]

We read with interest the article by Shi *et al*[6] published in *Cell Death and Differentiation* online on 14 October 2016. In this article, the authors implicate the glycoprotein gp130 and the tetraspanin CD9 as vital to maintaining the stem-like characteristics of GSCs.[6] Employing RNA interference techniques, they observed a reduction in the stem-like properties of GSCs in the absence of gp130 when cultured in complete media.[6] Our laboratory has also explored the role of gp130 in GSCs, using neutralizing antibodies (B-K5 clone) to pharmacologically alter its functions. To better reflect the *in vivo* endothelial microenvironment, our study was performed in human brain endothelial cell-conditioned serum-free mitogen-free media (EC-CM).[5] We too observed a drastic reduction in the stem-like properties in GSCs treated with the anti-gp130 blocking antibodies, assessed by both tumorsphere formation (Supplementary Figure S1a) and limiting dilution assays (Supplementary Figure S1b), as previously described.[7,8] However, and in contrast to the Shi *et al* work, no significant impact of anti-gp130 blocking antibodies was observed when GSCs were grown in complete media (Supplementary Figure S1a-b). Moreover, blocking gp130 had no overt impact on cell viability in any of the four GSCs tested (data for GSC4 and GSC9 not shown) in either EC-CM (Supplementary Figure S1c) or complete media (Supplementary Figure S1c).[9] Although our findings confirm the involvement of gp130 in stem maintenance, our data also suggest that the gp130 function in GSCs might vary along with cytokine and growth factor availability in the milieu.

The main differences in the two studies reside in the means employed in order to interfere with gp130 function: silencing *versus* blocking antibodies. Indeed, while Shi *et al*[6] reported decreased stem characteristics and cell viability with gp130 silencing in complete medium, our study using antibody-directed targeting of gp130 did not recapitulate these findings. From these results, it is tempting to speculate that gp130 scaffolds a ligand-independent biased intracellular signaling in complete medium that could be affected by gp130 silencing but not by antibodies. Conversely, the gp130 extracellular domain-ignited signaling action may be unmasked in EC-CM by neutralizing antibodies, while growth factor overload in complete medium might circumvent the need for gp130 extracellular domain-based signaling. Consequently, gp130 silencing or neutralization could target different signaling functions.

Taken together, our data reiterate the importance of gp130 in GSC maintenance, although therapeutic targeting of the gp130 complex alone might not lead to a full annihilation of its signaling functions as obtained through a genetic approach. Therefore, this indicates that we should remain cautious in our interpretations of such results as they may differ greatly when coming to the pre-clinical stage.

Conflict of Interest

The authors declare no conflict of interest.

Acknowledgements. The authors wish to thank Nicolas Bidère (SOAP team, Nantes, France) for careful reading of the manuscript. This research was funded by a grant from Région Pays-de-la-Loire and Nantes Métropole (Connect Talent), Ligue Nationale contre le Cancer (comité Loire-Atlantique, Maine-et-Loire, Morbihan, Sarthe, Vendée), Institut National du Cancer (INCA), Fondation ARC pour la Recherche contre le Cancer.

Kathryn A Jacobs[1], Elizabeth Harford-Wright[1] and Julie Gavard[*,1]*

[1] CRCINA, Team SOAP, Inserm, CNRS, Universite de Nantes, 8 quai Moncousu, Nantes, France

* Corresponding authors: J Gavard, Team SOAP, Signaling in Oncogenesis, Angiogenesis and Permeability, IRS-UN blg, Room 416, 8 quai Moncousu, Nantes 44000, France. Tel: +33 2 2808 0327
E-mail: julie.gavard@inserm.fr

1. Chen J *et al. Nature* 2012; **488**(7412): 522–526.
2. Singh SK *et al. Nature* 2004; **432**(7015): 396–401.
3. Bao S *et al. Nature* 2006; **444**(7120): 756–760.
4. Calabrese C *et al. Cancer Cell* 2007; **11**(1): 69–82.
5. Galan-Moya EM *et al. EMBO Rep* 2011; **12**(5): 470–476.
6. Shi Y *et al. Cell Death Differ* 2017; **24**: 167–180.
7. Tropepe V *et al. Dev Biol* 1999; **208**(1): 166–188.
8. Harford-Wright E *et al. Oncotarget*, e-pub ahead of print 1 September 2016, 10.18632/oncotarget.11784.
9. Galan-Moya EM *et al. PLoS O*ne 2014; **9**(3): e93505.

Supplementary Information accompanies this paper on *Cell Death and Differentiation* website (http://www.nature.com/cdd)

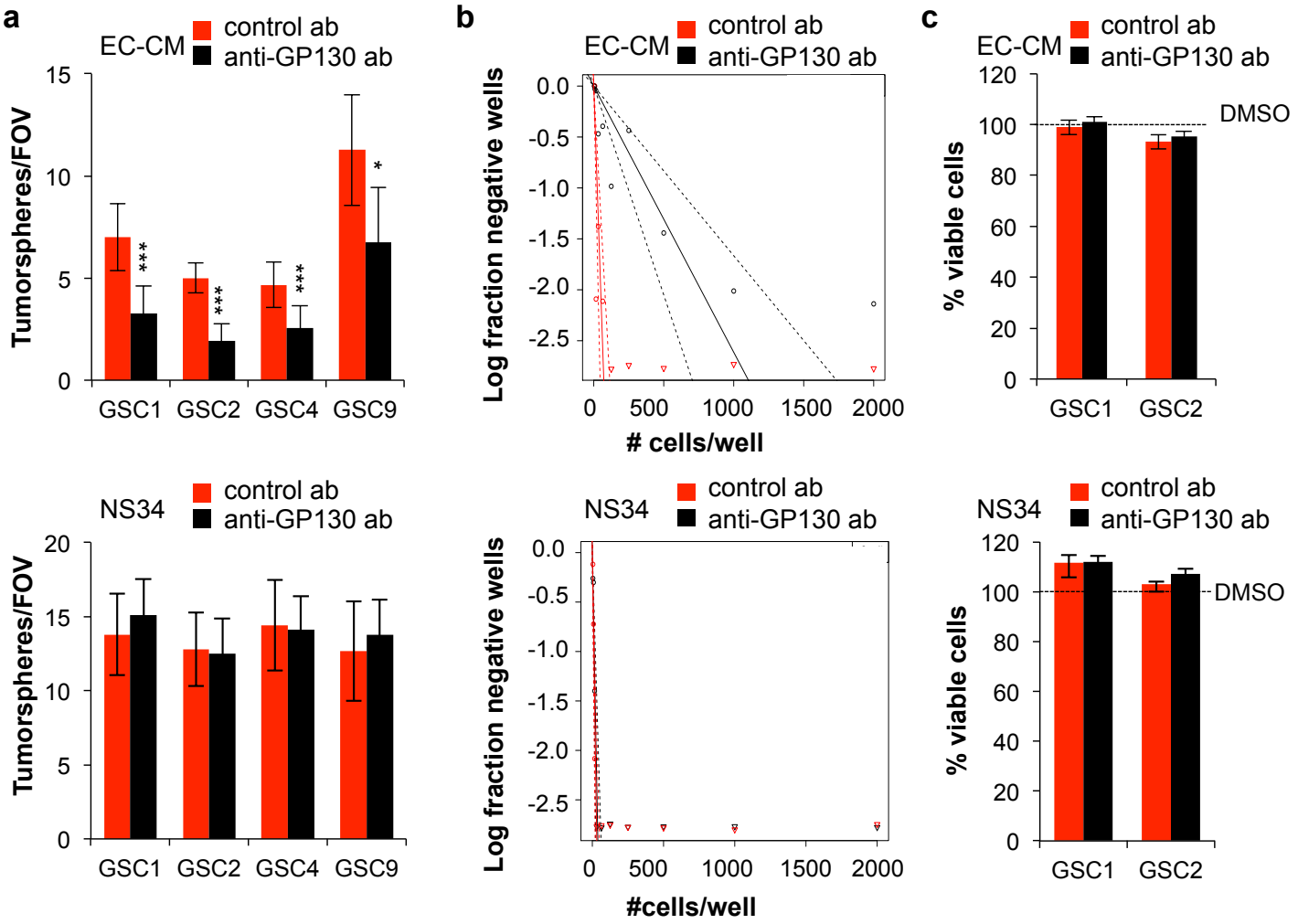

Figure S1. anti-gp130 blocking antibodies reduce GSC expansion in EC-CM.

(A) Tumorsphere formation per field of view (FOV) in mesenchymal (#1, #2 and #4) and classical (#9) glioblastoma stem-like cell (GSC)[8] subtypes in response to anti-gp130 (2 μmol.l^{-1}, B-K5 clone, Abcam) or control (swap70, 2 μmol.l^{-1}, Abcam) antibodies in endothelial cell-conditioned serum-free mitogen-free media, prepared as previously described[5,9] (EC-CM, top panel) and in mitogen-defined complete medium (NS34, bottom panel). n=3, mean±SEM, ns $p>0.05$ *$p<0.05$, ***$p<0.001$. (B) Linear regression plot of *in vitro* limiting dilution assay (LDA) for GSC#2 in EC-CM (top) and NS34 (bottom), in the presence of anti-gp130 or control antibodies. Data were analyzed as described by Tropepe *et al.*[7] n=2 (C) Cell viability using the UptiBlue reagent (Interchim), a fluorometric/colormetric growth indicator in response to treatment with anti-gp130 or control antibodies in EC-CM top) and NS34 (bottom). n=3, mean±SEM, ns $p>0.05$.

Second Article

Paracaspase MALT1 regulates Glioma Cell Survival by Controlling Endo-lysosomal Homeostasis

GBM are heterogeneous tumors with a characteristically abnormal vasculature, which allows for hypoxic and necrotic zones to develop within the tumor. In addition to their protective vascular niche, GSCs have been shown to survive in these harsh regions of the tumor. In the absence of oxygen and nutrients, they reduce receptor recycling to sustain signaling for longer and overcome microenvironmental stress (Man et al., 2018; Shingu et al., 2016). Therefore, there may be other autocrine signaling pathways employed by GSCs to maintain themselves outside the protective vascular niche.

To address this question, we decided to explore signaling involved in non-oncogene addiction in cancer, a process by which cancer cells exploit non-mutated cellular functions for their propagation and survival. While there are numerous pathways that fall into this category, NF-κB signaling converges on cytokine release, in addition to cell proliferation and survival. As NF-κB impacts both tumor cells and the microenvironment, we analyzed the TCGA for known mediators of the NF-κB pathway, and identified the paracaspase mucosa-associated lymphoid tissue l (MALT1) as the gene most significantly correlated with probability of survival in GBM patients.

MALT1 is a unique protease with a scaffold function, linked to immune responses, and aggressive lymphoma but whose role is underestimated in CNS cancer. Upon antigen receptor engagement in lymphocytes, a multiprotein complex named the CARMA1/BCL10/MALT1 complex or CBM forms. This signalosome is composed of a scaffold protein caspase recruitment domain family member 11 (CARD11 or CARMA1), an adaptor protein B Cell CLL/lymphoma-10 (BCL-10), and MALT1. CARMA1 has an autoinhibitory linker region which masks the CARD domain in unstimulated cells. Antigen receptor activation in T/B lymphocytes allows protein kinase Cθ/β (PKC θ/β) to phosphorylate CARMA1, changing its conformation (Ruland

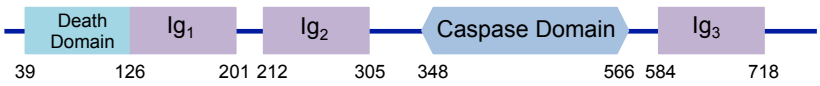

Figure 28: MALT1 construct map, featuring N-terminal death domain, 3 Ig domains, and a paracaspase domain

and Hartjes, 2019). Now in an open conformation, CARMA1 associates with BCL10 via the CARD domain of BCL10 to form a CARD/CARD interaction. BCL10 forms a constitutive heterodimer with MALT1 via its C-terminal serine/threonine rich domain, which interacts with the Ig domains for MALT1 (Figure 28). Once formed, the CBM complex organizes in a filamentous structure, which then allows the NF-κB activating machinery to dock (Qiao et al., 2013). The transcription factor NF-κB can subsequently translocate to the nucleus and bind its targets, enabling their expression (Bonizzi and Karin, 2004).

Caspases represent a family of cysteine proteases essential in the regulation of cell death. Paracaspases maintain their conserved catalytic cysteine and histidine combination, but unlike caspases have a specificity towards uncharged residues in the P1 position of substrates (Uren et al., 2000). In 2008, it was confirmed that the caspase-like domain in the C-terminus of MALT1 was indeed functional through pivotal findings of Margot Thome's and Rudi Beyaert's groups (Coornaert et al., 2008a; Rebeaud et al., 2008). Beyaert's laboratory established that A20, also known as TNFAIP3, a negative regulator of NF-κB was cleaved and inactivated by MALT1 (Coornaert et al., 2008a). Thome's group identified the MALT1 binding partner BCL10 as a substrate of MALT1 after T cell activation, and showed that this proteolysis was critical for integrin-mediated adhesion of T cells (Rebeaud et al., 2008). Both groups showed that MALT1 trimming of substrates was arginine specific and cysteine dependent (Coornaert et al., 2008a; Rebeaud et al., 2008). Later, structural analysis studies were performed to determine that MALT1 proteolytic activity occurs within the S/P-R↓G/A consensus motif (Table 2)(Wiesmann et al., 2012).

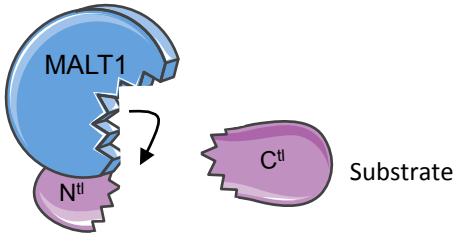

Figure 29: MALT1 is a protease. MALT1 cleaves substrates with a S/P-R↓G/A consensus motif

MALT1 knockout mice develop normally and have functional immune systems (Brüstle et al., 2017; Ruefli-Brasse et al., 2003; Ruland et al., 2003). With the creation of mice expressing a catalytically inactivated MALT1, it was discovered that the proteolytic activity of MALT1 specifically plays a crucial part in immune cell maturation as these mice did not properly develop regulatory T cells (Bornancin et al., 2015; Gewies et al., 2014; Jaworski et al., 2014; Yu et al., 2015). Catalytically dead MALT1 mice develop a lethal multi-organ inflammatory syndrome due to

abnormal secretion of interferon gamma, in addition to the tissue specific problems of neurodegeneration, and gastric inflammation (Gewies et al., 2014). Lung immune infiltration and eye inflammation were also reported (Bornancin et al., 2015; Yu et al., 2015). These mice also develop autoimmune gastritis (Jaworski et al., 2014). In contrast, the MALT1 knockout mice do not have any obvious phenotypes (Ruland et al., 2003), underlining an importance of each of the MALT1 protein functions: as a scaffold and as a protease.

Substrate	Cleavage Site	Function
A20	GAS**R**^{439}GEA	NF-κB
RELB	LVS**R**^{85}GAA	NF-κB
HOIL1	LQP**R**^{165}GPL	NF-κB
MALT1	LCC**R**^{149}ATG… HCS**R**^{781}TPD	NF-κB
NIK	CLS**R**^{325}GAH	NF-κB
LIMA1	PDS**R**^{206}ASS… FKSK^{269}GNY	B-cell Growth, Adhesion
CYLD	FMS**R**^{324}GVG	JNK/ AP1
ROQUIN 1	LIP**R**^{510}GTD… MVP**R**^{579}GSQ	mRNA Stability
ROQUIN 2	LIS**R**^{509}TDS	mRNA Stability
REGNASE 1	LVP**R**^{111}GGS	mRNA Stability
BCL10	LRS**R**^{228}TVS	Adhesion

Table 2: MALT1 substrates, cleavage sites and cellular functions

Of the already identified MALT1 substrates, half of them (A20, RELB, HOIL-1, MALT1, and NIK) play a role in NF-κB signaling. In addition to A20, HOIL-1, a component of the linear ubiquitination complex (LUBAC) involved in IKK activation, was identified as a MALT1 substrate by three independent groups, including our own (Douanne et al., 2016; Elton et al., 2016; Klein et al., 2015). Klein et al. suggest that the processing of HOIL-1 affects NF-κB signaling by destabilizing the LUBAC and therefore reducing its capacity for linear ubiquitination. Conversely, our laboratory showed that HOIL-1 cleavage inactivates it and therefore limits its function as a repressor of NF-κB.

Similarly, RELB, a component of the NF-κB pathway, was also identified as a MALT1 substrate by Margot Thome's laboratory (Hailfinger et al., 2011). RELB belongs to the NF-κB transcription family, which is composed of five members (RELA, RELB, c-Rel, p105/p50, p100/p52) all sharing a REL homology domain which

is responsible for DNA binding and oligomerization. It negatively regulates the canonical pathway in two ways, first by competing for DNA binding sites and second by forming inactive heterodimers with canonical REL family members RELA and c-REL (Hailfinger et al., 2011). This group showed that processed RELB is rapidly degraded by the proteasome. Further, when an uncleavable RELB mutant was expressed in Jurkat T cells, NF-κB signaling was reduced (Hailfinger et al., 2011). Therefore, among the NF-κB related substrates of MALT1, there exists a subgroup of negative regulators, whose processing permits their disabling.

From another axis, MALT1 protease activity can affect NF-κB activation by auto-cleavage at arginine 149 and arginine 781 (Baens et al., 2014, 2018; Wu et al., 2018). Baens et al illustrated that uncleavable mutants of this paracaspase reduced the MALT1 dependent production of interleukin-2, without affecting processing of other substrates or MALT1 scaffold function. Instead, this auto-processing appears to be essential for the expression of NF-κB target genes upon activation of T cells (Baens et al., 2014). Also, Wu et al. further extended the role of auto-processing to be important in regulatory T cell activation (Wu et al., 2018). These findings add another layer to MALT1's proteolytic activity in NF-κB signaling; not only does it inactivate negative regulators but also it self-regulates.

Additionally, Staal et al showed that MALT1 processes the deubiqutinating enzyme CYLD to inactivate it (Staal et al., 2011). CYLD is a negative regulator of the JNK and AP-1 pathways. Indeed, previously it was shown that MALT1 deficient T cells had impaired JNK activation upon T cell receptor stimulation (Ruland et al., 2003). Accordingly, uncleavable CYLD expression leads to decrease in JNK and AP-1 targets interleukin 2, interleukin-8 and c-Jun (Staal et al., 2011). Interestingly, the mice expressing catalytically inactive MALT1 did not show striking defects in JNK and AP-1 (Bornancin et al., 2015) which may signify other roles of CYLD processing outside of this signaling context.

As already described, Thome's group first identified MALT1 proteolytic activity in the context of BCL10 processing. Not only did they show that MALT1 was indeed a protease, but they also demonstrated that BCL10 processing is important for cell adhesion, though the mechanism of action remains poorly understood (Rebeaud et al., 2008). Moreover, Nakaya et al. showed that MALT1 proteolytic activity is necessary for glutamine uptake and mTOR activation upon antigen receptor engagement. Inhibition of MALT1 paracaspase activity with the competitive inhibitor

zVRPR led to decreased mTOR signaling, as evaluated through phosphorylation of S6 kinase and S6 (Nakaya et al., 2014). Concurrently, Hamilton et al. showed similar effects, and demonstrated that MALT1 protease activity is necessary for metabolic switch upon T cell activation (Hamilton et al., 2014). However, to date no specific substrates of MALT1 within the mTOR signaling pathway have been identified, so the exact molecular mechanism by which MALT1 controls mTOR signaling upon TCR engagement remains to be explored.

A rather surprising role for MALT1 in regulating RNA binding proteins emerged with the discovery of Regnase-1, also known as ZC3H12A or MCPIP-1, as a bona fide MALT1 substrate (Uehata et al., 2013). The RNA binding protein Regnase-1 contains a zinc finger domain, which tethers directly to mRNAs, as well as a PilT N-terminus like domain which has an RNase catalytic center activated upon interaction with N-terminus of the protein (Xu et al., 2012a, 2012b). It facilitates the mRNA stability of different genes including c-REL, OX40, and IL2 and prevents the generation of aberrant CD4+ T cells (Uehata et al., 2013). Indeed, Regnase-1 deficient mice have systematic inflammation due to hyperactive B and T cells (Iwasaki et al., 2011). In this vein, Uehata and colleagues showed that MALT1 inhibition led to destabilization of mRNAs and deregulated T cell activation (Uehata et al., 2013). Additionally, Heissmeyer's group linked Regnase-1 to Roquin 1 and Roquin 2, two other RNA binding proteins, in the production of IL17. They also demonstrated that Roquins 1/2 are MALT1 substrates upon antigen receptor engagement (Jeltsch et al., 2014). In addition to the zinc finger RNA binding domain, Roquins have a RING (Really Interesting New Gene) finger domain known to be present in E3 ubiquitin ligases (Schaefer and Klein, 2016). To date Roquin 1 has not been demonstrated to have any E3 ligase activity, while Roquin 2 has been shown to promote ubiquitination of MAP3K5, a protein involved in reactive oxygen species (ROS)-induced cell death (Maruyama et al., 2014). The role of MALT1 in regulating RNA binding proteins demonstrates a multi-level function of the protease in gene expression. Not only does it modify gene transcription through its role in NF-κB, MALT1 also regulates the stability and therefore translation of mRNA.

MALT1 has been shown to be constitutively active and involved in disease progression in a subset of diffuse large B-cell lymphoma (DLBCL) known as Activated B Cell diffuse large B cell lymphoma, or ABC DLBCL (Ferch et al., 2009; Hailfinger et al., 2009). Concurrently, Margot Thome's and Jurgen Ruland's

laboratories demonstrated that the competitive inhibitor of MALT1, zVRPR, as well as overexpression of a catalytically dead MALT1 could reduce growth and survival of ABC DLBCL (Ferch et al., 2009; Hailfinger et al., 2009). This work was expanded upon by studies with the small compound MI2 or phenothiazines, especially mepazine, which were shown to bind specifically to MALT1 and were selectively toxic to ABC DLBCL *in vitro* and *in vivo* without displaying toxicity in mice (Fontan et al., 2012; Nagel et al., 2012a; Schlauderer et al., 2013). However, the role of MALT1 in solid tumors has not been extensively explored.

Confirming my *in silico* TCGA analysis, knockdown or pharmacological inhibition of MALT1 in a panel of patient-derived GSCs abolished cell viability *in vitro*. MALT1 blockade also reduced tumor growth *in vivo*. In addition, these cells observed an increase in their endo-lysosomal compartment accompanied by a defect in autophagic flux. Moreover, inhibition or silencing of MALT1 reduced mTOR activation and lysosomal localization. We also demonstrated that MALT1 interacts with the lysosomal regulator QKI. This interaction was disturbed in response to pharmacological intervention. Consequently, QKI knockdown rescued MALT1-induced phenotype. Thus, targeting MALT1 is a potential strategy for the treatment of GBM.

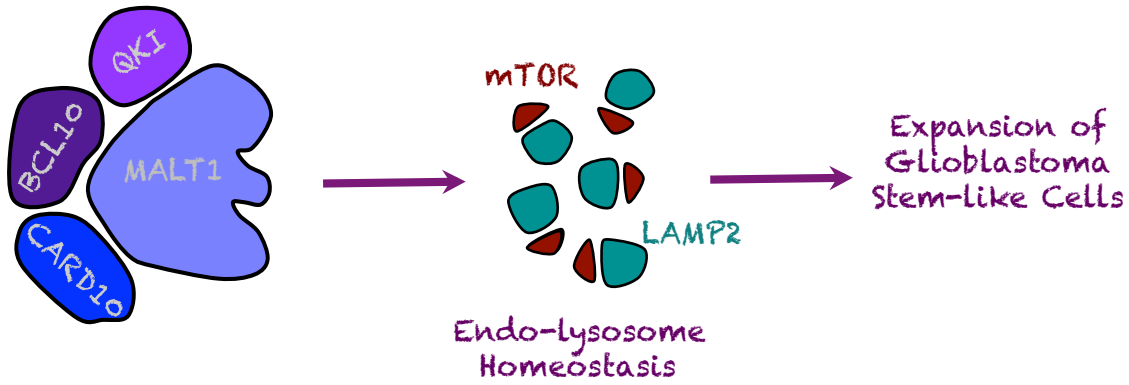

Figure 30: Overview of MALT1 action in GSCs. MALT1 activity regulates lysosomal homeostasis and mTOR signaling to promote GSC expansion.

- Expression and catalytic activity of MALT1 are required for GSC expansion.
- Pharmacological targeting of MALT1 is lethal to GSCs and reduces the expansion of established tumors in mice.
- MALT1 depletion results in an increased endo-lysosomal compartment and decreased mTOR signaling.

- MALT1 expression negatively correlates to that of RNA-binding protein Quaking to control endo-lysosomal biogenesis.


THE
EMBO
JOURNAL
Volume 39 Issue 1 | 2 January 2020
MALT1 regulates endo-lysosome abundance
EMBOpress

Second Publication

Article

SOURCE DATA | TRANSPARENT PROCESS

THE EMBO JOURNAL

Paracaspase MALT1 regulates glioma cell survival by controlling endo-lysosome homeostasis

Kathryn A Jacobs[1], Gwennan André-Grégoire[1,2], Clément Maghe[1], An Thys[1], Ying Li[3], Elizabeth Harford-Wright[1], Kilian Trillet[1], Tiphaine Douanne[1], Carolina Alves Nicolau[1], Jean-Sébastien Frénel[2], Nicolas Bidère[1] & Julie Gavard[1,2,*]

Abstract

Glioblastoma is one of the most lethal forms of adult cancer with a median survival of around 15 months. A potential treatment strategy involves targeting glioblastoma stem-like cells (GSC), which constitute a cell autonomous reservoir of aberrant cells able to initiate, maintain, and repopulate the tumor mass. Here, we report that the expression of the paracaspase mucosa-associated lymphoid tissue l (MALT1), a protease previously linked to antigen receptor-mediated NF-κB activation and B-cell lymphoma survival, inversely correlates with patient probability of survival. The knockdown of MALT1 largely impaired the expansion of patient-derived stem-like cells *in vitro*, and this could be recapitulated with pharmacological inhibitors, *in vitro* and *in vivo*. Blocking MALT1 protease activity increases the endo-lysosome abundance, impairs autophagic flux, and culminates in lysosomal-mediated cell death, concomitantly with mTOR inactivation and dispersion from endo-lysosomes. These findings place MALT1 as a new druggable target involved in glioblastoma and unveil ways to modulate the homeostasis of endo-lysosomes.

Keywords glioma; lysosome; MALT1; mTOR; protease
Subject Categories Cancer; Autophagy & Cell Death; Membranes & Trafficking
DOI 10.15252/embj.2019102030 | Received 18 March 2019 | Revised 16 October 2019 | Accepted 25 October 2019
The EMBO Journal (2019) e102030

Introduction

Glioblastoma multiforme (GBM) represents the most lethal adult primary brain tumors, with a median survival time of 15 months following diagnosis (Stupp *et al*, 2009, 2015). The current standard-of-care for the treatment of GBM includes a surgical resection of the tumor followed by treatment with alkylating agent temozolomide and radiation. While these standardized strategies have proved beneficial, they remain essentially palliative (Stupp *et al*, 2009; Chinot *et al*, 2014; Brown *et al*, 2016). Within these highly heterogeneous tumors exists a subpopulation of tumor cells named glioblastoma stem-like cells (GSCs). Although the molecular and functional definition of GSCs is still a matter of debate, there is compelling evidence that these cells can promote resistance to conventional therapies, invasion into normal brain, and angiogenesis (Singh *et al*, 2004; Bao *et al*, 2006; Chen *et al*, 2012; Yan *et al*, 2013; Lathia *et al*, 2015). As such, they are suspected to play a role in tumor initiation and progression, as well as recurrence and therapeutic resistance. Owing to their quiescent nature, GSCs resist to both chemotherapy and radiation, which target highly proliferative cancer cells (Bao *et al*, 2006; Chen *et al*, 2012). Hence, there is a clear need to identify novel therapeutic targets, designed to eradicate GSCs, in order to improve patient outcome.

GSCs constantly integrate external maintenance cues from their microenvironment and as such represent the most adaptive and resilient proportion of cells within the tumor mass (Lathia *et al*, 2015). Niches provide exclusive habitat where stem cells propagate continuously in an undifferentiated state through self-renewal (Lathia *et al*, 2015). GSCs are dispersed within tumors and methodically enriched in perivascular and hypoxic zones (Calabrese *et al*, 2007; Jin *et al*, 2017; Man *et al*, 2017). GSCs essentially received positive signals from endothelial cells and pericytes, such as ligand/receptor triggers of stemness pathways and adhesion components of the extracellular matrix (Calabrese *et al*, 2007; Galan-Moya *et al*, 2011; Pietras *et al*, 2014; Harford-Wright *et al*, 2017; Jacobs *et al*, 2017). GSCs are also protected in rather unfavorable conditions where they resist hypoxic stress, acidification, and nutrient deprivation (Shingu *et al*, 2016; Jin *et al*, 2017; Man *et al*, 2017). Recently, it has been suggested that this latter capacity is linked to the function of the RNA-binding protein Quaking (QKI), in the down-regulation of endocytosis, receptor trafficking, and endo-lysosome-mediated degradation. GSCs therefore down-regulate lysosomes as one adaptive mechanism to cope with the hostile tumor environment (Shingu *et al*, 2016).

Lysosomes operate as central hubs for macromolecule trafficking, degradation, and metabolism (Aits & Jaattela, 2013). Cancer cells usually show significant changes in lysosome morphology and composition, with reported enhancement in volume, protease activity, and membrane leakiness (Fennelly & Amaravadi, 2017). These

1 Team SOAP, CRCINA, Inserm, CNRS, Université de Nantes, Université d'Angers, Nantes, France
2 Integrated Center for Oncology, ICO, St. Herblain, France
3 Tsinghua University-Peking University Joint Center for Life Sciences, Technology Center for Protein Sciences, School of Life Sciences, Tsinghua University, Beijing, China
*Corresponding author. Tel: +33 2808 0327; E-mail: julie.gavard@inserm.fr

modifications can paradoxically serve tumor progression and drug resistance, while providing an opportunity for cancer therapies. The destabilization of the integrity of these organelles might indeed ignite a less common form of cell death, known as lysosomal membrane permeabilization (LMP). LMP occurs when lysosomal proteases leak into the cytosol and induce features of necrosis or apoptosis, depending on the degree of permeabilization (Aits & Jaattela, 2013). Recent reports also highlighted that lysosomal homeostasis is essential in cancer stem cell survival (Shingu *et al*, 2016; Mai *et al*, 2017; Le Joncour *et al*, 2019). Additionally, it has been shown that targeting the autophagic machinery is an effective treatment against apoptosis-resistant GBM (Shchors *et al*, 2015; Zielke *et al*, 2018). The autophagic flux inhibitor chloroquine can decrease cell viability and acts as an adjuvant for TMZ treatment in GBM. However, this treatment might cause neural degeneration at the high doses required for GBM treatment (Weyerhäuser *et al*, 2018). Therefore, it is preferable to find alternative drugs that elicit antitumor responses without harmful effects on healthy brain cells.

A growing body of literature supports the concept of non-oncogene addiction (NOA) in cancer. Although neither mutated nor involved in the initiation of tumorigenesis, NOA genes are essential for the propagation of the transformed phenotype (Luo *et al*, 2009). Because NOA gene products are pirated for the benefit of tumor cells' own survival, their targeting therefore constitutes an Achilles' heel. Among reported NOA genes and pathways (Staudt, 2010), the paracaspase mucosa-associated lymphoid tissue l (MALT1) might be of particular interest in GBM (please see Fig 1). This arginine-specific protease plays a key role in NF-κB signaling upon antigen receptor engagement in lymphocytes, via the assembly of the CARMA-BCL10-MALT1 (CBM) complex. In addition to this scaffold role in NF-κB activation, MALT1 regulates NF-κB activation, cell adhesion, mRNA stability, and mTOR signaling through its proteolytic activity (Rebeaud *et al*, 2008; Staal *et al*, 2011; Uehata *et al*, 2013; Hamilton *et al*, 2014; Jeltsch *et al*, 2014; Nakaya *et al*, 2014). MALT1 has been shown to be constitutively active in activated B-cell-like diffuse large B-cell lymphoma (ABC DLBCL), and its inhibition is lethal (Ngo *et al*, 2006; Hailfinger *et al*, 2009; Nagel *et al*, 2012). MALT1 was also recently reported to exert pro-metastatic effects in solid tumors (McAuley *et al*, 2019). However, the role of MALT1 in solid tumors has not been extensively investigated.

Here, we provide evidence of the role of MALT1 in disrupting GSC lysosomal homeostasis, which is associated with autophagic features. We found that targeting MALT1, notably through the phenothiazine family of drugs, including mepazine (MPZ), is lethal to GBM cells. We further established that MALT1 sequesters QKI and maintains low levels of lysosomes, while its inhibition unleashes QKI and hazardously increases endo-lysosomes, which subsequently impairs autophagic flux. This leads to cell death concomitant with mTOR inhibition and dispersion from lysosomes. Disrupting lysosomal homeostasis therefore represents an interesting therapeutic strategy against GSCs.

Results

MALT1 expression sustains glioblastoma cell growth

Glioblastoma stem-like cells (GSCs) are suspected to be able to survive outside the protective vascular niche, in non-favorable environments, under limited access to growth factors and nutrients (Calabrese *et al*, 2007; Shingu *et al*, 2016; Jin *et al*, 2017). While many signaling pathways can influence this process, the transcription factor NF-κB has been demonstrated to be instrumental in many cancers as it centralizes the paracrine action of cytokines, in addition to playing a major role in cell proliferation and survival of tumor cells and surrounding cells (Bargou *et al*, 1996; Davis *et al*, 2001; Karin & Greten, 2005; Li *et al*, 2009; McAuley *et al*, 2019). Because of this dual influence on both tumor cells and their microenvironment, we revisited The Cancer Genome Atlas (TCGA) for known mediators of the NF-κB pathway (Fig 1A). We found that *MALT1* expression was more significantly correlated with survival than other tested genes of the pathway (Fig 1B). This arginine-specific protease is crucial for antigen receptor-mediated NF-κB activation and B-cell lymphoma survival (Ngo *et al*, 2006). In addition, when GBM patients were grouped between low and high *MALT1* expression levels, there was a significant survival advantage for patients with lower *MALT1* expression (Fig 1C). Moreover, levels of *MALT1* mRNA are elevated in GBM (Grade IV) when compared with lower grade brain tumors (grades II and III) or non-tumor samples (Fig 1D and E).

Although this increased *MALT1* expression may be due to tumor-infiltrating immune cells, we first explored whether MALT1 was engaged in patient-derived GSCs, as these cells recapitulated *ex vivo* features of the tumor of origin (Lathia *et al*, 2015). The functional impact of MALT1 knockdown was thus evaluated by their viability and expansion *in vitro* (Fig 1F–J). Two individual short hairpin RNA sequences targeting MALT1 (sh*MALT1*) cloned in a lentiviral bi-cistronic GFP-expressing plasmid were delivered into GSC#1 (mesenchymal) and GSC#9 (classical) cells. We observed a reduced fraction of GFP-positive cells over time, while cells expressing non-silencing RNA plasmids (shc) maintained a steady proportion of GFP-positive cells, indicating that *MALT1* silencing was detrimental to GSCs (Fig 1F). Likewise, cells transfected with si*MALT1* had a lower percentage of EdU-positive cells as compared to non-silenced control cells (Fig 1G) and a higher incorporation of propidium iodide (PI) (Fig 1H). Additionally, GSCs either expressing sh*MALT1* or transfected with si*MALT1* had less stem traits, as evaluated by limited dilution assay and tumorsphere formation (Fig 1I and J). Taken together, these results indicate that MALT1 expression may be important for glioblastoma cell *ex vivo* expansion.

Pharmacological inhibition of MALT1 is lethal to glioblastoma cells

Next, to evaluate the potential of targeting MALT1 pharmacologically, we treated GSC #1 (mesenchymal), #4 (mesenchymal), #9 (classical), and #12 (neural) with the MALT1 allosteric inhibitor mepazine (MPZ) at a dose of 20 μM, as initially described (Nagel *et al*, 2012). All four GSCs showed a significant reduction in stemness by both limited dilution and tumorsphere assays (Fig 2A–C). Additionally, the competitive inhibitor Z-VRPR-FMK induced similar decrease in tumorsphere formation (Fig 2C). This was accompanied by a marked reduction in the abundance of SOX2 and NESTIN stemness markers (Fig 2D). Alongside the *in vitro* self-renewal impairment, GSC viability was largely annihilated by MPZ treatment, including reduction in EdU staining and increase in PI incorporation (Fig 2E–G). In contrast, MPZ had no significant effect on viability of

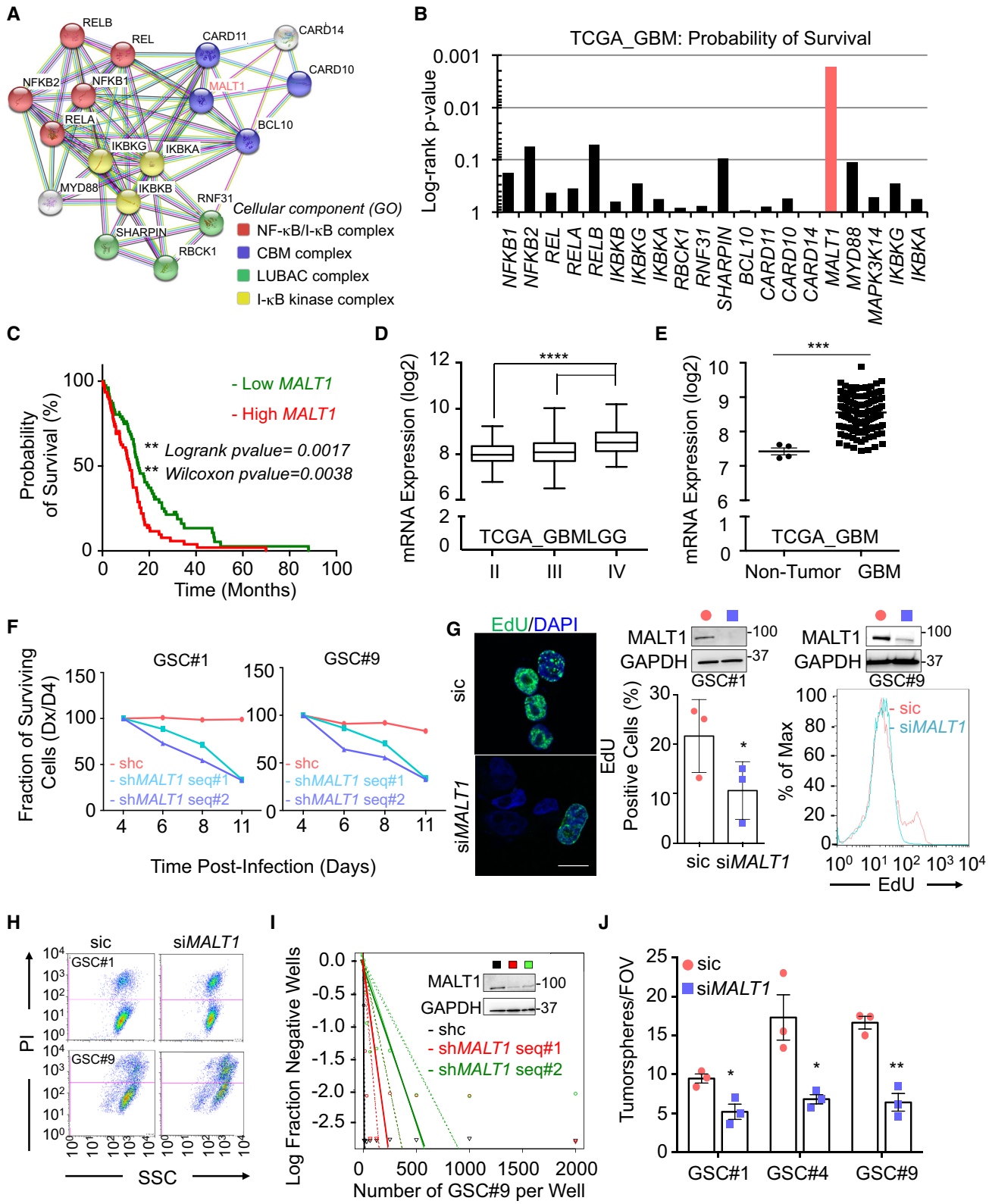
A
RELB
REL
CARD11
CARD14
CARD10
NFKB2
NFKB1
MALT1
RELA
BCL10
IKBKG
IKBKA
MYD88
IKBKB
RNF31
SHARPIN
RBCK1
Cellular component (GO)
NF-κB/I-κB complex
CBM complex
LUBAC complex
I-κB kinase complex
B
TCGA_GBM: Probability of Survival
Log-rank p-value
0.001
0.01
0.1
1
NFKB1 NFKB2 REL RELA RELB IKBKB IKBKG IKBKA RBCK1 RNF31 SHARPIN BCL10 CARD11 CARD10 CARD14 MALT1 MYD88 MAPK3K14 IKBKG IKBKA
C
Probability of Survival (%)
- Low MALT1
- High MALT1
** Logrank pvalue= 0.0017
** Wilcoxon pvalue=0.0038
Time (Months)
D
mRNA Expression (log2)
****
TCGA_GBMLGG
II III IV
E
mRNA Expression (log2)
***
TCGA_GBM
Non-Tumor GBM
F
Fraction of Surviving Cells (Dx/D4)
GSC#1
GSC#9
- shc
- shMALT1 seq#1
- shMALT1 seq#2
Time Post-Infection (Days)
G
EdU/DAPI
sic
siMALT1
EdU
MALT1
GAPDH
GSC#1
GSC#9
Positive Cells (%)
sic siMALT1
% of Max
sic
siMALT1
EdU
H
sic
siMALT1
GSC#1
GSC#9
PI
SSC
I
Log Fraction Negative Wells
MALT1
GAPDH
- shc
- shMALT1 seq#1
- shMALT1 seq#2
Number of GSC#9 per Well
J
Tumorspheres/FOV
sic
siMALT1
GSC#1 GSC#4 GSC#9

Figure 1.

Figure 1. MALT1 expression sustains glioblastoma cell growth.

A STRING diagram representation of the network of proteins involved in NF-κB pathway.

B The Cancer Genome Atlas (TCGA RNAseq dataset) was used on the GlioVis platform (Bowman *et al*, 2007) to analyze the probability of survival (log-rank *P*-value) of 155 GBM patients, for each gene encoding for the mediators of the NF-κB pathway.

C Kaplan–Meier curve of the probability of survival for 155 GBM patients with low or high *MALT1* RNA level, using median cutoff, based on the TCGA RNAseq dataset.

D, E Box and whisker plot of *MALT1* mRNA expression in low-grade glioma (LGG, grades II and III) or in GBM (grade IV) (TCGA GBMLGG, RNAseq dataset) (D). Horizontal line marks the median, box limits are the upper and lower quartiles, and error bars show the highest and lowest values. Alternatively, *MALT1* mRNA expression was plotted in non-tumor samples versus GBM samples (TCGA RNAseq dataset) (E). Each dot represents one clinical sample.

F Fraction of surviving cells over time in GSC#1 and GSC#9, transduced with control (shc) or bi-cistronic GFP plasmids using two different short hairpin RNA (sh*MALT1* sequences, seq #1 and #2). Data are plotted as the percentage of GFP-positive cells at the day of the analysis (Dx), normalized to the starting point (day 4 post-infection, D4).

G EdU incorporation (green, 2 h) was visualized by confocal imagery in GSC#1 or by FACS in GSC#9 transfected with sic or si*MALT1*. In GSC#1, the percentage of EdU-positive cells was quantified. Nuclei (DAPI) are shown in blue. $n > 240$ cells per replicate. Scale bar: 10 μm. Data are presented as the mean ± SEM on three independent experiments.

H FACS analysis of propidium iodide (PI) incorporation in GSC #1 and #9 transfected with non-silencing duplexes (sic) or *MALT1* siRNA duplexes (si*MALT1*) and analyzed 72 h later.

I Linear regression plot of *in vitro* limiting dilution assay (LDA) for control (shc) or sh*MALT1* seq#1 and seq#2 transduced GSC#9. Data are representative of $n = 2$. Knockdown efficiency was verified at day 3 by Western blot using anti-MALT1 antibodies. GAPDH served as a loading control.

J Tumorspheres per field of view (fov) were manually counted in sic or si*MALT1* transfected GSC#1, #4, and #9. Data are presented as the mean ± SEM on three independent experiments.

Data information: All data are representative of $n = 3$, unless specified. Statistics were performed using pairwise comparisons (Tukey's honest significant difference (HSD) with a 95% confidence interval for panels C–E), and a two-tailed *t*-test with a 95% confidence interval for panels (G and J), $*P < 0.05$, $**P < 0.01$, $***P < 0.001$, and $****P < 0.0001$.

Source data are available online for this figure.

brain-originated human cells (endothelial cells, astrocytes, and neurons), ruling out a non-selectively toxic effect (Fig 2E). Differentiated sister GSCs (DGCs) also showed reduced viability in response to MPZ, indicating that targeting MALT1 may have a pervasive effect on differentiated GBM tumor cells (Fig 2H).

MPZ is a drug, belonging to the phenothiazine family, and was formerly used in the treatment of schizophrenia (Lomas, 1957). Several anti-psychotic phenothiazines have been shown to potentially reduce glioma growth (Tan *et al*, 2018). We therefore evaluated whether clinically relevant phenothiazines could affect GSC viability (Fig EV1A–E). The effect on MALT1 inhibition was reflected in cell viability, with chlorpromazine (Oliva *et al*, 2017) and fluphenazine having robust effects on cell viability (Fig 2I). In addition to its effect on MALT1 protease activity (Fig EV1B and C) (Nagel *et al*, 2012; Schlauderer *et al*, 2013), MPZ may also exert off-target biological effects (Meloni *et al*, 2018). We took advantage of the well-characterized MPZ-resistant E397A MALT1 mutant (Schlauderer *et al*, 2013) to challenge the toxic action of phenothiazines in GSCs (Fig EV1F). E397A MALT1 expression in GSCs partially restored cell viability in phenothiazine-treated cells, suggesting that the main target of phenothiazine-mediated death involves MALT1 inhibition (Fig EV1F). Because MPZ has been shown to efficiently and safely obliterate MALT1 activity in experimental models (Nagel *et al*, 2012; McGuire *et al*, 2014; Kip *et al*, 2018; Di Pilato *et al*, 2019; Rosenbaum *et al*, 2019), ectopically implanted GSC#9 mice were challenged with MPZ. Daily MPZ administration reduced tumor volume in established xenografts, as well as NESTIN-positive staining (Fig 2J and K). This effect was prolonged for the week of measurement following treatment withdrawal (Fig 2J). Together, these data demonstrate that targeting MALT1 pharmacologically is toxic to GBM cells *in vitro* and *in vivo*.

GSCs maintain basal protease activity of MALT1

In addition to its scaffold function in the modulation of the NF-κB pathway, MALT1 also acts as a protease for a limited number of substrates (Juilland & Thome, 2018; Thys *et al*, 2018). No hallmarks of NF-κB activation such as phosphorylation and degradation of IκBα, or p65 and cREL nuclear translocation were observed, unless GSCs were treated with TNFα (Fig 3A and B). Nevertheless, the deubiquitinating enzyme CYLD (Staal *et al*, 2011) and the RNA-binding proteins ROQUIN 1 and 2 (Jeltsch *et al*, 2014), two known MALT1 substrates, were constitutively cleaved in GSCs (Fig 3C–F). This was, however, not the case of the MALT1 target HOIL1 (Douanne *et al*, 2016), suggesting that only a subset of MALT1 substrates is cleaved in GSCs (Fig 3C). Of note, CYLD proteolysis was not further increased upon stimulation with PMA plus ionomycin, in contrast to Jurkat lymphocytes, most likely due to a failure to co-opt this signaling route in GSCs (Fig 3C). However, CYLD processing was reduced in cells treated with MPZ or upon siRNA-mediated *MALT1* knockdown (Fig 3D and E). The same was true when MALT1 competitive inhibitor Z-VRPR-FMK was used (Fig 3F). Further supporting a role for MALT1 enzyme in GSCs, the expression of a protease-dead version of MALT1 (C464A) weakened CYLD trimming (Fig 3G and H). Interestingly, we found that refreshing medium also reduced CYLD cleavage, suggesting that MALT1 basal activity may rely on outside-in signals rather than cell autonomous misactivation (Fig 3I).

The activation of MALT1 habitually occurs within the microenvironment of the CBM complex (Thys *et al*, 2018). Accordingly, the knocking down of the CBM components *BCL10* or *CARD10* (i.e., CARMA3) also decreased CYLD processing (Fig 3J and K). In keeping with this, *BCL10*-silenced GSC#9 cells showed a reduction in cell viability (Fig 3K), therefore recapitulating the effect of knocking down MALT1. These data reinforce the hypothesis that a fraction of MALT1 is most likely active in growing GSCs, outside its canonical role in antigen receptor signaling and immune cancer cells.

MALT1 inhibition alters endo-lysosome homeostasis

To evaluate cell death modality triggered by MALT1 inhibition, transmission electron microscopy (TEM) was deployed to visualize

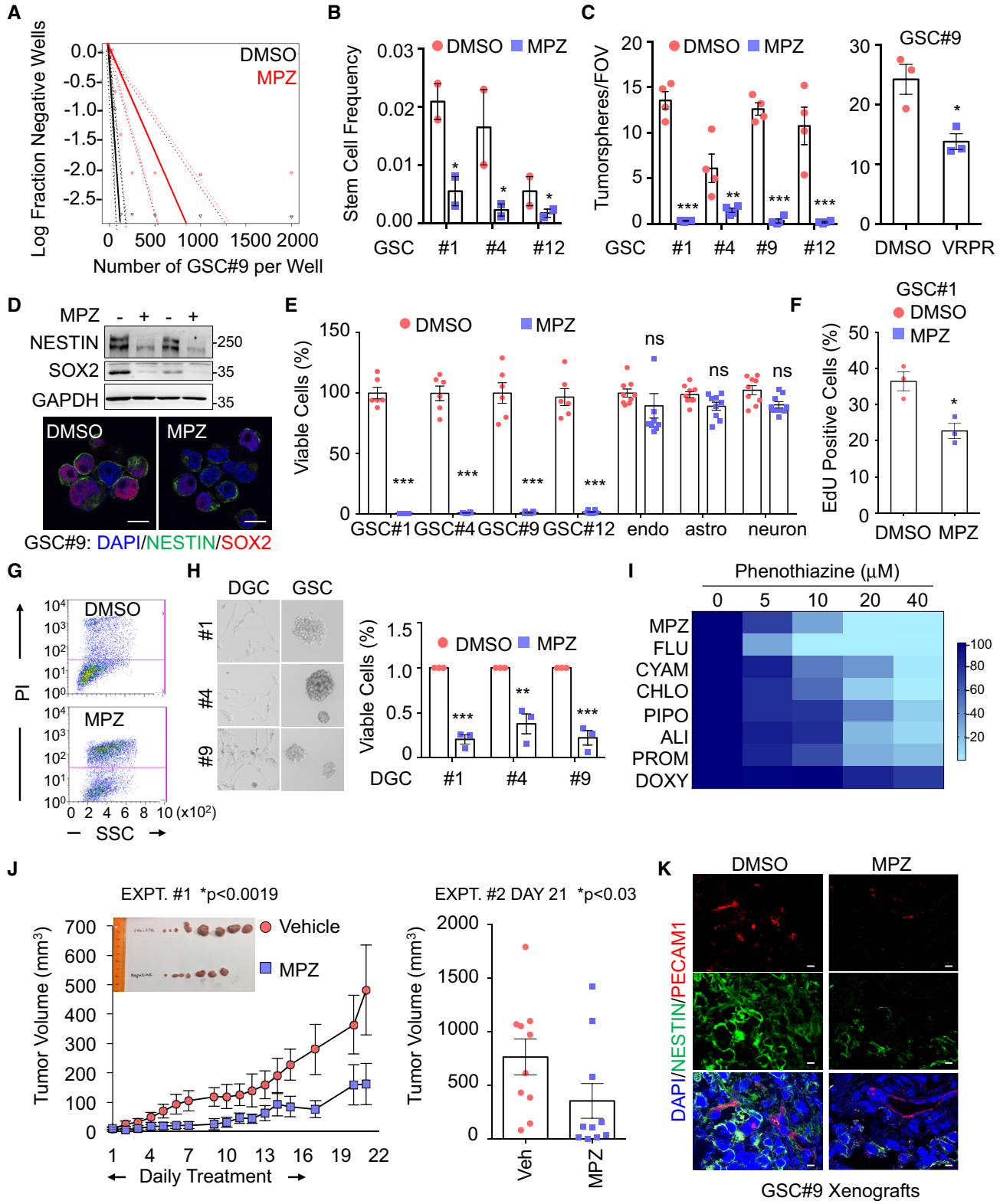
A
Log Fraction Negative Wells
DMSO
MPZ
Number of GSC#9 per Well
B
Stem Cell Frequency
DMSO MPZ
GSC #1 #4 #12
C
Tumorspheres/FOV
DMSO MPZ
GSC #1 #4 #9 #12
GSC#9
DMSO VRPR
D
MPZ - + - +
NESTIN
SOX2
GAPDH
DMSO
MPZ
GSC#9: DAPI/NESTIN/SOX2
E
Viable Cells (%)
DMSO MPZ
ns
GSC#1 GSC#4 GSC#9 GSC#12 endo astro neuron
F
GSC#1
DMSO
MPZ
EdU Positive Cells (%)
DMSO MPZ
G
DMSO
MPZ
PI
SSC
H
DGC GSC
#1
#4
#9
Viable Cells (%)
DMSO MPZ
DGC #1 #4 #9
I
Phenothiazine (μM)
0 5 10 20 40
MPZ
FLU
CYAM
CHLO
PIPO
ALI
PROM
DOXY
J
EXPT. #1 *p<0.0019
Vehicle
MPZ
Tumor Volume (mm3)
Daily Treatment
EXPT. #2 DAY 21 *p<0.03
Tumor Volume (mm3)
Veh
MPZ
K
DMSO
MPZ
DAPI/NESTIN/PECAM1
GSC#9 Xenografts

Figure 2.

Figure 2. MALT1 pharmacological inhibition is lethal to glioblastoma cells.

A Linear regression plot of *in vitro* limiting dilution assay (LDA) for GSC#9 treated with MALT1 inhibitor, mepazine (MPZ, 20 μM, 14 days). DMSO vehicle was used as a control. Data are representative of $n = 2$.

B Stem cell frequency was calculated from LDA in GSCs #1, #4, and #12 treated with MPZ treatment (20 μM, 14 days). Data are presented as the mean ± SEM on two independent experiments.

C Tumorspheres per field of view (fov) were manually counted in GSCs #1, #4, #9, and #12 in response to MPZ (20 μM) and vehicle (DMSO), and in GSC#9 treated with Z-VRPR-FMK (75 μM) and vehicle (H_2O) for 4 days. Data are presented as the mean ± SEM on 4 independent experiments for MPZ and three independent experiments for Z-VRPR-FMK.

D The expression of the stemness markers SOX2 and NESTIN was evaluated by Western blot and immunofluorescence (SOX2 in red NESTIN in green) in MPZ (+, 20 μM, 16 h) and vehicle (−, DMSO, 16 h) treated GSC#9. GAPDH served as a loading control. Scale bar: 10 μm.

E Cell viability was measured using Cell TiterGlo luminescent assay in GSCs #1, #4, #9, and #12, human brain endothelial cells (endo), human astrocytes (astro), and human neuron-like cells (neuron) treated for 48 h with DMSO or MPZ (20 μM). Data were normalized to their respective DMSO-treated controls and are presented as the mean ± SEM of three independent experiments in triplicate.

F FACS analysis of EdU staining was performed on GSC#1 treated overnight with MPZ (10 μM). Data are presented as the mean ± SEM on three independent experiments.

G FACS analysis of propidium iodide (PI) incorporation in GSC#9 treated for 48 h with vehicle (DMSO) or MPZ (20 μM).

H Cell viability was measured using Cell TiterGlo luminescent assay in differentiated GSC#1 #4, and #9 (DGCs) treated for 48 h with vehicle (DMSO) or MPZ (20 μM). Data were normalized to their respective DMSO-treated controls and are presented as the mean ± SEM of three independent experiments. Morphology of GSCs #1, #4, #9, and DGCs #1, #4, #9 was shown using brightfield images.

I Heatmap of cell viability of GSC#9 using increasing doses (0, 5, 10, 20, 40 μM) of phenothiazines: mepazine (MPZ), fluphenazine (FLU), cyamemazine (CYAM), chlorpromazine (CHLO), pipotiazine (PIPO), alimemazine (ALI), promethazine (PRO), and doxylamine (DOXY). Data were normalized to their respective DMSO-treated controls.

J Nude mice were implanted with GSC#9 (10^6 cells) in each flank, and randomized cages were treated with either vehicle (DMSO) or MPZ (8 mg/kg) daily i.p., for 14 consecutive days, once tumors were palpable. Tumor volume was measured from the start of treatment until 1 week after treatment was removed. Graph of tumor volume on day 21 post-treatment is presented. Data are presented as the mean ± SEM $n = 10$/group.

K Cryosections from GSC-xenografted tumors were stained for the endothelial marker PECAM1 (red) and tumor marker NESTIN (green). Nuclei (DAPI) are shown in blue. Scale bar: 20 μm.

Data information: All data are representative of $n = 3$, unless specified. Statistics were performed using a two-tailed *t*-test with a 95% confidence interval for panels (B, C, E, F, H), a two-way ANOVA with Bonferroni post-test at 95% confidence interval for panel (J), a Wilcoxon–Mann–Whitney test for Expt #2 with *P*-values stated for panel (J). $*P < 0.05$ $**P < 0.01$, $***P < 0.001$.

Source data are available online for this figure.

morphological changes upon MPZ treatment. TEM images showed increased vacuoles and lysosomes compared to control cells (Fig 4A). The augmentation was also visible in si*MALT1*-transfected cells (Fig EV2A). In fact, the abundance of the endo-lysosome protein LAMP2 was amplified upon MALT1 inhibition with MPZ, in a time-dependent manner (Figs 4B and EV2B). Additionally, treatment with the MALT1 competitive inhibitor Z-VRPR-FMK, other phenothiazines, or *MALT1* knockdown resulted in similar LAMP2 increase (Figs 4C–E and EV1D), therefore militating against putative drug-related action or deleterious accumulation in lysosomes. Moreover, the ectopic expression of a protease-dead MALT1 mutant (C464A) mimicked MPZ effect on lysosome staining, using the lysotracker probe (Fig 4D). In addition, CTSD and Rab7 endo-lysosomal protein levels were up-regulated as well upon MALT1 blockade (Figs 4C and EV2C). Conversely, other cellular organelles (early endosomes, mitochondria, Golgi, and peroxisomes) remained unchanged upon MPZ treatment (Fig EV2B and D). Furthermore, ectopic tumors, excised from mice challenged with a MPZ 2-week regime, showed a marked gain in LAMP2 staining intensity and protein amount, as compared to vehicle-treated tumors (Fig 4F). Finally, the treatment with MPZ of the ABC DLBCL lymphoma cell line HBL1, which displays constitutive MALT1 activity, also led to an increase in LAMP2 protein amount (Fig EV2E), indicating that MALT1's effect on lysosomal homeostasis might not be limited to GSCs.

The newly formed endo-lysosomes in GSCs appeared to be at least partially functional, as evidenced by pH-based Lysotracker staining, DQ-ovalbumin, and transferrin uptake (Figs 4G and EV2F). Of note, at a later time point (16 h) in MPZ-treated cells, DQ-ovalbumin staining was dimmer as compared to early time points (4 h), which might signify lysosomal membrane permeabilization (Fig EV2F). Our data demonstrated that MALT1 knockdown and pharmacological inhibition provoke a meaningful endo-lysosomal increase.

MALT1 inhibition induces autophagic features in GBM cells

Because autophagy is fueled by endo-lysosomal activity, the impact of MALT1 inhibition on autophagy in GSCs was explored and estimated by LC3B modifications. The turnover of LC3B and the degradation of the autophagy substrate P62 also reflect autophagic flux (Loos *et al*, 2014). Treatment with MPZ led to a significant increase in LC3B puncta at later time points (16 h), subsequent to lysosomal increase (4 h) (Fig 5A, left panel). Super-resolution microscopy using structured illumination microscopy (SIM) further revealed that these LC3 structures were covered with LAMP2-positive staining (Fig 5A, right panel). Upon MPZ treatment, there was also an accumulation of lipidated LC3B (LC3B-II) and P62 protein amount over time, suggesting impaired autophagic flux (Fig 5B). Likewise, there was an increase in lipidated LC3B protein amount in cells that received phenothiazines or were knocked down for MALT1 (Figs EV1D and 5C). Of note, chloroquine treatment did not further augment LC3 lipidation (Fig 5C and D). The effect of MPZ was concomitant with a reduced LC3B turnover, as evaluated via luciferase assay (Fig 5E), and P62 puncta accumulation in cells treated with MPZ and Z-VRPR-FMK, or knocked down for MALT1 (Fig 5F). Taken together, this suggests that MALT1 inhibition impairs autophagic flux in GSCs.

Lysosomes are the cornerstone of MPZ-induced cell death

To evaluate precisely the mechanism of cell death by MPZ, caspases were simultaneously blocked with Q-VD-OPh (QVD) (Fig 5G and H). However, this did not thwart MPZ-mediated cell death, suggesting another mechanism than apoptosis. Meanwhile, chloroquine treatment did not impact GSC#9 viability (Fig EV3A). Further, cells, in which autophagy was inhibited via knockdown of *BECN1* (*i.e.*,

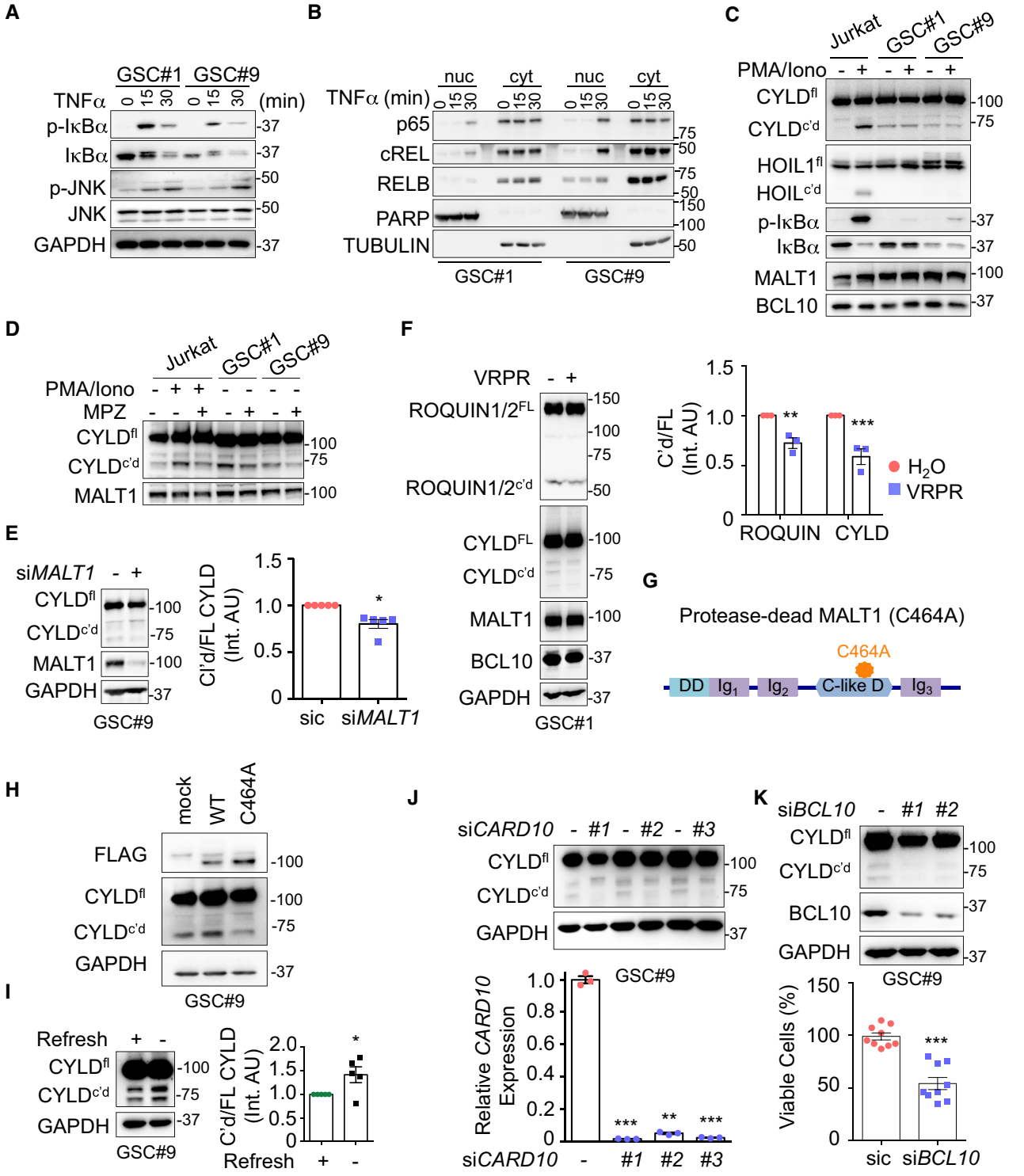

Figure 3.

Figure 3. MALT1 is active in GSCs.

A Total protein lysates from GSCs #1 and #9 challenged with TNFα (10 ng/ml, for the indicated times) were analyzed by Western blot for p-IκBα, IκBα, and p-JNK. Total JNK and GAPDH served as loading controls.

B Western blot analysis of p65, cREL, and RELB in cytosolic (cyt) and nuclear (nuc) cell fractionation from GSC#1 and GSC#9 stimulated with TNFα (10 ng/ml, for the indicated times). TUBULIN and PARP served as controls for each fraction.

C Jurkat T cells, GSC#1, and GSC#9 were stimulated with PMA (20 ng/ml) and ionomycin (Iono, 300 ng/ml) for 30 min. Total protein lysates were analyzed by Western blot for CYLD (full length, FL, and cleaved, c'd), HOIL1 (full length, FL, and cleaved, c'd), p-IκBα and IκBα. MALT1 and BCL10 served as loading controls.

D Jurkat T cells, GSC#1, and GSC#9 were treated with vehicle (DMSO) and mepazine (MPZ, 20 μM) for 4 h. PMA/ionomycin mixture was also administered to Jurkat cells for the last 30 min. Total protein lysates were analyzed by Western blot for CYLD (full length, FL, and cleaved, c'd). MALT1 served as a loading control.

E Western blot analysis of CYLD (full length, FL, and cleaved, c'd) and MALT1 in total protein lysates from GSC#9 transfected with non-silencing RNA duplexes (sic) or *MALT1* targeting duplexes (si*MALT1*). GAPDH served as a loading control. Densitometric analysis of c'd CYLD/FL CYLD was performed (right). Data are presented as the mean ± SEM on five independent experiments.

F (Left) Western blot analysis of CYLD, ROQUIN1/2, MALT1, and BCL10 in total protein lysates from GSC#9 treated for 4 h with vehicle (H_2O) or Z-VRPR-FMK (75 μM). GAPDH served as a loading control. (Right) Densitometric analysis of c'd/FL was performed for ROQUIN1/2 and CYLD. Data are presented as the mean ± SEM on three independent experiments.

G Schematic drawing of MALT1 structures highlighting the C464A substitution in the protease-dead version. DD: death domain, C-like D: caspase-like domain, Ig: immunoglobulin domain.

H Western blot analysis of CYLD and FLAG in total protein lysates from GSC#9 transfected with WT or C464A MALT1-FLAG. GAPDH served as a loading control.

I Western blot of CYLD (full length, FL, and cleaved, c'd) in total protein lysates from GSC#9 after refreshing the medium (+), as compared to 3-day-old culture (−). GAPDH served as a loading control. Densitometric analysis of c'd/FL CYLD was performed. Data are presented as the mean ± SEM on five independent experiments.

J Western blot analysis of CYLD (full length, FL, and cleaved, c'd) in total protein lysates from GSC#9 transfected with non-silencing RNA duplexes (sic) or *CARD10* targeting duplexes (si*CARD10 seq#1*, *seq#2*, and *seq#3*). GAPDH served as a loading control. qPCR analysis confirmed the knockdown of *CARD10* in GSC#9. Data are presented as the mean ± SEM on three independent experiments.

K Western blot analysis of CYLD and BCL10 in total protein lysates from GSC#9 transfected with non-silencing RNA duplexes (sic) or *BCL10* targeting duplexes (si*BCL10, seq#1*, and *seq#3*). GAPDH served as a loading control. Cell viability was measured using Cell TiterGlo luminescent assay in sic and seq#1 si*BCL10*-transfected cells. Data were normalized to their respective sic-treated controls and are presented as the mean ± SEM of three independent experiments, in triplicate.

Data information: All data are representative of $n = 3$, unless specified. Statistics were performed using a two-tailed *t*-test with a 95% confidence interval. $*P < 0.05$, $**P < 0.01$, $***P < 0.001$.

Source data are available online for this figure.

BECLIN1), were not protected either, suggesting that autophagy might be secondary to MPZ-induced cell death (Fig EV3B). Nonetheless, there was increased CTSD release by GSCs treated with MPZ or silenced for *MALT1*, which could signify either lysosomal membrane permeabilization or increased secretion of lysosomal enzymes (Fig 5I). Accordingly, treatment with lysosomal enzyme inhibitors partially rescued cells from MPZ-induced cell death (Fig 5J). Thus, lysosomes participate in MPZ-induced cell death, while MALT1 appears to be required to maintain innocuous level of endo-lysosomes in GSCs.

MALT1 modulates the lysosomal mTOR signaling pathway

In order to further characterize the mode of action of MALT1 inhibition in GSCs, we performed RNA-sequencing analysis on GSCs treated with MPZ for 4 h, prior to any functional sign of death. Our results identified 7474 differentially expressed genes, among which 9/10 randomly chosen top candidates were validated in both MPZ-treated and MALT1-silenced cells (Figs 6A and EV3C, Table EV1). No obvious endo-lysosomal protein encoding genes were found, which was further confirmed by qPCR (Fig 6A–E, Table EV1). Of note, VGF, recently shown to promote GSC/DGC survival, was down-regulated upon MPZ treatment (Wang *et al*, 2018a) (Figs 6E and EV3C, Table EV1). In line with a non-transcriptional regulation of lysosome biogenesis, knockdown of the master regulator of lysosomal transcription TFEB (Sardiello *et al*, 2009) failed to reduce autophagy signature and CTSD protein up-regulation upon MPZ treatment (Fig 6F). We thus hypothesized that the observed endo-lysosomal increase was due to modulation in their translation and/or RNA metabolism. When translation was blocked with cycloheximide, MPZ failed to increase endo-lysosomal protein amounts (Fig EV3D). Likewise, RNAseq analysis unveiled putative changes in translation (peptide chain elongation, ribosome, co-translational protein targeting, 3′-UTR mediated translational regulation), RNA biology (influenza viral RNA, nonsense mediated decay), metabolism (respiratory electron transport, ATP synthesis, oxidative phosphorylation, respiratory electron transport), and an mTOR signature (referred as Bilanges serum and rapamycin-sensitive genes) (Fig 6C and D). Because mTOR sustains GSC expansion and its activation is linked to lysosomal biogenesis (Yu *et al*, 2010; Galan-Moya *et al*, 2011; Settembre *et al*, 2012), we further explored this possibility. Notably, MALT1 activity has been shown to participate in mTOR activation upon antigen receptor engagement, although the mechanism of action remains poorly understood (Hamilton *et al*, 2014; Nakaya *et al*, 2014). In fact, MPZ and phenothiazine pharmacological challenge, as well as *MALT1* siRNA blunted mTOR activation in GSCs, as evaluated through the phosphorylation of AKT, p70S6K, and S6 ribosomal protein (Figs 6G–I and EV3E). MPZ treatment also reduced inhibitory phosphorylation of autophagy regulator ULK1 at serine 757 (Fig 6G), which may partially account for increased autophagic features upon MPZ treatment. In addition, the enforced expression of protease-dead MALT1 (C464A) reduced S6 phosphorylation levels, reiterating the importance of MALT1 catalytic activity in the observed phenotype (Fig 6J). Furthermore, as phosphorylation of 4EBP1 increases protein translation by releasing it from EIF4E (Gingras *et al*, 1998), and as it can be resistant to mTOR inhibition (Qin *et al*, 2016), we evaluated 4EBP1 phosphorylation levels over time in response to MPZ (Fig EV3F). Although reduced shortly upon MPZ addition, phosphorylation returned at later time points, which may allow for the observed translational effect despite mTOR inhibition. As mTOR signaling is intimately linked to lysosomes (Korolchuk *et al*,

2011), we explored the impact of MPZ treatment on mTOR positioning. Confocal microscopy analysis revealed that mTOR staining no longer colocalized with LAMP2-positive structures upon treatment with MPZ (Figs 6K and EV3G). Interestingly, TFEB silencing did not influence mTOR recruitment at endo-lysosomes (Fig EV3H). Conversely, mTOR staining appears dispersed from LAMP2 puncta upon Z-VRPR-FMK, phenothiazines treatment, or knockdown of MALT1 (Fig 6K). These results suggest that MALT1 affects lysosomal homeostasis post-transcriptionally, and that the increase in endo-lysosomes coincides with weakening of the mTOR signaling, which may be due to displacement of mTOR from its lysosomal signaling hub.

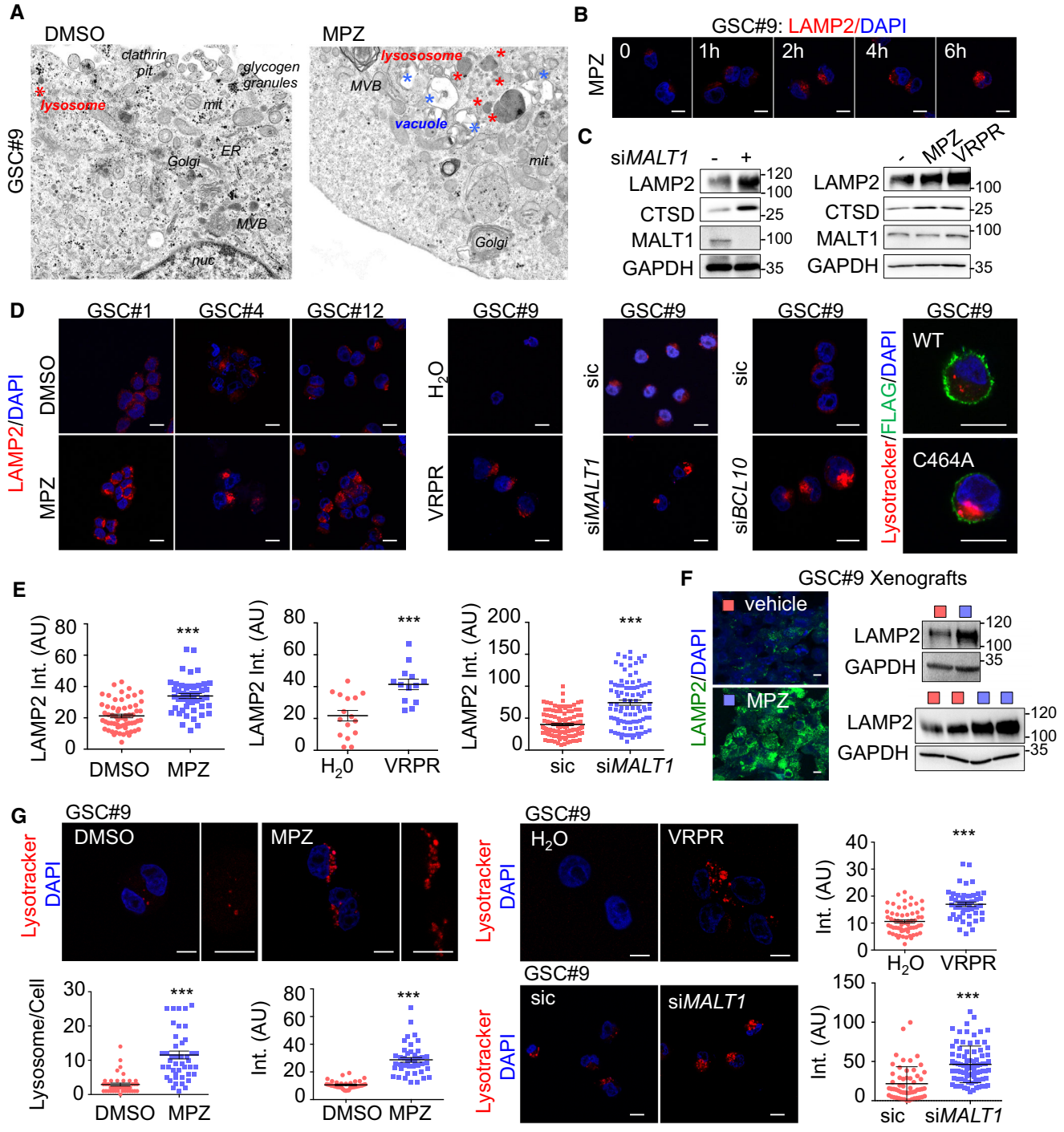

Figure 4.

Figure 4. MALT1 pharmacological inhibition alters endo-lysosome homeostasis.

A Transmission electron microscopy of GSC#9 treated with vehicle (DMSO) or MPZ (20 μM) for 16 h. ER: endoplasmic reticulum; MVB: multivesicular bodies; lys: lysosome; mit: mitochondria; nuc: nucleus. Red stars denote lysosomes; blue stars vacuoles.

B Confocal analysis of LAMP2 staining (red) at 0, 1, 2, 4, and 6 h post-MPZ (20 μM) treatment. Nuclei (DAPI) are shown in blue. Scale bar: 10 μm.

C Western blot analysis was performed in total protein lysates from GSC#9 transfected with non-silencing duplexes (sic) or *MALT1* targeting siRNA duplexes (si*MALT1*). Alternatively, Western blot analysis of LAMP2, CTSD, and MALT1 was done in total protein lysates from GSC#9 treated for 16 h with MPZ (20 μM) or Z-VRPR-FMK (75 μM). DMSO was used as vehicle. GAPDH served as a loading control.

D Confocal analysis of LAMP2 staining (red) in GSCs #1, #4, #12 treated for 16 h with vehicle (DMSO) or MPZ (20 μM). Alternatively, GSC#9 were either treated for 16 h with H_2O or Z-VRPR-FMK (75 μM). Additionally, cells were transfected with non-silencing duplexes (sic) or MALT1 and BCL10 targeting siRNA duplexes (si*MALT1* and si*BCL10*). Alternatively, lysotracker staining (red) was used to track for lysosomes in either GSC#9 expressing either wild-type (WT) or C464A FLAG-MALT1 (green). Scale bar: 10 μm.

E Quantification of LAMP2 staining pixel intensity on GSC#9 treated as described in panel (D). Data are presented as the mean ± SEM on three independent experiments. Each dot represents one cell. $n > 30$.

F Cryosections from GSC#9-xenografted tumors in vehicle and MPZ-challenged animals (as described in Fig 2J) and assessed for LAMP2 staining (green). Nuclei (DAPI) are shown in blue. Scale bar: 10 μm. Western blot analysis of LAMP2 was performed in tumor lysates. GAPDH served as a loading control.

G Confocal analysis of lysotracker staining (red) in GSC#9 treated for 16 h with vehicle (DMSO) or MPZ (20 μM). Alternatively, GSC#9 were either treated for 16 h with H_2O or Z-VRPR-FMK (75 μM) (upper panel) or transfected with sic and si*MALT1* (bottom panel). As indicated, number of lysotracker-positive puncta and lysotracker pixel intensity (arbitrary unit, AU) were quantified per cell. Data are presented as the mean ± SEM on three independent experiments. Each dot represents one cell. $n > 30$. Nuclei (DAPI) are shown in blue. Scale bars: 10 μm.

Data information: All data are representative of $n = 3$, unless specified. Statistics were performed using a two-tailed *t*-test with a 95% confidence interval. ***$P < 0.001$.

Source data are available online for this figure.

MALT1 is negatively linked to the endo-lysosomal regulator QKI

Shinghu *et al* recently demonstrated that the RNA-binding protein Quaking (QKI) regulates endo-lysosomal levels in GBM. They showed that GBM-initiating cells maintain low levels of endo-lysosomal trafficking in order to reduce receptor recycling (Shingu *et al*, 2016). QKI was suggested to regulate RNA homeostasis of endo-lysosome elements, independently of the TFEB-driven endo-lysosome biogenesis. TCGA analysis confirmed the prognosis value of QKI expression in GBM, as patients with higher expression of QKI had a slight survival advantage (Fig 7A). As our data suggest a counterbalancing role of MALT1 in lysosomal biogenesis, we revisited the TCGA and compared the expression of *MALT1* with that of *QKI* in GBM patients. Interestingly, there was a negative correlation between the levels of expression of the two genes (Fig 7A). In addition, *QKI* and *MALT1* were both linked to the expression of 7 common lysosomal lumen genes (Fig 7A). This prompted us to examine QKI pattern in GBM. First, QKI was indeed expressed in a panel of GSCs, as well as in ectopic xenografts (Fig EV4A). Similarly, human GBM samples from two patients showed pervasive QKI staining (Fig EV4B). As expected (Wu *et al*, 1999), QKI displayed cytosolic and nuclear forms, as evidenced by cellular fractionation and immunofluorescence (Fig EV4C and D). Given these findings, we decided to explore the possible link between MALT1 and QKI in GSCs. Co-immunoprecipitation experiments were thus deployed using QKI and the MALT1 binding partner BCL10 as baits. This showed that MALT1 was pulled down with QKI in GSC#1 and GSC#9, and *vice versa* (Fig 7B). Because MALT1 appeared excluded from nuclear fractions, the QKI/MALT1 interaction most likely occurs in the cytosol (Fig EV4C). Binding was, however, reduced in cells exposed to MPZ or Z-VRPR-FMK (Fig 7C). This suggests that active MALT1 tethered QKI in GSCs, while blocking MALT1 unleashed a fraction of QKI from the BCL10/MALT1 complex. Of note, QKI and MALT1 readily interacted in HBL1 ABC DLBCL lymphoma cells with constitutive MALT1 activation (Fig EV4E).

To next challenge the function of this putative neutralizing interaction of MALT1 and QKI, QKI expression was manipulated to alter QKI/MALT1 stoichiometry in GSCs. Strikingly, transient overexpression of QKI phenocopied the effect of MALT1 inhibition on endo-lysosomes. Reinforcing pioneer findings of QKI action on endo-lysosome components in transformed neural progenitors (Shingu *et al*, 2016), ectopically expressed QKI was sufficient to increase Lysotracker staining, LAMP2 protein amount and lipidated LC3B (Fig 7D–F). Accordingly, the augmented endo-lysosome staining synchronized with mTOR dispersion from a focalized organization, together with a decrease in the level of S6 phosphorylation (Fig 7G and H). Corroborating the surge of endo-lysosomes, the fraction of cells overexpressing QKI was drastically reduced over time, while the fraction of cells expressing an empty vector remained stable, suggesting that exacerbated QKI expression hampered cell viability (Fig 7I). Conversely, cells knocked down for *QKI* did not show the same MPZ-driven increase in LAMP2, CTSD, and lipidated LC3B (LC3B-II), suggesting that *QKI* knockdown can partially rescue cells from endo-lysosomal increase (Fig 7J and K). Reinforcing this idea, the dissipation of mTOR staining from endo-lysosomes and the reduction of S6 protein phosphorylation both provoked upon MPZ treatment were no longer observed without QKI (Fig 7K and L). Finally, double knockdown of QKI and MALT1 rescued cells from decreased proliferation and increased cell death triggered by MALT1 depletion (Figs 7M and N, and EV4F). Thus, *QKI* silencing rescued phenotype upon MALT1 inhibition or knockdown, further indicating that MALT1 is negatively linked to the endo-lysosomal regulator QKI.

Discussion

Here, we provide evidence that the activity of the paracaspase MALT1 is decisive for growth and survival of GBM cells. Our data indicate that MALT1 inhibition causes indiscipline of endo-lysosomal and autophagic proteins, which appears to occur in conjunction with a deficit in mTOR signaling. In addition to the known MALT1 inhibitor mepazine (Nagel *et al*, 2012), we show that several other clinically relevant phenothiazines can potently suppress MALT1 enzymatic activity and have similar effects to MPZ on endo-lysosomes and cell death in GSCs. Our data with MALT1

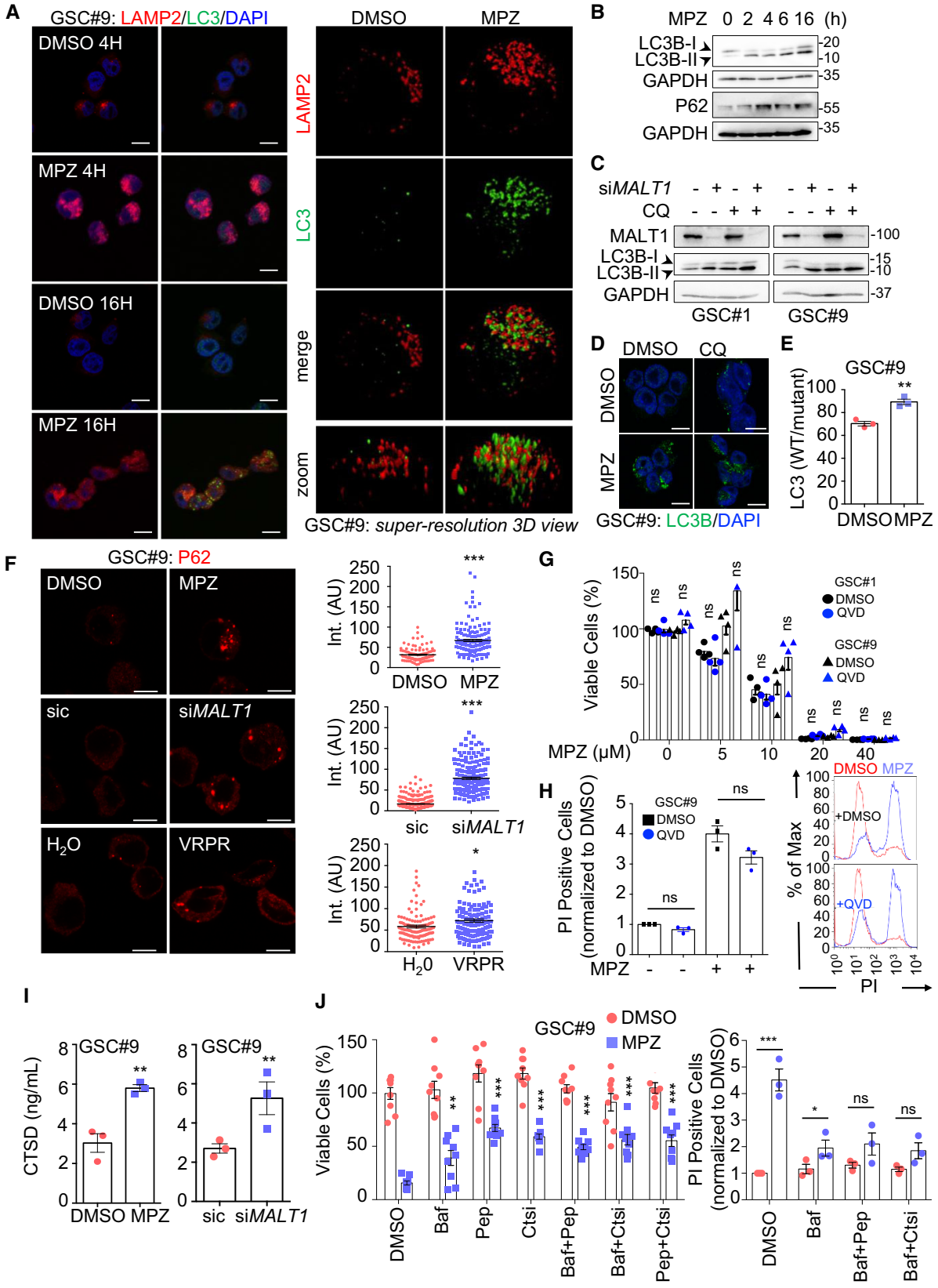
A
GSC#9: LAMP2/LC3/DAPI
DMSO 4H
MPZ 4H
DMSO 16H
MPZ 16H
DMSO
MPZ
LAMP2
LC3
merge
zoom
GSC#9: super-resolution 3D view
B
MPZ 0 2 4 6 16 (h)
LC3B-I
LC3B-II
GAPDH
P62
GAPDH
C
siMALT1
CQ
MALT1
LC3B-I
LC3B-II
GAPDH
GSC#1
GSC#9
D
DMSO
CQ
DMSO
MPZ
GSC#9: LC3B/DAPI
E
GSC#9
LC3 (WT/mutant)
DMSO MPZ
F
GSC#9: P62
DMSO
MPZ
sic
siMALT1
H2O
VRPR
Int. (AU)
DMSO MPZ
sic siMALT1
H2O VRPR
G
Viable Cells (%)
MPZ (μM)
GSC#1
DMSO
QVD
GSC#9
DMSO
QVD
ns
H
PI Positive Cells (normalized to DMSO)
GSC#9
DMSO
QVD
MPZ
% of Max
DMSO MPZ
+DMSO
+QVD
PI
I
CTSD (ng/mL)
GSC#9
DMSO MPZ
sic siMALT1
J
GSC#9
DMSO
MPZ
Viable Cells (%)
DMSO
Baf
Pep
Ctsi
Baf+Pep
Baf+Ctsi
Pep+Ctsi
PI Positive Cells (normalized to DMSO)
DMSO
Baf
Baf+Pep
Baf+Ctsi

Figure 5.

Figure 5. MALT1 inhibition induces autophagic features in GSCs.

A (Left) Confocal analysis of LAMP2 (red) and LC3B (green) in GSC#9 treated for 4 and 16 h with vehicle (DMSO) and MPZ (20 μM). Nuclei (DAPI) are shown in blue. Scale bars: 10 μm. (Right) Super-resolution imaging (SIM, Structured Illumination Microscopy) of LAMP2 (red) and LC3B (green) staining in GSC#9 treated for 16 h with vehicle (DMSO) or MPZ (20 μM).

B Western blot analysis of LC3B and P62 in total protein lysates from GSC#9 at 0, 2, 4, 6, and 16 h post-MPZ treatment (20 μM). GAPDH served as a loading control.

C Western blot analysis of LC3B in total protein lysates from GSCs #1 and #9 at 72 h post-transfection with sic or si*MALT1* and subsequently treated 4 h with vehicle (DMSO) or chloroquine (CQ, 20 μM). Knockdown was verified by MALT1 blotting and GAPDH served as a loading control.

D Confocal analysis of LC3B (green) in GSC#9 treated for 16 h with vehicle (DMSO) and MPZ (20 μM) with or without chloroquine (CQ, 20 μM). Nuclei (DAPI) are shown in blue. Scale bars: 10 μm.

E GSC#9 were transfected with LC3B reporters (wild-type WT or G120A mutant, which cannot be lipidated), treated 24 h later with vehicle (DMSO) or MPZ (20 μM) for 6 more hours. Ratios of WT/mutant luciferase signals are presented as the mean ± SEM of three independent experiments.

F Confocal analysis of P62 staining (red) in GSC#9 treated for 16 h with vehicle (DMSO) or MPZ (20 μM). Alternatively, GSC#9 was either transfected with sic or si*MALT1* (middle) or treated for 16 h with H_2O or Z-VRPR-FMK (75 μM) (bottom). Quantification of P62 staining pixel intensity on GSC#9 treated for 16 h with vehicle (DMSO or H_2O), MPZ (20 μM) or Z-VRPR-FMK (75 μM) or sic and si*MALT1*. Data are presented as the mean ± SEM on three independent experiments. Each dot represents one cell. $n > 30$.

G Cell viability was measuring using Cell TiterGlo in GSCs #1 and #9 pre-treated for 1 h with vehicle (DMSO) or QVD (20 μM) and treated for 72 h more with the indicated doses of MPZ. Data were normalized to the vehicle-treated controls and are presented as the mean ± SEM of 4 independent experiments.

H FACS analysis of propidium iodide (PI) incorporation in GSC#9 treated for 48 h with vehicle (DMSO) or MPZ (15 μM) in combination with QVD (20 μM). (Left) Percentage of PI-positive cells, normalized to vehicle-treated controls are presented as the mean ± SEM on three independent experiments. (Right) Histogram plots for representative experiment (DMSO in red and MPZ in blue).

I CTSD ELISA was performed on culture media from GSC#9 treated for 8 h with vehicle (DMSO) or MPZ (20 μM). Alternatively, cells were transfected with sic or si*MALT1* and analyzed 72 h later. Data are presented as the mean ± SEM of three independent experiments.

J (Left) Cell viability was measured using Cell TiterGlo luminescent assay in GSC#9 treated for 48 h with vehicle (DMSO) or MPZ (10 μM), following a 30-min pre-treatment with the following drugs: Bafilomycin A1 (Baf, 100 nM), pepstatin A (Pep, 1 μg/ml), or CTS inhibitor 1 (Ctsi, 1 μM). Data were normalized to the vehicle-treated controls and are presented as the mean ± SEM of three independent experiments in triplicate, stars refer to comparison to vehicle + MPZ group (blue squares). (Right) FACS analysis of propidium iodide (PI) incorporation in GSC#9 treated for 48 h with vehicle (DMSO) or MPZ (15 μM) in combination with Baf, Pep, and Ctsi. Percentage of PI-positive cells normalized to vehicle-treated controls are presented as the mean ± SEM on three independent experiments.

Data Information: All data are representative of $n = 3$, unless specified. Statistics were performed using a two-tailed *t*-test with a 95% confidence interval for all experiments with *P*-values stated, except panel (G, H, J), which used a two-way ANOVA with Bonferroni post-test at 95% confidence interval. $*P < 0.05$, $**P < 0.01$, $***P < 0.001$.

Source data are available online for this figure.

and BCL10 silencing, as well as the expression of catalytically dead MALT1, clearly support a role for MALT1 in maintaining the endo-lysosomal homeostasis in GSCs. Although pharmacological inhibitors largely recapitulated the phenotype obtained with molecular interference, nonselective action of drugs remains of concern when it comes to clinics. Indeed, because some of the less potent MALT1 inhibitors, such as promethazine (Nagel *et al*, 2012; Schlauderer *et al*, 2013), also provoke changes LAMP2 and LC3B-II increase, we cannot exclude that some of the lysosomal effects of phenothiazine derivatives result from potential off-target accumulation in the lysosome. Likewise, it has been shown that Z-VRPR-FMK can efficiently inhibit cathepsin B (Eitelhuber *et al*, 2015). Nevertheless, since these drugs efficiently cross the blood–brain barrier in humans (Korth *et al*, 2001) and since they are currently used in the clinic, they represent an exciting opportunity for drug repurposing.

The disruption of endo-lysosomal homeostasis appears to be the main cause of death upon MALT1 inhibition in GSCs. This is aligned with recent findings that define lysosomes as an Achilles' heel of GBM cells (Shingu *et al*, 2016; Le Joncour *et al*, 2019). As CTSD release is accelerated upon MALT1 blockade, and as inhibitors of lysosomal cathepsins (cathepsin inhibitor 1 and pepstatin A), but not pan-caspase blockade (QVD), can partially rescue cell viability, we hypothesize that cells may be dying from a form of caspase-independent lysosomal cell death (LCD) (Aits & Jaattela, 2013). During this form of death, which may also be initiated by cathepsins, lysosomal membrane permeabilization (LMP) allows cathepsins to act as downstream mediators of cell death upon leakage into the cytosol (Aits & Jaattela, 2013). Additional studies will determine how exactly MALT1 inhibition drives lysosomal death in GSCs. Nevertheless, we found that inhibition of cathepsins provides only partial protection to cells treated with MPZ (Fig 4K). Autophagic features may also play a part in cell death. Induction of autophagy likely occurs due to reduced inhibition of ULK1 (Fig 6G) as a consequence of mTOR dispersion from endo-lysosomes (Yu *et al*, 2010; Settembre *et al*, 2012) (Fig 6K). Whether inducing or blocking autophagy is preferable therapeutic strategy in treating GBM remains up for debate, with some groups reporting beneficial effects of blocking autophagy, and others preferring its activation as a therapeutic strategy (Shchors *et al*, 2015; Rahim *et al*, 2017). Here, we show that the observed increased autophagic features are associated with reduced autophagic flux. Impairment in autophagic flux reduces a cell's ability for bulk degradation (Loos *et al*, 2014). Others have shown that lysosomal dysfunction, such as LMP, can impede upon autophagic flux and eventually lead to cell death (Elrick & Lieberman, 2013; Wang *et al*, 2018b). Because of this, we infer that reduced autophagic flux is a downstream consequence of LMP and ultimately contributes to LCD in our cells.

MALT1 has previously been linked to mTOR activity (Hamilton *et al*, 2014; Nakaya *et al*, 2014). For instance, MALT1 was reported to be necessary for glutamine uptake and mTOR activation after T-cell receptor engagement (Nakaya *et al*, 2014). Subsequently, the inhibition of MALT1 with Z-VRPR-FMK causes a reduction in the phosphorylation of S6 and p70S6K (Hamilton *et al*, 2014). Our data now extend these findings to GSCs, although the exact mechanism by which mTORC1 inhibition occurs remains to be explored in both cellular backgrounds. Immunofluorescence analysis of mTOR positioning after MPZ treatment suggests that inhibition of mTOR is linked to its dispersion from the endo-lysosomes, concurrent with

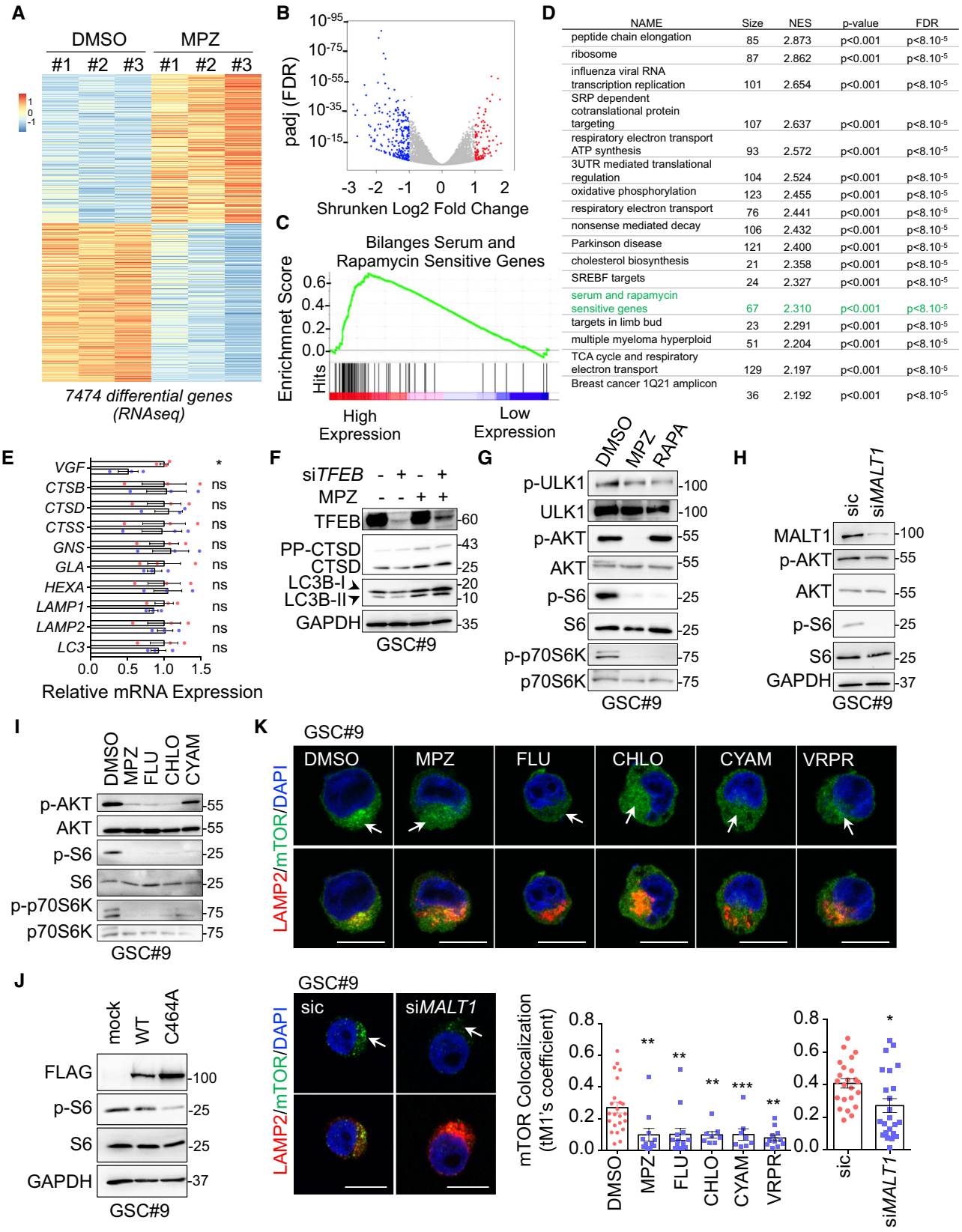

Figure 6.

Figure 6. MALT1 modulates the lysosomal mTOR signaling pathway.

A Heatmap of differentially expressed genes obtained from RNAseq analysis of GSC#9 treated for 4 h with vehicle (DMSO) or MPZ (20 μM), from three biological replicates.

B Volcano plot of differentially expressed genes in RNAseq analysis of GSC#9, expressed as fold changes between vehicle (DMSO) and MPZ-treated cells.

C GSEA (gene set enrichment analysis) plot showing enrichment of "Bilanges serum and rapamycin sensitive genes" signature in vehicle (DMSO) versus MPZ-treated triplicates.

D Table of top differential pathways in DMSO versus MPZ-treated triplicates. Size of each pathway, normalized enrichment scores (NES), *P*-value, and false discovery rate q value (FDR) were indicated.

E qRT–PCR was performed on total RNA from GSC#9 treated for 4 h with vehicle (DMSO) or MPZ (20 μM). Histograms showed changes in RNA expression of indicated targets. Data were normalized to two housekeeping genes (*ACTB*, *HPRT1*) and are presented as the mean ± SEM of technical triplicates.

F Western blot analysis of LC3B, CTSD, and TFEB in total protein lysates from GSC#9 transfected with non-silencing duplexes (sic) or siRNA duplexes targeting *TFEB* (si*TFEB*) and treated with vehicle (DMSO) or MPZ (20 μM) for 16 h. GAPDH served as a loading control.

G Western blot analysis of p-ULK1, p-AKT, p-S6, and p-p70S6K in GSC#9 treated for 1 h with MPZ (20 μM) or rapamycin (RAPA, 50 nM). Total ULK, AKT, S6, and p70S6K served as loading controls. DMSO was used as a vehicle.

H Western blot analysis of MALT1, p-AKT, and p-S6 in total protein lysates from GSC#9 transfected with non-silencing duplexes (sic) or *MALT1* targeting siRNA duplexes (si*MALT1*). Total AKT and S6, as well as GAPDH served as loading controls.

I Western blot analysis of p-AKT, p-S6, and p-p70S6K in total protein lysates from GSC#9 treated for 1 h with vehicle (DMSO) or 20 μM of phenothiazine compounds (MPZ, FLU, CHLO, and CYAM). Total AKT, total S6, and total p70S6K served as loading controls.

J Western blot analysis of p-S6 and FLAG in GSC#9 expressing WT or C464A MALT-FLAG. Total S6 and GAPDH served as loading controls.

K Confocal analysis of LAMP2 (red) and mTOR (green) staining in GSC#9 treated with vehicle (DMSO) or MPZ (20 μM), Z-VRPR-FMK (75 μM), FLU (20 μM), CHLO (20 μM), and CYAM (20 μM). Alternatively, cells were transfected with sic or si*MALT1*. Nuclei (DAPI) are shown in blue. Arrows point to LAMP2-positive area. Scale bars: 10 μm. Quantification of mTOR colocalization score with LAMP2 is shown. The Coloc2 plug-in from ImageJ was used to measure Mander's tM1 correlation factor in LAMP2-positive ROI, using Costes threshold regression. Data are presented as the mean ± SEM on three independent experiments. Each dot represents one cell. $n > 10$.

Data information: All data are representative of $n = 3$, unless specified. Statistics were performed using a two-tailed *t*-test with a 95% confidence interval for all experiments with *P*-values stated. $*P < 0.05$, $**P < 0.01$, $***P < 0.001$.

Source data are available online for this figure.

Figure 7. MALT1 is negatively linked to the endo-lysosomal regulator QKI.

A (Left) Kaplan–Meier curve of the probability of survival for 155 GBM patients with low or high *QKI* RNA level, using median cutoff, based on the TCGA RNAseq dataset. (Right) Differential expression analysis related to either *MALT1* or *QKI* expression highlighted a lysosomal lumen GO function. Venn diagram of overlapping lysosomal enriched protein encoding genes from this comparison showed 7 shared genes, together with 9 and 10 specific genes for *MALT1* and *QKI* expression, respectively. (Bottom) Correlation between *MALT1* and *QKI* expression was analyzed using The Cancer Genome Atlas (TCGA, HG-U133A dataset) on the GlioVis platform (Bowman *et al*, 2007). Pearson correlation factor = −0.21, *P*-value = 0.03.

B GSCs #1 and #9 protein lysates (input) were processed for immunoprecipitation (IP) using control immunoglobulins (Ig), anti-QKI, or anti-BCL10 antibodies. Input and IP fractions were separated on SDS–PAGE and Western blots for MALT1, QKI, and BCL10 antibodies were performed as specified.

C Total protein lysates (input) from GSC#9 treated with vehicle (-, DMSO) or MPZ (+, 20 μM, 1 h) or with vehicle (-, H_2O) or Z-VRPR-FMK (+, 75 μM, 4 h), were processed for control immunoglobulins (Ig) or anti-QKI antibodies immunoprecipitation (IP). Western blots were performed with indicated antibodies. Western blots were performed with indicated antibodies.

D Confocal analysis of Lysotracker (green) or FLAG (red) in GSC#9 overexpressing either empty vector (mock) or FLAG-QKI. Scale bars: 10 μm. Nuclei (DAPI) are shown in blue.

E Confocal analysis of LAMP2 (green) or FLAG (red) in GSC#9 transfected with either empty vector (mock) or FLAG-QKI. Scale bars: 10 μm. Nuclei (DAPI) are shown in blue. Quantification of LAMP2 staining pixel intensity on GSC#9 transfected with mock and FLAG-QKI. Data are presented as the mean ± SEM on three independent experiments. Each dot represents one cell. $n > 15$.

F Western blot analysis of QKI, LAMP2, and LC3B in GSC#9 overexpressing either empty vector (mock) or FLAG-QKI. GAPDH served as a loading control.

G Confocal analysis of mTOR (green) or FLAG (red) in GSC#9 transfected with either empty vector (mock) or Flag-QKI. Nuclei (DAPI) are shown in blue. Scale bars: 10 μm.

H GSC#1 were transfected with either empty vector (mock) or FLAG-QKI. Total protein lysates were processed for Western blots against p-S6 and FLAG. Total S6 served as a loading control.

I Fraction of surviving cells over time in GSCs #1 and #9, transduced with empty vector (mock) or FLAG-QKI bi-cistronic GFP plasmids. Data are plotted as the percentage of GFP-positive cells at the day of the analysis (Dx), normalized to the starting point (Day 4 post-infection, D4). Data are representative of $n = 3$.

J GSC#9 transfected with non-silencing RNA duplexes (sic) or *QKI* targeting siRNA duplexes (si*QKI*) were treated for 16 h with vehicle (DMSO) or MPZ (10 μM). Total protein lysates were processed for Western blots against LAMP2, CTSD, QKI, and LC3B expression, as indicated. GAPDH served as a loading control.

K Confocal analysis of mTOR (green) and LAMP2 (red) in GSC#9 transfected with sic or si*QKI* and treated for 16 h with vehicle (DMSO) or MPZ (20 μM). Nuclei (DAPI) are shown in blue. Scale bars: 10 μm. Quantification of mTOR colocalization score with LAMP2 is shown. The Coloc2 plug-in from ImageJ was used to measure Mander's tM1 correlation factor in LAMP2-positive ROI, using Costes threshold regression. Data are presented as the mean ± SEM on three independent experiments. Each dot represents one cell. $n > 10$.

L GSC#9 transfected with non-silencing RNA duplexes (sic) or *QKI* targeting siRNA duplexes (si*QKI*) were treated for 1 h with vehicle (DMSO) or MPZ (20 μM). Total protein lysates were processed for Western blots against QKI and p-S6. TUBULIN and total S6 served as loading controls.

M FACS analysis of EdU staining was performed on GSC#9 cells transfected with non-silencing RNA duplexes (sic, pink), *QKI* targeting siRNA duplexes (si*QKI*, light purple), *MALT1* targeting siRNA duplexes (si*MALT1*, blue), or double-transfected with si*QKI* and si*MALT1* (purple).

N FACS analysis of propidium iodide (PI) incorporation in GSC#9 transfected with non-silencing RNA duplexes (sic), *QKI* targeting siRNA duplexes (si*QKI*), *MALT1* targeting siRNA duplexes (si*MALT1*) or double-transfected with si*QKI* and si*MALT1* and analyzed 72 h later. Percentage of PI-positive cells normalized to vehicle-treated controls are presented as the mean ± SEM on three independent experiments.

Data information: All data are representative of $n = 3$, unless specified. Statistics were performed using a two-tailed *t*-test with a 95% confidence interval for all experiments with *P*-values stated. $*P < 0.05$.

Source data are available online for this figure.

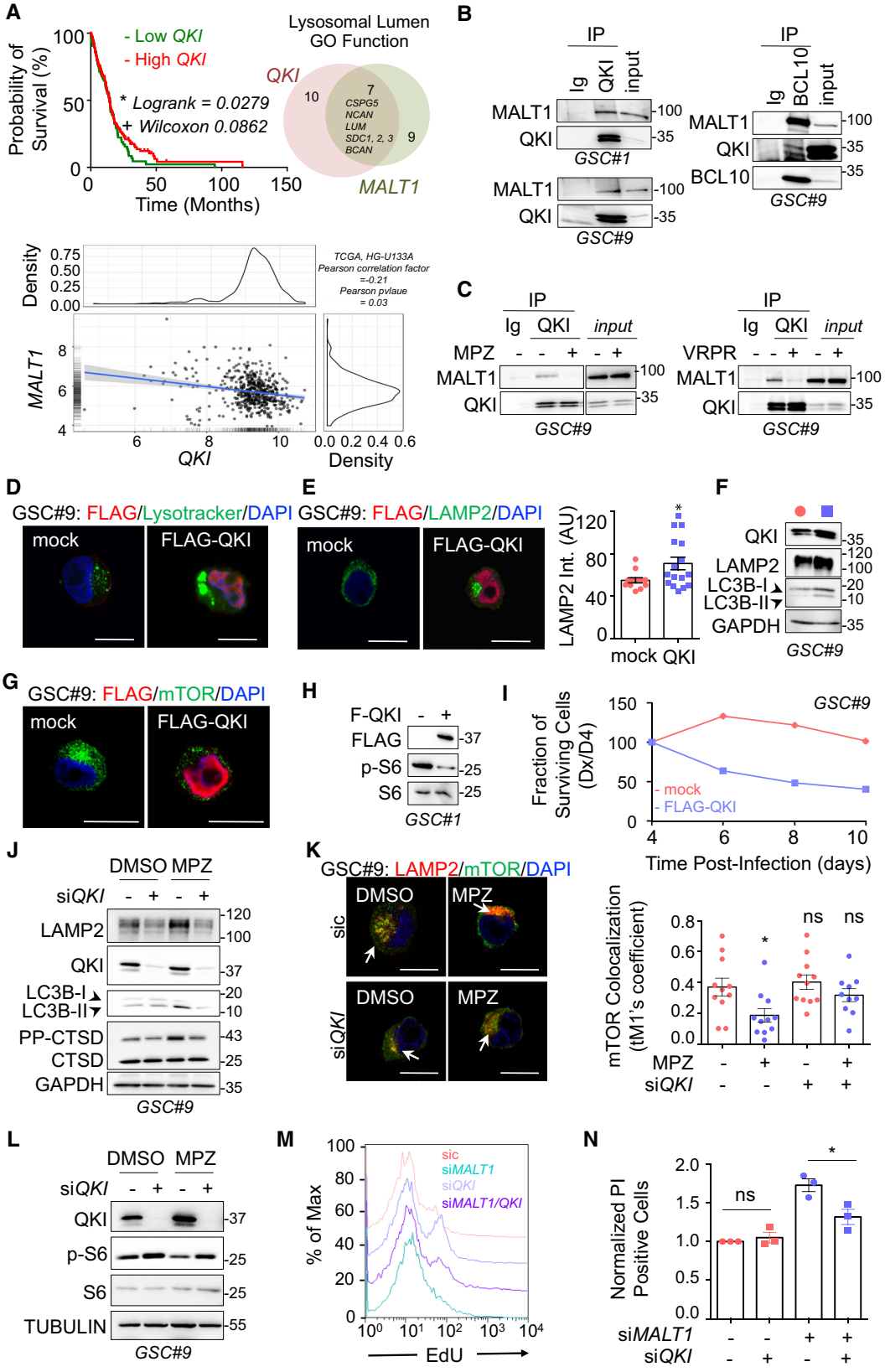
A
Probability of Survival (%)
- Low QKI
- High QKI
* Logrank = 0.0279
+ Wilcoxon 0.0862
Time (Months)
Lysosomal Lumen GO Function
QKI
MALT1
7
CSPG5
NCAN
LUM
SDC1, 2, 3
BCAN
10
9
Density
TCGA, HG-U133A
Pearson correlation factor =-0.21
Pearson pvlaue = 0.03
B
IP
Ig
QKI
input
BCL10
MALT1
GSC#1
GSC#9
C
MPZ
VRPR
D
GSC#9: FLAG/Lysotracker/DAPI
mock
FLAG-QKI
E
GSC#9: FLAG/LAMP2/DAPI
LAMP2 Int. (AU)
mock QKI
F
LAMP2
LC3B-I
LC3B-II
GAPDH
G
GSC#9: FLAG/mTOR/DAPI
H
F-QKI
FLAG
p-S6
S6
I
Fraction of Surviving Cells (Dx/D4)
Time Post-Infection (days)
- mock
- FLAG-QKI
J
DMSO MPZ
siQKI
PP-CTSD
CTSD
K
GSC#9: LAMP2/mTOR/DAPI
sic
DMSO
MPZ
mTOR Colocalization (tM1's coefficient)
ns
L
TUBULIN
M
% of Max
EdU
sic
siMALT1
siQKI
siMALT1/QKI
N
Normalized PI Positive Cells
siMALT1

Figure 7.

lysosomal increase. In addition to a reduction in mTORC1 signaling, AKT phosphorylation was also impaired upon MALT1 inhibition in GSCs. It is thus possible that perturbed lysosome positioning might also influence specific pools of mTORC2 and AKT, as recently demonstrated (Jia & Bonifacino, 2019). Accordingly, AKT activity modulated the lysosomal membrane dynamics during autophagy (Arias *et al*, 2015). We and others speculate that there may exist unidentified substrates of MALT1, which link its protease activity directly to mTOR activation (Juilland & Thome, 2018; Thys *et al*, 2018). This may also rationalize the need for constitutive MALT1 activity in GSCs, as mTOR is constantly functioning in these cells (Galan-Moya *et al*, 2011). Moreover, it was suggested that down-regulation of lysosomes reduces recycling of receptors, including EGFR, which allows signaling to continue even in unfavorable niche where GSCs often reside and/or travel (Shingu *et al*, 2016). Less turnover of EGFR may also explain increased mTOR activation despite lysosomal down-regulation (Li *et al*, 2016). In addition, AKT can be central to balance between proliferation and apoptosis, by integrating multiple signaling networks besides mTOR in GBM. One hypothesis is that mTOR inhibition and/or dissociation from endo-lysosomes originate from lack of processing of unknown MALT1 substrates and is then exacerbated once homeostasis is disrupted.

How is QKI involved? Based on our data, we hypothesize that MALT1 sequesters QKI to prevent it from carrying out its RNA-binding function. Interestingly, MALT1 is already known to regulate other RNA-binding proteins Regnase-1/ZC3H12A, Roquin-1/RC3H1, and Roquin-2/RC3H2 (Uehata *et al*, 2013; Jeltsch *et al*, 2014). We propose that upon MALT1 inhibition QKI is released and free to bind its RNA-binding partners. QKI has already been shown to bind directly to lysosomal RNAs in progenitor cells (Shingu *et al*, 2016). It is thus tempting to speculate that QKI-dependent stabilization of lysosomal RNAs would preference the system toward more translation of these genes upon MALT1 inhibition, leading in turn to dysregulated endo-lysosomal protein expression and LMP. Indeed, our RNA-sequencing data suggest changes in translation and RNA biology upon MPZ treatment; however, further study is needed to validate whether there is increased QKI binding to lysosomal RNAs upon MALT1 inhibition. Notably, QKI-dependent lysosomal increase appears to be a post-transcriptional effect, independent of TFEB. As such, we propose a method of dual lysosomal control in GSCs whereby transcriptional biogenesis is tightly checked by known mTOR/TFEB pathway, and MALT1 acts on post-transcriptional regulation by isolating QKI from RNAs.

These findings place MALT1 as a new druggable target operating in non-immune cancer cells and involved in endo-lysosome homeostasis. Lysosomal homeostasis appears vital for glioblastoma cell survival and thus presents an intriguing axis for new therapeutic strategies in GBM.

Materials and Methods

Ethics statement

Informed consent was obtained from all patients prior to sample collection for diagnostic purposes. This study was reviewed and approved by the institutional review boards of Sainte Anne Hospital, Paris, France, and Laennec Hospital, Nantes, France, and performed in accordance with the Helsinki Protocol. Animal procedures were conducted as outlined by the European Convention for the Protection of Vertebrate Animals used for Experimental and other Scientific Purposes (ETS 123) and approved by the French Government (APAFIS#2016-2015092917067009).

The Cancer Genome Atlas (TCGA) analysis

The Cancer Genome Atlas (TCGA) was explored via the Gliovis platform (http://gliovis.bioinfo.cnio.es/) (Bowman *et al*, 2007). RNAseq databases (155 patients) were used to interrogate data related to *MALT1* and *QKI* expression (levels of RNA, probability of survival, correlation with *QKI* expression). Optimal cutoffs were set. All subtypes were included and histology was the only selective criteria.

Cell culture, siRNA and DNA transfection, and lentiviral transduction

GBM patient-derived cells with stem-like properties (GSCs) were isolated as previously described (Treps *et al*, 2016; Harford-Wright *et al*, 2017). GSC#1 (mesenchymal, 68-year-old male), GSC#4 (mesenchymal, 76-year-old female), GSC#9 (classical, 68-year-old female), and GSC#12 (neural, 59-year-old male) were cultured as spheroids in NS34 medium (DMEM-F12, with N2, G5, and B27 supplements, glutamax, and antibiotics). In order to induce differentiation, GSCs were grown in DMEM with 10% fetal bovine serum (FBS), glutamax, and antibiotics, for at least 2 weeks. Differentiation of sister cells (DGC) was monitored through their morphology and NESTIN and/or SOX2 loss of expression. Human brain microvascular endothelial cells (hCMEC/D3, a gift from PO Couraud, Institut Cochin, Paris, France) and HEK-293T cells (ATCC) were cultured as previously described (Treps *et al*, 2016). Human fetal astrocytes SVG-p12 (ATCC) and human neuronal-like cells SK-N-SH (ATCC) were cultured in MEM with 10% fetal bovine serum (FBS), and antibiotics.

Stealth non-silencing control duplexes (low-GC 12935200, Life Technologies), and small interfering RNA duplexes (Stealth RNAi, Life Technologies) were transfected using RNAiMAX lipofectamine (Life Technologies). The following duplexes targeting the respective human genes were as follows: CAGCAUUCUGGAUUGGCAAAUGG AA (*MALT1*), CCTTGAGTATCCTATTGAACCTAGT (*QKI*), UCAGAU GAGAGUAAUUUCUCUGAAA and GGGCUCCUCCUUUGCCACCAGA UCU (*BCL10*), CCCUUUGCGUGAAAGCCCAAGAGAU, ACAUCAC AGGGAGUGUGACACUUAA, and GACAAGGGACCAGAUGGACUG UCGU (*CARD10*), AGACGAAGGUUCAACAUCA (*TFEB*), CCACTCT GTGAGGAATGCACAGATA (*BECN1*).

pFRT/FLAG/HA-DEST QKI was purchased from Addgene and was subsequently cloned into a pCDH1-MSCV-EF1α-GreenPuro vector (SBI). pMSCV-MALT1A-WT and pMSCV-MALT1A-E397A were a gift from Daniel Krappmann (German Research Center for Environmental Health, Neuherberg, Germany). pMSCV-MALT1A-WT was subsequently mutated to C464A. Lentiviral GFP-expressing GIPZ sh*MALT1* (V2LHS_84221 TATAATAACCCATATACTC and V3LHS378343 TCTTCTGCAACTTCATCCA) or non-silencing short hairpin control (shc) was purchased from Open Biosystems. Lentiviral particles were obtained from psPAX2 and pVSVg co-transfected HEK-293T cells and infected as previously described (Dubois *et al*, 2014). pFRT/FLAG/HA-DEST QKI was a gift from Thomas Tuschl

(Landthaler *et al*, 2008); pRluc-LC3wt and pRluc-LC3BG120A were a gift from Marja Jaattela (Farkas & Jaattela, 2017). They were introduced in GSCs using Neon electroporation system according to manufacturer's instructions (Life technologies).

Antibodies and reagents

Cathepsin inhibitor 1 was purchased from SelleckChem, rapamycin from Tocris Bioscience, and mepazine from Chembridge. Bafilomycin A1, cycloheximide, chloroquine, phorbol myristate acetate (PMA), pepstatin A, fluphenazine, cyamemazine, chlorpromazine, pipotiazine, alimemazine, promethazine, and doxylamine were all from Sigma-Aldrich. Z-VRPR-FMK was purchased from Enzo Life Sciences. Q-VD-OPh and tumor necrosis factor-alpha (TNFα) were obtained from R&D Systems. Ionomycin was purchased from Calbiochem. The following primary antibodies were used: NESTIN (Millipore MAB5326), SOX2 (Millipore AB5603), GAPDH (Santa Cruz SC-25778 and SC-32233), TUBULIN (Santa Cruz SC-8035), MALT1 (Santa Cruz SC-46677), LAMP2 (Santa Cruz SC-18822), BCL10 (Santa Cruz SC-13153), BCL10 (Santa Cruz SC-5273), CYLD (Santa Cruz SC-137139), HOIL1 (Santa Cruz SC-393754), QKI (Santa Cruz SC-517305), PARP (Santa Cruz SC-8007), IκBα (CST 9242), p-S32/S36-IκBα (CST 9246), P62 (CST 5114), P62 (CST 88588), mTOR (CST 2983), p-S473-AKT (CST 4060), AKT (CST 9272), p-S235/S236-S6 (CST 2211), p-T183/Y185-JNK (CST 9255), JNK (CST 9258), p-S757-ULK1 (CST 6888), LC3B (CST 3868), p-T37/T46-4E-BP1 (CST 2855), p-T70-4E-BP1 (CST 9455), p-S65-4E-BP1 (CST 9451), 4E-BP1 (CST 9644), eIF4E (CST 2067), TOM20 (CST 42406), p-T421/S424-p70S6K (CST 9204), p70S6K (CST 14130), EEA1 (BD Bioscience 610456), CTSD (BD Bioscience 610800), PEX1 (BD Bioscience 611719), PECAM (BD Bioscience 557355), TFEB (Bethyl A303-673A), PDI (Abcam ab2792), GM130 (Abcam ab52649), QKI (Atlas HPA019123), CTSD (Atlas HPA063001), ULK1 (Sigma A7481), and FLAG (Sigma F1804). HRP-conjugated secondary antibodies (anti-rabbit, mouse Ig, mouse IgG1, mouse IgG2a, and mouse IgG2b) were purchased from Southern Biotech. Alexa-conjugated secondary antibodies were from Life Technologies.

Tumorsphere formation

To analyze tumorsphere formation, GSCs (100/μl) were seeded in triplicate in NS34 media as previously described (Harford-Wright *et al*, 2017). Cells were dissociated manually each day to reduce aggregation influence and maintained at 37°C 5% CO_2 until day 5 (day 4 for siRNA). Tumorspheres per field of view (fov) were calculated by counting the total number of tumorspheres in 5 random fov for each well. The mean of each condition was obtained from the triplicates of three independent experiments.

Limiting dilution assays

In order to evaluate the self-renewal of GSCs, limited dilution assays (LDA) were performed as previously described (Tropepe *et al*, 1999). GSCs were plated in a 96-well plate using serial dilution ranging from 2,000 to 1 cell/well with 8 replicates per dilution and treated as indicated. After 14 days, each well was binarily evaluated for tumorsphere formation. Stemness frequency was then calculated using ELDA software (Hu & Smyth, 2009). The mean stemness frequency for each treatment was calculated by averaging across two independent experiments.

Cell viability

Cell viability was measured using Cell TiterGlo luminescent cell viability assay, according to the manufacturers' protocol. Briefly, cells were seeded at 5,000 cells per well in triplicate per indicated treatment. Two days later, 100 μl of Cell TiterGlo reagent was added to each condition, cells were shaken vigorously, using an orbital shaker, to aid in their lysis, and then, luminescence was measured on a FluStar Optima plate reader (BMG).

ELISA

10×10^6 GSCs were cultured with 20 μM MPZ or DMSO and culture media was collected at 8 h, centrifuged, and filtered. Alternatively, cells were transfected with sic or si*MALT1* and supernatants were collected on day 3 post-transfection, centrifuged, and filtered. Human CTSD ELISA (Sigma) was performed on the culture media according to the manufacturer's instructions.

Animal procedures

Tumor inoculation was performed on female Balb/C nude mice aged 6–7 weeks, as described previously (Harford-Wright *et al*, 2017). Animals were randomly assigned to each group and group-housed in specific pathogen-free (SPF) conditions at 24°C on a 12-h day–night cycle. At all times, animals were allowed access to standard rodent pellets and water *ad libitum*. Mice were subcutaneously injected in each flank with 10^6 GSC#9 in 100 μl of PBS and growth factor-free Matrigel. Once tumors were palpable, mice were injected intraperitoneally daily with MPZ (8 mg/kg) or vehicle (DMSO) for two consecutive weeks, based on previous reports (Nagel *et al*, 2012; McGuire *et al*, 2014). Tumor size was measured daily during treatment and for 1 week following treatment withdrawal, with calipers and tumor volume calculated using the following equation $(\text{width}^2 \times \text{length})/2$.

Luciferase assays

Rluc-LC3B luciferase assay was performed as previously described (Farkas & Jaattela, 2017). Briefly, GSC#9 was transfected with 1 μg plasmid using a Neon Transfection System. 24 h later, cells were treated for 4 h with DMSO or MPZ and then assayed using Dual-Glo Luciferase assay system according to the manufacturers' guidelines. Luminescence was measured on a FluStarOptima plate reader.

Flow cytometry

For EdU analysis, cells we incubated with EdU (10 μM) for 2 h followed by fixation and Click-it reaction according to the manufacturers' protocol. For propidium iodide (PI) staining, cells were incubated for 15 min at room temperature with PI (100 μg/ml) following treatment according to manufacturer's protocol. Flow cytometry analyses were performed on FACSCalibur (BD Biosciences, Cytocell, SFR Francois Bonamy, Nantes, France) and processed using FlowJo software.

Immunostaining

After treatment, cells were seeded onto poly-lysine slides, fixed for 10 min with 4% PFA diluted in PBS, permeabilized in 0.04% Triton X-100, and blocked with PBS–BSA 4% prior to 1 h primary antibody incubation. After PBS washes, cells were incubated with AlexaFluor-conjugated secondary antibodies for 30 min. Next, cells were incubated with DAPI for 10 min and mounted with prolong gold anti-fade mounting medium. For Lysotracker Red DND-99 staining, cells were incubated with 50 nM Lysotracker during the last 30 min of treatment, and cells were fixed for 10 min in 4% PFA. To monitor changes in lysosomal enzyme activity, DQ-ovalbumin assay was performed, as previously described (Ebner *et al*, 2018). Cells were incubated with 10 μg/ml DQ-ovalbumin for 1 h at the end of treatment. Cells were then fixed for 10 min in 4% PFA. For transferrin uptake assay, following treatment, cells were washed in medium and incubated with Alexa596-conjugated transferrin (25 μg/ml) for 30 min at 37°C. Cells were then acid-washed for 40 s and fixed for 10 min in 4% PFA. Mouse tissue sections, 7 μm thickness, were obtained after cryosectioning of xenograft tumor embedded in OCT (Leica cryostat, SC3M facility, SFR Francois Bonamy, Nantes, France). Mouse tissue sections and human GBM samples from patients (IRCNA tumor library IRCNA, CHU Nantes, Integrated Center for Oncology, ICO, St. Herblain, France) were stained as followed. Sections were fixed 20 min in 4% PFA, permeabilized 10 min with PBS–Triton 0.2%, and blocked with 4% PBS–BSA 2 h prior to staining. Primary antibodies were incubated overnight at 4°C. All images were acquired on confocal Nikon A1 Rsi, using a 60× oil-immersion lens (Nikon Excellence Center, MicroPicell, SFR Francois Bonamy, Nantes, France). Structure illumination microscopy (SIM) images were acquired with a Nikon N-SIM microscope. Z-stacks of 0.12 μm were performed using a 100× oil-immersion lens with a 1.49 aperture and reconstructed in 3D using the NIS-Element Software. All images were analyzed and quantified using the ImageJ software.

Immunoblotting and immunoprecipitation

Cells were harvested with cold PBS followed by cellular lysis in TNT lysis buffer (50 mM Tris pH 7.4, 150 mM NaCl, 1% Triton X-100, 1% Igepal, 2 mM EDTA, supplemented with protease inhibitor) for 30 min on ice. Samples were centrifuged at 8,000 *g* to remove insoluble fraction. Tissue samples were lysed in RIPA lysis buffer for 2 h under agitation, following homogenization with mortar and pestle. Lysates were cleared in centrifuge at max speed for 30 min. Cytosol and nuclei separation were performed as previously described (Dubois *et al*, 2014). Briefly, cells were lysed in Buffer A (HEPES 10 mM, KCl 10 mM, EDTA 0.1 mM, EGTA 0.1 mM, DTT 1 mM, Na_3VO_4 1 mM, plus protease inhibitor) on ice for 5 min and then Buffer A + 10% Igepal was added for 5 min. Samples were centrifuged at 1,000 *g* for 3 min. Soluble fraction was cleared at 8,000 *g*. Immunoprecipitation was performed as previously described (Dubois *et al*, 2014). Briefly, cells were lysed in TNT lysis buffer for 30 min and cleared by centrifugation at 8,000 *g*. Samples were precleared by a 30-min incubation with Protein G agarose and then incubated for 2 h at 4°C with Protein G agarose and 5 μg of indicated antibodies. Protein concentrations were determined by BCA. Equal amount of 5–10 μg proteins were resolved by SDS–PAGE and transferred to nitrocellulose membranes. Membranes were revealed using a chemiluminescent HRP substrate and visualized using the Fusion imaging system.

Electron microscopy

After treatment, 1 volume of warm 2.5% glutaraldehyde (0.1M PB buffer, pH 7.2, 37°C) was added to 1 volume of cell suspension for 5 min, RT. Fixative was removed by centrifugation, and cells were treated 2.5% glutaraldehyde for 2 h, RT. Samples were then stored at 4°C in 1% paraformaldehyde until processed. After washes (10 min × 3), cells are post-fixed by 1% OsO_4/1.5% $K_3[Fe(CN)_6]$ for 30 min following washed by ddH_2O 10 min × 3, then dehydrated by 50, 70, 80, 90, 100% ethanol, 100% ethanol/100% acetone (1:1) for 5 min, 100% acetone for 3 min. Cells were infiltrated by 100% acetone/pure resin 1:1, 1:2, 1:3 for 1 h, pure resin overnight, pure resin for 1 h, then cells were embedded in the pure resin and polymerized at 60°C for 48 h. 70-nm sections were stained by uranyl acetate and lead citrate then observed under TEM at 80 kV (Technology Center for Protein Sciences, School of Life Sciences, Tsinghua University, Beijing, China).

RNAseq analysis

5×10^6 GSC#9 were treated with vehicle (DMSO) and MPZ (20 μM) for 4 h, in three biological replicates and snap-frozen on dry ice. RNA extraction (all RIN > 9.0), library preparation, RNAseq, and bioinformatics analysis were performed at Active Motif (Carlsbad, California, USA). Briefly, 2 μg of total RNA was isolated using the Qiagen RNeasy Mini Kit and further processed in Illumina's TruSeq Stranded mRNA Library kit. Libraries are sequenced on Illumina NextSeq 500 as paired-end 42-nt reads. Sequence reads are analyzed with the STAR alignment—DESeq2 software pipeline described in the Data Explanation document. The list of differentially expressed genes from DESeq2 output was selected based on 10% adjusted *P*-value level and FDR of 0.1 (please see Fig 6A and D, Table EV1). Gene ontology and KEGG pathway enrichment analysis were done using DAVID bioinformatics resources portal.

qPCR

3×10^6 GSC#9 were treated with vehicle (DMSO) and MPZ (20 μM) for 4 h, in three biological replicates and were snap-frozen. RNA extraction was done using Qiagen RNeasy kit. Equal amounts of RNA were reverse-transcribed using the Maxima Reverse Transcriptase kit, and 30 ng of the resulting cDNA was amplified by qPCR using PerfeCTa SYBR Green SuperMix Low ROX. Data were analyzed using the 2-ΔΔCt methods and normalized by the housekeeping genes ACTB and HPRT1.

The following primers were used: VGF forward GACCCTCCTCTC CACCTCTC, VGF reverse ACCGGCTCTTTATGCTCAGA, GNS forward CCCATTTTGAGAGGTGCCAGT, GNS reverse TGACGT TACGGCCTTCTCCTT, HEXA forward CAACCAACACATTCTTCTC CA, HEXA reverse CGCTATCGTGACCTGCTTTT, GLA forward AGCCAGATTCCTGCATCAGTG, GLA reverse ATAACCTGCATCCTT CCAGCC, CTSD forward CAACAGCGACAAGTCCAGC, CTSD reverse CTGAATCAGCGGCACGGC, LAMP2 forward CGTTCTGGTCTGCC TAGTC, LAMP2 reverse CAGTGCCATGGTCTGAAATG, LAMP1

forward ACCTGTCGAGTGGCAACTTCA, LAMP1 reverse GGGCA CAAGTGGTGGTGAG, CSTB forward AGTGGAGAATGGCACACC CTA, CSTB reverse AAGAAGCCATTGTCACCCCA, CTSS forward GCCTGATTCTGTGGACTGG, CTSS reverse GATGTACTGGAAAGCC GTTG, LC3B forward GCTCATCAAGATAATTAGAAGGCG, LC3B reverse CTGGGAGGCATAGACCATGT, ACTB forward GGACTTC GAGCAAGAGATGG, ACTB reverse AGCACTGTGTTGGCGTACAG, HPRT1 forward TGACACTGGCAAAACAA TGCA, HPRT1 reverse GGTCCTTTTCACCAGCAAGCT, CAV1 forward CGTAGACTCG GAGGGACATC, CAV1 reverse GCCTTCCAAATGCCGTCAAA, CTGF forward CATCTTCGGTGGTACGGTGT, CTGF reverse TTCCAGT CGGTAAGCCGC, EGR3 forward GTGCTATGACCGGCAAACTC, EGR3 reverse TGTCCATTACATTCTCTGTAGCCA, GLIPR1 forward TACACTCAGGTTGTTTGGGCA, GLIPR1 reverse ACGTTTGAC TTGGTCTCGCT, IL7R forward ACGATGTAGCTTACCGCCAG, IL7R reverse TAGGATCCATCTCCCCTGAGC, CXCL10 forward TGGCATT CAAGGAGTACCTCTC, CXCL10 reverse TGATGGCCTTCGATT CTGGA, DRP2 forward CCGTGTGAGTGGCTATCGTA, DRP2 reverse AGCTCTAACCTGAGGGTGGG, ITGAM forward CGATATCAG CACATCGGCCT, ITGAM reverse AGCCCTCTGCCCCCTG, MSLN forward ACTCCCGTCTGCTGTGACG, MSLN reverse AAGAGCAGG AACAGGAGGCT, CARD10 forward GGACCTGAGCCTCACAACTC, CARD10 reverse CCACCCTTTGCTCTCTTGGT.

Statistics

Data are representative of at least three independent experiments, unless otherwise stated. Statistical analysis was performed with GraphPad Prism5 using one-way analysis of variance (ANOVA), two-way ANOVA, or an unpaired two-tailed *t*-test (Student's *t*-test). For each statistical test, *P*-value of < 0.05 was considered significant.

Data availability

The datasets produced in this study are available in the following databases:

RNA-seq data: Gene Expression Omnibus GSE139018 (https://www.ncbi.nlm.nih.gov/geo/query/acc.cgi?acc=GSE139018).

Expanded View for this article is available online.

Acknowledgements

We thank SOAP team members (Nantes, France). We thank Steven Nedellec from MicroPicell, as well as Cytocell, and UTE facilities (SFR Santé François Bonamy, Nantes, France). We are also grateful to Daniel Krappmann (German Research Center for Environmental Health, Neuherberg, Germany), Rudi Beyaert (VIB, Ghent, Belgium), and Li Yu (Tsinghua University, Beijing, China) for reagents and helpful discussion. This research was funded by Fondation pour la Recherche Medicale (Equipe labellisée DEQ20180339184), Fondation ARC contre le Cancer (JG PJA20171206146), Ligue nationale contre le cancer comités de Loire-Atlantique, Maine et Loire, Vendée, Ille-et-Vilaine (JG, NB), Région Pays de la Loire et Nantes Métropole under Connect Talent Grant (JG), and SIRIC ILIAD INCa-DGOS-Inserm_12558. KAJ received PhD fellowships from Nantes Métropole and Fondation ARC; TD received PhD fellowship from Nantes Métropole; GAG and AT hold postdoctoral fellowships from Fondation de France and Fondation ARC, respectively.

Author contributions

KAJ, JG, NB: conception and design, acquisition of data, analysis and interpretation of data, drafting or revising the article; GA-G, CM, AT, YL, EH-W, KT, TD, CAN: acquisition of data, analysis and interpretation of data; J-SF: conception and interpretation of data. All authors approved the manuscript. All data needed to evaluate the conclusions in the paper are present in the paper and/or the Supplementary Materials. Additional data related to this paper may be requested from the authors.

Conflict of interest

The authors declare that they have no conflict of interest.

References

Aits S, Jaattela M (2013) Lysosomal cell death at a glance. *J Cell Sci* 126: 1905 – 1912

Arias E, Koga H, Diaz A, Mocholi E, Patel B, Cuervo AM (2015) Lysosomal mTORC2/PHLPP1/Akt regulate chaperone-mediated autophagy. *Mol Cell* 59: 270 – 284

Bao S, Wu Q, McLendon RE, Hao Y, Shi Q, Hjelmeland AB, Dewhirst MW, Bigner DD, Rich JN (2006) Glioma stem cells promote radioresistance by preferential activation of the DNA damage response. *Nature* 444: 756 – 760

Bargou RC, Leng C, Krappmann D, Emmerich F, Mapara MY, Bommert K, Royer HD, Scheidereit C, Dörken B (1996) High-level nuclear NF-kappa B and Oct-2 is a common feature of cultured Hodgkin/Reed-Sternberg cells. *Blood* 87: 4340 – 4347

Bowman RL, Wang Q, Carro A, Verhaak RGW, Squatrito M (2007) GlioVis data portal for visualization and analysis of brain tumor expression datasets. *Neuro Oncol* 19: 139 – 141

Brown CE, Alizadeh D, Starr R, Weng L, Wagner JR, Naranjo A, Ostberg JR, Blanchard MS, Kilpatrick J, Simpson J *et al* (2016) Regression of glioblastoma after chimeric antigen receptor T-cell therapy. *N Engl J Med* 375: 2561 – 2569

Calabrese C, Poppleton H, Kocak M, Hogg TL, Fuller C, Hamner B, Oh EY, Gaber MW, Finklestein D, Allen M *et al* (2007) A perivascular niche for brain tumor stem cells. *Cancer Cell* 11: 69 – 82

Chen J, Li Y, Yu TS, McKay RM, Burns DK, Kernie SG, Parada LF (2012) A restricted cell population propagates glioblastoma growth after chemotherapy. *Nature* 488: 522 – 526

Chinot OL, Wick W, Mason W, Henriksson R, Saran F, Nishikawa R, Carpentier AF, Hoang-Xuan K, Kavan P, Cernea D *et al* (2014) Bevacizumab plus radiotherapy-temozolomide for newly diagnosed glioblastoma. *N Engl J Med* 370: 709 – 722

Davis RE, Brown KD, Siebenlist U, Staudt LM (2001) Constitutive nuclear factor kappaB activity is required for survival of activated B cell-like diffuse large B cell lymphoma cells. *J Exp Med* 194: 1861 – 1874

Di Pilato M, Kim EY, Cadilha BL, Prüßmann JN, Nasrallah MN, Seruggia D, Usmani SM, Misale S, Zappulli V, Carrizosa E *et al* (2019) Targeting the CBM complex causes Treg cells to prime tumours for immune checkpoint therapy. *Nature* 570: 112 – 116

Douanne T, Gavard J, Bidere N (2016) The paracaspase MALT1 cleaves the LUBAC subunit HOIL1 during antigen receptor signaling. *J Cell Sci* 129: 1775 – 1780

Dubois SM, Alexia C, Wu Y, Leclair HM, Leveau C, Schol E, Fest T, Tarte K, Chen ZJ, Gavard J *et al* (2014) A catalytic-independent role for the LUBAC in NF-kappaB activation upon antigen receptor engagement and in lymphoma cells. *Blood* 123: 2199 – 2203

Ebner P, Poetsch I, Deszcz L, Hoffman T, Zuber J, Fumiyo I (2018) The IAP family member BRUCE regulates autophagosome-lysosome fusion. *Nat Commun* 9: 599

Eitelhuber AC, Vosyka O, Nagel D, Bognar M, Lenze D, Lammens K, Schlauderer F, Hlahla D, Hopfner KP, Lenz G *et al* (2015) Activity-based probes for detection of active MALT1 paracaspase in immune cells and lymphomas. *Chem Biol* 22: 129 – 138

Elrick MJ, Lieberman AP (2013) Autophagic dysfunction in a lysosomal storage disorder due to impaired proteolysis. *Autophagy* 9: 234 – 235

Farkas T, Jaattela M (2017) Chapter one - renilla luciferase-LC3B based reporter assay for measuring autophagic flux. *Methods Enzymol* 588: 1 – 13

Fennelly C, Amaravadi RK (2017) Lysosomal biology in cancer. *Methods Mol Biol* 1594: 293 – 308

Galan-Moya EM, Le Guelte A, Lima Fernandes E, Thirant C, Dwyer J, Bidere N, Couraud PO, Scott MG, Junier MP, Chneiweiss H *et al* (2011) Secreted factors from brain endothelial cells maintain glioblastoma stem-like cell expansion through the mTOR pathway. *EMBO Rep* 12: 470 – 476

Gingras AC, Kennedy SG, O'Leary MA, Sonenberg N, Hay N (1998) 4EBP1, a repressor of mRNA translation, is phosphorylated and inactivated by the AKT (PKB) signaling pathway. *Genes Dev* 12: 502 – 513

Hamilton KS, Phong B, Corey C, Cheng J, Gorentla B, Zhong X, Shiva S, Kane LP (2014) T cell receptor-dependent activation of mTOR signaling in T cells is mediated by Carma1 and MALT1, but not Bcl10. *Sci Signal* 7: ra55

Hailfinger S, Lenz G, Ngo V, Posvitz-Fejfar A, Rebeaud F, Guzzardi M, Penas EMM, Dierlamm J, Chan WC, Staudt LM *et al* (2009) Essential role of MALT1 protease activity in activated B cell-like diffuse large B-cell lymphoma. *Proc Natl Acad Sci USA* 106: 19946 – 19951

Harford-Wright E, Andre-Gregoire G, Jacobs KA, Treps L, Le Gonidec S, Leclair HM, Gonzalez-Diest S, Roux Q, Guillonneau F, Loussouarn D *et al* (2017) Pharmacological targeting of apelin impairs glioblastoma growth. *Brain* 140: 2939 – 2954

Hu Y, Smyth GK (2009) ELDA: extreme limiting dilution analysis for comparing depleted and enriched populations in stem cell and other assays. *J Immunol Methods* 347: 70 – 78

Jacobs KA, Harford-Wright E, Gavard J (2017) Neutralizing gp130 interferes with endothelial-mediated effects on glioblastoma stem-like cells. *Cell Death Differ* 24: 384

Jeltsch KM, Hu D, Brenner S, Zöller J, Heinz GA, Nagel D, Vogel KU, Rehage N, Warth SC, Edelmann SL *et al* (2014) Cleavage of roquin and regnase-1 by the paracaspase MALT1 releases their cooperatively repressed targets to promote TH17 differentiation. *Nat Immunol* 15: 1079 – 1089

Jia R, Bonifacino JS (2019) Lysosome positioning influences mTORC2 and AKT signaling. *Mol Cell* 75: 26 – 38

Jin X, Kim LJY, Wu Q, Wallace LC, Prager BC, Sanvoranart T, Gimple RC, Wang X, Mack SC, Miller TE *et al* (2017) Targeting glioma stem cells through combined BMI1 and EZH2 inhibition. *Nat Med* 23: 1352 – 1361

Juilland M, Thome M (2018) Holding all the CARDs: how MALT1 controls CARMA/CARD-dependent signaling. *Front Immunol* 9: 1927

Karin M, Greten FR (2005) NF-kappaB: linking inflammation and immunity to cancer development and progression. *Nat Rev Immunol* 5: 749 – 759

Kip E, Staal J, Verstrepen L, Tima HG, Terryn S, Romano M, Lemeire K, Suin V, Hamouda A, Kalai M *et al* (2018) MALT1 controls attenuated rabies virus by inducing early inflammation and T cell activation in the brain. *J Virol* 92: e02029 – 17

Korolchuk VI, Saiki S, Lichtenberg M, Siddiqi FH, Roberts EA, Imarisio S, Jahreiss L, Sarkar S, Futter M, Menzies FM *et al* (2011) Lysosomal positioning coordinates cellular nutrient responses. *Nat Cell Biol* 13: 453 – 460

Korth C, May BC, Cohen FE, Prusiner SB (2001) Acridine and phenothiazine derivatives as pharmacotherapeutics for prion disease. *Proc Natl Acad Sci USA* 98: 9836 – 9841

Landthaler M, Gaidatzis D, Rothballer A, Chen PY, Soll SJ, Dinic L, Ojo T, Hafner M, Zavolan M, Tuschl T (2008) Molecular characterization of human Argonaute-containing ribonucleoprotein complexes and their bound target mRNAs. *RNA* 14: 2580 – 2596

Lathia JD, Mack SC, Mulkearns-Hubert EE, Valentim CL, Rich JN (2015) Cancer stem cells in glioblastoma. *Genes Dev* 29: 1203 – 1217

Le Joncour V, Filppu P, Hyvonen M, Holopainen M, Turunen SP, Sihto H, Burghardt I, Joensuu H, Tynninen O, Jaaskelainen J *et al* (2019) Vulnerability of invasive glioblastoma cells to lysosomal membrane destabilization. *EMBO Mol Med* 11: e9034

Li J, Jia H, Xie L, Wang X, Wang X, He H, Lin Y, Hu L (2009) Association of constitutive nuclear factor-kappaB activation with aggressive aspects and poor prognosis in cervical cancer. *Int J Gynecol Cancer* 19: 1421 – 1426

Li W, Wu C, Chen N, Gu H, Yen A, Cao L, Wang E, Wang L (2016) PI3K/Akt/mTOR signaling pathway and targeted therapy for glioblastoma. *Oncotarget* 7: 33440 – 33450

Lomas JL (1957) Treatment of schizophrenia. *Br Med J* 2: 78 – 80

Loos B, du Toit A, Hofmeyr JHS (2014) Defining and measuring autophagosome flux-concept and reality. *Autophagy* 10: 2087 – 2096

Luo J, Solimini NL, Elledge SJ (2009) Principles of cancer therapy: oncogene and non-oncogene addiction. *Cell* 138: 807

Mai TT, Hamai A, Hienzsch A, Caneque T, Müller S, Wicinski J, Cabaud O, Leroy C, David A, Acevedo V *et al* (2017) Salinomycin kills cancer stem cells by sequestering iron in lysosomes. *Nat Chem* 10: 1025 – 1033

Man J, Yu X, Huang H, Zhou W, Xiang C, Huang H, Miele L, Liu Z, Bebek G, Bao S *et al* (2017) Hypoxic induction of vasorin regulates Notch1 turnover to maintain glioma stem-like cells. *Cell Stem Cell* 22: 104 – 118

McAuley JR, Bailey KM, Ekambaram P, Klei LR, Kang H, Hu D, Freeman TJ, Concel VJ, Hubel NE, Lee JL *et al* (2019) MALT1 is a critical mediator of PAR1-driven NF-κB activation and metastasis in multiple tumor types. *Oncogene*. https://doi.org/10.1038/s41388-019-0958-4

McGuire C, Elton L, Wieghofer P, Staal J, Voet S, Demeyer A, Nagel D, Krappmann D, Prinz M, Beyaert R *et al* (2014) Pharmacological inhibition of MALT1 protease activity protects mice in a mouse model of multiple sclerosis. *J Neuroinflammation* 11: 124

Meloni L, Verstrepen L, Kreike M, Staal J, Driege Y, Afonina IS, Beyaert R (2018) Mepazine inhibits RANK-induced osteoclastogenesis independent of its MALT1 inhibitory function. *Molecules* 23: 3144

Nagel D, Spranger S, Vincendeau M, Grau M, Raffegerst S, Kloo B, Hlahla D, Neuenschwander M, Peter von Kries J, Hadian K *et al* (2012) Pharmacologic inhibition of MALT1 protease by phenothiazines as a therapeutic approach for the treatment of aggressive ABC-DLBCL. *Cancer Cell* 22: 825 – 837

Nakaya M, Xiao Y, Zhou X, Chang JH, Chang M, Cheng X, Blonska M, Lin X, Sun SC (2014) Inflammatory T cell responses rely on amino acid transporter ASCT2 facilitation of glutamine uptake and mTORC1 kinase activation. *Immunity* 40: 692 – 705

Ngo VN, Davis RE, Lamy L, Yu X, Zhao H, Lenz G, Lam LT, Dave S, Yang L, Powell J *et al* (2006) A loss-of-function RNA interference screen for molecular targets in cancer. *Nature* 441: 106 – 110

Oliva CR, Zhang W, Langford C, Suto MJ, Griguer CE (2017) Repositioning chlorpromazine for treating chemoresistant glioma through the inhibition of cytochrome c oxidase bearing the COX4-1 regulatory subunit. *Oncotarget* 8: 37568 – 37583

Pietras A, Katz AM, Ekström EJ, Wee B, Halliday JJ, Pitter KL, Werbeck JL, Amankulor NM, Huse JT, Holland EC (2014) Osteopontin-CD44 signaling in the glioma perivascular niche enhances cancer stem cell phenotypes and promotes aggressive tumor growth. *Cell Stem Cell* 14: 357 – 369

Qin X, Jiang B, Zhang Y (2016) 4E-BP1, a multifactor regulated multifunctional protein. *Cell Cycle* 15: 781 – 786

Rahim SAA, Dirkse A, Oudin A, Schuster A, Bohler J, Barthelemy V, Muller A, Vallar L, Janji B, Golebiewska A *et al* (2017) Regulation of hypoxia – induced autophagy in glioblastoma involves ATG9A. *Br J Cancer* 117: 813 – 825

Rebeaud F, Hailfinger S, Posevitz-Fejfar A, Tapernoux M, Moser R, Rueda D, Gaide O, Guzzardi M, Lancu EM, Rufer N *et al* (2008) The proteolytic activity of the paracaspase MALT1 is key in T cell activation. *Nat Immunol* 9: 272 – 281

Rosenbaum M, Gewies A, Pechloff K, Heuser C, Engleitner T, Gehring T, Hartjes L, Krebs S, Krappmann D, Kriegsmann M *et al* (2019) Bcl10-controlled Malt1 paracaspase activity is key for the immune suppressive function of regulatory T cells. *Nat Commun* 10: 2352

Sardiello M, Palmieri M, di Ronza A, Medina DL, Valenza M, Gennarino VA, Di Malta C, Donaudy F, Embrione V, Polishchuk RS *et al* (2009) A gene network regulating lysosomal biogenesis and function. *Science* 325: 473 – 477

Schlauderer F, Lammens K, Nagel D, Vincendeau M, Eitelhuber AC, Verhelst SH, Kling D, Chrusciel A, Ruland J, Krappman D *et al* (2013) Structural analysis of phenothiazine derivatives as allosteric inhibitors of the MALT1 paracaspase. *Angew Chem Int Ed Engl* 52: 10384 – 10387

Settembre C, Zoncu R, Medina DL, Vetrini F, Erdin S, Erdin S, Huynh T, Ferron M, Karsenty G, Vellard MC *et al* (2012) A lysosome-to-nucleus signalling mechanism senses and regulates the lysosome via mTOR and TFEB. *EMBO J* 31: 1095 – 1108

Shchors K, Massaras A, Hanahan D (2015) Dual targeting of autophagic regulatory circuitry in gliomas with repurposed drugs elicits cell-lethal autophagy and therapeutic benefit. *Cancer Cell* 28: 456 – 471

Shingu T, Ho AL, Yuan L, Zhou X, Dai C, Zheng S, Wang Q, Zhong Y, Chang Q, Horner JW *et al* (2016) Qki deficiency maintains stemness of glioma stem cells in suboptimal environment by downregulating endolysosomal degradation. *Nat Genet* 49: 75 – 86

Singh SK, Hawkins C, Clarke ID, Squire JA, Bayani J, Hide T, Henkelman RM, Cusimano MD, Dirks PB (2004) Identification of human brain tumour initiating cells. *Nature* 432: 396 – 401

Staal J, Driege Y, Bekaert T, Demeyer A, Muyllaert D, Van Damme P, Gevaert K, Beyaert R (2011) T-cell receptor-induced JNK activation requires proteolytic inactivation of CYLD by MALT1: CYLD is cleaved by MALT1. *EMBO J* 30: 1742 – 1752

Staudt LM (2010) Oncogenic activation of NF-kappaB. *Cold Spring Harb Perspect Biol* 2: a000109

Stupp R, Hegi ME, Mason WP, van den Bent MJ, Taphoorn MJ, Janzer RC, Ludwin SK, Allgeier A, Fisher B, Belanger K *et al* (2009) Effects of radiotherapy with concomitant and adjuvant temozolomide versus radiotherapy alone on survival in glioblastoma in a randomised phase III study: 5-year analysis of the EORTC-NCIC trial. *Lancet Oncol* 10: 459 – 466

Stupp R, Taillibert S, Kanner AA, Kesari S, Steinberg DM, Toms SA, Taylor LP, Lieberman F, Silvani A, Fink KL *et al* (2015) Maintenance therapy with tumor-treating fields plus temozolomide vs temozolomide alone for glioblastoma: a randomized clinical trial. *JAMA* 314: 2535 – 2543

Tan SK, Jermakowicz A, Mookhtiar Adnan K, Nemeroff CB, Schurer SC, Ayad NG (2018) Drug repositioning in glioblastoma: a pathway perspective. *Front Pharmacol* 9: 218

Thys A, Douanne T, Bidere N (2018) Post-translational modifications of the CARMA1-BCL10-MALT1 complex in lymphocytes and activated B-cell like subtype of diffuse large B-cell lymphoma. *Front Oncol* 8: 498

Treps L, Edmond S, Harford-Wright E, Galan-Moya EM, Schmitt A, Azzi S, Citerne A, Bidere N, Ricard D, Gavard J (2016) Extracellular vesicle-transported Semaphorin3A promotes vascular permeability in glioblastoma. *Oncogene* 35: 2615 – 2623

Tropepe V, Sibilia M, Ciruna BG, Rossant J, Wagner EF, van der Kooy D (1999) Distinct neural stem cells proliferate in response to EGF and FGF in the developing mouse telencephalon. *Dev Biol* 208: 166 – 188

Uehata T, Iwasaki H, Vandenbon A, Matsushita K, Hernandez-Cuellar E, Kuniyoshi K, Satoh T, Mino T, Suzuki Y, Standley DM *et al* (2013) Malt1-induced cleavage of Regnase-1 in $CD4^+$ helper T cells regulates immune activation. *Cell* 153: 1036 – 1049

Wang F, Salvati A, Boya P (2018a) Lysosome-dependent cell death and deregulated autophagy induced by amine-modified polystyrene nanoparticles. *Open Biol* 8: 170271

Wang X, Prager BC, Wu Q, Kim LJY, Gimple RC, Shi Y, Yang K, Morton AR, Zhou W, Zhu Z *et al* (2018b) Reciprocal signaling between glioblastoma stem cells and differentiated tumor cells promotes malignant progression. *Cell Stem Cell* 22: 514 – 528

Weyerhäuser P, Kantelhardt SR, Kim EL (2018) Re-purposing chloroquine for glioblastoma: potential merits and confounding variables. *Front Oncol* 8: 335

Wu J, Zhou L, Tonissen K, Tee R, Artzt K (1999) The quaking 1-5 protein (QKI-5) has a novel nuclear localization signal and shuttles between the nucleus and the cytoplasm. *J Biol Chem* 274: 29202 – 29210

Yan K, Yang K, Rich JN (2013) The evolving landscape of glioblastoma stem cells. *Curr Opin Neurol* 26: 701 – 707

Yu L, McPhee CK, Zheng L, Mardones GA, Rong Y, Peng J, Mi N, Zhao Y, Liu Z, Wan F *et al* (2010) Termination of autophagy and reformation of lysosomes regulated by mTOR. *Nature* 465: 942 – 946

Zielke S, Meyer N, Mari M, Abou-El-Ardat K, Reggiori F, van Wijk SJL, Kögel D, Fulda S (2018) Loperamide, pimozide, and STF-62247 trigger autophagy-dependent cell death in glioblastoma cells. *Cell Death Dis* 9: 994

Expanded View Figures

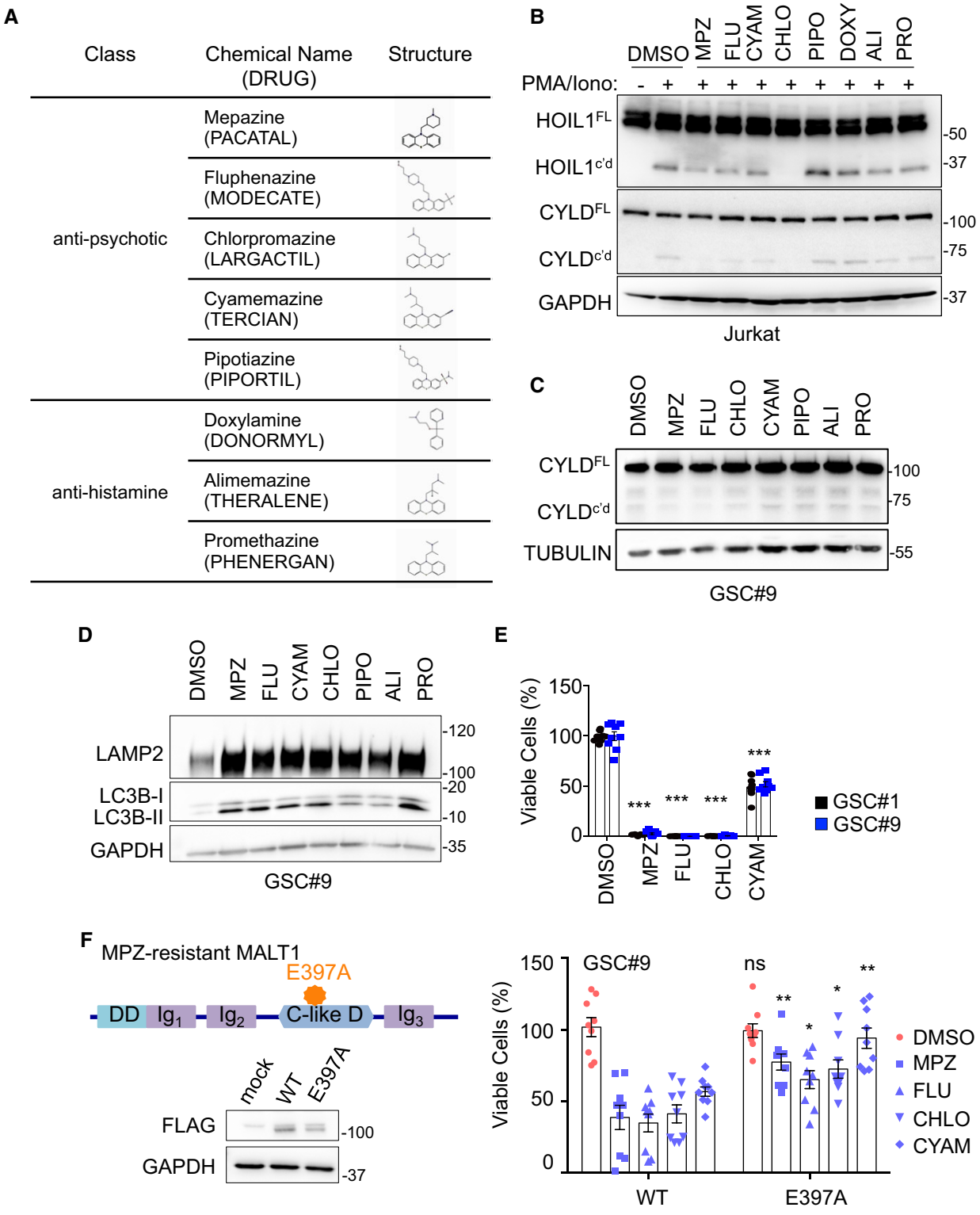

Figure EV1.

◀ **Figure EV1. Impact of phenothiazines on MALT1 protease activity and lysosomes.**

A Table summarizing eight phenothiazines used in clinics as either anti-psychotic or anti-histaminic, along with their generic and brand names (cap letters), and chemical structures.

B Western blot analysis of two MALT1 substrates, HOIL1 and CYLD, either full length (FL) or cleaved (c'd) in Jurkat T cells treated with vehicle (DMSO) or phenothiazines, as follows: 20 μM CYAM (cyamemazine), CHLO (chlorpromazine), PIPO (pipotiazine), DOXY (doxylamine), ALI (alimemazine), and PRO (promethazine), and 10 μM MPZ (mepazine) and FLU (fluphenazine) for 30 min and stimulated for 30 min more with PMA (20 ng/ml) and Ionomycin (Iono, 300 ng/ml). TUBULIN served as a loading control.

C Western blot analysis of CYLD processing in GSC#9 treated with vehicle (DMSO) or phenothiazines (20 μM CYAM, CHLO, PIPO, DOXY, ALI, and PRO, 10 μM MPZ and FLU) for 60 min. GAPDH served as a loading control.

D Western blot analysis of LAMP2 and LC3B in equal amount of total protein lysates from GSC#9 treated for 6 h with vehicle (DMSO) or 20 μM phenothiazines (MPZ, FLU, CYAM, CHLO, ALI, PRO). GAPDH served as a loading control.

E Cell viability of GSC#1 and GSC#9 using 20 μM of MPZ, FLU, CHLO, and CYAM, using Cell TiterGlo assays. Data were normalized to their respective DMSO-treated controls and are presented as the mean ± SEM of three independent experiments in triplicate.

F Schematic drawing of MALT1 structures highlighting the E397A substitution in the mepazine-resistant version. DD: death domain, C-like D: caspase-like domain, Ig: immunoglobulin domain. Western blot analysis of FLAG in equal amount of total protein lysates from HEK-293T cells transfected with empty vector (mock), MALT-WT, or MALT1-E397A. GAPDH serves as a loading control. GSC#9 were transduced with MALT-WT or MALT1-E397A and treated with phenothiazines (10 μM of MPZ, FLU, CYAM, CHLO) for 24 h. Cell Viability was analyzed using Cell TiterGlo assay. Data were normalized to their respective DMSO-treated controls and are presented as the mean ± SEM of three independent experiments in triplicate.

Data information: All data were repeated in three independent experiments. Statistics were performed using a one-way ANOVA with a 95% confidence interval for all experiments with *P*-values stated. *$P < 0.05$, **$P < 0.01$, ***$P < 0.001$.

Source data are available online for this figure.

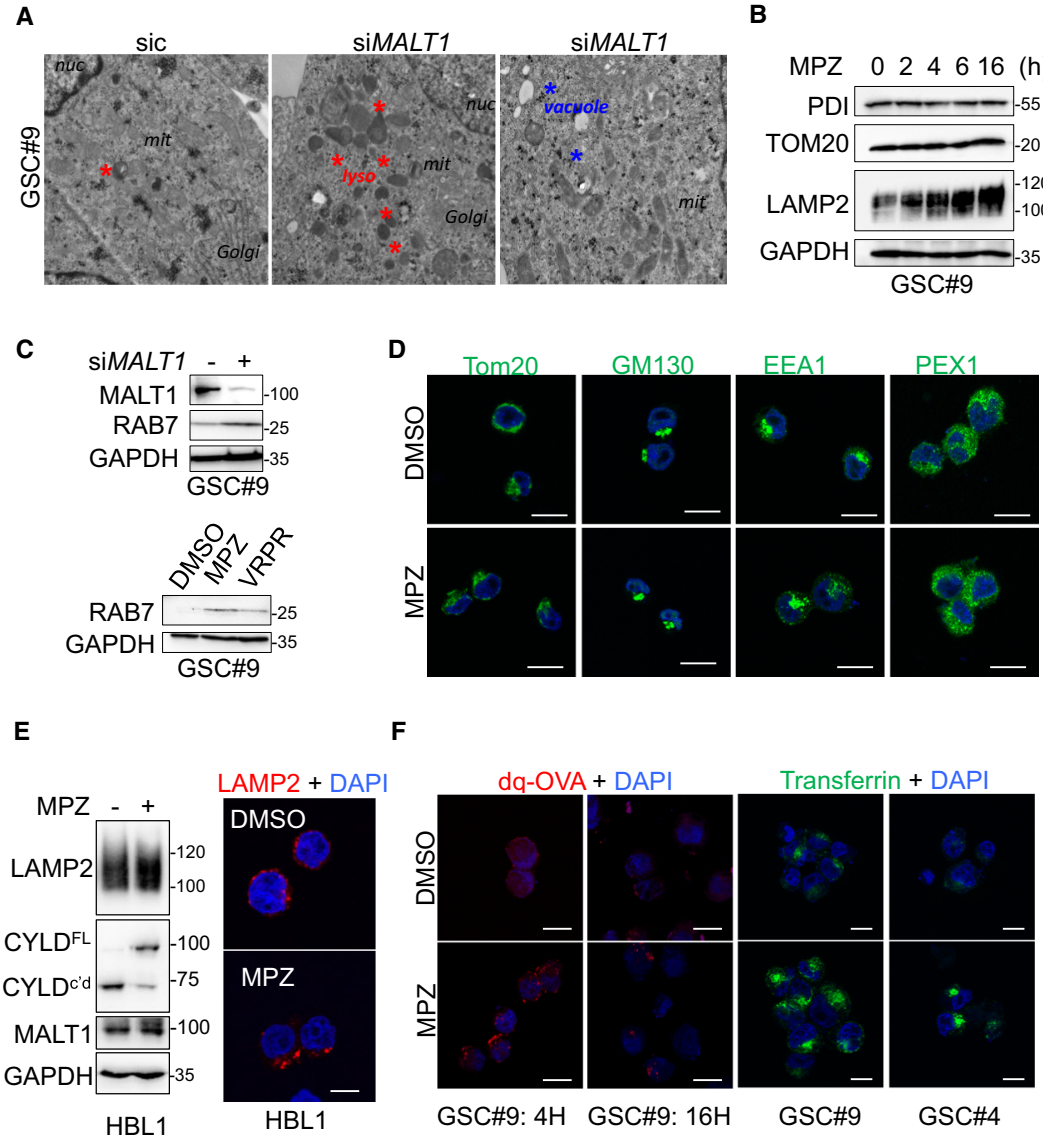

Figure EV2. Impact of MALT1 inhibition on intracellular organelles.

A Transmission electron microscopy images from GSC#9 transfected with non-silencing duplexes (sic) or siRNA duplexes targeting *MALT1* (si*MALT1*). Multiple images and sections from one experiment were analyzed. Red stars denote lysosomes; blue stars vacuoles.

B Western blot analysis of PDI, TOM20, and LAMP2 in total protein lysates from GSC#9 treated vehicle (DMSO) or MPZ (20 μM) for the indicated times. GAPDH serves as a loading control.

C Western blot analysis of RAB7 and MALT1 in GSC#9 in total protein lysates from GSC#9 transfected with non-silencing duplexes (sic) or siRNA duplexes targeting *MALT1* (si*MALT1*). Alternatively, GSC#9 received Z-VRPR-FMK (VRPR, 75 μM, 16 h) and mepazine (MPZ, 20 μM, 16 h). GAPDH serves as a loading control.

D Confocal analysis of TOM20, GM130, EEA1, and PEX1 immunostaining (green) in GSC#9 treated with vehicle (DMSO) or MPZ (20 μM) for 4 h. Nuclei (DAPI) are shown in blue. Scale bars: 10 μm.

E ABC DLBCL lymphoma cells HBL1 treated with vehicle (DMSO) or MPZ (20 μM) for 4 h. (Left) Western blot analysis of LAMP2 and CYLD (full length, FL, or cleaved, c'd) in total protein lysates. MALT1 and GAPDH serve as loading controls. (Right) Confocal analysis of LAMP2 (red). Nuclei (DAPI) are shown in blue. Scale bars: 10 μm.

F Confocal analysis of dq-ovalbumin (dq-OVA, red) in GSC#9 treated with vehicle (DMSO) or MPZ (20 μM) for 4 or 16 h. Nuclei (DAPI) are shown in blue. Alternatively, confocal analysis of transferrin uptake (green) in GSC#9 and GSC#4 treated with vehicle (DMSO) or MPZ (20 μM) for 4 h. Nuclei (DAPI) are shown in blue. Scale bars: 10 μm.

Data information: All data were repeated in three independent experiments, unless specified.
Source data are available online for this figure.

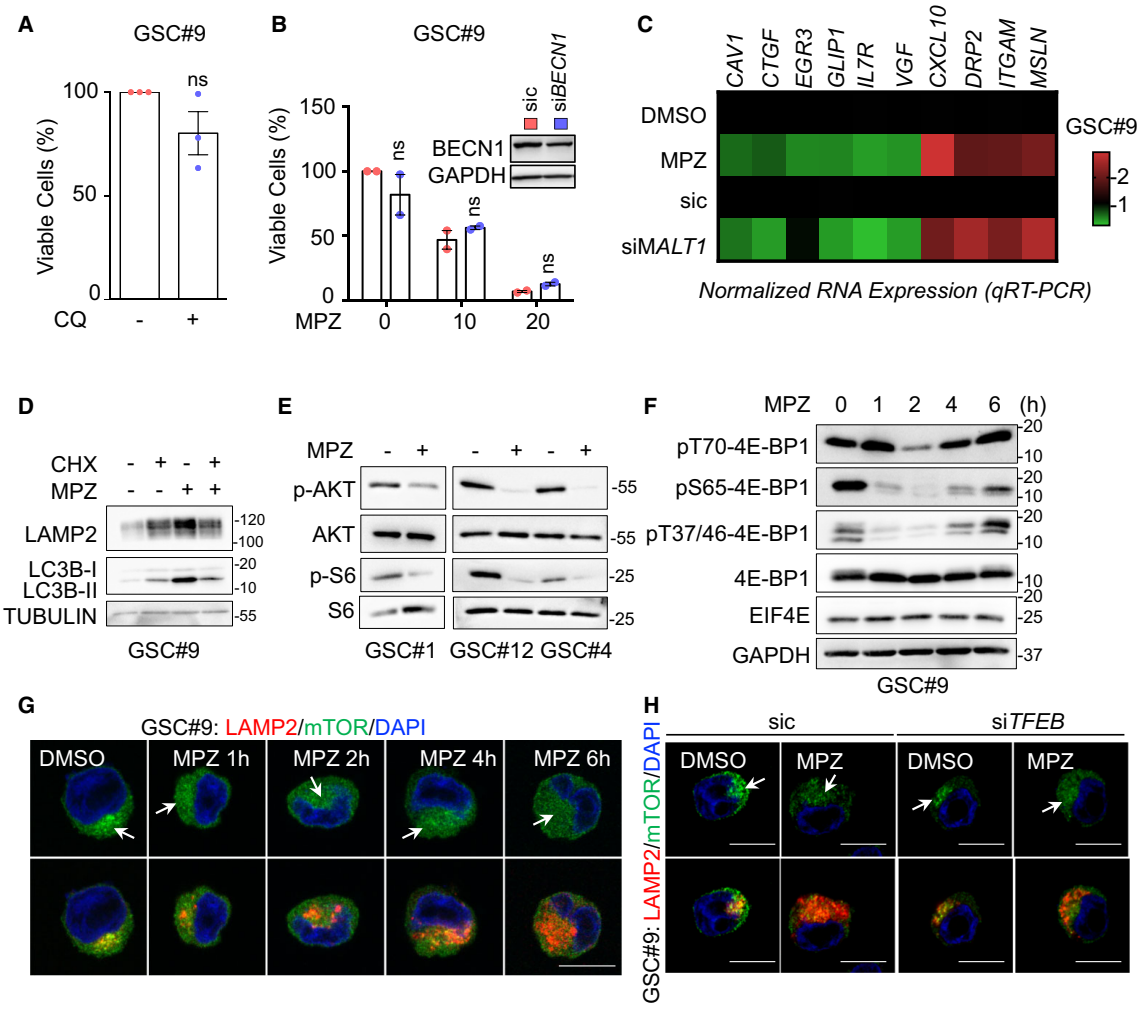

Figure EV3. Impact of MALT1 inhibition on cell death and mTOR signaling.

A Cell viability was measured using Cell TiterGlo luminescent assay in GSC#9 treated for 72 h with vehicle (DMSO) or chloroquine (CQ, 20 μM). Data were normalized to the vehicle-treated controls and are presented as the mean ± SEM of three independent experiments in triplicate.

B Cell viability was measured using Cell TiterGlo luminescent assay in GSC#9 transfected with non-silencing duplexes (sic, red) or siRNA duplexes targeting *BECLIN1* (si*BECN1*, blue) and further treated with vehicle (DMSO) and MPZ (10 and 20 μM) for 72 h. Data were normalized to the vehicle-treated controls and are presented as the mean ± SEM of two independent experiments in triplicate. Knockdown efficiency was checked at the end point by Western blot. GAPDH serves as a loading control.

C GSC#9 were treated with vehicle (DMSO) and mepazine (MPZ, 20 μM) for 16 h. Alternatively, GSC#9 were transfected with non-silencing duplexes (sic) or siRNA duplexes targeting *MALT1* (si*MALT1*). RNAs were processed for qRT–PCR on 10 gene candidates from RNAseq data (Table EV1). Data are represented as heatmap representation of RNA expression, normalized to two housekeeping genes (*HPRT1* and *ACTB*).

D Western blot analysis of LAMP2 and LC3B in total protein lysates from GSC#9 treated with vehicle (DMSO) and mepazine (MPZ, 20 μM) in the presence of cycloheximide (CHX, 50 μg/ml) for 16 h. TUBULIN served as a loading control.

E Western blot analysis of indicated antibodies in total protein lysates from GSC#1, GSC#12, and GSC#4 that received vehicle (DMSO, –) or mepazine (MPZ, 20 μM, 1 h).

F Western blot analysis of indicated antibodies in total protein lysates from GSC#9 treated vehicle (DMSO) or mepazine (MPZ, 20 μM) for the indicated times. GAPDH serves as a loading control.

G Confocal analysis of LAMP2 (red) and mTOR (green) staining in GSC#9 treated vehicle (DMSO) or MPZ (20 μM) for the indicated times. Arrows point to LAMP2-positive area. Nuclei (DAPI) are shown in blue. Scale bars: 10 μm.

H GSC#9 were transfected with sic or si*TFEB* and treated with vehicle (DMSO) or MPZ (20 μM) for 16 h. Samples were analyzed as described in (G). Arrows point to LAMP2-positive area. Nuclei (DAPI) are shown in blue. Scale bars: 10 μm.

Data information: All data were repeated in three independent experiments, unless specified.
Source data are available online for this figure.

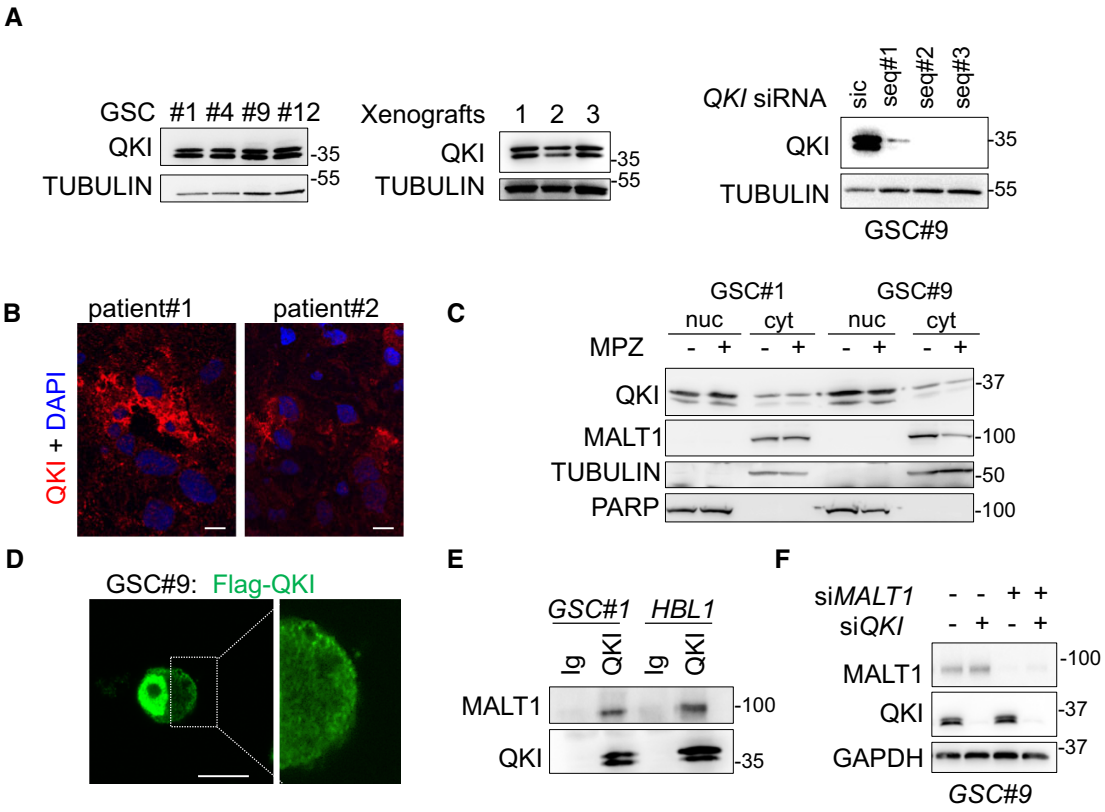

Figure EV4. Characterization of the RNA-binding protein QKI in glioblastoma cells.

A Western blot analysis of QKI in total protein lysates from GSC #1, #4, #9, #12, and from GSC-xenografted tumors. Alternatively, GSC#9 were transfected with sic or si*QKI* using three different duplexes. TUBULIN served as a loading control.

B Confocal analysis of QKI immunostaining (red) in glioblastoma tissue sections from two patients. Nuclei (DAPI) are shown in blue. Scale bars: 10 μm.

C Western blot analysis of QKI in cytosolic (cyt.) and nuclear (nuc.) cell fractionation from GSC#1 and GSC#9, treated with vehicle (–) and mepazine (MPZ, 20 mM, 1 h). TUBULIN and PARP served as loading controls for each fraction. Each panel was replicated at least twice.

D Confocal analysis of FLAG-QKI (green) localization in transfected GSC#9. Scale bars: 10 μm.

E GSC#1 and HBL1 protein lysates were processed for immunoprecipitation using control immunoglobulins (Ig) and anti-QKI antibodies. Western blots were performed using anti-MALT1 and anti-QKI, as specified.

F GSC#9 were transfected with non-silencing RNA duplexes (sic), *QKI* targeting siRNA duplexes (si*QKI*), *MALT1* targeting siRNA duplexes (si*MALT1*), or double-transfected with si*QKI* and si*MALT1* and analyzed 72 h later. Knockdown efficiency was checked by Western blot analysis using the indicated antibodies.

Source data are available online for this figure.

Discussion

Discussion

1. Intercellular Signaling

The first goal of this study was to identify novel targets involved in intercellular signaling between GSCs and endothelial cells. We identified that the transmembrane glycoprotein gp130 is important for stemness maintenance in response to endothelial cues, as blocking antibodies against gp130 abolish functional properties of GSCs cultured in a medium enriched with endothelial cell-secreted factors. However, how gp130 affects self-renewal in GSCs, and the nature of the downstream signaling pathways altered upon its inhibition have not been fully defined.

1.1 Defining the Role of gp130 in Downstream GSC Signaling

In order to better understand its role in the pathways regulating stemness of GSCs, we generated two gp130 KO clones in one patient-derived GSC from a Mesenchymal tumor origin, via CRISPR/Cas9 editing. In both clones, we detected a marked decrease in STAT3 phosphorylation at Y705, as compared to wildtype (WT) cells analyzed by western-blot (Figure 31A). Moreover, transcriptome data from RNA sequencing highlight a “LIF signaling” signature between KO and WT cells (Figure

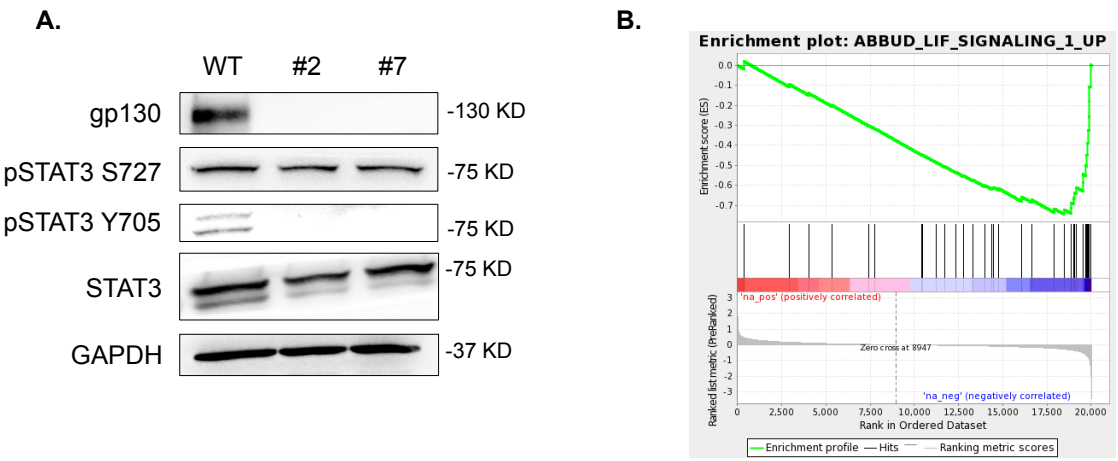

Figure 31: Downstream Signaling upon gp130 Knockout.
(A) Briefly, wildtype and KO clones #2 and #7 were lysed in TNT lysis buffer and blotted for gp130 and p-STAT3 (Y705 and S727). Total STAT3 and Tubulin serve as loading controls. (B) RNA sequencing was performed on wildtype versus KO clones #2 and #7. GSEA (gene set enrichment analysis) plot showing enrichment of “LIF signaling” signature in wildtype versus KO #2 and #7 triplicates. Data are representative of 3 independent experiments in A and 3 Biological replicates in B. Detailed methods can be found in Annex 5.

31B). In contrast, there was no obvious repertoire switch, which may occur due to subpopulation selection from cloning pressure.

The leukemia inhibitory factor (LIF) is a member of the IL-6 family of cytokines. The LIF receptor is a co-receptor of gp130 and activates downstream JAK[45]/ STAT3[46] signaling upon its triggering (Gearing et al., 1991). After dimerization of the LIF receptor and gp130, the kinase cascade of JAKs leads to the activating Y705 phosphorylation of the transcription factor STAT3, which subsequently promotes the expression of its target genes. These include classical stemness markers, such as SOX2, angiogenic modifiers like VEGF, as well as gene products involved in survival pathways, including AKT (Niu et al., 2002, 2002; Wang et al., 2017a).

In glioma, several studies have implicated STAT3 as a marker of poor prognosis (Abou-Ghazal et al., 2008; Ganguly et al., 2018; Tu et al., 2011). Additionally, the therapeutic potential of blocking STAT3 action was explored by multiple groups (Ashizawa et al., 2013; Fuh et al., 2009; Gao et al., 2010; Li et al., 2010; Shi et al., 2018). Likewise, the upstream activator of STAT3, IL-6 was linked to worse survival in GBM and targeting either the receptor or ligand reduces tumor growth (Choi et al., 2002; Tchirkov et al., 2007; Wang et al., 2009). Moreover, the gp130-IL6 receptor complex is stabilized by the tetraspanin CD9 and this increases STAT3 signaling in GSCs (Shi et al., 2017). Therefore, one remaining question in our experimental models is whether IL-6 secretion is altered in KO cells. This can be answered with ELISAs of the WT vs KO secretome.

Combination studies inhibiting STAT3 have also been performed. Indirect blockade of STAT3 signaling using resveratrol enhanced the effects of radiotherapy (Yang et al., 2012). Furthermore, STAT3 inhibitors resensitized TMZ-resistant cell lines to TMZ-induced cell death by downregulating the MGMT (Kohsaka et al., 2012). Therefore, targeting gp130 in combination with standard of care therapy could prove effective in the treatment of GBM.

[45] Janus Kinase
[46] Signal Transducer and Activator of Transcription 3

1.2 Is gp130 Action on Stemness linked to Apelin Signaling?

As we also reported a potent effect of the endothelial-released peptide, Apelin, in stemness maintenance (Annex 2), we revisited gp130 in the context of Apelin signaling. Under cell culture with Apelin factor alone, pharmacological blockade of gp130 with either blocking antibodies or the drug LMT-28 abrogated the effect of Apelin on GSC expansion. Furthermore, this phenotype was recapitulated in gp130 KO clones (Figure 32).

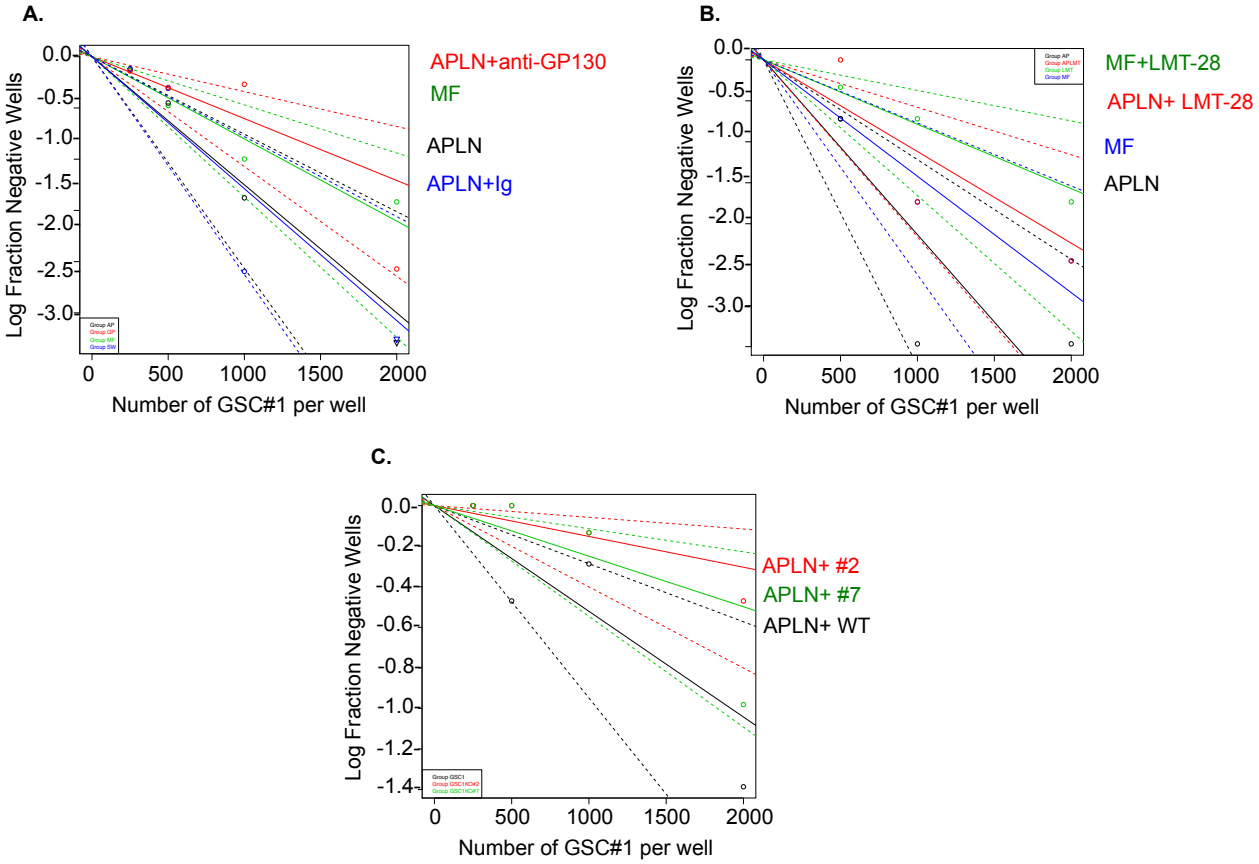

Figure 32: Inhibition of gp130 alters Apelin Signaling.
(A) Limited Dilution Assay (LDA) of GSC#1 +/- Apelin and +/- anti-gp130 blocking antibody. The more stem the cells, the closer the slope is to a vertical line. (B) LDA of GSC#1 +/- Apelin +/- LMT28. (C) LDA of GSC#1 in Apelin-containing media. WT= wildtype cells, #2= clone #2 KO gp130, #7 = clone #7 KO gp130. N= 2 independent experiments for each panel. Detailed methods can be found in Annex 5.

Additionally, gp130 is a co-receptor for multiple membrane receptors, including IL-6R, LIF, IL-11R, CTNF-R[47], and WSX-1 (IL-27) (White and Stephens, 2011). We therefore investigated the possibility that a portion of gp130 could be

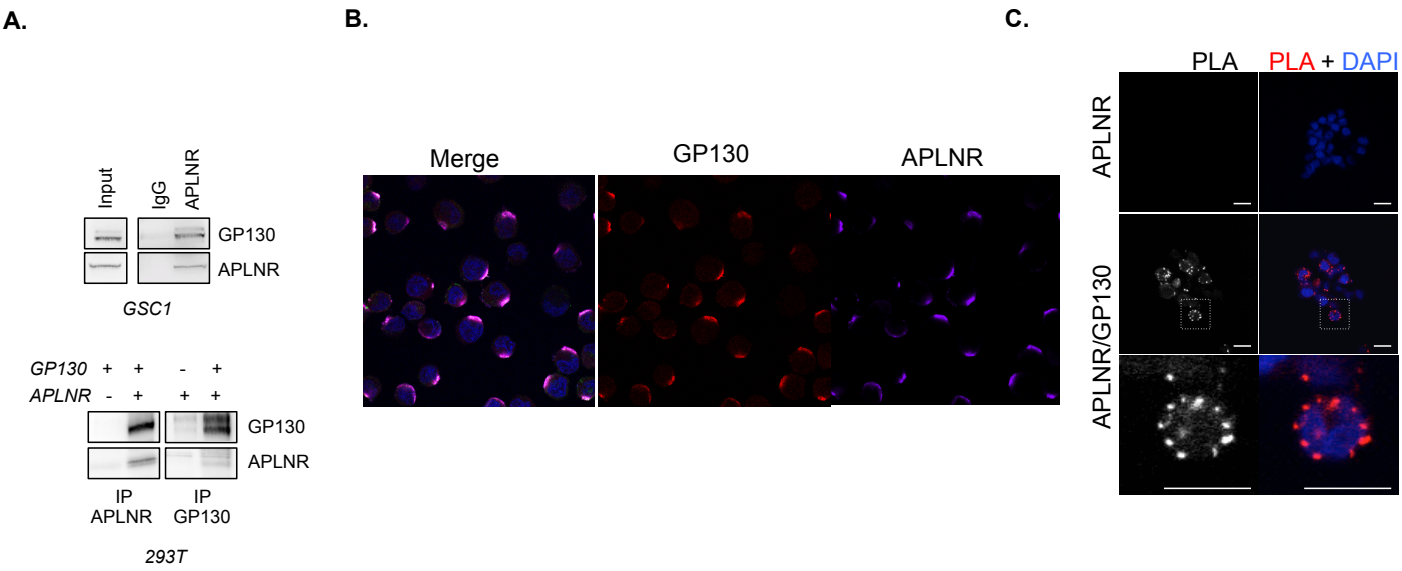

Figure 33: Apelin Receptor interacts with gp130 in GSCs.
(A) gp130 co-immunoprecipitates with APLNR in endogenous GSC#1 (Top) and in a HEK-293T overexpression system. (B) Costaining of gp130 (red) and APLNR (purple) in GSC#1. (C) Proximity ligation assay (PLA) in GSC#1 of APLNR and gp130. Data are representative of 3 independent experiments. Detailed information on methods can be found in Annex 5.

interacting with the Apelin receptor (APLNR), a GPCR[48], in GSCs. In order to explore this possibility, we performed co-immunoprecipitation (Co-IP) experiments in endogenous and ectopic systems. In the over-expression system, APLNR falls into the gp130 immunocomplex and *vice versa*. The same was true endogenously in GSC#1 (Figure 33A). Moreover, immunofluorescence analysis of APLNR and gp130 showed polarized co-staining of the receptors in GSC#1 (Figure 33B). Using proximity ligation assay (PLA), we confirmed the close contact (less than 40 nm) between gp130 and APLNR. Therefore, we concluded that gp130 interacts with the Apelin receptor in GSCs.

GPCRs are maintained at the plasma membrane through association with eachother or with scaffold proteins. For example, GABA receptors form heterodimers to anchor them at the cell surface (White et al., 1998). Additionally, the GPCR mGluR5, involved in synaptic signaling in neurons, is maintained at the plasma membrane by the scaffold Homer (Ango et al., 2000). Moreover, a previous report

[47] Ciliary neurotrophic factor
[48] G protein-coupled receptor

demonstrated that gp130 is stabilized by the tetraspanin CD9 to prevent its recycling and extend STAT3 signaling (Shi et al., 2017). With this in mind, we hypothesized that gp130 and the APLNR might secure eachother at the membrane. Our data suggest that gp130 associates with the APLNR, and blockade or KO of gp130 abolishes the effects of Apelin on stemness. Indeed, in cells KO for gp130, there was less APLNR on the surface as compared to WT (Figure 34A). Importantly, the overall level of APLNR expression, as tested by qRT-PCR, was similar between WT and gp130 KO cells (data not shown). Moreover, re-expression of ectopic gp130 restored APLNR to the membrane (Figure 34B).

In GSCs, gp130 acts as a novel co-receptor of APLNR, stabilizing this protein at the

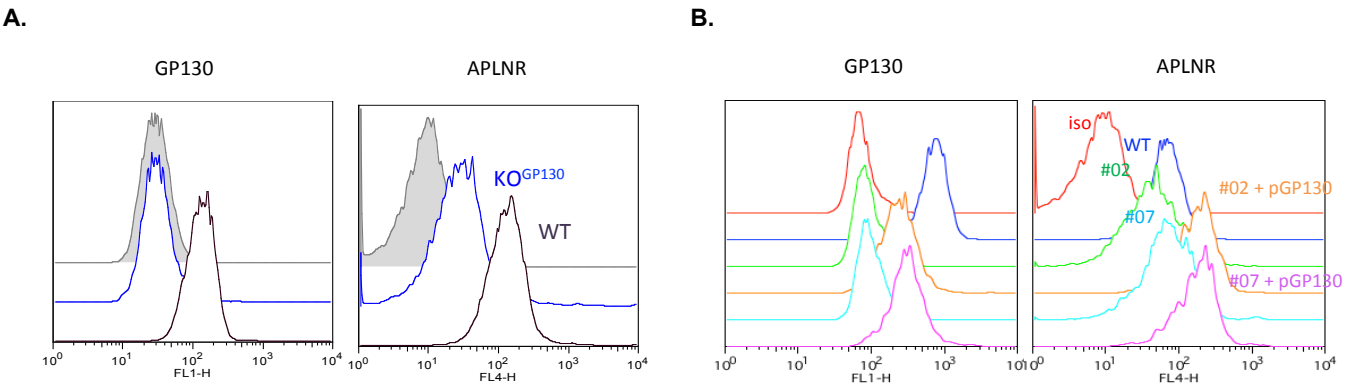

Figure 34: gp130 regulates APLNR availability at the membrane.
(A) FACS analysis of surface expression of gp130 and APLNR in WT or KO gp130 cells. (B) FACS analysis of gp130 and APLNR surface expression in WT, KO clone #2 and KO clone #7 +/- gp130 reexpression. Detailed information on methods can be found in Annex 5.

membrane to enhance signaling. Hence, our recent data point to a scaffold role for gp130 in stemness maintenance (Figure 35).

Recent papers have emphasized an important role of Apelin signaling in cancer. Following our study about the role of Apelin in GSCs, work by Roland Kälin's group emphasized the pro-angiogenic nature of Apelin action in GBM. They found that blockade of VEGF/VEGFR triggering diminishes Apelin expression and that reducing Apelin signaling reduced tumor angiogenesis. Additionally, their *in vivo* data confirms the importance of Apelin in tumor growth as syngenic grafts were smaller when implanted in *Apln* KO background mice, as compared to WT animals (Mastrella et al., 2019b). These data emphasize the potential of Apelin blockade in

GBM therapy, as it targets tumor growth from two axes: both by reducing both the stem-like properties of GSCs and by reducing tumor angiogenesis.

Moreover, the role of Apelin signaling can now be expanded to other cancers. Josef Penninger's laboratory recently demonstrated that targeting Apelin improves vessel function and prevents resistance to receptor-tyrosine kinase (RTK) therapy in lung and breast cancer models. Metastases were also reduced. Moreover, high Apelin expression was correlated with poor prognosis in these cancers (Uribesalgo et al., 2019). Therefore, Apelin may be a ubiquitous marker of poor prognosis across a variety of cancers.

In a recent study by Patel and colleagues, the APLNR was identified as an important gene for cancer immunotherapy, as loss of this gene or point mutation identified in melanoma reduced the efficacy of these treatments. Interestingly, APLNR could co-immunoprecipitate with JAK1 in such tumor cells (Patel et al., 2014). As JAK1 can bind to gp130, this converges with our findings that gp130 is a novel co-receptor of the APLNR. Further study will unveil whether or not JAK1 is a component of the APLNR-gp130 signaling complex in GSCs.

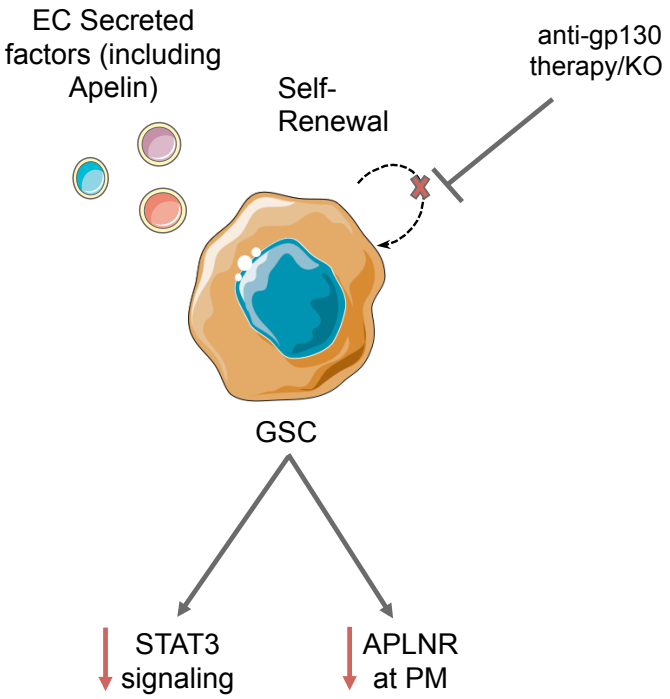

Figure 35: Effects of gp130 inhibition or deletion in GSCs.

Additionally, Ralf Adam's group, in the context of bone marrow transplantation, explored the role Apelin in vascular regeneration after irradiation. Radiation therapy induced vessel permeability and morphological changes. Apelin positive EC's are necessary for the restoration of vessel integrity in this context, as they are critical for the maintenance of hematopoietic stem cells in the niche (Chen et al., 2019b). These results can be extrapolated, to form hypotheses about the

therapeutic potential of this mechanism in tumors. If radiotherapy induces similar changes in the tumor vasculature, one can hypothesize that anti-apelin/APLNR therapy may enhance the effectiveness of this treatment. Indeed, preliminary data from our lab suggest an increased expression of apelin in irradiated brain ECs (data not shown). Moreover, our *in vitro* results show a synergism between TMZ and anti-APLNR therapy. Therefore, further study combining anti-APLNR therapy with standard of care treatment could prove effective against GBM growth.

Based on our data and the work of others, Apelin appears to play a reciprocal role in maintaining the integrity of the vascular niche. Not only does it promote angiogenesis, but also it is critical for maintaining stem properties in GSCs. Targeting the apelin/APLNR signaling axis could prove more effective than current anti-angiogenic therapy, as it targets multiple actors within the niche.

2. Intracellular signaling

The second goal of this research was to identify novel mechanisms governing non-oncogene addiction, *ie* pathways not necessarily involved in the initiation of the transformed phenotype of tumor cells but rather in their persistence. Through analysis of the TCGA, we identified that the protease MALT1 is correlated with GBM patient probability of survival. Accordingly, knockdown or pharmacological blockade of MALT1 reduced patient-derived cell viability *in vitro*. This was accompanied by decreased mTOR activation and an increase in the abundance of endo-lysosomes. However, how MALT1 acts on mTOR activation, and how this lysosomal increase leads to cell death remain undefined.

2.1 MALT1 in Solid Tumors

The importance of MALT1 in ABC DLBCL has been extensively investigated, due to its constitutive activity in these lymphoma cells (Ferch et al., 2009; Hailfinger et al., 2009). Inhibitors of MALT1, including zVRPR, phenothiazines (especially MPZ) and MI2, were selectively toxic to these cancer cells *in vitro* and *in vivo* (Fontan et al., 2012; Hailfinger et al., 2009; Nagel et al., 2012b; Schlauderer et al., 2013). As such, a MALT1 inhibitor, JNJ-67856633 is currently in phase I clinical trials (NCT03900598) for the treatment of this disease.

In addition to our study of MALT1 in GSCs, the paracaspase was also explored in several solid tumors including non-small cell lung cancer (NSCLC), GBM, pancreatic cancer, osteosarcoma, and breast cancer (Konczalla et al.; McAuley et al., 2019; Pan et al., 2016; Yang et al., 2017). In NSCLC and GBM, the scaffold role of MALT1 in NF-κB activation, but not its protease activity, was shown to be important for cell growth and migration (Pan et al., 2016; Yang et al., 2017). However, the study in GBM was primarily done in established cell lines, U87, in which NF-κB status may differ from patient-derived cells, which more accurately represent human tumors (Galan-Moya et al., 2011; Harford-Wright et al., 2017; Lathia et al., 2015). Indeed, our results did not demonstrate obvious CBM-dependent activation of NF-κB in GSCs. Also, a recent study by Konczalla et al. demonstrated that MALT1 was highly expressed and active in pancreatic ductal adenocarcinomas and that inhibition reduced growth both *in vitro* and *in vivo* (Konczalla et al., 2019). Concurrently, McAuley and colleagues showed that protease-activated receptor 1 (PAR1) induced CBM-dependent NF-κB activation and MALT1 protease activity in both breast cancer and osteosarcoma cells (McAuley et al., 2019). Hence, the role of MALT1 in CBM-dependent NF-κB activation may be more pervasive across different cancers. One drawback to these studies is that they did not fully delve into the protease function of MALT1, and the effects of its processed substrates. Therefore, more extensive investigation to understand all of MALT1's functions in solid tumors will help to inform its use as a target in cancer therapy.

2.2 How does MALT1 affect mTOR?

Our experimental results clearly demonstrate a potent effect of MALT1 inhibition on mTORC1 activation in GSCs. Moreover, we show that mTOR is less associated with LAMP2 staining upon MALT1 silencing or blockade, indicating that lack of downstream signaling may be due to displacement of mTORC1 at the lysosomes. However, our current data cannot not discriminate between the possibility that either mTOR is re-localized from the lysosome or whether signaling is dampened due to expansion of the endo-lysosomal compartment. Co-IP for Raptor and the lysosomal Rags, or lysosomal IPs (Abu-Remaileh et al., 2017) may serve to answer this question.

The decrease in downstream mTOR signaling upon MALT1 inhibition in GSCs confirms two previous studies in lymphocytes. These studies showed that MALT1 inhibition abrogates antigen receptor-dependent activation of the mTOR pathway (Hamilton et al., 2014; Nakaya et al., 2014). However, to date no MALT1 substrates involved in the mTOR cascade have been identified.

In order to be considered as a MALT1 substrate, proteins must contain an S/P-R↓G/A consensus motif. Upon MALT1 activation, protein levels of the full-length substrate should be reduced, while restored upon inhibition of the protease. Additionally, mutation of the arginine in the consensus motif should protect against MALT1-driven cleavage. We and others speculate that there do exist MALT1 substrates within mTOR pathway. As MALT1 inhibition blocks mTOR signaling, the most likely candidates are negative regulators of mTOR activity, which would prevent mTORC1 docking at the lysosome. Likewise, MALT1 proteolytic action has been shown to inactivate negative regulators of the NF-κB pathway, in order to amplify the

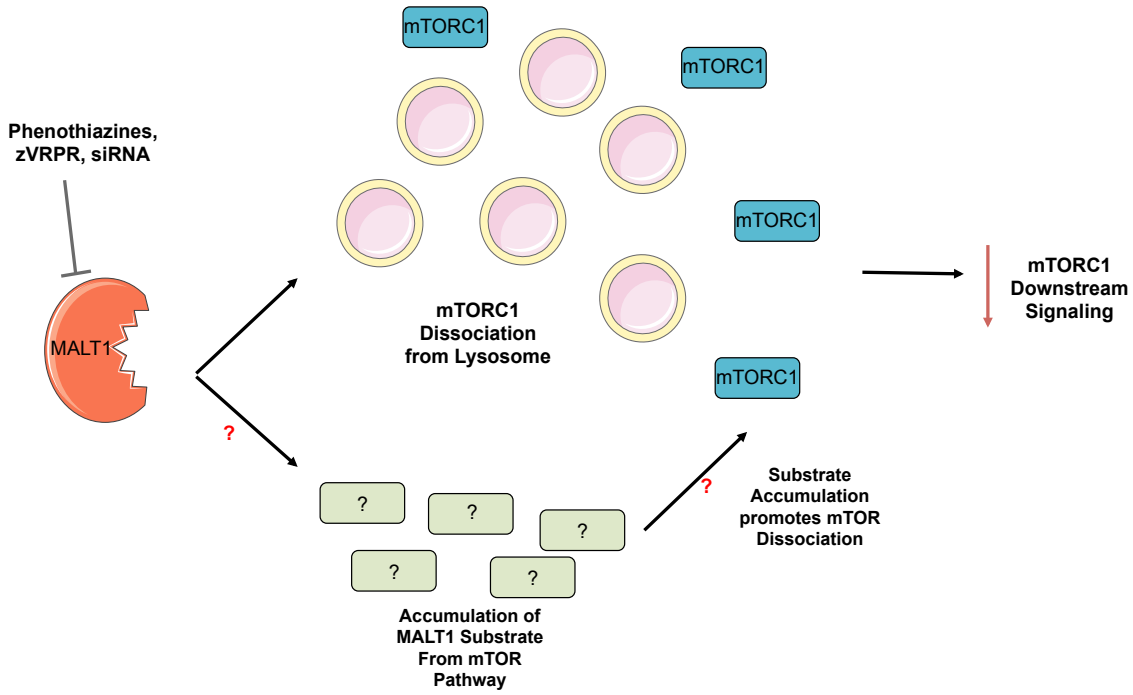

Figure 36: MALT1 action on mTOR activation.

downstream action of the transcription factor (Coornaert et al., 2008b; Douanne et al., 2016; Hailfinger et al., 2011). So it is feasible that MALT1 exerts a similar role in fine-tuning mTOR signaling nexus. Of note, overexpression of catalytically dead MALT1 reduced mTOR activation in GSCs, signifying that the protease activity is

important for mTOR triggering in these cells. With this in mind, we plan to perform *in silico* analysis of the mTOR pathway components to uncover putative MALT1 substrates. While we cannot exclude that MALT1 inhibition indirectly affects the mTOR pathway, our data points to a mechanistic link between MALT1 and mTOR in GSCs, which prompts further investigation.

In brief, most GBM tumors display aberrant mTOR activation likely due to PTEN deletion and EGFR amplification or mutation. However, rapalogs failed in clinical trials, probably owing to continued mTORC2 activation (Cancer Genome

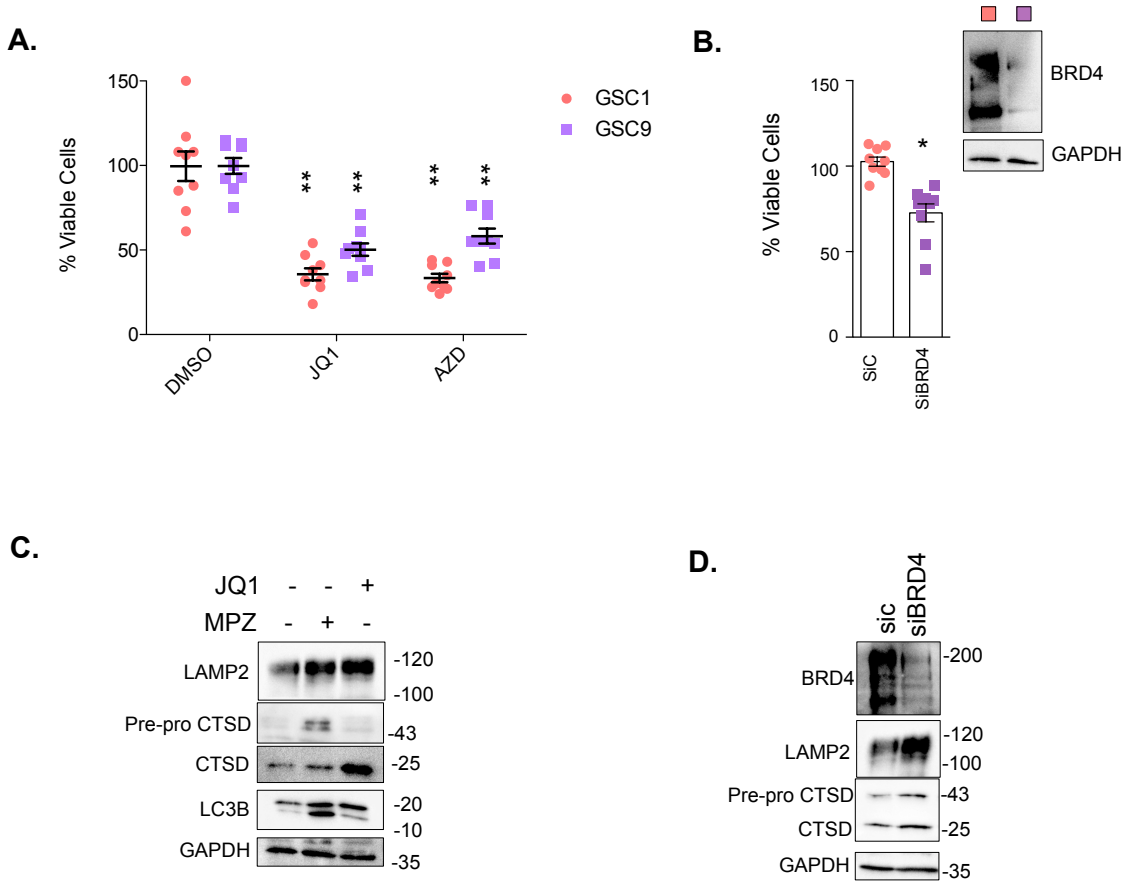

Figure 37: BRD4 blockade increases lysosomes and reduces GSC viability. (A and B) Cell titer Glo assay of GSCs treated 48 hrs with BRD4 inhibitors, JQ1 and AZD5153 (A) or 72 hrs after knocked-down for BRD4 using siRNA (B). % viable cells refers to the % viable/DMSO. BRD4 expression was controled by Western-blot where GAPDH served as a loading control. (C and D) Western-blot of lysosomal protein amount LAMP2 and cathepsin D (CTSD) in response to mepazine (MPZ) or JQ1 (C) or BRD4 KD (D). GAPDH served as a loading control. All data are representative of 3 independent experiments. *p<0.05 **p<0.01

Atlas Research Network, 2008; Fine et al., 2009). Therefore, novel therapies, which

potently inhibit mTORC signaling could prove effective in the treatment of this disease.

2.3. TFEB-Independent Regulation of Lysosomal Biogenesis

The MITF family transcription factor TFEB is an established master regulator of lysosomal biogenesis. Upon mTOR inhibition, TFEB is translocated to the nucleus to bind to the CLEAR element in the promoter of many lysosomal and autophagy genes which enhances both the formation of new lysosomes and the induction of the autophagy pathway (Napolitano and Ballabio, 2016b).

Recent studies have identified the existence of TFEB-independent control of lysosomal biogenesis. The first, reported by Kevin Ryan's laboratory, identified that BRD4 is a transcriptional repressor of CLEAR network genes independent of TFEB. BRD4 inhibition enhanced the induction of autophagy under several signaling cues including starvation, hypoxia, rapamycin treatment, and oncogenic Ras expression, however it had no effect on mitophagy, the organelle specific degradation of mitochondria. Moreover, BRD4 inactivation occurs in response to AMPK stimulation, suggesting that its repression of the CLEAR network has a function in the cellular nutrient sensing response (Sakamaki et al., 2017). Our preliminary data using BRD4 knockdown or inhibition with the BET bromodomain pharmacological inhibitor JQ1 confirms that this protein regulates lysosomal biogenesis in GSCs (Figure 37 C-D).

In conjunction with this, an interesting report demonstrated a role of AMPK in TFEB-dependent transcription via its regulation of CARM1[49], a co-activator of the CLEAR network (Shin et al., 2016). AMPK senses changes in cellular energy through the detection of AMP levels. Upon activation, AMPK inhibits mTOR and activates autophagy through its kinase activity. When mTOR is stimulated, it phosphorylates TFEB to prevent nuclear shuttling. As AMPK promotes TFEB action (via mTOR inactivation and CARM1 stimulation), while also inactivating BRD4, this metabolic enzyme seems to act as a key link between both pathways that converge on lysosome formation. Hence, one can envision a model of lysosomal regulation where AMPK rather than TFEB may be the "master" regulator of lysosomal biogenesis.

[49] Co-activator-associated arginine methyltransferase 1

Similarly, lysosomal biogenesis can be regulated post-transcriptionally. Shingu et al. identified that the RNA binding protein QKI associates directly to stabilize lysosomal RNAs in NSCs and GSCs, independently of TFEB. Moreover, QKI expression is lower in GSCs as compared to NSCs resulting in fewer lysosomes (Shingu et al., 2016). Our data implicates the paracaspase MALT1 in this process. Rather than reducing QKI expression, our study indicates that in patient-derived GSCs, MALT1 alters QKI availability to binding to its targets (including lysosomal RNAs) resulting in turn in reduced number of lysosomes. Indeed, QKI co-immunoprecipitates with the MALT1 binding partner BCL10, while MALT1 interacts with QKI. Moreover, inhibition of MALT1 reduces this association.

This gives rise to two major hypotheses as to how MALT1 alters QKI accessibility: either QKI is a substrate of MALT1, or MALT1 sequesters QKI to prevent it from binding to target RNAs. *In silico* analysis of the QKI amino acid sequence revealed a potential MALT1 cleavage site are R106 (on the human sequence). QKI as a MALT1 substrate is an intriguing possibility because MALT1 is already known to cleave other RNA binding proteins, namely Roquin1/2 and Regnase-1 (Jeltsch et al., 2014; Uehata et al., 2013). Also, preliminary western-blots for QKI in GSCs showed a specific band at ~25kDa that disappears upon QKI silencing, consistent with the expected size of a C-terminus cleavage fragment (Figure 38A). This band was present in a panel of four patient-derived GSCs (Figure 38B). However, there was no clear induction of the 25kDa fragment in Jurkat T cells upon stimulation (data not shown), calling into question the possibility that QKI is a substrate upon tonic activation of MALT1. More experiments need to be done with MALT1 inhibitors, and catalytically dead MALT1, including introduction of an “uncleavable” QKI mutant, in order to determine whether or not this RNA binding protein is indeed a substrate of MALT1.

If QKI is not a direct MALT1 substrate, this favors the possibility that the RNA binding protein is sequestered by MALT1 and is kept silent when in complex with MALT1. In this scenario, MALT1 inhibition allows QKI to be liberated from MALT1 isolation and free to bind and stabilize its targets. Because the catalytic activity of MALT1 is also engaged in this process, as per our data with zVRPR and protease dead mutant, this likely excludes steric hindrance. Rather this would suggest that MALT1 activity helps in maintaining QKI at the vicinity of the CBM complex, possibly by processing an intermediate substrate involved in regulating this process. Further

studies would be required to delineate how MALT1 modulate QKI localization and acitivity in GSCs.

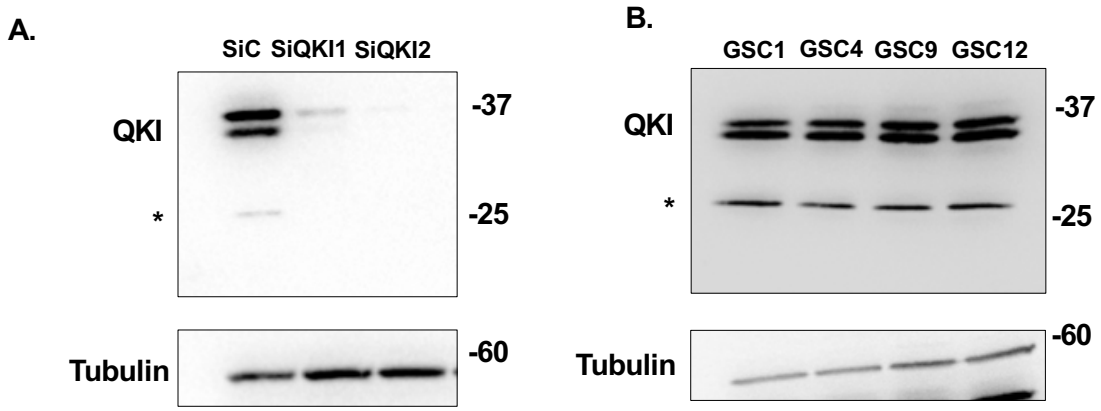

Figure 38: Potential QKI cleavage in GSCs. (A) Western-blot of GSC9 transfected with 2 siRNA sequences against QKI or non-silencing control (SiC) to evaluated QKI expression. (*) denotes potential C-termiunus cleavage fragment. Tubulin serves as a loading control. (B) Western-blot for QKI (37 KD) of 4 patient derived GSCs (*) denotes potential C-termiunus cleavage fragment.

2.4 Does MALT1 inhibition induce LMP?

Our data clearly show that lysosomes play an important role in MALT1-dependent cell death. Inhibition, with phenothiazines or zVRPR, induces an increase in endo-lysosomes, and lysosomal drugs partially rescue these cells from death. Additionally, MALT1 silencing or overexpression of catalytically dead MALT1 recapitulate the drug induced effects. Moreover, silencing of the lysosomal regulator QKI (Shingu et al., 2016) assuages MALT1 inhibition phenotype. However, whether or not these cells experience LMP remains to be determined.

LMP can be difficult to detect because the ultrastructure of lysosomes is not always changed (Aits and Jäättelä, 2013). In terms of my results, DQ-Ovalbumin data hints at phenothiazine-induced LMP. Staining is indeed dimmer at later time points upon MPZ treatment, suggesting the lysosomal compartment is less acidic. However, there was still a strong lysotracker staining of cells at 16 hours, and all experiments with transferrin were performed in a shorter time frame (4 hrs), therefore longer timer courses need to be performed in these settings to confirm this observation. Moreover, MALT1 blockade or silencing, causes an impairment in

autophagic flux in GSCs, as certified with a clear accumulation of lipidated LC3 and P62. LMP is often accompanied by a reduction in autophagic flux due to “defective” lysosomes (Elrick and Lieberman, 2013; Wang et al., 2018). Galectins (including Gal3) are recruited to leaky lysosomes upon LMP; which can therefore be experimentally visualized by the formation of galectin puncta at lysosomes (Aits et al., 2015; Chauhan et al., 2016). In our settings, Galectin-3 and LAMP2 co-staining will be analyzed upon MALT1 knockdown or inhibition to address this question.

Moreover, our data do not exclude the possibility that some deleterious effects on the lysosomes are due to non-selective actions of the drugs used in this study, as less potent MALT1 inhibitors, like promethazine, also expand the lysosomal compartment (Nagel et al., 2012b; Schlauderer et al., 2013). Indeed, phenothiozines have a cationic amphiphilic nature, due to their hydrophilic amine groups and a hydrophobic aromatic ring structures. As previously mentioned CADs can freely diffuse across the lysosomal membrane and disrupt ASM stability (Gulbins and Kolesnick, 2013; Kirkegaard et al., 2010; Petersen et al., 2013). Therefore we cannot discount that some of the effect of phenothiozines on the lysosomes is independent of MALT1 action. Also other drugs, such as clemastine, induce LMP and lysosomal compartment increase in GBM cells (Le Joncour et al., 2019). Indeed, though not of the same drug family, zVRPR can also affect lysosomes by inhibiting Cathepsin B (Eitelhuber et al., 2015). Off target actions do not eliminate the therapeutic potential of phenothiazines. For example, despite the lysomotrophic properties of Sunitinib, it is commonly used as an anti-angiogenic treatment in cancer therapy. The lysomotropic nature of a molecule does not therefore preclude it from being an effective anti-cancer agent. (Meadows and Hurwitz, 2012; Zhitomirsky and Assaraf, 2014). Thus, as phenothiazines efficiently cross the blood-brain barrier in humans (Korth et al., 2001), and as these molecules are currently used in the clinic, they represent an interesting possibility for drug repurposing.

Certainly, targeting lysosomes has emerged as a potent and effective strategy in cancer therapy. Due to an altered lysosomal compartment, cancer cells are more susceptible to death upon treatment with LMP-inducers than normal cells (Gyrd-Hansen et al., 2004; Ono et al., 2003). In GBM, several studies have also illustrated the potential at targeting lysosomal stability (Le Joncour et al., 2019; Mora et al., 2010; Shingu et al., 2016). Mora and colleagues showed that altered sphingolipid

metabolism in GBM cells increased susceptibility to sphingosine kinase inhibitors (Mora et al., 2010). Comparably, Le Joncour et al used a lysomotrophic drug, clemastine, to disrupt lysosomal stability (Le Joncour et al., 2019). In a similar vein, Shingu's work demonstrates that GSCs downregulate lysosomal expression as a survival mechanism (Shingu et al., 2016). In addition, our preliminary data using BRD4 knockdown or blockade with JQ1 and AZD5153 revealed an increase in lysosomal proteins in conjunction with reduced cell viability, underlining the vulnerability of GSCs towards disruption in lysosome homeostasis (Figure 37). Hence, our study expands upon the idea that lysosomes act as the "Achilles heels"

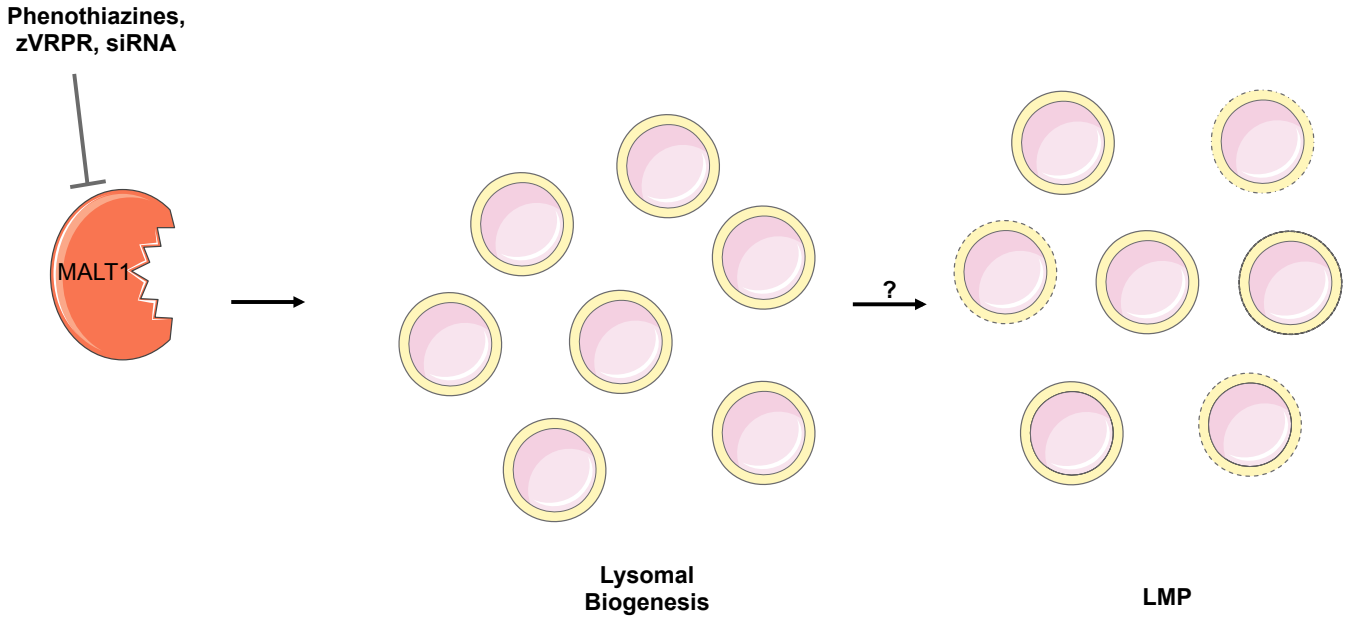

Figure 39: Does MALT1 induce LMP?

of GSC viability.

How could MALT1 contribute to LMP? Our data indicate that MALT1 sequesters QKI, most likely away from binding its RNA targets. As Shingu and colleagues previously demonstrated that QKI associates directly with lysosomal RNAs in GSCs (Shingu et al., 2016), we hypothesize that MALT1 inhibition biases the system towards an increase in lysosomal biogenesis. However, currently, we do not know whether the freshly synthesized lysosomes are fully functional. It is indeed possible, that these newly formed lysosomes lack certain components, making them "leaky" and susceptible to cathepsin release. We plan to explore the composition of these neo-lysosomes by performing lysosomal IPs (Abu-Remaileh et al., 2017)

followed by mass spectrometry, upon MALT1 inhibition or silencing, to determine the presence of lysosomal alterations.

As MALT1 is a protease, and as the expression of a catalytically dead MALT1 leads to an increase in the lysosomal compartment, another possibility is that MALT1 directly cleaves a substrate involved in lysosomal stability, such as QKI itself (see discussion 2.3). However, further study needs to be done to identify other potential candidates.

2.5 Lysosomes and Stem Cell Fate

In addition to the established lysosomal vulnerability of cancer cells, emerging evidence highlights a potential role of lysosomes in the stem cell fate. A recent study by Villegas et al used a CRISPR genome wide screen to identify regulators of embryonic stem cell (ESC) differentiation. This classified TFE3 as a governor of ESC pluripotency. In fact, this study unveiled a novel role for Rag C and D outside their canonical function in

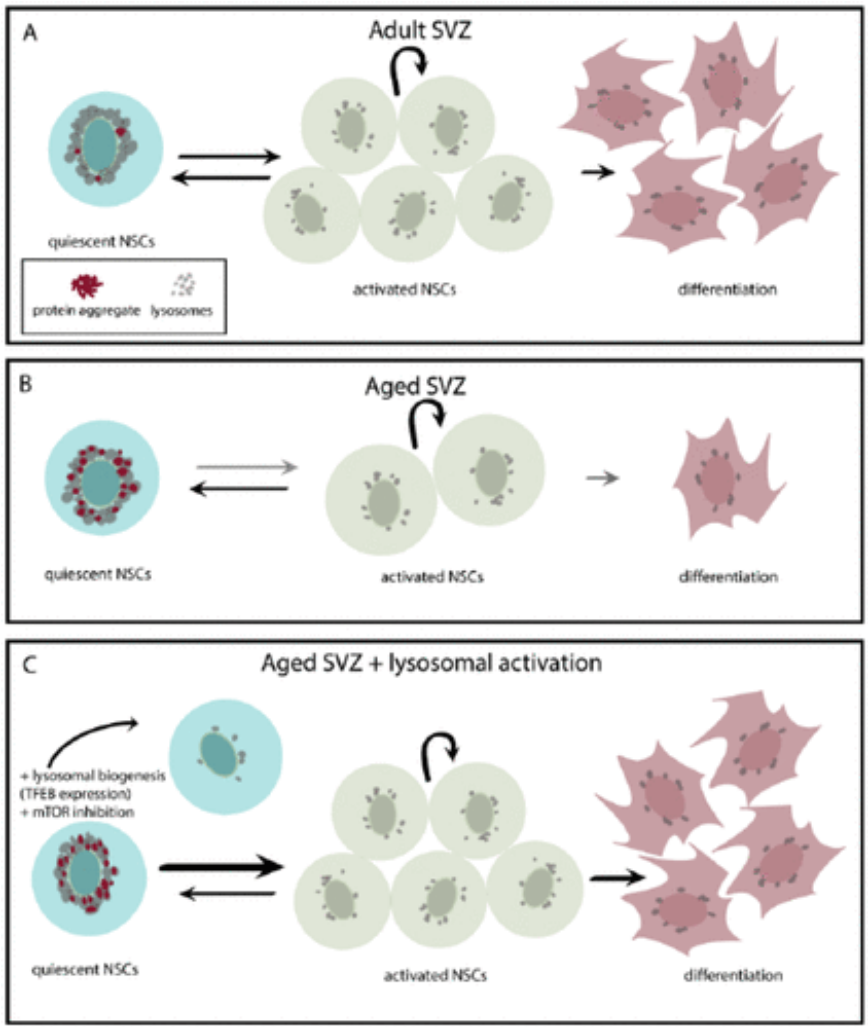

Figure 40: Lysosomal involvement in NSC differentiation from Audesse and Webb 2018. (A) Quiescent NSCs have more lysosomes than activated NSCs. (B)In aged NSCs there are less functional lysosomes and more protein aggregates leading to reduction in NSC activation. (c) Lysosomal restoration could ameliorate the phenotype of aged NSCs.

mTOR recruitment. Instead, in this context, these Rags retain TFE3 in the cytoplasm to prevent nuclear translocation and cellular differentiation. As TFE3 directly binds to CLEAR network targets, this implies that increased lysosomal protein expression and degradation promotes differentiation. Likewise, this mechanism also occurs in neural progenitor cells, suggesting that TFE3 may ubiquitously regulate the differentiation process (Villegas et al., 2019). Therefore, this study highlights a potential impact of lysosomes on stem cell fate.

Furthermore, damaged and misfolded proteins are cleared either by the ubiquitin proteasome system or through the autophagy/lysosome degradation pathway. Disruption of either system can lead to protein aggregate accumulation, which can affect cellular functioning and viability. One area of the body especially sensitive to protein aggregates is the central nervous system, as protein aggregates play a key role in the development of neurodegenerative diseases (Balch et al., 2008). With this in mind, a recently discovered characteristic of aging NSCs is the development of defective lysosomes, which leads to the accumulation of protein aggregates. A study by Anne Brunet's group demonstrated that quiescent NSCs (qNSCs) had more numerous and larger lysosomes than activated NSCs. However, when older qNSCs were compared to younger qNSCs, there was a reduction in lysosome expression and an accumulation of protein aggregates. Moreover, these cells were less able to initiate differentiation than their younger counterparts. These data suggest that restoration of lysosomal function in aging qNSCs could improve their capacity to clear aggregates and activate in response to stimuli (Figure 40) (Audesse and Webb, 2018; Leeman et al., 2018). Also, Kobayashi and colleagues confirmed an important role of lysosomes in NSC quiescence. There was higher lysosomal receptor recycling in qNSCs than in proliferating ones. Likewise, when lysosomal degradation was blocked in qNSCs, these cells exited the quiescent state. These results suggest that lysosomes play an important role in qNSC maintenance.

The RNA binding protein QKI is mostly expressed in the brain, and has recently been reported as a lysosomal regulator in NSCs and GSCs (Shingu et al., 2016). Interestingly, QKI has previously been implicated in Parkinson's disease. QKI null mice display dysmyelination in the central nervous system and a phenotype of tonic seizures, as well as deletions in *Parkin*, a protein known to be altered in many cases of Parkinson's disease (Lorenzetti et al., 2004). Furthermore, QKI gene expression was found to correlate with severity in Alzheimer's disease, (Gómez

Ravetti et al., 2010). Therefore, lysosomal dysfunction may be a common link in the process of aging, culminating with neurodegenerative diseases and with GBM development. Lysosomal integrity is of high importance for NSC maintenance, which may explain the increased sensitivity of their GSC counterparts to disruptions in lysosomal homeostasis.

In the course of this study, we identified two possible axes by which to target GSCs. As GSCs are known to engage in close contacts with endothelial cells, we first sought to disrupt their reciprocal communication. Interfering with the gp130/APLNR signaling axis can perturb stemness maintenance within the protective vascular niche. This molecular target has the potential to combine with standard of care therapies. Not all GSCs are found in this nutrient rich environment. We therefore explored at intrinsic survival mechanisms that could be exploited for therapeutic purposes. MALT1 proved important in GSC viability due to its role in lysosomal homeostasis. Our work and that of other groups point to the exciting therapeutic potential of perturbing lysosomal stability in GSCs. Thus, MALT1 inhibitors and other LMP inducing drugs may prove to be an effective strategy in the treatment of this lethal disease.

ANNEXES

ANNEX 1

Mini CV

Scientific Communication

Oral communications

- Oral Communication, ADELIH Meeting, Paris, March 2018. “Apelin Signaling in Glioblastoma Stem-like Cells”

Posters

- EMBO Autophagy, Creiff, Scotland, August 2019. ”The Paracaspase MALT1 regulates Endolysosome Levels in Glioblastoma Stem-Like Cells”
- Conference Cellular Proteolysis, SFBBM, Montpelier, France, October 2018. ”The Paracaspase MALT1 regulates Endolysosome Levels in Glioblastoma Stem-Like Cells” – Poster Prize winner
- EMBO Conference Lysosomes and Metabolism, Naples, Italy, May 2018. “Regulation of QKI by the Paracaspase MALT1 is required for Glioblastoma Stem Cell Survival”
- GDR MicroNIT Meeting, Marseille, France, January 2018. “Regulation of QKI by the Paracaspase MALT1 is required for Glioblastoma Stem Cell Survival”
- Brain Tumor Conference, Berlin, Germany, May 2017. “Neutralizing gp130 interferes with endothelial-mediated effects on glioblastoma stem-like cells”

Courses

- Course, Autophagy in the Healthy and Diseased Brain, Lake Como School for advanced studies, Lake Como, Italy, October 2018.

ANNEX 2

Pharmacological Targeting of Apelin impairs Glioblastoma Growth

doi:10.1093/brain/awx253 BRAIN 2017: 140; 2939–2954 | 2939

BRAIN
A JOURNAL OF NEUROLOGY

Pharmacological targeting of apelin impairs glioblastoma growth

Elizabeth Harford-Wright,[1,2] Gwennan Andre-Gregoire,[1,*] Kathryn A. Jacobs,[1,*] Lucas Treps,[2] Sophie Le Gonidec,[3] Heloise M. Leclair,[1,2] Sara Gonzalez-Diest,[1,2] Quentin Roux,[1] François Guillonneau,[4] Delphine Loussouarn,[5,6] Lisa Oliver,[5,6] François M. Vallette,[6,7] Fabienne Foufelle,[8] Philippe Valet,[3] Anthony P. Davenport,[9] Robert C. Glen,[10,11] Nicolas Bidere[1,2] and Julie Gavard[1,2]

*These authors contributed equally to this work.

Glioblastoma are highly aggressive brain tumours that are associated with an extremely poor prognosis. Within these tumours exists a subpopulation of highly plastic self-renewing cancer cells that retain the ability to expand *ex vivo* as tumourspheres, induce tumour growth in mice, and have been implicated in radio- and chemo-resistance. Although their identity and fate are regulated by external cues emanating from endothelial cells, the nature of such signals remains unknown. Here, we used a mass spectrometry proteomic approach to characterize the factors released by brain endothelial cells. We report the identification of the vasoactive peptide apelin as a central regulator for endothelial-mediated maintenance of glioblastoma patient-derived cells with stem-like properties. Genetic and pharmacological targeting of apelin cognate receptor abrogates apelin- and endothelial-mediated expansion of glioblastoma patient-derived cells with stem-like properties *in vitro* and suppresses tumour growth *in vivo*. Functionally, selective competitive antagonists of apelin receptor were shown to be safe and effective in reducing tumour expansion and lengthening the survival of intracranially xenografted mice. Therefore, the apelin/apelin receptor signalling nexus may operate as a paracrine signal that sustains tumour cell expansion and progression, suggesting that apelin is a druggable factor in glioblastoma.

1 CRCINA, Inserm, Team SOAP, CNRS, Universite de Nantes, Nantes, France
2 Institut Cochin, Team SOAP, Inserm, CNRS, Universite Paris Descartes, Paris, France
3 I2MC, Inserm, Universite Paul Sabatier, Toulouse, France
4 3P5 Proteomics Facility of the Universite Paris Descartes, Paris, France
5 Centre Hospitalier Universitaire (CHU) de Nantes, Nantes, France
6 CRCINA, Inserm, Universite de Nantes, Nantes, France
7 Institut de Cancérologie de l'Ouest, René Gauducheau, St Herblain, France
8 Centre de Recherches des Cordeliers, Inserm, Universite Paris Descartes, Paris, France
9 Experimental Medicine and Immunotherapeutics, University of Cambridge, Cambridge, UK
10 The Centre for Molecular Informatics, Department of Chemistry, University of Cambridge, Cambridge, UK
11 Computational and Systems Medicine, Department of Surgery and Cancer, Faculty of Medicine, Imperial College London, UK

Correspondence to: Dr Julie Gavard,
Team SOAP, Signaling in Oncogenesis, Angiogenesis and Permeability, IRS-UN blg, Room 416, 8 quai Moncousu, Nantes 44000, France
E-mail: julie.gavard@inserm.fr
Twitter: @LabSoap

Keywords: glioblastoma initiating cells; vascular niche; apelin; APJ; antagonist

Received January 25, 2017. Revised July 27, 2017. Accepted August 5, 2017. Advance Access publication October 3, 2017

Abbreviations: EC-CM = endothelial cell conditioned media; GSC = glioblastoma stem-like cells; MF = mitogen-free; NS = mitogen-supplemented; TMZ = temozolomide

Introduction

Glioblastoma is the most common and lethal primary brain tumour in adults. Although there has been notable progress in strategies to fight glioblastoma (Stupp *et al.*, 2009; Chinot *et al.*, 2014; Brown *et al.*, 2016), the prognosis remains extremely poor with average survival reported to be less than 15 months following diagnosis (Stupp *et al.*, 2009, 2015). A subpopulation of tumorigenic cells termed glioblastoma stem-like cells (GSCs), also known as cancer-initiating cells (Lathia *et al.*, 2015), has been implicated in tumour initiation, resistance to current therapies and disease recurrence (Singh *et al.*, 2004; Bao *et al.*, 2006; Chen *et al.*, 2012; Yan *et al.*, 2013). Similar to how normal stem and progenitor cells participate in tissue development and repair, cancer stem-like cells pervert these processes to facilitate the initiation and progression of tumours. Moreover, GSCs contribute to both radiation and chemoresistance as these treatments target cycling, highly proliferative cancer cells, whereas GSCs are comparatively quiescent, and thus survive to repopulate the tumour post-treatment (Bao *et al.*, 2006; Chen *et al.*, 2012). As such, GSCs represent an important target for future therapies and a better understanding of how GSCs interact with their environment is required.

Studies have proposed that GSC tumorigenicity relies on the surrounding tumour microenvironment, with brain tumour-initiating cells reported to reside in close contact with brain microvascular cells (Calabrese *et al.*, 2007; Galan-Moya *et al.*, 2011; Shingu *et al.*, 2017). The localization of GSCs in proximity to endothelial cells facilitates communication between these cells (Calabrese *et al.*, 2007) allowing the tumour vascular bed to provide factors essential to maintain GSC resistance to therapies, identity and fate (Garcia-Barros *et al.*, 2003; Folkins *et al.*, 2007; Evers *et al.*, 2010; Galan-Moya *et al.*, 2011, 2014). Among the putative candidates of this angiocrine signalling, soluble growth factors emanating from the vascular niche have been reported in various physiological and pathological models (Andreu-Agullo *et al.*, 2009; Beck *et al.*, 2011; Cao *et al.*, 2014, 2017). However, to date, the specific endothelial secreted factors involved in this process remain to be identified. Here, we used a mass spectrometry proteomic analysis of the endothelial cell secretome and identified the vasoactive peptide apelin as a central regulator of the expansion of glioblastoma patient-derived cells with stem-like properties. As such, targeting apelin may represent an effective novel therapeutic approach to treat glioblastoma.

Materials and methods

Ethics statement

Informed consent was obtained from all patients prior to sample collection for diagnostic purposes. Clinical tissue samples were provided by the Regional Institute for Cancer in Nantes Atlantique (IRCNA) tumour library (Nantes, France). This study was reviewed and approved by the institutional review boards of Sainte Anne Hospital, Paris, France, and Laennec Hospital, Nantes, France, and performed in accordance with the Declaration of Helsinki Protocol. Animal procedures were conducted as outlined by the European Convention for the Protection of Vertebrate Animals used for Experimental and other Scientific Purposes (ETS 123) and approved by the French Government (APAFIS#2016-2015092917067009).

Analysis of human clinical databases

The Cancer Genome Atlas (TCGA, HG-UG133A and Agilent-4502A data), Rembrandt and Gravendeel microarrays were interrogated through the Gliovis platform (http://gliovis.bioinfo.cnio.es/) (Bowman *et al.*, 2017). Data were plotted based on histology criteria only. For reverse protein phase arrays (RPPA), optimal cut-offs were set to define high versus low expression of *APLNR*, as indicated on the plots. Pairwise *t*-tests were run.

Cell culture, conditioned media preparation and mass spectrometry

Glioblastoma patient-derived cells with stem-like properties (GSCs) were isolated as previously described (Treps *et al.*, 2016). Briefly, tumours were dissociated using the MACsDissociator (Miltenyi) and each GSC characterized for their self-renewal capabilities, cell surface antigens, expression of stemness markers, their ability to differentiate, and to initiate tumour formation (Supplementary Table 1). GSCs 1–16 were maintained as spheres in NS medium (DMEM-F12, with N2, G5 and B27 supplements, GlutaMAX^{TM} and antibiotics, Life Technologies). To induce differentiation in GSCs, the three supplements were omitted and 10% foetal bovine serum added to the media.

Human brain microvascular endothelial cells (hCMEC/D3, PO Couraud), HEK-293T and SVEC4-10 mouse endothelial cells (ATCC) were cultured as previously described (Treps *et al.*, 2016). Tumour-derived endothelial cells (tEC) were isolated from mechanically homogenized mice orthotopic brain tumours using CD31 MicroBeads (Miltenyi).

Stealth non-silencing control (low-GC 12935111) and selected siRNA targeting human *APLN* (HSS113086), *APLNR* (HSS100325) and *GSK3B* (HSS104522) (Life Technologies,

50 nM) were transfected using RNAiMAX Lipofectamine® (Life Technologies). GIPZ lentiviral shRNAs against human *APLNR* sequences 1–3, with identification numbers V3LHS_307344, V3LHS_307345 and V3LHS_307346, respectively, were purchased from Thermo Fisher Scientific. Lentiviral particles were collected from pGIPZ, pSPAX2 and pVSVg co-transfected HEK-293T cells (Dubois *et al.*, 2014).

Conditioned media (CM) from hCMEC/D3 (hEC-CM), tumour xenograft-derived endothelial cells (tEC-CM), SVEC4-10 (mEC) and HEK-293T (293T-CM) cells were obtained from 72-h-old monolayers in serum-free EBM2 (Lonza). Conditioned media from GSC#1 was obtained from 72-h-old tumourspheres. For acidic stress simulation, EBM2 (Lonza, pH 8.2) was adjusted to pH 6.8 using HCl before preparing hEC-CM. Apelin concentrations were quantified using the human apelin-12 EIA kit according to the manufacturer's instructions (cross-reactivity with apelin-12, apelin-13, and apelin-36, Phoenix Pharmaceuticals).

Protein and peptide identification was performed in the University Paris Descartes Proteomics Facility (3P5, Paris, France), without trypsin proteolysis for peptidome analysis, as previously described in Luissint *et al.* (2012). Mass spectra were measured with a 4800 MALDI-TOF-TOF mass spectrometer (ABSciex) equipped with a Nd:YAG pulsed laser (355 nm wavelength, <500 ps pulse and 200 Hz repetition rate). Spectra acquisition and processing were performed using the 4000 series explorer software (ABSciex).

Drugs

MM54 (cyclo[1-6]CRPRLCKHcyclo[9-14]CRPRLC) and MM193 were prepared as previously described (Macaluso *et al.*, 2011). Temozolomide (TMZ) and tideglusib were purchased from Sigma, and apelin peptides were from Phoenix Pharmaceuticals (pyr1-apelin-13 pyr1-QRPRLSHKGPMPF, apelin-13 QRPRLSHKGPMPF, and apelin-36 LVQPRGSRN GPGPWQGGRRKFRRQRPRLSHKGPMPF).

Tumoursphere formation

To test the tumoursphere formation, GSCs (100 cells/µl) were plated in triplicate in indicated media as previously described (Harford-Wright *et al.*, 2016). Cells were manually dissociated each day and a single cell suspension maintained until Day 5. Tumourspheres were counted in five random fields of view, and the mean from the triplicate of each condition calculated from three independent experiments.

Limiting dilution assays

To test the clonal capacity of GSCs, a limiting dilution assay was performed as previously described (Tropepe *et al.*, 1999). GSCs were seeded in the tested media (NS, MF and EC-CM) in a 96-well plate with serial dilutions ranging from 4 to 2000 cells/well, with eight wells per dilution for each plate and treated as indicated. Two weeks later, each well was scored for tumoursphere formation and the frequency of stem cells calculated using ELDA software (Hu and Smyth, 2009). The mean stem cell frequency for each condition was determined by averaging the stem cell frequencies of two independent experiments.

Radioligand binding and calcium mobilization assays

Radioligand binding and calcium mobilization assays to assess the putative off-target effects of MM54 were performed by Eurofins Cerep Panlabs, according to the manufacturer's instructions.

Cell viability

Cell viability in response to MM54 was tested using the UptiBlue reagent (Interchim), a fluorometric/colorimetric growth indicator based on the detection of metabolic activity. Briefly, cells were seeded at a density of 2×10^3 per well, UptiBlue added at a concentration of 10% v/v and cells maintained at 37°C 5% CO_2 until analysis. Absorbance was measured at Day 5 following treatment at 570 and 600 nm on a FLUOStar OPTIMA (BMG Labtech) plate reader, and the percentage of cell viability calculated according to the manufacturer's instructions.

Cell survival in adherent cells was evaluated using the MTT assay [1-(4,5-dimethylthiazol-2-yl)-3,5-diphenylformazan, thiazolyl blue formazan; Sigma], which is reduced to formazan based on the mitochondrial activity of living cells. Cells were seeded in a 96-well plate in triplicate at a density of 5×10^3 per well and treatments administered 24 h after seeding. Absorbance values were read at 590 nm and expressed as a percentage of cell viability relative to basal conditions.

Animal procedures

Tumour inoculation experiments were performed on female Balb/C nude mice (Janvier) aged 5–6 weeks. For toxicity experiments 6-week-old female C57/Bl6J (Janvier) mice were used. Animals were randomly assigned to each group and group housed in specific pathogen-free conditions at 24°C on a 12-h day-night cycle. At all times, animals were allowed access to standard rodent pellets and water *ad libitum*.

To test potential toxic effects of MM54 and MM193 *in vivo*, mice were administered 2 mg/kg of MM54, MM193 or vehicle bi-weekly for 4 weeks. At sacrifice, blood was taken for analysis and the heart, kidney, aorta and liver removed, weighed and fixed for histological analysis. For the glycaemic study, animals were starved for 6 h prior to sacrifice.

For the ectopic models, mice were subcutaneously injected with 5×10^5 GSC#9 in 100 µl of phosphate-buffered saline (PBS) and growth factor-free Matrigel® (Corning) in each flank. Tumourspheres were dissociated prior to injection for all *in vivo* experiments to ensure implantation of a single cell suspension. To analyse tumour initiation, mice were examined weekly to monitor tumour growth and sacrificed between 6 and 7 weeks following implantation. For pharmacological studies, mice were treated twice per week once tumours were palpable, with MM54 (2 mg/kg), MM193 (2 mg/kg) or vehicle (PBS) by intraperitoneal injection. Tumour size was measured once a week with callipers and tumour volume calculated using the following equation (width^2 × length)/2.

Intracranial injection of GSC#9 was performed using a free hand injection technique as described in detail elsewhere (Treps *et al.*, 2016). Briefly, mice were anaesthetized with a mixture of ketamine (100 mg/kg) and xylazine (10 mg/kg) and a midline

incision performed. A small burr hole was made 2 mm to the right of bregma, 1 mm anterior and 3 mm ventral to the coronal suture. A 5 µl Hamilton syringe was inserted to a depth of 3 mm and 10^5 GSC#9 injected slowly. One minute after completion of the injection, the needle was retracted, surgical site closed and animals allowed to recover. At 3 weeks following GSC#9 inoculation, treatment with PBS or MM54 (2 mg/kg) was commenced three times per week until death due to tumour burden or the conclusion of the experiment at Day 70.

Immunostaining

Both cellular and tissue analysis was performed using immunostaining and haematoxylin and eosin standard protocols (Treps *et al.*, 2016). The following primary antibodies were used: PECAM (BD), pS9-GSK3β (Cell Signaling), APLN and APLNR (Abcam), and Ki67, SOX2 and NESTIN (Millipore). Cell death was estimated through the TUNEL assay kit (Trevigen). A minimum of three tumour sections per condition was used for analysis, with at least five different fields of view. For blood vessel surface analysis, PECAM pixel intensity was calculated (ImageJ) in randomly chosen fields of view and mean ± standard error of the mean (SEM) of the total field of view was represented. Cell proliferation was assessed through the percentage of Ki67-positive cells normalized to the total number of nuclei. NESTIN-positive and pS9-GSK3β-positive cells were counted per field of view. Image acquisitions were performed on Spinning Disk Leica microscope (Institut Cochin) and confocal Nikon A1 RSi (Micropicell).

Flow cytometry

For cell surface expression analysis, cells were incubated with antibodies for 1 h and washed twice with cold PBS. For total expression, cells were fixed (4% paraformaldehyde-PBS, 15 min) and permeabilized (iced-cold methanol, 10 min) prior incubation with antibodies. APC-APLNR, and isotype control Ig (R&D systems) antibodies were used.

Analysis of aldehyde dehydrogenase (ALDH) activity was performed using the ALDEFLUOR™ assay kit (Stem Cell Technologies). Briefly, cells were incubated with ALDEFLUOR alone or in combination with an ALDH activity inhibitor (DAEB) at 37°C for 45 min. This flow cytometry-based staining allows monitoring ALDH activity in stem, progenitor and cancer precursor cells. The ALDH activity is considered positive in comparison to cells incubated with DEAB reagent.

Flow cytometry analyses were performed on Accuri C6 and FACsCalibur (BD Biosciences, Cytocell) and processed using CFlow plus or FlowJo software (BD Biosciences).

Western blots

Following stimulation with the relevant treatment, cells were collected and washed in PBS before lysis at 4°C with TNT buffer (50 mM Tris pH 7.4, 150 mM NaCl, 2 mM EDTA, 1% Triton™ X-100, 1% IGEPAL®) supplemented with protease inhibitors (ThermoFisher Scientific). Equal amounts of protein were loaded on tris-glycine gels and transferred onto nitrocellulose membranes (GE Healthcare). Antibodies against pS9-GSK3β, GSK3β, KDM1A, pS473-AKT, AKT, pS235/S236-S6 and pT202/Y204-ERK1/2 (Cell Signaling, Ozyme), GAPDH (Santa Cruz Biotech) and APLNR (Abcam) were incubated with the membrane overnight at 4°C and followed by incubation with the relevant secondary antibodies (Southern Biotech) for 1 h at room temperature. Membranes were revealed using a chemiluminescent HRP substrate (Millipore) and visualized using the Fusion imaging system (Vilber Lourmat).

RNA extraction and RT-PCR

RNA was extracted using the Qiagen RNeasy® Mini Kit as per the manufacturer's directions. Equal amounts of RNA were reverse transcribed using the SuperScript® III RT kit (Life Technologies) and the resulting cDNA was used to amplify mRNA by PCR using gene-specific primer sets in the presence of REDTaq® DNA polymerase (Sigma). *ACTB* and *GAPDH* were also amplified as control for input. See Supplementary Table 2 for primer details.

Statistics

Data are representative of three independent experiments, unless otherwise stated. Statistical analysis was performed with GraphPad Prism6 using two-way ANOVA and an unpaired two-tailed *t*-test (Student's *t*-test). In Kaplan-Meier survival curves, differences were compared by log-rank analysis and Gehan-Breslow-Wilcoxon. In all experiments a *P*-value of <0.05 was considered significant.

Results

Endothelial cells produce the vasoactive peptide apelin

To identify endothelial-secreted factors potentially involved in the maintenance of GSCs, we performed an unbiased tandem mass spectrometry proteomic analysis of the human brain endothelial secretome using human brain endothelial cell (hCMEC/D3)-conditioned media (EC-CM) and compared it to epithelial-like HEK-293T CM. Hits that were shared by the two cell lines were discarded, and 22 peptides or proteins specific to the EC-CM identified (Fig. 1A, Supplementary Table 3 and Supplementary Fig. 1A). Apelin peptides revealed the highest exponentially modified protein index and were selected for further characterization (Fig. 1B, Supplementary Table 3 and Supplementary Fig. 1B and C).

Enzyme immunoassay analysis demonstrated that endothelial cells secreted significant amounts of apelin, as the peptide was robustly detected in the conditioned media produced by human, mouse and xenograft tumour-derived endothelial cells, supporting endothelial cells as a source of apelin (Fig. 1C and D). In contrast, apelin was not detected in patient-derived GSC#1, #2, #9 and #12 RNA lysates, and concentrations were found lower than the limit of ELISA sensitivity (0.07 ng/ml) (Fig. 1C and D). Furthermore, to challenge apelin production in conditions that recapitulate the tumour microenvironment, we assessed apelin secretion from human brain endothelial cells under acidic stress (Fig. 1D). Interestingly, acidification of the milieu did not affect the overall production of apelin.

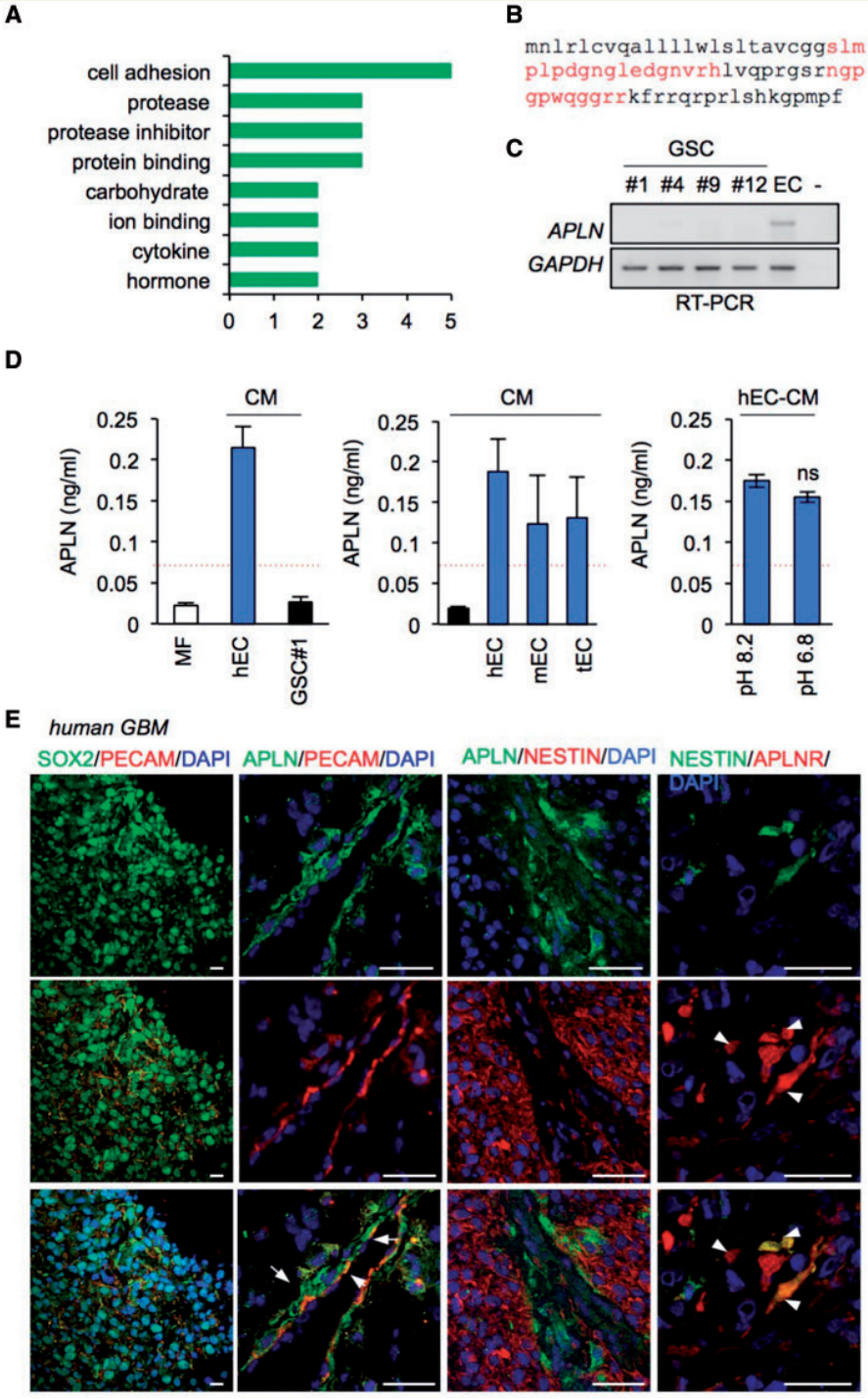

Figure 1 Endothelial cells produce the vasoactive peptide apelin. (**A**) Mass spectrometry analysis of the brain microvascular endothelial cell (hEC) secretome identified 22 peptides and proteins specific to endothelial cells. (**B**) Apelin peptide coverage (37%) is indicated in red on the full-length sequence. (**C**) RT-PCR for *APLN* and *GAPDH* is shown for hEC and glioblastoma patient-derived cells with stem properties (GSCs) #1, #4, #9 and #12 RNA total cell lysates. (**D**) Apelin secretion in mitogen-free control media (MF), and in conditioned media (CM) prepared from GSC#1, human brain microvascular EC (hEC), mouse macrovascular EC (mEC) and orthotopic mouse brain tumour-isolated EC (tEC). Apelin secretion was measured in CM from hEC cultured in acidified medium (pH 6.8) or control conditions (pH 8.2). Data are representative of $n \geqslant 2$ with mean ± SEM. Red dashed lines indicate the minimum sensitivity range of APLN detection. (**E**) Confocal analysis of SOX2 (green) + PECAM (red), APLN (green) + PECAM (red), APLN (green) + NESTIN (red), NESTIN (green) + APLNR (red) in glioblastoma clinical samples. Nuclei are shown in blue (DAPI). Arrowheads and arrows indicate APLNR/NESTIN and APLN/PECAM-double positive cells respectively. Scale bars = 25 μm. Data are representative of $n = 4$ newly diagnosed patient samples. All panels are representative of $n = 3$, unless specified.

Moreover, we detected apelin and its receptor, the G-protein coupled receptor APLNR (APJ), in clinical glioblastoma samples in the vicinity of PECAM-labelled endothelial cells and cells positive for the stem cell markers NESTIN and SOX2 (Fig. 1E), suggesting a potential role for apelin in the tumour vascular niche (Calabrese *et al.*, 2007). However, APLN staining did not coincide with NESTIN-positive tumour cells, but rather with vascular tracks (Fig. 1E), supporting endothelial cells as a potential source for apelin in glioblastoma, consistent with a recent report in colorectal cancer-derived endothelial cells (Zuurbier *et al.*, 2017). To explore the clinical relevance of apelin further, we performed a retrospective analysis using The Cancer Genome Atlas (TCGA), Rembrandt and Gravendeel databases. Analysis of all three databases revealed a significant increase in *APLN* mRNA in glioblastoma tissue, as compared to non-tumour samples, which might be due to endothelial abundance in these grade IV tumours (Supplementary Fig. 1D).

Apelin sustains GSC expansion *in vitro*

We next evaluated the response of patient-derived GSCs, which have been extensively characterized both *in vitro* and *in vivo* (Supplementary Table 1 and Supplementary Fig. 2A and B) to the biologically active apelin fragments: apelin-13, pyr-apelin-13 and apelin-36 (see 'Materials and methods' section for more information). Although all of the apelin peptides increased the number of tumourspheres compared to mitogen-free media (MF), apelin-13 was the most potent at sustaining GSCs (Fig. 2A). Subsequently, we assessed the effect of increasing concentrations of apelin-13 (termed apelin hereafter) on GSC#1 and observed a potent and sustained increase in tumourspheres from the lowest concentration (Fig. 2B). Consistent with our previous work (Galan-Moya *et al.*, 2011, 2014), both mitogen-supplemented medium (NS) and EC-CM maintained the expression of stem markers NESTIN and SOX2 (Fig. 2C). Accordingly, mitogen withdrawal resulted in the loss of expression of these markers and the reduced ability to form tumourspheres, which was rescued by the addition of synthetic apelin to this MF media (Fig. 2C). To determine whether apelin alone maintained GSC self-renewal, a limiting dilution assay was performed in GSC#1 (Fig. 2D). As expected, we observed the highest frequency of colony-forming cells in GSCs grown in NS and EC-CM. Nonetheless, compared to MF conditions, GSC#1 grown in apelin-supplemented MF demonstrated an increase in the frequency of colony-forming cells. Moreover, we observed in a panel of 16 patient-derived GSCs (Supplementary Table 1) that apelin-supplemented media significantly increased the ability of GSCs to expand as tumourspheres (Fig. 2E), and increased the frequency of stem cells in a panel of five representative GSCs (Fig. 2F), indicating that *in vitro* apelin addition sustains GSC growth and substitutes, at least partially, to cell culture supplements provided in the NS (Fig. 2D–F). Similar effects were obtained with apelin-containing conditioned media derived from mouse brain tumour endothelial cells (tEC-CM) (Figs 1C and 2G), indicating that tumour-derived endothelial cells may provide a source of bioactive apelin *in situ*, although the intratumoural concentration and the apelin forms are not experimentally available. Consistent with these findings, EC-CM obtained from *APLN*-silenced endothelial cells was no longer able to maintain the stem properties of GSCs, while the addition of exogenous apelin into the depleted EC-CM restored this effect (Fig. 2H–J). Furthermore, we did not observe any obvious effect of apelin-supplemented mitogen-free media on the proliferation of GSCs (Fig. 2K), indicating that apelin may maintain GSCs by enhancing their self-renewal capabilities.

Apelin modulates GSCs via activation of the G-protein coupled receptor APLNR

Apelin is known to signal through the G-protein coupled receptor APLNR (also known as APJ), which is reported to be highly expressed throughout the brain and act as paracrine and autocrine factor that supports embryonic and tumour angiogenesis (Kaelin *et al.*, 2007). In the present study, we observed a heterogeneous expression of APLNR in our panel of GSCs, at both a RNA and protein level (Fig. 3A and B). In keeping with a role for apelin in the stem cell maintenance, we found that differentiated GSCs were associated with a decrease in APLNR expression compared to tumourspheres (Fig. 3C and D) and reduced tumour-initiating ability (Supplementary Fig. 2C). Moreover, analysis of the stem marker PROM1 (CD133) revealed that expression of APLNR was detected in the PROM1 (CD133)-positive GSC population, further supporting a role for apelin and its receptor in the stem population (Fig. 3E). Consistent with this, APLNR silencing in GSC#1 impaired the ability of these cells to form SOX2-positive spheres cultured in both EC-CM and apelin conditions (Fig. 3F and G). Of note, the optimal concentration of exogenous mitogens in the NS medium allows maintaining *APLNR*-knocked down GSC#1 expansion *in vitro* (Fig. 3F and G). Similar results were obtained in three additional GSCs with variable APLNR expression level (Fig. 3A, B and H), highlighting the potential importance of this receptor in GSC maintenance in response to APLN. Subsequently, GSC#9 was transduced with short hairpin (sh) RNA against *APLNR* and grafted subcutaneously into the flanks of nude mice. Reducing APLNR levels in GSC#9 markedly decreased tumour development, NESTIN overall staining and only mildly affect tumour vascularization (Fig. 3I and J). To observe the impact of APLNR signalling on tumour development in the brain microenvironment, shAPLNR GSC#9 were orthotopically implanted into the striatum of nude mice and assessed for histological signs of tumour growth at Week 5, when tumours are largely developed but neurological signs

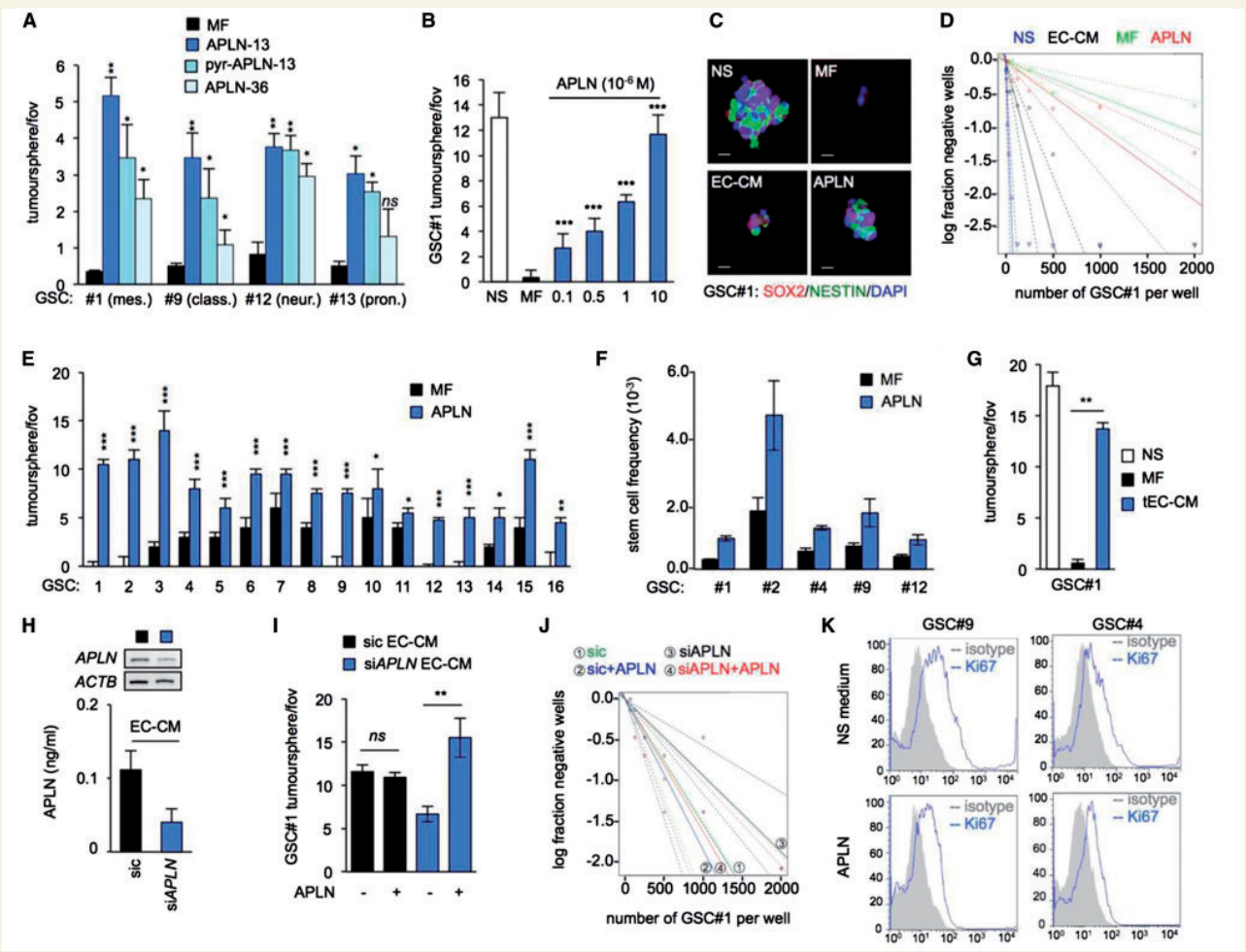

Figure 2 Apelin sustains GSC expansion *in vitro*. (**A**) Tumoursphere per field of view (fov) in GSCs #1, #9, #12 and #13 in response to apelin 13 (APLN-13), pyr-apelin-13 (pyr-APLN-13) or apelin 36 (APLN-36) treatment (1 μM, diluted in mitogen-free medium, MF). $^{**}P < 0.01$, $^{*}P < 0.05$ compared to the MF condition. (**B**) Tumourspheres per field of view were counted in GSC#1 cultured in complete mitogen-supplemented medium (NS), MF and MF supplemented with the indicated APLN concentration. $^{***}P < 0.001$ compared to the MF condition. (**C**) Confocal analysis of NESTIN (green), SOX2 (red) and nuclei (DAPI, blue) in GSC#1 grown in NS, MF, human brain endothelial cell-conditioned medium (EC-CM) or MF + APLN (1 μM). Scale bars = 20 μm. (**D**) Linear regression plot of *in vitro* limiting dilution assay (LDA) for GSC#1 in NS, EC-CM, MF, and MF + APLN (1 μM). Data are representative of $n = 2$. (**E**) Tumourspheres per field of view were quantified in GSCs #1 to #16 cultured in MF or with apelin. $^{*}P < 0.05$; $^{**}P < 0.01$; $^{***}P < 0.001$ compared to the MF condition. (**F**) Stem cell frequency in GSCs #1, #2, #4, #9 and #12 in response to MF and APLN conditions. (**G**) Tumourspheres per field of view in GSC #1 in NS, MF and EC-CM derived from mouse tumour endothelial cells (tEC-EM). $^{**}P < 0.01$ compared to the MF condition. (**H**) EC received non-silencing RNA (sic) or siRNA targeting APLN (si*APLN*) and APLN knockdown efficiency assessed by RT-PCR and ELISA. (**I** and **J**) GSCs #1 were cultured with sic and si*APLN* EC-CM, with or without apelin (1 μM). $^{**}P < 0.01$ compared to the corresponding control condition for both tumoursphere and LDA assays. (**K**) FACS analysis of the proliferation marker Ki67 in GSCs #4 and #9 in NS and MF + APLN conditions. All panels are representative of $n = 3$, unless otherwise specified.

were not yet evident. In these conditions, the number of progressing tumours was modestly reduced in *APLNR* shRNA (Supplementary Fig. 2D). Whether the reduction of *APLNR* expression also decreases tumour volume would require in-depth measurement over time. This slight decrease in tumour formation suggested that APLNR contributes to tumour expansion, although compensatory mechanisms may take place due to alternate signalling or an incomplete knockout of *APLNR* gene. Collectively, these results suggest that endothelial-secreted apelin sustains GSCs both *in vitro* and *in vivo* via activation of the apelin receptor.

Pharmacological inhibition of APLNR impairs the effects of the endothelial secretome on GSCs by inhibition of GSK3β signalling

To next evaluate the potential of targeting apelin/APLNR, we investigated the properties of a novel bi-cyclic peptide [cyclo(1–6)CRPRLC-KH-cyclo(9–14)CRPRLC], MM54, which acts as a competitive antagonist of APLNR (Fig. 4A) (Macaluso *et al.*, 2011; Brame *et al.*, 2015). To identify

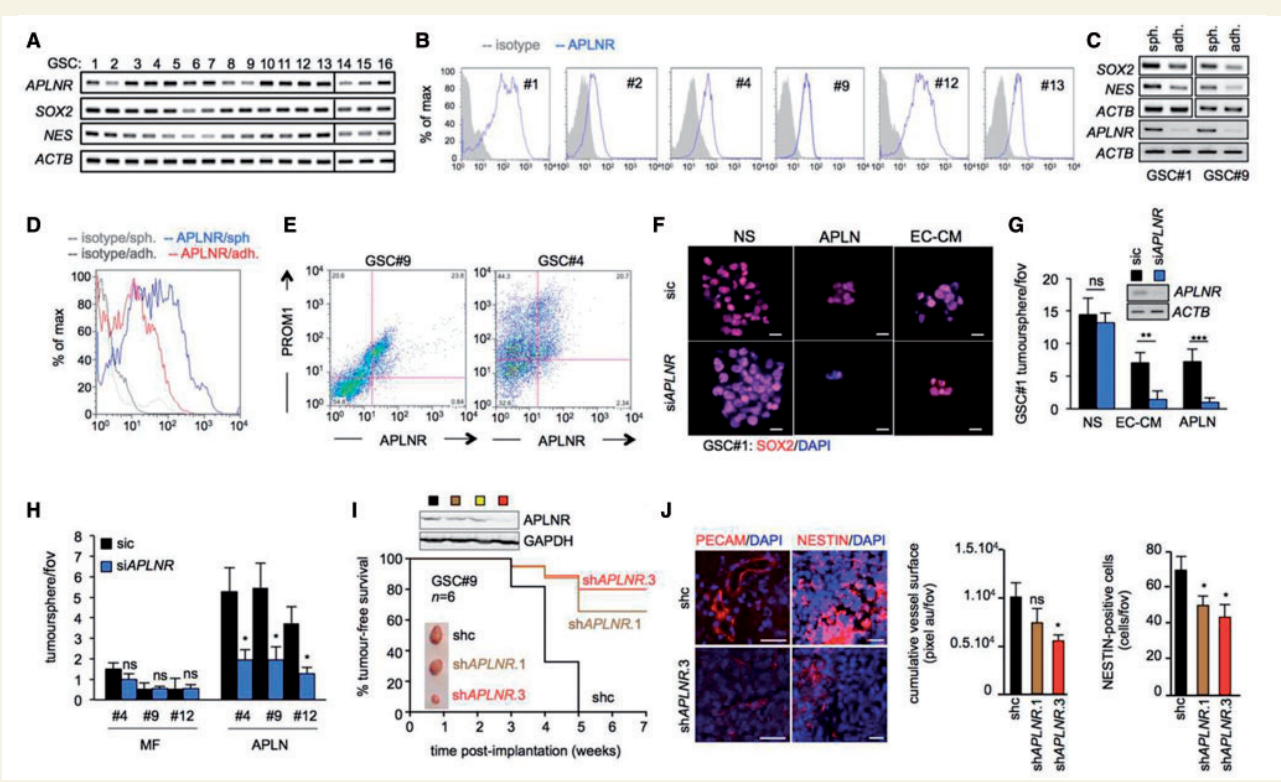

Figure 3 Apelin modulates GSCs via activation of the G-protein coupled receptor APLNR. (**A**) RT-PCR in a panel of 16 GSCs for *APLNR* and stemness markers *NES* and *SOX2*. *ACTB* is shown as internal PCR control. (**B**) FACS analysis of APLNR surface expression in GSCs #1, #4, #9, #12 and #13. (**C** and **D**) Differentiation was induced in GSCs #1 and #9 by growth in serum-containing media. RT-PCR and FACS analysis of APLNR and stem markers in GSCs #1 and #9 grown as both tumourspheres (sph.) and differentiated adherent cells (adh.). (**E**) FACS analysis of the stemness marker PROM1 (CD133) and APLNR in GSCs #4 and #9. Data are representative of $n = 2$. (**F**) GSC #1 received non-silencing RNA (sic) or *APLNR* targeting siRNA (si*APLNR*) and were maintained in complete medium (NS), human brain endothelial cell-conditioned medium (EC-CM), and MF supplemented with purified apelin (APLN, 1 μM). Confocal analysis of SOX2 (red) and nuclei (DAPI, blue). Scale bars = 20 μm. (**G**) Tumourspheres per field of view (fov) in sic (small interfering control) or si*APLNR* GSC#1 maintained in NS, EC-CM or APLN. *APLNR* knockdown was assessed with RT-PCR. $^{**}P < 0.01$; $^{***}P < 0.001$ compared to the sic condition. (**H**) Tumourspheres per field of view in non-silencing duplexes (sic) or *APLNR* targeting siRNA (si*APLNR*) transfected GSC#4, #9 and #12 in MF alone or supplemented with APLN. (**I**) GSCs#9 were infected with control shRNA (shc, black), and shRNA targeting *APLNR* (seq#1, orange; seq#2, yellow; and seq#3, red). Knockdown efficiency was checked by western blots. Female nude mice were implanted with 5×10^5 shcontrol (black line), sh*APLNR* seq#1 (orange line) or seq#3 (red line) and monitored for tumour-free survival over 7 weeks. $n = 4$ mice/group. (**J**) Sections of tumour tissue were analysed for PECAM and NESTIN expression using immunofluorescence. Scale bar = 40 μm. $n \geqslant 4$ mice/group. All panels are representative of $n = 3$, unless specified.

possible off-target G-protein coupled receptor or ion channels that may interact with MM54, we performed radioligand competitive binding experiments to investigate the specificity of the compound. MM54 inhibited more than 95% of apelin binding to APLNR at the dose of 10 μM (Fig. 4B). In addition to APLNR, of the 55 receptors tested, five G-protein coupled receptors (CXCR2, M3, NK2, NOP, and 5HT1B) and one ion channel (SKCa) demonstrated over 50% inhibition of agonist binding in response to MM54 (10 μM) (Fig. 4B). However, using a cell-based second messenger assay to measure G-protein coupled receptor-mediated calcium flux we again observed that MM54 was very effective at inhibiting APLNR, while having little or no effect towards other identified off-targets (Fig. 4C). Thus, MM54 may behave as a potent and selective inhibitor of apelin binding and APLNR activation. In both EC-CM and apelin-supplemented mitogen-free (MF) media, MM54 induced a dose-dependent decrease in the number of tumourspheres that was significant from a concentration of 2 μM (Fig. 4D). In keeping with this, we observed a significant reduction in the frequency of sphere-forming cells in GSCs #1, #4, #9 and #12 following treatment with MM54 (Fig. 4E and F). Furthermore, inhibition of APLNR with MM54 clearly decreased the percentage of the stem marker aldehyde dehydrogenase (ALDH)-positive cells compared to untreated GSC#1 controls (Fig. 4G), consistent with the MM54-mediated decrease in the number of SOX2- and NESTIN-positive spheres (Fig. 4H). However, GSC#1 were resistant to MM54 treatment when cultured in mitogen-containing defined medium (NS) that does not contain apelin, consistent with our RNA interference data (Fig. 3). Analysis of downstream mechanisms

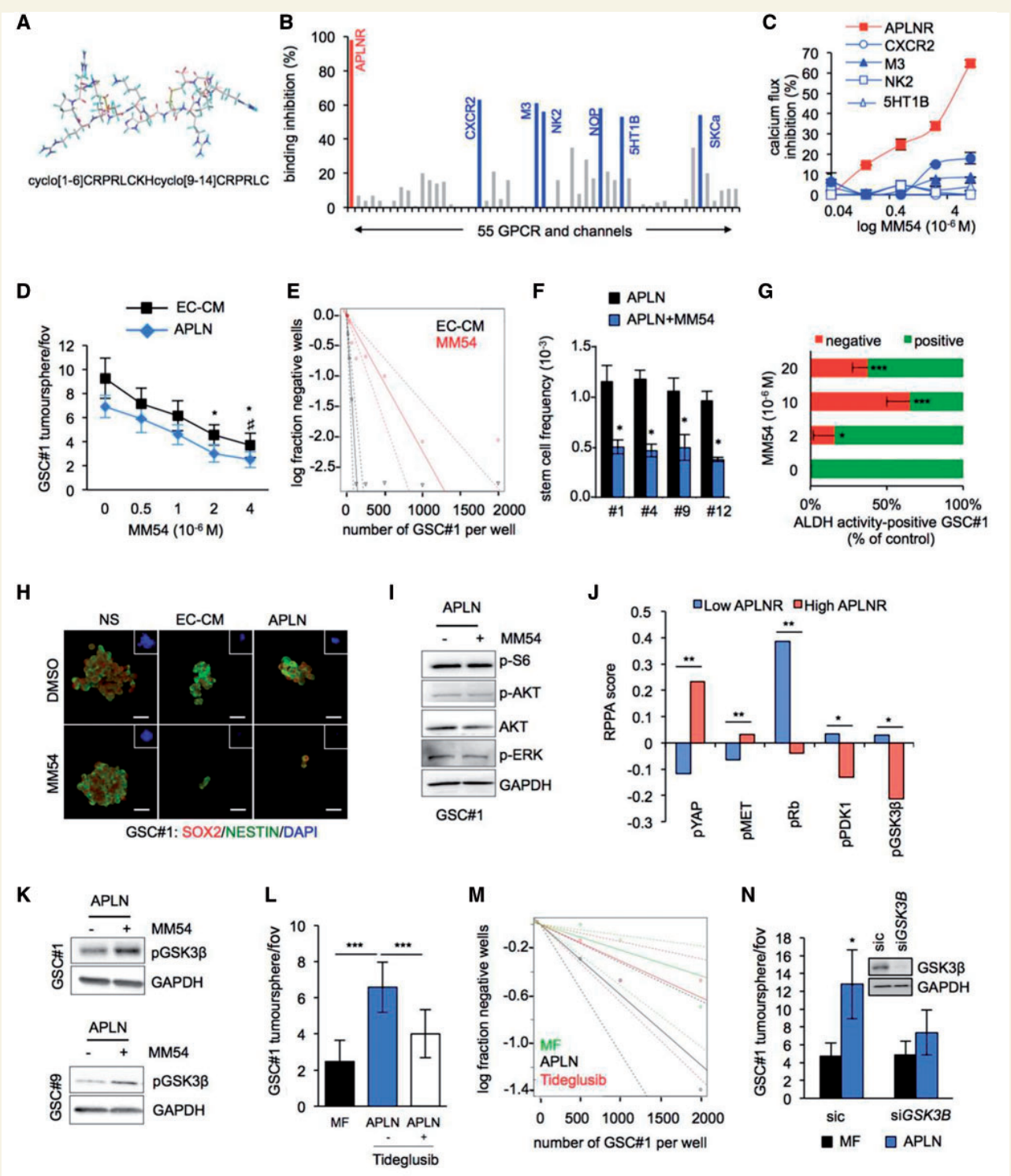

Figure 4 Pharmacological inhibition of APLNR impairs the effects of the endothelial secretome on GSCs by inhibition of GSK3β signalling. (**A**) Molecular structure and primary sequence of the competitive APLNR antagonist MM54. (**B**) A radioligand binding assay of 55 G-protein coupled receptors and ion channels identified APLNR (indicated in red) and six putative off-targets (indicated in blue) that demonstrated >50% inhibition of agonist binding following administration of APLNR antagonist MM54 (10 μM). (**C**) The percentage of calcium flux inhibition following MM54 treatment (0.4–10 μM) in the G-protein coupled receptor hits. (**D**) Tumoursphere per field of view (fov) in response to MM54 (0–4 μM) treatment in GSC#1 maintained in human brain endothelial cell-conditioned medium (EC-CM) and apelin-supplemented mitogen-free MF media (APLN, 1 μM) for 5 days. $^{*}P < 0.05$ compared to EC-CM DMSO control, $^{\#}P < 0.05$ compared to apelin DMSO control. (**E**) Linear regression plot of *in vitro* limiting dilution assay (LDA) for GSC#1 in EC-CM or EC-CM + MM54 (2 μM). (**F**) Stem cell frequency in apelin supplemented media in response to MM54 (2 μM) in GSCs #1, #4, #9 and #12. $^{*}P < 0.05$ compared to the vehicle condition.

(continued)

associated with apelin/APLNR activation revealed that MM54 did not induce any changes to major components of the PI3K/AKT and ERK signalling pathways (Fig. 4I). To explore the APLNR downstream signalling further, we interrogated the TCGA database for reverse phase protein array (RPPA) in glioblastoma patients with high and low APLNR expression (Fig. 4J). This analysis unmasks two significantly upregulated phospho-proteins, namely pYAP and pMET, and three downregulated (pRb, pPDK1, and pGSK3β) in high APLNR glioblastoma samples (Fig. 4J). Interestingly, glycogen synthase kinase 3β (GSK3β) activity has recently been shown to participate in gliomagenesis via maintenance of the stem population of cancer cells (Zhou *et al.*, 2016). This process occurs through the GSK3β-dependent stabilization of KDM1A. Moreover, GSK3β inactivation by phosphorylation on serine 9 was associated with a loss of stemness traits in GSCs (Zhou *et al.*, 2016). In keeping with this, incubation with MM54 (2 μM, overnight) in apelin-supplemented MF media resulted in an increase in phosphorylation of GSK3β at serine 9 in both GSCs #1 and #9 (Fig. 4K), consistent with an inhibitory effect on GSK3β signalling. Consequently, we treated patient-derived GSCs with the GSK3β inhibitor tideglusib (2.5 μM) and observed that apelin was less potent at increasing tumourspheres and self-renewal (Fig. 4L and M). Furthermore, silencing GSK3β in GSC#1 resulted in a significant decrease in apelin-mediated tumoursphere formation (Fig. 4N), suggesting that apelin may sustain GSCs via activation of GSK3β signalling.

Pharmacological inhibition of APLNR by MM54 impairs the *in vitro* expansion of temozolomide-resistant GSCs

The chemotherapeutic agent TMZ is commonly used in the treatment of glioblastoma, although it has been reported that GSCs are resistant to TMZ (Chen *et al.*, 2012; Hale *et al.*, 2013). To test the specificity of MM54 towards GSCs, we treated a panel of normal human and primary glioblastoma cell lines with increasing concentrations of MM54, as compared to TMZ. MM54 demonstrated no overtly toxic effects on any of the cell lines tested, whilst TMZ significantly reduced the viability of glioblastoma cell lines (namely U87 and LN229) but not GSCs (Fig. 5A and B). Similarly to GSC#1, #4, #9 and #12, the *in vitro* viability of U87 glioblastoma cell line grown as spheroids was not modified upon high dose of TMZ (Fig. 5C). Conversely, TMZ reduces the viability of U87 glioblastoma cell line and GSCs #1, #4 and #9, when grown as adherent differentiated cells (Fig. 5C).

Combined treatment of MM54 with TMZ did not significantly alter GSC#1 viability in NS or EC-CM even at the highest concentrations of both compounds (Fig. 5D). Moreover, MM54 was significantly better at impairing GSC#1 tumoursphere formation and ALDH activity at low doses compared to TMZ, which required much higher concentrations to achieve comparable results (Fig. 5E and F). Drugs were then combined at constant MM54:TMZ ratios (1:2.5, 1:5, and 1:10) and ALDH activity measured (Fig. 5E). At MM54 suboptimal dose, i.e. <2 μM MM54 (Fig. 4), TMZ significantly potentiates the effects of MM54. To further assess whether MM54 and TMZ do synergize, data were processed according to the Chou combination index (CI) method (Chou, 2010) (Fig. 5G). In this representation, a CI value of 1 indicates an additive effect, <1 synergism and >1 antagonism. TMZ and MM54 therefore displayed a striking synergism (Fig. 5H). In line with this, co-administration of low doses of both MM54 (0.5 μM) and TMZ (1.25, 2.5, and 5 μM) decreased the percentage of ALDH activity in GSCs (Fig. 5I), indicating that APLNR antagonists may enhance the therapeutic efficacy of TMZ.

Pharmacological inhibition of APLNR by MM54 reduces xenograft progression

Pharmacodynamics studies revealed that MM54 demonstrated good solubility in the tested solutions, and was detected in the plasma and the brain *in vivo* following intraperitoneal administration in healthy animals (Supplementary Table 4). Next, to determine the bio-

Figure 4 Continued

(**G**) Flow cytometry analysis of the percentage of ALDH positive and negative GSC #1 in response to 2, 10 or 20 μM of MM54 at Day 5. ALDH activity corresponds to the percentage of cells that contains ALDH activity (positive) or not (negative), normalized to the vehicle condition. $^{*}P < 0.05$; $^{***}P < 0.001$ compared to the vehicle condition. (**H**) Confocal analysis of GSC #1 treated with DMSO or MM54 (2 μM) for SOX2 (red), NESTIN (green) and nuclei (DAPI, blue). Scale bars = 20 μm. (**I**) Western blot analysis of components of the mTOR and ERK signalling pathways in GSC#1 with APLN in the presence or absence of MM54 (2 μM). (**J**) Reverse protein phase array (RPPA) from the TCGA database were analysed in low and high *APLNR* expressing glioblastoma samples. $^{*}P < 0.05$; $^{**}P < 0.01$ compared to the low APLNR condition. (**K**) Western blot analysis of pS9-GSK3β in GSCs #1 and #9 following MM54 treatment in APLN containing MF media. (**L**) Tumoursphere per field of view in GSC#1 in response to APLN treatment (1 μM) in the presence or absence of the GSK3β inhibitor (tideglusib, 2.5 μM). $^{***}P < 0.001$ compared to the MF condition. (**M**) Linear regression plot of limiting dilution assay (LDA) for GSC #1 in MF and APLN (1 μM) alone or with tideglusib. (**N**) GSC #1 received sic (control) or *GSK3B* targeting siRNA (si*GSK3B*) and tumoursphere per field of view was quantified in MF supplemented with purified apelin (APLN, 1 μM). $^{*}P < 0.05$ compared to the sic MF condition. All panels are representative of $n = 3$, unless otherwise specified.

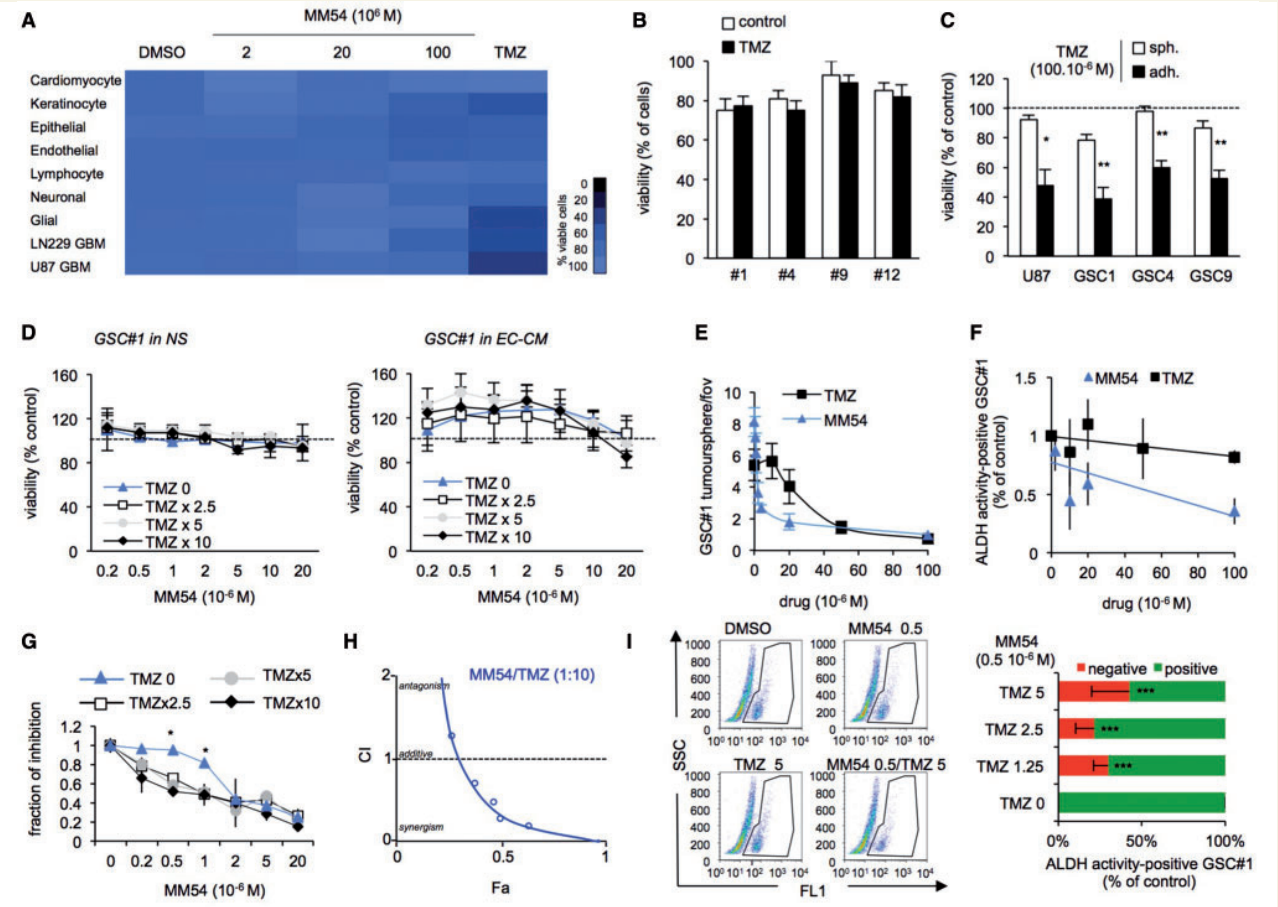

Figure 5 Pharmacological inhibition of APLNR by MM54 impairs the *in vitro* expansion of temozolomide-resistant GSCs. (**A**) Cell viability following treatment with DMSO, MM54 (2, 20 and 100 μM) or temozolomide (TMZ, 50 μM) was measured using UptiBlue in different cell types for 3 days. Cardiomyocytes (mouse primary cardiomyocytes), keratinocytes (HaCAT), epithelial cells (CaCo2), endothelial (hCMEC/D3), lymphocyte (Jurkat), neuronal (SH-SY5Y), glial (SVGp12). (**B** and **C**) Cell viability following treatment with DMSO or TMZ (100 μM) was measured using UptiBlue in GSCs #1, #4, #9, and #12 for 3 days. Similar experiments were conducted U87 glioblastoma cell line and GSCs #1, #4, and #9 grown as spheroids (sph.) in NS medium or as differentiated adherent cells (adh.) in serum-containing medium. (**D**) GSC#1 viability was assessed following combined treatment with MM54 (0.2–20 μM) and TMZ (constant ratios TMZ:MM54 2.5:1, 5:1, and 10:1) in NS and human brain endothelial cell-conditioned medium (EC-CM) conditions. (**E** and **F**) Tumoursphere per field of view (fov) and ALDH activity were assessed in response to MM54 (0.2–100 μM) or TMZ (10–100 μM) treatment at Day 5. (**G**) Drugs were combined at a constant MM54:TMZ ratio (1:2.5, 1:5, and 1:10) and ALDH activity measured. *$P < 0.05$ compared to the TMZ 0 condition. (**H**) Combination index plot for TMZ with MM54. Combination index (CI) was plotted against fractions affected (Fa) and analysed using COMPUSYN (http://www.combosyn.com/). A result < 1 indicated an additive effect of the two compounds, while values closer to 0 suggest the drugs may behave synergistically. (**I**) Flow cytometry analysis of ALDH activity in GSC #1 at Day 5 following combined treatment with MM54 (0.5 μM) and the indicated TMZ doses. ALDH activity corresponds to the percentage of cells that contains ALDH activity (positive) or not (negative). ***$P < 0.001$ compared to the TMZ 0 condition. All panels are representative of $n = 3$, unless otherwise specified.

safety of MM54 *in vivo*, tumour-bearing mice were administered 2 mg/kg of MM54 bi-weekly for 4 weeks. Due to the known physiological roles of apelin on the cardiovascular system and glucose metabolism (Maguire *et al.*, 2009; Scimia *et al.*, 2012; Fournel *et al.*, 2015), cardiac frequency, blood pressure and glycaemic index were measured. MM54 did not induce alterations to these parameters, reflecting no obvious detrimental action of APLNR antagonism in tumour-bearing animals (Fig. 6A and B). Complete blood count analysis revealed no significant differences between mice treated with MM54 and vehicle in healthy animals (Supplementary Table 5). Similarly, histological and biochemical analysis of heart, kidney and liver revealed no differences between MM54-treated animals and vehicle controls (Supplementary Fig. 3), indicating that at the present dose following repeated administration, MM54 does not exert any overt adverse effects *in vivo*.

We next tested the effect of pharmacological inhibition of APLNR with MM54 in an ectopic xenograft tumour model. MM54 treatment dramatically reduced tumour

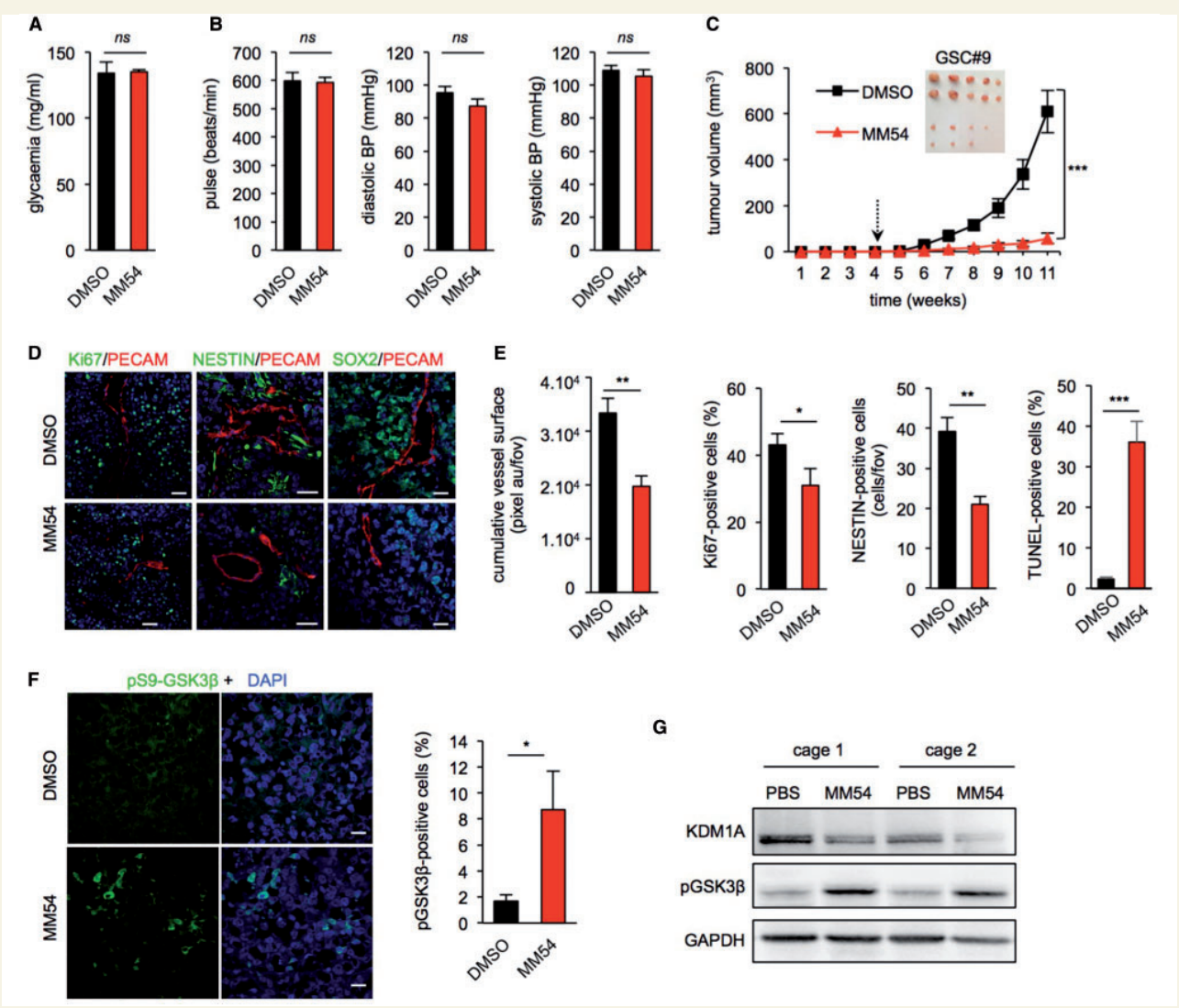

Figure 6 Pharmacological inhibition of APLNR by MM54 reduces xenograft progression. (**A**) Tumour-bearing mice were fasted for 6 h and the effect of either MM54 (2 mg/kg) or DMSO vehicle treatment on glycaemia measured via blood analysis. (**B**) Cardiac frequency and blood pressure were measured in random-fed tumour-bearing animals. (**C**) Nude mice were implanted with GSC#9 (5×10^5 cells) in each flank and treated with either DMSO vehicle or the APLNR antagonist (MM54, 2 mg/kg) bi-weekly from Week 4. Tumour volume was measured weekly until Week 11. $n = 10$/group. (**D** and **E**) Cryosections from GSC tumours were assessed for PECAM (red), Ki67 (green), NESTIN (green), SOX2 (green) and apoptosis (TUNEL). (**F**) Tumour sections were assessed for pS9-GSK3β staining in DMSO vehicle- and MM54-treated animals. Scale bars = 40 μm. (**G**) Western blot analysis of KDM1A and pS9-GSK3β was performed on two independent tumours from each treatment group. $n = 6$ mice/group. $^*P < 0.05$; $^{**}P < 0.01$; $^{***}P < 0.001$ compared to the DMSO vehicle control group. All panels are representative of $n = 3$, unless specified.

growth over 11 weeks when compared to DMSO control group (Fig. 6C). The decreased tumour volume was associated with a reduction in the staining of SOX2 and NESTIN-positive cells, overall proliferation and viability that was accompanied by a diminution in tumour vascularization (Fig. 6D and E). Additionally, MM54 treatment led to a significant increase in phospho-GSK3β positive cells within the tumour (Fig. 6F and G). In line with Zhou *et al*'s (2016) studies, this increased GSK3β phosphorylation was correlated with a decrease in KDM1A levels (Fig. 6G). To further validate our findings with MM54, we tested a second recently developed and structurally different APLNR antagonist, MM193 (Glen and Davenport, unpublished observation). Increasing doses of MM193 in GSCs counteracted the effect of apelin on tumourspheres *in vitro* (Supplementary Fig. 4A). Moreover, administration of MM193 (2 mg/kg) in GSC#9-inoculated mice resulted in significant impairment of tumour growth compared to vehicle controls (Supplementary Fig. 4B). Likewise, blockade of APLNR with MM193 did not induce any adverse

changes to cardiac frequency, blood pressure or glycaemia in healthy animals (Supplementary Fig. 4C). Together, these *in vivo* data indicate that pharmacological inhibition of APLNR efficiently and safely reduces tumour growth in xenografted female animals.

Pharmacological blockade of APLNR by MM54 prolongs survival of xenografted mice

To gain further insight into the therapeutic potential of APLNR antagonism in glioblastoma, nude mice were orthotopically implanted with GSC#9 into the striatum and treated with MM54 (2 mg/kg) three times a week. Experimental models of brain tumours are commonly associated with the development of neurological symptoms as well as cachexia as the tumour progresses. MM54 treatment was sufficient to impair the development of tumour-associated neurological symptoms and weight loss (Fig. 7A and B), which was coupled with a marked reduction in tumour size (Fig. 7C). Importantly, MM54 administration significantly improved the overall survival of tumour-bearing mice compared to their vehicle-treated counterparts (Fig. 7D). Additionally, blockade of APLNR was associated with a reduction in vascularization, proliferation, and SOX2 and NESTIN-positive cells (Fig. 7E). Collectively, these *in vivo* data provide a strong basis for the clinical potential of apelin/APLNR signalling as a therapeutic target in glioblastoma.

Discussion

The present study has identified the vasoactive peptide apelin as a critical factor involved in glioma growth. It is now well accepted that GSCs reside in proximity to vascular beds, into which endothelial cells secrete factors that regulate their self-renewal and fate. With that view, apelin is highly expressed in endothelial cells and once released has been proposed to act as a local mediator (Kleinz and Davenport, 2005; Kaelin *et al.*, 2007). In keeping with this, a recent study reports the high expression of apelin in colorectal cancer-isolated endothelial cells, which further correlates with refractoriness to anti-angiogenic treatment (Zuurbier *et al.*, 2017). Here, we demonstrate that apelin is released by human, mouse and tumour-derived endothelial cells *in vitro*, although this secretion

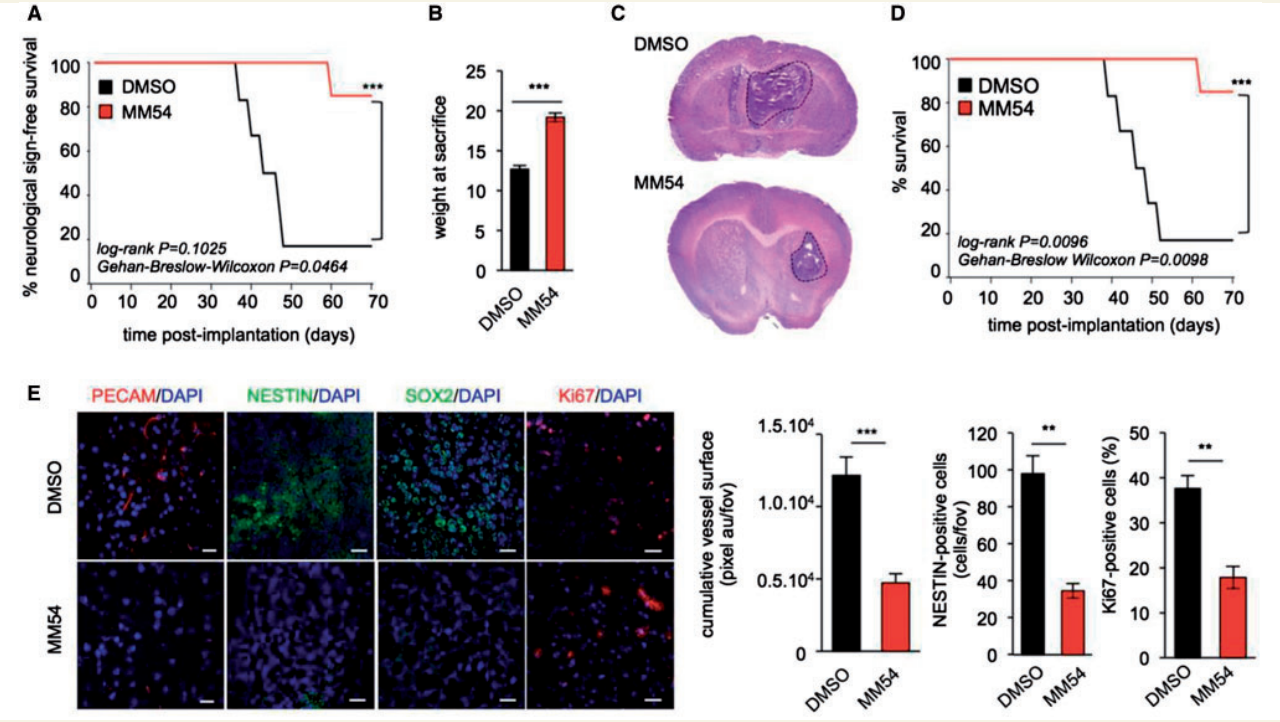

Figure 7 Pharmacological blockade of APLNR by MM54 prolongs survival of xenografted mice. (**A–E**) 10^5 GSC #9 were implanted into the striatum of female nude mice and treated three times a week with DMSO or MM54 (2 mg/kg) from Week 3 and the appearance of neurological symptoms monitored over time (**A**). The weight of mice at sacrifice was recorded for each treatment group (**B**). Haematoxylin and eosin (H&E) staining of tumour-inoculated brains following MM54 (2 mg/kg) or DMSO vehicle treatment (**C**). Kaplan-Meier survival curve of GSC #9 bearing mice in response to vehicle or MM54 treatment. $n = 6$/group. (**D**) Cryosections of brain tumour tissue stained for PECAM (red), NESTIN (green), SOX2 (green), Ki67 (red), and DAPI (blue) and quantified. Scale bars = 40 μm. $^{**}P < 0.01$; $^{***}P < 0.001$ compared to the DMSO control group (**E**). All panels are representative of $n = 3$, unless otherwise specified.

was not overtly affected by the acidification of the milieu. Additionally, we show that apelin increases GSC self-renewal *in vitro* in tumoursphere and limiting dilution assays, and that this effect appears to be independent of cell proliferation, consistent with the previously reported action on microvascular endothelial cells (Kaelin *et al.*, 2007).

In both subcutaneous ectopic and intracranial orthotopic xenograft models, inhibition of APLNR was associated with a significant reduction in tumour volume together with a reduction in vascularization, proliferation and an increase in apoptosis. Moreover, animals implanted with *APLNR* knocked down cells (shAPLNR GSC#9) were associated with a reduction in tumour burden compared to control groups, indicating that APLNR may be intrinsically important for tumour development. Additionally, APLNR knockdown and MM54 treatment diminished the number of NESTIN-positive cells within the xenografts again strengthening our hypothesis that apelin is particularly essential for the maintenance of GSCs.

Moreover, apelin has been implicated in physiological and pathological angiogenesis (Kaelin *et al.*, 2007). Apelin induces proliferation and vessel sprouting in endothelial cells, as well as stabilizing contacts between adjacent endothelial cells (Kleinz and Davenport, 2005). In keeping with this, a recent study proposed apelin as a marker for monitoring tumour vessel normalization and response to anti-angiogenic therapy (Zhang *et al.*, 2016; Zuurbier *et al.*, 2017). Accordingly, pharmacological blockade of apelin (Figs 6, 7 and Supplementary Fig. 3), but not the reduction of APLNR expression in GSCs (Supplementary Fig. 2D), may also contribute to the reduction of tumour volume observed in this study *in vivo*, by blocking angiogenesis and depriving tumour cells of the nutrients they require to survive. Although we cannot discount alternative sources of apelin peptides are involved *in vivo*, taken together the results of this study indicate that endothelial-derived apelin is an important factor for glioma growth.

The poor response of glioblastoma to chemotherapies has been in part attributed to the population of resistant initiating cells within the tumour. Therefore, identification of agents that improve GSC sensitivity to TMZ, the current standard-of-care, is of great interest. It has been reported that vascular niche maintains GSCs in a quiescent state thereby protecting them from radiation and chemotherapies. Our study demonstrates that the APLNR antagonist MM54 synergizes with TMZ *in vitro*. We further demonstrate that TMZ alone does not alter the activity of the stem marker ALDH, however when combined with sub-optimal dose of MM54, we observed profound alterations in the percentage of ALDH-positive cells. High *ALDH1A1* expression has been associated with poor prognosis in glioblastoma, and its overexpression *in vitro* a predictor of TMZ resistance (Schafer *et al.*, 2012). These alterations to the stem identity of GSCs suggest that combined treatment with MM54 and TMZ may provide an interesting opportunity to further target populations of cells currently resistant to chemotherapeutic drugs.

Although the precise molecular mechanisms that connect the apelin/APLNR axis to GSC maintenance will require further investigation, our data suggest that it may act through the GSK3β signalling pathway. GSK3β was shown to be upregulated in glioblastoma cells, and assist in stem cell maintenance by phosphorylating and stabilizing KDM1A (Zhou *et al.*, 2016). Paralleling the effect of the GSK3β inhibitor tideglusib (Zhou *et al.*, 2016) (Fig. 4L), we found that the APLNR antagonist MM54 reduced GSC self-renewal and potentiated sensitivity to TMZ (Fig. 5). APLNR inhibition was accompanied by an increased phosphorylation of GSK3β at S9, both *in vitro* and *in vivo* further supporting an inhibitory effect of MM54 compound on GSK3β signalling.

Here, we provide evidence that both *in vitro* and *in vivo* inhibition of APLNR results in a significant reduction in tumour growth. Given the concerns about the current therapeutic regime and the intrinsic resistance to TMZ, targeting apelin signalling presents a new opportunity for use in the treatment of glioblastoma.

Acknowledgements

The authors wish to thank the present and past members of SOAP laboratory at Institut Cochin, Paris and CRCINA, Nantes, France. We are grateful to Pierre-Olivier Couraud and Cecile Godard (Institut Cochin, Paris, France), Herve Chneiweiss and Marie-Pierre Junier (Institut de Biologie Paris-Seine/Neurosciences, Paris, France), Soumaya El Moghrabi and Fawaz Alzaid (Centre de Recherches des Cordeliers, Paris, France), Patrick Gizzi (TechMed, Strasbourg, France), and Lixin Zheng (NIAID, NIH, Bethesda, USA), for helpful discussions and reagents. The following core-facilities from SFR Francois Bonamy (FED 4203/UMS Inserm 016/CNRS 3556, Nantes, France) are acknowledged: cellular and tissular imaging core facility of Nantes University (MicroPICell), flow cytometry and cell sorting (Cytocell), functional exploration core facility for small animals (Therassay), SC3M/Histology, and UTE IRS-UN.

Funding

This research was funded by: *Connect Talent award* from *Region Pays-de-la-Loire and Nantes Metropole* (J.G), *Fondation ARC Association pour la Recherche sur le Cancer* (J.G and N.B), *Institut National du Cancer INCA* (J.G), *Ligue nationale contre le cancer* comité Loire-Atlantique, Maine-et-Loire, Morbihan, Sarthe, Vendée (J.G and N.B), and *SATT IDF Innov* (J.G). R.C.G thanks Unilever for support of the Centre for Molecular Informatics. A.P.D thanks the Wellcome Trust (WT107715/Z/15/Z).

Supplementary material

Supplementary material is available at *Brain* online.

References

Andreu-Agullo C, Morante-Redolat JM, Delgado AC, Farinas I. Vascular niche factor PEDF modulates Notch-dependent stemness in the adult subependymal zone. Nat Neurosci 2009; 12: 1514–23.

Bao S, Wu Q, McLendon RE, Hao Y, Shi Q, Hjelmeland AB, et al. Glioma stem cells promote radioresistance by preferential activation of the DNA damage response. Nature 2006; 444: 756–60.

Beck B, Driessens G, Goossens S, Youssef KK, Kuchnio A, Caauwe A, et al. A vascular niche and a VEGF-Nrp1 loop regulate the initiation and stemness of skin tumours. Nature 2011; 478: 399–403.

Brame AL, Maguire JJ, Yang P, Dyson A, Torella R, Cheriyan J, et al. Design, characterization, and first-in-human study of the vascular actions of a novel biased apelin receptor agonist. Hypertension 2015; 65: 834–40.

Bowman RL, Wang Q, Carro A, Verhaak RGW, Squatrito M. GlioVis data portal for visualization and analysis of brain tumor expression datasets. Neuro Oncol 2017; 19: 139–41.

Brown CE, Alizadeh D, Starr R, Weng L, Wagner JR, Naranjo A, et al. Regression of glioblastoma after chimeric antigen receptor T-cell therapy. N Engl J Med 2016; 375: 2561–9.

Calabrese C, Poppleton H, Kocak M, Hogg TL, Fuller C, Hamner B, et al. A perivascular niche for brain tumor stem cells. Cancer Cell 2007; 11: 69–82.

Cao Z, Ding BS, Guo P, Lee SB, Butler JM, Casey SC, et al. Angiocrine factors deployed by tumor vascular niche induce B cell lymphoma invasiveness and chemoresistance. Cancer Cell 2014; 25: 350–65.

Cao Z, Scandura JM, Inghirami GG, Shido K, Ding BS, Rafii S. Molecular checkpoint decisions made by subverted vascular niche transform indolent tumor cells into chemoresistant cancer stem cells. Cancer Cell 2017; 31: 110–26.

Chen J, Li Y, Yu TS, McKay RM, Burns DK, Kernie SG, et al. A restricted cell population propagates glioblastoma growth after chemotherapy. Nature 2012; 488: 522–6.

Chinot OL, Wick W, Mason W, Henriksson R, Saran F, Nishikawa R, et al. Bevacizumab plus radiotherapy-temozolomide for newly diagnosed glioblastoma. N Engl J Med 2014; 370: 709–22.

Chou TC. Drug combination studies and their synergy quantification using the Chou-Talalay method. Cancer Res 2010; 70: 440–6.

Dubois SM, Alexia C, Wu Y, Leclair HM, Leveau C, Schol E, et al. A catalytic-independent role for the LUBAC in NF-kappaB activation upon antigen receptor engagement and in lymphoma cells. Blood 2014; 123: 2199–203.

Evers P, Lee PP, DeMarco J, Agazaryan N, Sayre JW, Selch M, et al. Irradiation of the potential cancer stem cell niches in the adult brain improves progression-free survival of patients with malignant glioma. BMC Cancer 2010; 10: 384.

Folkins C, Man S, Xu P, Shaked Y, Hicklin DJ, Kerbel RS. Anticancer therapies combining antiangiogenic and tumor cell cytotoxic effects reduce the tumor stem-like cell fraction in glioma xenograft tumors. Cancer Res 2007; 67: 3560–4.

Fournel A, Drougard A, Duparc T, Marlin A, Brierley SM, Castro J, et al. Apelin targets gut contraction to control glucose metabolism via the brain. Gut 2015; 66: 258–69.

Galan-Moya EM, Le Guelte A, Lima Fernandes E, Thirant C, Dwyer J, Bidere N, et al. Secreted factors from brain endothelial cells maintain glioblastoma stem-like cell expansion through the mTOR pathway. EMBO Rep 2011; 12: 470–6.

Galan-Moya EM, Treps L, Oliver L, Chneiweiss H, Vallette FM, Bidere N, et al. Endothelial secreted factors suppress mitogen deprivation-induced autophagy and apoptosis in glioblastoma stem-like cells. PLoS One 2014; 9: e93505.

Garcia-Barros M, Paris F, Cordon-Cardo C, Lyden D, Rafii S, Haimovitz-Friedman A, et al. Tumor response to radiotherapy regulated by endothelial cell apoptosis. Science 2003; 300: 1155–9.

Hale JS, Sinyuk M, Rich JN, Lathia JD. Decoding the cancer stem cell hypothesis in glioblastoma. CNS Oncol 2013; 2: 319–30.

Harford-Wright E, Bidere N, Gavard J. β-escin selectively targets the glioblastoma-initiating cell population and reduces cell viability. Oncotarget 2016; 7: 66865–79.

Hu Y, Smyth GK. ELDA: extreme limiting dilution analysis for comparing depleted and enriched populations in stem cell and other assays. J Immunol Methods 2009; 347: 70–8.

Kaelin RE, Kretz MP, Meyer AM, Kispert A, Heppner FL, Brändli AW. Paracrine and autocrine mechanisms of apelin signaling govern embryonic and tumor angiogenesis. Dev Biol 2007; 305: 599–614.

Kleinz MJ, Davenport AP. Emerging roles of apelin in biology and medicine. Pharmacol Ther 2005; 107: 198–211.

Lathia JD, Mack SC, Mulkearns-Hubert EE, Valentim CL, Rich JN. Cancer stem cells in glioblastoma. Genes Dev 2015; 29: 1203–17.

Luissint AC, Federici C, Guillonneau F, Chretien F, Camoin L, Glacial F, et al. Guanine nucleotide-binding protein Galphai2: a new partner of claudin-5 that regulates tight junction integrity in human brain endothelial cells. J Cereb Blood Flow Metab 2012; 32: 860–73.

Macaluso NJ, Pitkin SL, Maguire JJ, Davenport AP, Glen RC. Discovery of a competitive apelin receptor (APJ) antagonist. Chem Med Chem 2011; 6: 1017–23.

Maguire JJ, Kleinz MJ, Pitkin SL, Davenport AP. [Pyr1]apelin-13 identified as the predominant apelin isoform in the human heart: vasoactive mechanisms and inotropic action in disease. Hypertension 2009; 54: 598–604.

Schafer A, Teufel J, Ringel F, Bettstetter M, Hoepner I, Rasper M, et al. Aldehyde dehydrogenase 1A1- a new mediator of resistance to temozolomide in glioblastoma. Neuro Oncol 2012; 14: 1452–64.

Scimia MC, Hurtado C, Ray S, Metzler S, Wei K, Wang J, et al. APJ acts as a dual receptor in cardiac hypertrophy. Nature 2012; 488: 394–8.

Shingu T, Ho AL, Yuan L, Zhou X, Dai C, Zheng S, et al. Qki deficiency maintains stemness of glioma stem cells in suboptimal environment by downregulating endolysosomal degradation. Nat Genet 2017; 49: 75–86.

Singh SK, Hawkins C, Clarke ID, Squire JA, Bayani J, Hide T, et al. Identification of human brain tumour initiating cells. Nature 2004; 432: 396–401.

Stupp R, Hegi ME, Mason WP, van den Bent MJ, Taphoorn MJ, Janzer RC, et al. Effects of radiotherapy with concomitant and adjuvant temozolomide versus radiotherapy alone on survival in glioblastoma in a randomised phase III study: 5-year analysis of the EORTC-NCIC trial. Lancet Oncol 2009; 10: 459–66.

Stupp R, Taillibert S, Kanner AA, Kesari S, Steinberg DM, Toms SA, et al. Maintenance therapy with tumor-treating fields plus temozolomide vs temozolomide alone for glioblastoma: a randomized clinical trial. JAMA 2015; 314: 2535–43.

Treps L, Edmond S, Harford-Wright E, Galan-Moya EM, Schmitt A, Azzi S, et al. Extracellular vesicle-transported Semaphorin3A promotes vascular permeability in glioblastoma. Oncogene 2016; 35: 2615–23.

Tropepe V, Sibilia M, Ciruna BG, Rossant J, Wagner EF, van der Kooy D. Distinct neural stem cells proliferate in response to EGF and FGF in the developing mouse telencephalon. Dev Biol 1999; 208: 166–88.

Yan K, Yang K, Rich JN. The evolving landscape of glioblastoma stem cells. Curr Opin Neurol 2013; 26: 701–7.

Zhang L, Takara K, Yamakawa D, Kidoya H, Takakura N. Apelin as a marker for monitoring the tumor vessel normalization window during antiangiogenic therapy. Cancer Sci 2016; 107: 36–44.

Zhou A, Lin K, Zhang S, Chen Y, Zhang N, Xue J, et al. Nuclear GSK3beta promotes tumorigenesis by phosphorylating KDM1A and inducing its deubiquitylation by USP22. Nat Cell Biol 2016; 18: 954–66.

Zuurbier L, Rahman A, Cordes M, Scheick J, Wong TJ, Rustenberg F, et al. Apelin: a putative novel predictive biomarker for bevacizumab response in colorectal cancer. Oncotarget 2017; 8: 42949–61.

ANNEX 3

3D Endothelial Cell Migration

Chapter 6

3D Endothelial Cell Migration

Kathryn A. Jacobs and Julie Gavard

Abstract

Endothelial cells have the capacity to shift between states of quiescence and angiogenesis. The early stage of angiogenesis, sprouting, occurs with the synchronized activities of tip cells, which lead the migration of the sprout, and stalk cells, which elongate this vessel sprout. Here, we describe a method to study in vitro this early and rapid stage of sprouting angiogenesis.

Key words Sprouting angiogenesis, Endothelial cell, VEGF, Tumor microenvironment, Fibrin matrix, Conditioned medium

1 Introduction

Blood vessels fuel organs and tissues throughout the body with oxygen, nutrients, hormones, and growth factors, while eliminating metabolic by-products. They also allow for circulation of immune cells that patrol the blood stream [1].

Blood vessels form a hierarchized and stereotyped network of many branches, which are lined with endothelial cells. Angiogenesis is defined as the expansion of this predefined network. This occurs, in physiological and pathological conditions, in response to changes in metabolic demands, with nutrient deprivation and a reduction in oxygen tension as the primary provocations for angiogenesis [2–4].

Endothelial cells are mainly found quiescent with a slow turnover in adult mature vessels. However, these differentiated cells remain highly plastic, with the ability to quickly switch between states of quiescence to rapid growth, i.e., vessel sprouting, when stimulated by growth factors or hypoxia. The most accepted model of vessel sprouting proposes a coordinated activity between endothelial cells in different states [4]. Schematically the leading cells—the first state—the so-called endothelial tip cells, navigate the vasculature and guide vessel elongation. The second one,

Alexis Gautreau (ed.), *Cell Migration: Methods and Protocols*, Methods in Molecular Biology, vol. 1749,
https://doi.org/10.1007/978-1-4939-7701-7_6,

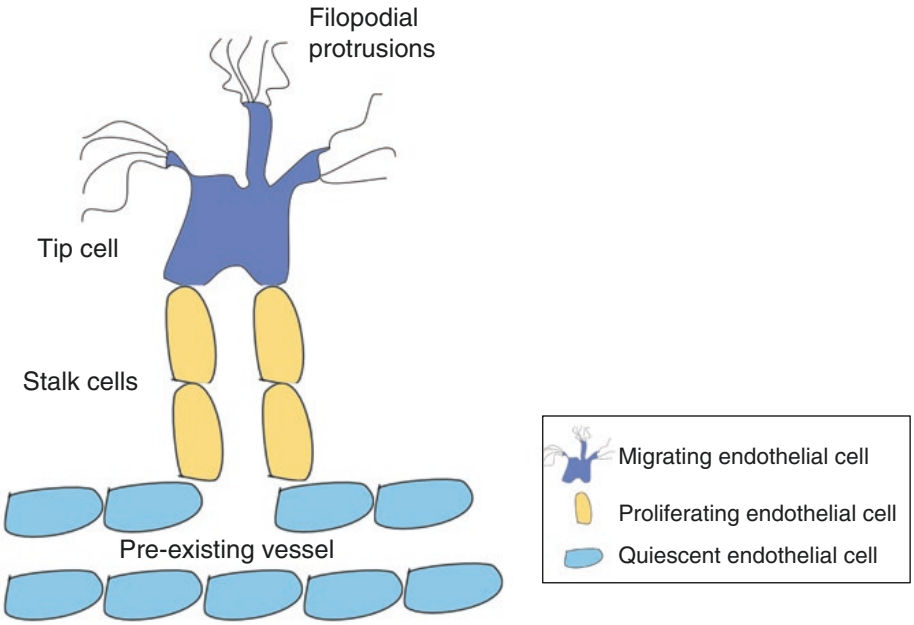

Fig. 1 Sprouting angiogenesis. A schematic model of vessel sprouting where stalk cells proliferate to expand the sprout, and the tip cells guide the vessel migration

endothelial stalk cells, elongates the branch through rapid proliferation (Fig. 1) [4].

Tip and stalk differentiation is notably regulated by VEGF (vascular endothelial growth factor) and Notch signaling. VEGF signals tip cell induction and prompts expression of Notch ligand Delta-like 4 (dll4). This activates Notch signaling in neighboring endothelial cells, and suppresses VEGF receptor 2 expression, to prevent tip cell behavior [4]. This mechanism selects therefore VEGFR2-positive dll4-positive tip cells and VEGFR2-negative Notch-positive stalk cells. However, cell fates are not permanently defined, there is a dynamic switch between tip and stalk cell phenotypes depending on the fitness of the cells [5]. From a mechanistic standpoint, this sprouting angiogenesis requires orchestrated tridimensional migration of endothelial cells together with cell invasion within a defined matrix (Fig. 1).

Angiogenesis is important for maintaining homeostasis, but it also has implications in disease. Endothelial cell dysfunction is indeed a characteristic of diabetes as a consequence of elevated oxidative stress [2, 6]. In cancer, tumor-induced angiogenesis allows tumors to grow by providing them with nutrients and oxygen [1]. How the tumor microenvironment operates on endothelial cells to drive sprouting is crucial to design antiangiogenic-based anticancer strategies.

The method presented here allows for the in vitro study of the early stages of angiogenesis, by recapitulating the endothelial behavior during sprouting angiogenesis (Fig. 2). This model can

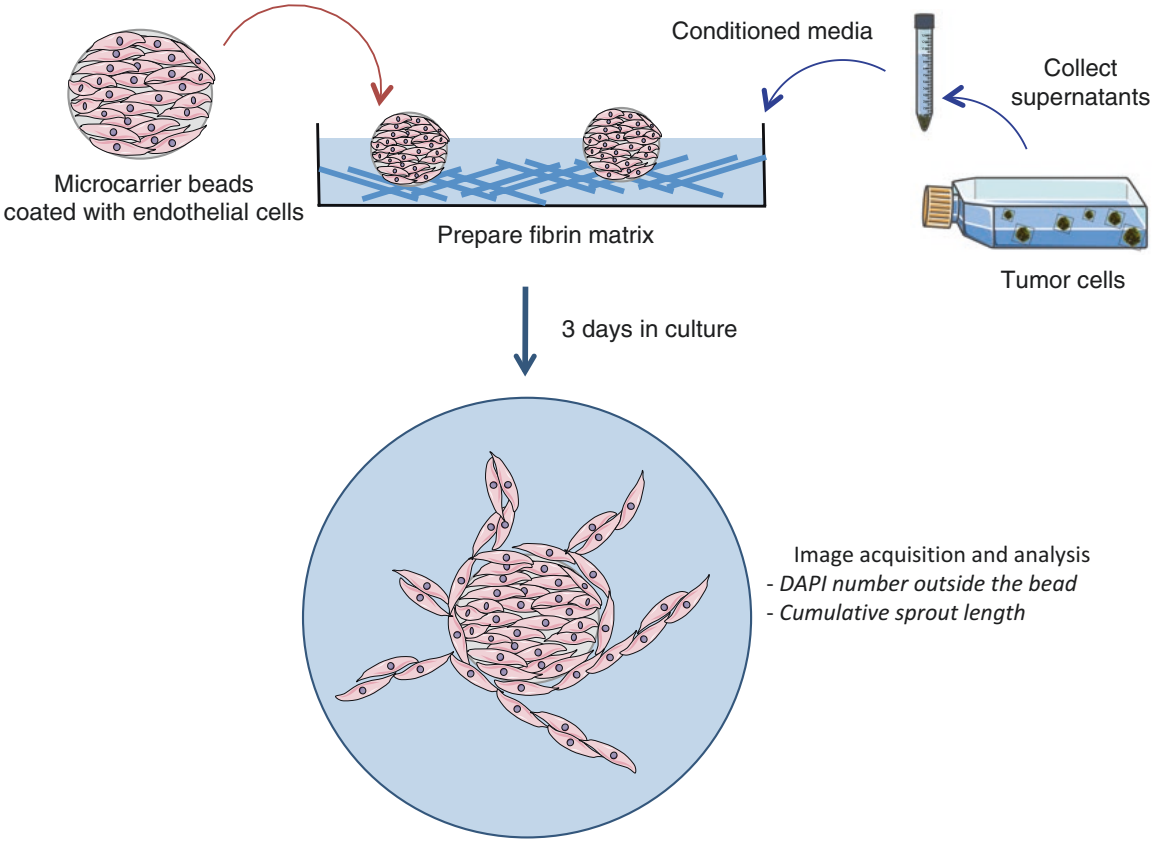

Fig. 2 In vitro sprouting assay procedure. Human umbilical vein endothelial cells (HUVEC) are coated on microcarrier beads, and allowed to sprout into a fibrin matrix, under exposure to malignant tumor cell conditioned media

have applications in a variety of disease studies, as conditions can be manipulated genetically or pharmacologically. For instance, recent studies from our lab had shown that conditioned media collected from patient-derived cancer cell cultures drive sprouting angiogenesis through secretion of growth factors [7]. In keeping with this idea, oncogenic transformation of endothelial cells also forces in vitro sprouting angiogenesis, a process that involves both the activation of intracellular aberrant signaling pathways and autocrine/paracrine cytokine action [8].

2 Materials

2.1 Reagents

1. HUVEC (human umbilical vein endothelial cells, Ea.hy926, ATCC).
2. U87-MG (human astrocytoma malignant glioma cell line, ATCC).
3. DMEM 4.5 g/L glucose.
4. GlutaMAX.

5. Fetal bovine serum (FBS).
6. Trypsin–EDTA (0.05%).
7. Cytodex-3 Beads (Sigma, C3275).
8. Rat tail collagen I.
9. Aprotinin.
10. Fibrinogen Type I.
11. bFGF solution (basic fibroblast growth factor solution, Sigma, F5392) 2 μL bFGF stock (10,000×) in 200 μL DMEM.
12. Thrombin.
13. 8-well Ibidi plate.
14. Sterile filter 0.2 μm.
15. PBS.
16. Paraformaldehyde.
17. Prolong Diamond antifade mountant (Life Technologies).
18. Alexa 488-conjugated phalloidin (Life Technologies).
19. Deionized water.

2.2 Equipment

1. Bench pipettes and small equipment (rocker, centrifuge).
2. Equipped cell culture room (37 °C/5%CO_2 incubator, hood).
3. Conventional microscope to visualize DAPI and Alexa 488.

3 Methods

3.1 Reagent Preparation

1. In order to prepare fibrinogen for use, first dissolve 2 mg/mL fibrinogen in DMEM-GlutaMAX medium. Make sure to note the clottable protein percentage and adjust accordingly. The solution should be heated in a 37 °C water bath to dissolve the fibrinogen. Filter solution through a sterile 0.2 μm filter (*see* **Note 1**).
2. To reconstitute aprotinin, dissolve lyophilized aprotinin in deionized water at 4 U/mL. Filter solution through a sterile 0.2 μm filter. Make aliquots of 1 mL each and store the solution at −20 °C (*see* **Note 2**).
3. For thrombin preparation, reconstitute thrombin in sterile water at 50 U/mL. Make aliquots of 500 μL each and store at −20 °C (*see* **Note 2**).
4. For a 10 mL fibrinogen solution, dissolve 25 mg of fibrinogen in 10 mL of DMEM, as described in **step 1**. Then add 20 μL of aprotinin (10 mg/mL) to the solution. Filter the resulting solution sterilely through a 0.2 μm filter. Finally, add 100 μL of the bFGF solution.
5. In order to prepare Cytodex beads for use, hydrate 0.5 g of dry beads in PBS (pH 7.4) for at least 3 h at room temperature.

This should be done in a 50 mL tube on a rocker, under gentle rotation. Next, let the beads settle down for approximately 15 min. Discard the supernatant and wash the beads for several minutes in 50 mL of fresh PBS. Then, discard the supernatant and replace again with fresh PBS. For 30,000 beads/mL (10 mg/mL), use 50 mL PBS.

6. Prepare all reagents for staining; paraformaldehyde (4% in PBS) for fixation, Triton X-100 (0.05% in PBS) for permeabilization. Prepare fresh solutions.

3.2 Cell Preparation

1. Grow HUVEC in DMEM-GlutaMAX +10% FBS in the days before beading. A concentration of 400 cells per bead is needed to perform the experiment. For 75 µL of bead solution, 10^6 HUVEC will be needed (*see* **Notes 3** and **4**).
2. Grow U87 in DMEM-GlutaMAX +10% FBS. To prepare U87-MG condition medium (CM), 250.000 cells are plated in 10 cm dish, grow for 2 days in DMEM-GlutaMAX, supplemented with 10% FBS. Cells are washed thrice with PBS and incubated at 37 °C overnight in DMEM-GlutaMAX serum-free media [9]. Two days later, media are decanted and cleared by centrifugation (300 × *g*, 5 min), followed by filtration through a 0.2 µm filter. CM are then used immediately or stored at −20 °C until use (*see* **Notes 2** and **5**).

3.3 Sprouting Assay

1. On day −1, coat beads with HUVEC. First, 4000 Cytodex microcarrier beads are incubated with collagen (1/50 dilution in PBS, 15 min, RT). Aspirate the supernatant and wash the beads in 1 mL of prewarmed DMEM. Trypsinize nonconfluent HUVEC and mix 75 µL of beads with 10^6 HUVEC in 1.5 mL of prewarmed DMEM in a 15 mL round tube. Make sure to place the tube vertically in the incubator (37 °C) (*see* **Note 6**).
2. Incubate the tube for 4 h at 37 °C, shaking the tube every 20 min. After 4 h, transfer the coated beads into a T75 flask, add 12 mL of DMEM and incubate overnight at 37 °C (*see* **Note** 7).
3. On day 0, coated beads should be embedded in fibrin gel. To do this, prepare the fibrinogen/aprotinin/bFGF solution (2.5 mg/mL) (*see* Subheading 3.1). Next, transfer the coated beads to a 15 mL conical tube. Let the beads settle. Wash the beads three times with 1 mL DMEM. Then, count the beads on a 10 µL coverslip and resuspend them in the fibrinogen solution at a concentration of approximately 500 beads per mL (*see* **Note 8**).
4. Add 0.625 U/mL of thrombin to each well of the IBIDI plate. Stock is at 100 U/mL, add 20 µL of the stock diluted 1–10 by adding 450 µL of DMEM to a 50 µL aliquot. Then add 400 µL

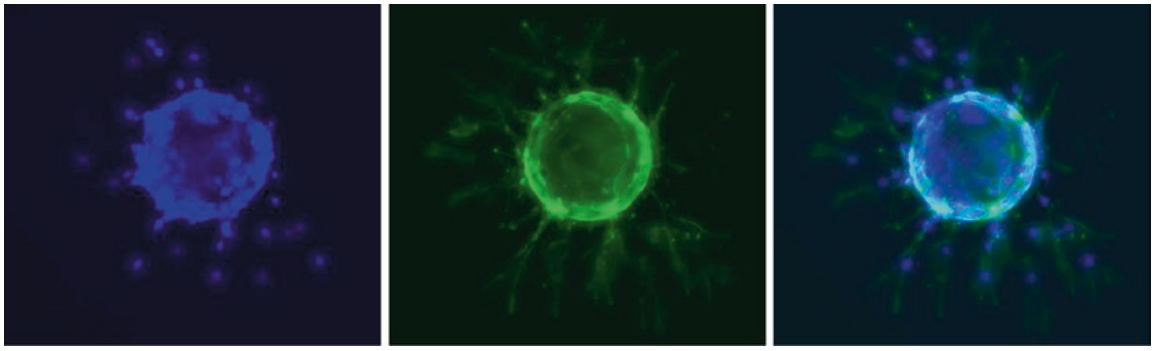

Fig. 3 Typical image of endothelial sprouting. Human endothelial cells were prepared for sprouting assays, as described and incubated for 3 days with conditioned media from malignant glioma cells. Nuclei are stained with DAPI (blue), actin cytoskeleton is visualized with Phalloidin (green)

of the fibrinogen/bead suspension to each well of the plate. Mix the thrombin and fibrinogen by pipetting up and down gently four or five times (*see* **Notes 1**, **9**, and **10**).

5. Leave the plate in the cell culture hood for 5 min. After, place plate in the incubator (37 °C) for 10 to 15 min in order to generate a clot. Once the clot is formed, add 1 mL of DMEM/bFGF dropwise to each well. Return the plate to the incubator (*see* **Note 11**).
6. On day 1, add the U87-CM on top of the fibrin gel. Return plate to incubator (37 °C) (*see* **Notes 12** and **13**).

3.4 Data Analysis

1. By day 3, sprouting should have occurred. Check under bright field microscope and harvest the experiment. Fix in paraformaldehyde 4% (15 min, RT) and permeabilized in Triton (5 min, RT). Wash once in PBS. Incubate with Alexa 488-conjugated phalloidin (1/1000 in PBS, 45 min, RT). Wash three times in PBS. Mount in DAPI-containing mounting medium (*see* **Note 14**).
2. Proceed to image acquisition, with a minimum of 5 random fields of views (Fig. 3) (*see* **Note 15**).
3. From individual bead, quantify (1) number of sprouted cells by counting DAPI-positive nuclei away from the beads, and, (2) sprout extension by measuring cumulative sprout length and mean sprout length (Fig. 2) (*see* **Note 16**).

4 Notes

1. Tubes should never be vortexed, instead mix by inverting the tube.
2. Avoid freeze–thaw cycles.

3. Antibiotics (penicillin/streptomycin) can be added to the medium.
4. Alternate endothelial cells could be used, such as from human, mouse, rat and porcine origin, as well as from any organs. Culture conditions vary and might need to be adapted.
5. Other tumor cell lines could be used. Cell density might need to be tested and adjusted. Usually 48 h is preferred to collect CM.
6. Allow the beads to settle, but do not centrifuge them.
7. Make sure to rinse the T75 flask with DMEM.
8. As a control of good coating, beads should look like golf balls.
9. Make sure to change the pipette tip each time.
10. Avoid creating large bubbles.
11. Tiny bubbles are usually formed in the fibrin gel. They should disappear by the end of the experiment.
12. Media on plate should be changed every other day. Control for evaporation, a humid chamber can be useful when CM volume is limited.
13. Do not forget negative control, such as DMEM-GlutaMAX media collected similarly to U87-CM from cell-free plates.
14. Experiment can be stopped after the fixation step and plate left in PBS, 4 °C overnight. Slowly aspirate medium by pipetting, avoid vacuum it.
15. Images can be acquired with any conventional large field microscope, equipped with DAPI and FITC filters, and automatized camera.
16. Image analysis can be performed with any image viewer software. We recommend Fiji software (Fiji is just Image J), free of use at https://fiji.sc/.

Acknowledgment

The authors are thankful to the present and past members of SOAP laboratory, in particular to Sandy Azzi and Lucas Treps who developed the sprouting assays in the team. Research in SOAP team was funded by: Fondation ARC pour la recherche contre le Cancer, Ligue Nationale contre le Cancer comité Pays-de-la-Loire, comité Maine-et-Loire and comité Vendée, and Connect Talent grant from Région Pays-de-la-Loire and Nantes Métropole. KAJ received a doctoral fellowship from Nantes Métropole.

References

1. De Bock K, Georgiadou M, Carmeliet P (2013) Role of endothelial cell metabolism in vessel sprouting. Cell Metab 18:634–647
2. Adams RH, Alitalo K (2007) Molecular regulation of angiogenesis and lymphangiogenesis. Nat Rev Mol Cell Biol 8:464–478
3. Herbert SP, Stainier DY (2011) Molecular control of endothelial cell behaviour during blood vessel morphogenesis. Nat Rev Mol Cell Biol 12:551–564
4. Potente M, Gerhardt H, Carmeliet P (2011) Basic and therapeutic aspects of angiogenesis. Cell 146:873–887
5. Jakobsson L, Franco CA, Bentley K, Collins RT, Ponsioen B, Aspalter IM, Rosewell I, Busse M, Thurston G, Medvinsky A et al (2010) Endothelial cells dynamically compete for the tip cell position during angiogenic sprouting. Nat Cell Biol 12:943–953
6. Yeh WL, Lin CJ, Fu WM (2008) Enhancement of glucose transporter expression of brain endothelial cells by vascular endothelial growth factor derived from glioma exposed to hypoxia. Mol Pharmacol 73:170–177
7. Azzi S, Treps L, Leclair HM, Ngo H, Harford-Wright E, Gavard J (2015) Desert Hedgehog/Patch2 axis contributes to vascular permeability and angiogenesis in glioblastoma. Front Pharmacol 6:281
8. Dwyer J, Azzi S, Leclair HM, Georges S, Carlotti A, Treps L, Galan-Moya A, Alexia C, Dupin N, Bidere N, Gavard J (2015) The guanine exchange factor SWAP70 mediates vGPCR-induced endothelial plasticity. Cell Commun Signal 13:12
9. Dwyer J, Hebda JK, Le Guelte A, Galan-Moya EM, Smith SS, Azzi S, Bidere N, Gavard J (2012) Glioblastoma cell-secreted interleukin-8 induces brain endothelial cell permeability via CXCR2. PLoS One 7:e45562

ANNEX 4
Scientific Communications

idw - Informationsdienst
Wissenschaft

27.11.2019 12:34

Exploring drug repurposing to treat glioblastoma

Dr. Tilmann Kiessling *EMBO Communications*
EMBO - excellence in life sciences

MALT1 blockers have long been in clinical use for the treatment of blood cancers. A study suggests that these drugs could potentially also be developed as a treatment option for glioblastoma, the most common and lethal type of brain tumour.

Heidelberg, 27 November 2019 – For a long time, cancer research has largely focused on so-called oncogenes – genes that can cause cancer when mutated. While targeting these genes has led to the successful development of a number of valuable drugs, this approach is hampered by the fact that tumours often become resistant to these treatments.

A study conducted by Julie Gavard at the Université de Nantes, CNRS, INSERM, France, and her team, published today in The EMBO Journal, is now based on a different concept, termed non-oncogene addiction. During disease progression, cancer cells become strongly dependent on normal genes and cell functions to survive. These genes could thus serve as potential targets to attack tumour growth more efficiently. A gene called mucosa-associated lymphoid tissue l (MALT1), for example, is highly active in lymphoma, a type of blood cancer, and blocking MALT1 causes lymphoma cells to die. MALT1 blockers have been viewed as a promising new treatment for lymphomas.

The researchers now addressed the role of MALT1 in solid tumours, namely glioblastoma. Using data from The Cancer Genome Atlas, a molecular characterization of over 20,000 primary cancers, they revealed that MALT1 levels strongly correlate with patients' survival in brain cancer – patients with less MALT1 tend to live longer.

Gavard and colleagues then focused their attention on so-called glioblastoma stem cells, a self-renewing subpopulation of cells within the tumour that are likely responsible for cancer recurrence after treatment. They uncovered that targeting MALT1 with MALT1 blockers caused glioblastoma stem cells to undergo a rare form of cellular suicide termed lysosomal cell death in human cell culture experiments. Lysosomes are organelles within the cell that serve as the cells' digestive system. MALT1 keeps lysosomes low in cancer cells, which is crucial for their survival. Blocking MALT1 leads to an increase in lysosomes, which in turn impairs the cells' waste disposal system, eventually killing them. This points to the possibility of further exploring MALT1 inhibitors as potential treatment of glioblastoma.

Originalpublikation:
Control of the Homeostasis of Endo-lysosomes by the Paracaspase MALT1 regulates Glioma Cell Survival

The EMBO Journal

Kathryn A. Jacobs, Gwennan André-Grégoire, Clément Maghe, An Thys, Ying Li, Elizabeth Harford-Wright1, Kilian Trillet, Tiphaine Douanne, Carolina Alves Nicolau, Jean-Sébastien Frénel, Nicolas Bidère, and Julie Gavard

DOI: 10.15252/embj.2019102030

UNNEWS
NE RIEN MANQUER DE NOTRE ACTUALITÉ
UNNEWS > Version française > Futurs

Thématiques:
- Recherche / Culture scientifique

Cerveau : les chercheurs décèlent le "talon d'Achille" d'une tumeur cancéreuse

Le 27 novembre 2019

Le glioblastome, une tumeur incurable du cerveau, est alimenté par un réservoir de cellules souches capables d'initier, maintenir et renouveler cette tumeur. Une étude menée par des chercheur.e.s du Centre de Recherche en Cancérologie et Immunologie Nantes-Angers (CRCINA / CNRS, Inserm, Université de Nantes, Université d'Angers), et récemment publiée dans The EMBO Journal, révèle qu'un gène (MALTI) agit comme un point de contrôle vie/mort des cellules souches cancéreuses.

Les glioblastomes multiformes (GBM) sont des tumeurs du cerveau parmi les plus dévastatrices de l'adulte, avec une survie médiane de 15 mois après le diagnostic. Le traitement standard actuel comprend une résection neurochirurgicale suivie de cycles répétés de chimiothérapie et radiothérapie. Bien que ces stratégies standardisées se soient révélées bénéfiques, elles demeurent essentiellement palliatives. Au sein de ces tumeurs hautement hétérogènes, existe une sous-population de cellules tumorales appelées cellules de type souche du glioblastome (GSC) qui jouent un rôle dans l'initiation et la progression de la tumeur, ainsi que dans les résistances thérapeutiques et la récurrence.

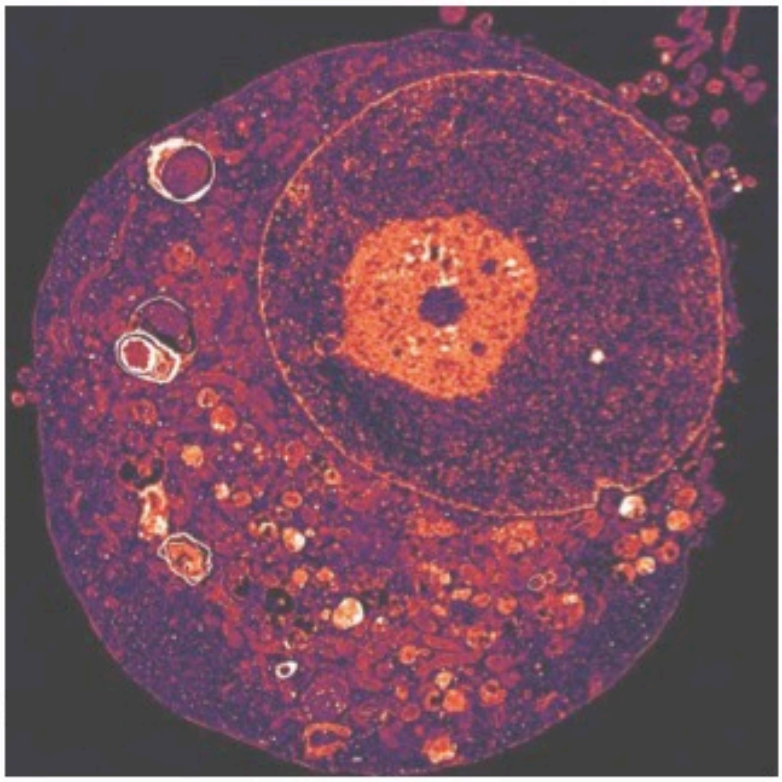

Les chercheur.e.s du **Centre de Recherche en Cancérologie et Immunologie Nantes-Angers (CRCINA)** se sont intéressé.e.s à l'expression d'un gène (MALT1) présent et actif dans les tumeurs humaines. Leurs études menées sur des cellules de patients atteints de glioblastome ont montré que le blocage moléculaire de l'expression de ce gène pouvait être toxique pour les cellules tumorales.

Par une approche d'imagerie cellulaire, les chercheur.e.s ont également remarqué que le blocage de l'activité du gène - ou la réduction de son expression - provoquait dans les GSCs une augmentation incontrôlée et fatale en lysosomes, les structures intracellulaires qui agissent normalement comme des stations de recyclage.

Crédit photo : © Julie Gavard

Mis à jour le 27 novembre 2019 par Julien PATRON.

Ressources

Control of the Homeostasis of Endo-lysosomes by the Paracaspase MALT1 regulates Glioma Cell Survival. Kathryn A. Jacobs, Gwennan André-Grégoire, Clément Maghe, An Thys, Ying Li, Elizabeth Harford-Wright, Kilian Trillet, Tiphaine Douanne, Carolina Alves Nicolau, Jean-Sébastien Frénel, Nicolas Bidère, Julie Gavard. The EMBO Journal

En savoir plus

> **La fiche du Centre de Recherche en Cancérologie Nantes-Angers**

MALT1 et Glioblastomes: Haro sur les Lysosomes !

02 décembre 2019

RÉSULTATS SCIENTIFIQUES PHYSIOLOGIE ET CANCER

Le glioblastome, une tumeur incurable du cerveau, est alimenté par un réservoir de cellules souches capables d'initier, maintenir et renouveler la tumeur. La cellule souche cancéreuse peut survivre en conditions hostiles notamment en atténuant les processus de dégradation intracellulaire médiée par les lysosomes. Cette étude publiée dans *The EMBO Journal* révèle que la protéase MALT1 agit comme un point de contrôle vie/mort des cellules souches cancéreuses en régulant la quantité de lysosomes.

Les glioblastomes multiformes (GBM) sont des tumeurs du cerveau parmi les plus dévastatrices de l'adulte, avec une survie médiane de 15 mois après le diagnostic. Le traitement standard actuel comprend une résection neurochirurgicale suivie de cycles répétés de chimiothérapie et radiothérapie. Bien que ces stratégies standardisées se soient révélées bénéfiques, elles demeurent essentiellement palliatives. Au sein de ces tumeurs hautement hétérogènes, existe une sous-population de cellules tumorales appelées cellules de type souche du glioblastome (GSC). Bien que la définition moléculaire des GSCs fasse encore l'objet de débat, ces cellules jouent un rôle dans l'initiation et la progression de la tumeur, ainsi que dans les résistances thérapeutiques et la récurrence.

Les GSCs sont dispersées dans la tumeur à la fois à proximité des vaisseaux sanguins et à distance dans des zones moins oxygénées. Tandis que la vasculature cérébrale leur offre une "niche" protectrice, enrichie en facteurs de croissance, les GSCs sont également capables de supporter des conditions de privation extrême. Cette résilience est notamment liée à leur capacité à prolonger et maintenir des voies de signalisation de survie cellulaire, en l'absence des activateurs exogènes de la "niche". Cette caractéristique s'appuie sur la baisse du trafic d'endocytose des récepteurs membranaires aux facteurs de croissance et de leur dégradation dans les lysosomes qui sont des organites au pH acide fonctionnant comme des centres névralgiques pour le trafic et le métabolisme des macromolécules. Les lysosomes sont notamment impliqués dans la voie de signalisation multiple mTOR (*mammalian Target of Rapamycin*).

Afin d'identifier des régulateurs de cette voie intrinsèque d'autoprotection, les chercheurs ont analysé les bases de données publiques de plusieurs centaines de patients atteints de glioblastome. Parmi les gènes non déjà connus pour leur implication dans l'initiation de la transformation tumorale, ils ont observé une corrélation entre la survie des patients et l'expression du gène MALT1 (*Mucosa-Associated lymphoid tissue Lymphoma Translocation protein 1*). Ce gène spécifie la paracaspase MALT1, une arginine-protéase qui orchestre la réponse immunitaire lors de l'activation des lymphocytes, tandis qu'elle est constitutivement active dans certains lymphomes. Son rôle dans le système nerveux central et en particulier dans les glioblastomes n'a cependant pas été exploré en détail.

En utilisant des cellules isolées à partir des pièces opératoires de patients atteints de glioblastome, les chercheurs ont constaté que le blocage moléculaire de l'expression de MALT1 est toxique pour ces cellules. C'est aussi le cas lorsque MALT1 est inhibée pharmacologiquement par le biais d'antipsychotiques de la famille des phénothiazines, dont la mépazine. Ce frein à

l'expansion tumorale est reproduit *in vivo* dans des souris greffées de tumeurs humaines.

Par des approches d'imagerie cellulaire, les chercheurs ont ensuite établi que l'activité protéolytique de MALT1 permet de maintenir des quantités faibles en lysosomes dans les GSCs. En revanche, le blocage de l'activité protéolytique de MALT1 ou la réduction de son expression provoque dans les GSCs un déferlement fatal en lysosomes. Ceci conduit à la mort cellulaire des GSCs, concomitante à une réduction de la voie de signalisation mTOR, normalement essentielle au maintien de leur caractère "souche".

La perturbation de l'homéostasie lysosomale pourrait donc représenter une nouvelle stratégie d'attaque contre les GSCs, faisant émerger MALT1 comme un "talon d'Achille" du glioblastome.

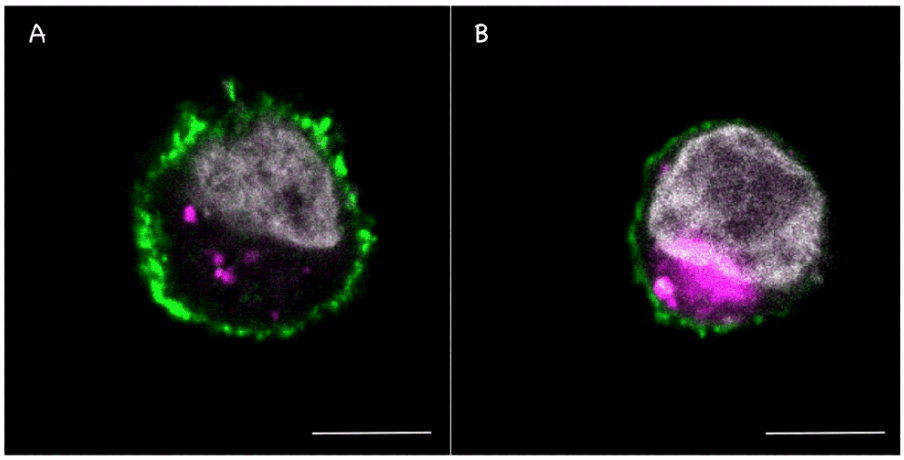

Figure : La forme sauvage (A) ou inactive (B) de l'arginine-protéase MALT1 a été introduite dans une cellule souche humaine de glioblastome. L'analyse en microscopie confocale permet de révéler les noyaux en gris, les lysosomes en magenta, et MALT1 en vert. Barre d'échelle : 10 mm.

Pour en savoir plus :

Paracaspase MALT1 regulates glioma cell survival by controlling endo-lysosome homeostasis.

Jacobs KA, André-Grégoire G, Maghe C, Thys A, Li Y, Harford-Wright E, Trillet K, Douanne T, Alves Nicolau C, Frénel JS, Bidère N, Gavard J.
EMBO J. 2019 Nov 27:e102030. doi: 10.15252/embj.2019102030 . [Epub ahead of print]

Contact

Julie Gavard
Chercheuse CNRS au Centre de recherche en cancérologie Nantes-Angers (CNRS / Inserm / Université de Nantes / Université d'Angers)

0228080327
Julie.gavard@inserm.fr

ANNEX 5

Supplemental methods for discussion

Annex 5

Supplemental methods :

CRISPR generation. For CRISPR, single-guide RNA (sgRNA) (sequence GTGGATGCTGTGTCTTCAGG) targeting gp130 was chosen in the sgRNA library (Shalem et al., 2014) and cloned into a lentiviral lentiCRISPRv2 (GeCKO, ZhangLab) backbone. For infections, lentiviral particles were produced in HEK293T by co-transfection of the construct together with pVSV-G and psPAX2 plasmids. Supernatants containing lentiviral particles were collected after 48 h and applied on GSC#1 during a 1,250 × g centrifugation for 90 min in presence of 8 µg ml−1 of polybrene (Sigma). Cells were cultured with 10 µg ml−1 of puromycin to select infected cells. Single cell clones were isolated by cell sorting of the negative cell population using an antibody against gp130 (abcam). Knockout of gp130 was confirmed by PCR and genomic sequencing.

RNA sequencing. 5.10^6 GSC#1 WT, GSC#1 KO clone #2, and GSC#1 KO clone #7 were snap-frozen on dry ice in 3 biological replicates. RNA extraction (all RIN >9.0), library preparation, RNAseq and bioinformatics analysis was performed at Active Motif (Carlsbad, California, USA). Briefly, 2 µg of total RNA were isolated using the Qiagen RNeasy Mini Kit and further processed in Illumina's TruSeq Stranded mRNA Library kit. Libraries are sequenced on Illumina NextSeq 500 as paired-end 42-nt reads. Sequence reads are analyzed with the STAR alignment – DESeq2 software pipeline described in the Data Explanation document. The list of differentially expressed genes from DESeq2 output were selected based on 10% adjusted P-value level and a FDR of 0.1.

Limiting Dilution Assays. In order to evaluate the self-renewal of GSCs, limited dilution assays (LDA) were performed. GSCs were seeded in a 96-well plate via a serial dilution ranging from 2000-1 cell/well. 8 replicates per dilution were performed and treated as indicated. After 14 days, each well was assessed for tumoursphere formation in a binary fashion. Stemness frequency was then calculated using ELDA software. Data are representative of N=2 experiments.

Immunostaining. Cells were seeded onto slides, fixed for 10 min with 4% PFA diluted in PBS, and blocked with PBS-BSA 4% prior to 1 hour primary antibody incubation with gp130 (santa cruz) and APLNR (R&D). No permeabilization step was performed. After PBS washes, cells were incubated with AlexaFluor-conjugated secondary antibodies for 30 minutes. Next, cells were mounted with prolong diamond anti-fade with DAPI mounting medium. All images were acquired on confocal Nikon A1 Rsi, using a 60x oil-immersion lens (Nikon Excellence Center, Micropicell, SFR Francois Bonamy, Nantes, France). All images were analyzed using Image J software.

Proximity Ligation Assay. APLNR/GP130 interaction was visualized through the Duolink in situ kit following manufacturer's instructions (Sigma) on GSC#1 using primary antibodies against ALPNR (R&D) and gp130 (Santa Cruz). All images were acquired on confocal Nikon A1 Rsi, using a 60x oil-immersion lens (Nikon Excellence Center, Micropicell, SFR Francois Bonamy, Nantes, France). All images were analyzed using the Image J software.

Flow cytometry analysis. GSC#1 and GSC#1 KO cells were isolated, washed, and incubated with antibodies against gp130 (abcam) and APLNR (R&D coupled APC) for 1 hour at RT. Alternatively, ectopic gp130 or empty vector was introduced in KO clones using a Neon transfection system and cells were analyzed 48 hrs later for surface gp130 and APLNR. Flow Cytometry analyses were performed on FACsCalibur (BD Biosciences, Cytocell, SFR Francois Bonamy, Nantes, France) and processed using FlowJo software.

Cell viability. 5000 GSC#1 and GSC#9 were treated with JQ1 (Sigma) or AZD5153 (Selleckchem) in triplicate for 48 hrs. Alternatively, GSC#9 were transfected with siRNA sic (Low GC duplex, Invitrogen) or siBRD4 (UUAGACUUGAUUGUGCUCATG) and analyzed 72 hrs later. Cell viability was measured using Cell titer glo reagent (Promega) according to the manufacturers protocol.

Immunoblotting and Immunoprecipitation. Cells were collected with cold PBS and lysed in TNT lysis Buffer (50 mM TRIS pH7.4, 150 mM NaCl, 1% Triton X-100, 1% Igepal, 2 mM EDTA, supplemented with Protease Inhibitor) for 30 minutes on ice. Samples were cleared at 8000g to remove insoluble fraction. Immunoprecipitation was performed as previously described (Douanne et al. 2016). Briefly, cell lysis was done in TNT lysis buffer for 30 minutes and samples were centrifuged at 8000g. Samples were precleared via a 30 minute-incubation with Protein G agarose, and then incubated for 2 hours at 4°C with Protein G agarose and 5 µg of indicated antibodies. Protein concentrations were determined by BCA. Equal amount of 5-10µg proteins were resolved by SDS-PAGE and transferred to

nitrocellulose membranes. Membranes were revealed using a chemiluminescent HRP substrate and visualized using the Fusion imaging system.

Statistics. Statistical analysis was performed with GraphPad Prism5 using One-way analysis of variance (ANOVA), or an unpaired two-tailed *t*-test (Student's t test). For each statistical test, p value of <0.05 was considered significant.

Abbott, N.J., Rönnbäck, L., and Hansson, E. (2006). Astrocyte-endothelial interactions at the blood-brain barrier. Nat. Rev. Neurosci. *7*, 41–53.

Abou-Ghazal, M., Yang, D.S., Qiao, W., Reina-Ortiz, C., Wei, J., Kong, L.-Y., Fuller, G.N., Hiraoka, N., Priebe, W., Sawaya, R., et al. (2008). The incidence, correlation with tumor-infiltrating inflammation, and prognosis of phosphorylated STAT3 expression in human gliomas. Clin. Cancer Res. Off. J. Am. Assoc. Cancer Res. *14*, 8228–8235.

Abu-Remaileh, M., Wyant, G.A., Kim, C., Laqtom, N.N., Abbasi, M., Chan, S.H., Freinkman, E., and Sabatini, D.M. (2017). Lysosomal metabolomics reveals V-ATPase and mTOR-dependent regulation of amino acid efflux from lysosomes. Science *358*, 807–813.

Affronti, M.L., Heery, C.R., Herndon, J.E., Rich, J.N., Reardon, D.A., Desjardins, A., Vredenburgh, J.J., Friedman, A.H., Bigner, D.D., and Friedman, H.S. (2009). Overall survival of newly diagnosed glioblastoma patients receiving carmustine wafers followed by radiation and concurrent temozolomide plus rotational multiagent chemotherapy. Cancer *115*, 3501–3511.

Aits, S., and Jäättelä, M. (2013). Lysosomal cell death at a glance. J. Cell Sci. *126*, 1905–1912.

Aits, S., Kricker, J., Liu, B., Ellegaard, A.-M., Hämälistö, S., Tvingsholm, S., Corcelle-Termeau, E., Høgh, S., Farkas, T., Holm Jonassen, A., et al. (2015). Sensitive detection of lysosomal membrane permeabilization by lysosomal galectin puncta assay. Autophagy *11*, 1408–1424.

Akhavan, D., Alizadeh, D., Wang, D., Weist, M.R., Shepphird, J.K., and Brown, C.E. (2019). CAR T cells for brain tumors: Lessons learned and road ahead. Immunol. Rev. *290*, 60–84.

Albertini, M.R. (2018). The age of enlightenment in melanoma immunotherapy. J. Immunother. Cancer *6*, 80.

Alcantara Llaguno, S., Chen, J., Kwon, C.-H., Jackson, E.L., Li, Y., Burns, D.K., Alvarez-Buylla, A., and Parada, L.F. (2009). Malignant astrocytomas originate from neural stem/progenitor cells in a somatic tumor suppressor mouse model. Cancer Cell *15*, 45–56.

Al-Hajj, M., Wicha, M.S., Benito-Hernandez, A., Morrison, S.J., and Clarke, M.F. (2003). Prospective identification of tumorigenic breast cancer cells. Proc. Natl. Acad. Sci. U. S. A. *100*, 3983–3988.

Allen, E., Jabouille, A., Rivera, L.B., Lodewijckx, I., Missiaen, R., Steri, V., Feyen, K., Tawney, J., Hanahan, D., Michael, I.P., et al. (2017). Combined antiangiogenic and anti–PD-L1 therapy stimulates tumor immunity through HEV formation. Sci. Transl. Med. *9*.

Allen, M., Bjerke, M., Edlund, H., Nelander, S., and Westermark, B. (2016). Origin of the U87MG glioma cell line: Good news and bad news. Sci. Transl. Med. *8*, 354re3-354re3.

Alonso, M.M., Jiang, H., Yokoyama, T., Xu, J., Bekele, N.B., Lang, F.F., Kondo, S., Gomez-Manzano, C., and Fueyo, J. (2008). Delta-24-RGD in Combination With RAD001 Induces Enhanced Anti-glioma Effect via Autophagic Cell Death. Mol. Ther. *16*, 487–493.

Alonso, M.M., Jiang, H., Gomez-Manzano, C., and Fueyo, J. (2012). Targeting brain tumor stem cells with oncolytic adenoviruses. Methods Mol. Biol. Clifton NJ *797*, 111–125.

André-Grégoire, G., and Gavard, J. (2016). Spitting out the demons: Extracellular vesicles in glioblastoma. Cell Adhes. Migr. *11*, 164–172.

André-Grégoire, G., Bidère, N., and Gavard, J. (2018). Temozolomide affects Extracellular Vesicles Released by Glioblastoma Cells. Biochimie *155*, 11–15.

Ango, F., Pin, J.P., Tu, J.C., Xiao, B., Worley, P.F., Bockaert, J., and Fagni, L. (2000). Dendritic and axonal targeting of type 5 metabotropic glutamate receptor is regulated by homer1 proteins and neuronal excitation. J. Neurosci. Off. J. Soc. Neurosci. *20*, 8710–8716.

Armulik, A., Abramsson, A., and Betsholtz, C. (2005). Endothelial/pericyte interactions. Circ. Res. *97*, 512–523.

Arnandis, T., Ferrer-Vicens, I., García-Trevijano, E.R., Miralles, V.J., García, C., Torres, L., Viña, J.R., and Zaragozá, R. (2012). Calpains mediate epithelial-cell death during mammary gland involution: mitochondria and lysosomal destabilization. Cell Death Differ. *19*, 1536–1548.

Ashizawa, T., Miyata, H., Iizuka, A., Komiyama, M., Oshita, C., Kume, A., Nogami, M., Yagoto, M., Ito, I., Oishi, T., et al. (2013). Effect of the STAT3 inhibitor STX-0119 on the proliferation of cancer stem-like cells derived from recurrent glioblastoma. Int. J. Oncol. *43*, 219–227.

Aumailley, M., and Smyth, N. (1998). The role of laminins in basement membrane function. J. Anat. *193 (Pt 1)*, 1–21.

Autier, L., Clavreul, A., Cacicedo, M.L., Franconi, F., Sindji, L., Rousseau, A., Perrot, R., Montero-Menei, C.N., Castro, G.R., and Menei, P. (2019). A new glioblastoma cell trap for implantation after surgical resection. Acta Biomater. *84*, 268–279.

Bach, M., Larance, M., James, D.E., and Ramm, G. (2011). The serine/threonine kinase ULK1 is a target of multiple phosphorylation events. Biochem. J. *440*, 283–291.

Bachoo, R.M., Maher, E.A., Ligon, K.L., Sharpless, N.E., Chan, S.S., You, M.J., Tang, Y., DeFrances, J., Stover, E., Weissleder, R., et al. (2002). Epidermal growth

factor receptor and Ink4a/Arf: convergent mechanisms governing terminal differentiation and transformation along the neural stem cell to astrocyte axis. Cancer Cell *1*, 269–277.

Baens, M., Bonsignore, L., Somers, R., Vanderheydt, C., Weeks, S.D., Gunnarsson, J., Nilsson, E., Roth, R.G., Thome, M., and Marynen, P. (2014). MALT1 auto-proteolysis is essential for NF-κB-dependent gene transcription in activated lymphocytes. PloS One *9*, e103774.

Baens, M., Stirparo, R., Lampi, Y., Verbeke, D., Vandepoel, R., Cools, J., Marynen, P., de Bock, C.E., and Bornschein, S. (2018). Malt1 self-cleavage is critical for regulatory T cell homeostasis and anti-tumor immunity in mice. Eur. J. Immunol. *48*, 1728–1738.

Baker, H., Sidorowicz, A., Sehgal, S.N., and Vézina, C. (1978). Rapamycin (AY-22,989), a new antifungal antibiotic. III. In vitro and in vivo evaluation. J. Antibiot. (Tokyo) *31*, 539–545.

Balch, W.E., Morimoto, R.I., Dillin, A., and Kelly, J.W. (2008). Adapting Proteostasis for Disease Intervention. Science *319*, 916–919.

Baldi, I., Huchet, A., Bauchet, L., and Loiseau, H. (2010). Épidémiologie des glioblastomes. Neurochirurgie *56*, 433–440.

Bao, S., Wu, Q., Sathornsumetee, S., Hao, Y., Li, Z., Hjelmeland, A.B., Shi, Q., McLendon, R.E., Bigner, D.D., and Rich, J.N. (2006a). Stem cell-like glioma cells promote tumor angiogenesis through vascular endothelial growth factor. Cancer Res. *66*, 7843–7848.

Bao, S., Wu, Q., McLendon, R.E., Hao, Y., Shi, Q., Hjelmeland, A.B., Dewhirst, M.W., Bigner, D.D., and Rich, J.N. (2006b). Glioma stem cells promote radioresistance by preferential activation of the DNA damage response. Nature *444*, 756–760.

Bardella, C., Al-Dalahmah, O., Krell, D., Brazauskas, P., Al-Qahtani, K., Tomkova, M., Adam, J., Serres, S., Lockstone, H., Freeman-Mills, L., et al. (2016). Expression of Idh1R132H in the Murine Subventricular Zone Stem Cell Niche Recapitulates Features of Early Gliomagenesis. Cancer Cell *30*, 578–594.

Bar-Peled, L., Schweitzer, L.D., Zoncu, R., and Sabatini, D.M. (2012). Ragulator Is a GEF for the Rag GTPases that Signal Amino Acid Levels to mTORC1. Cell *150*, 1196–1208.

Bar-Peled, L., Chantranupong, L., Cherniack, A.D., Chen, W.W., Ottina, K.A., Grabiner, B.C., Spear, E.D., Carter, S.L., Meyerson, M., and Sabatini, D.M. (2013). A Tumor suppressor complex with GAP activity for the Rag GTPases that signal amino acid sufficiency to mTORC1. Science *340*, 1100–1106.

Basel-Vanagaite, L., Hershkovitz, T., Heyman, E., Raspall-Chaure, M., Kakar, N., Smirin-Yosef, P., Vila-Pueyo, M., Kornreich, L., Thiele, H., Bode, H., et al. (2013).

Biallelic SZT2 Mutations Cause Infantile Encephalopathy with Epilepsy and Dysmorphic Corpus Callosum. Am. J. Hum. Genet. *93*, 524–529.

Bashir, T., Cloninger, C., Artinian, N., Anderson, L., Bernath, A., Holmes, B., Benavides-Serrato, A., Sabha, N., Nishimura, R.N., Guha, A., et al. (2012). Conditional Astroglial Rictor Overexpression Induces Malignant Glioma in Mice. PLOS ONE *7*, e47741.

Batchelor, T.T., Sorensen, A.G., di Tomaso, E., Zhang, W.-T., Duda, D.G., Cohen, K.S., Kozak, K.R., Cahill, D.P., Chen, P.-J., Zhu, M., et al. (2007). AZD2171, a Pan-VEGF Receptor Tyrosine Kinase Inhibitor, Normalizes Tumor Vasculature and Alleviates Edema in Glioblastoma Patients. Cancer Cell *11*, 83–95.

Beaumatin, F., O'Prey, J., Barthet, V.J.A., Zunino, B., Parvy, J.-P., Bachmann, A.M., O'Prey, M., Kania, E., Gonzalez, P.S., Macintosh, R., et al. (2019). mTORC1 Activation Requires DRAM-1 by Facilitating Lysosomal Amino Acid Efflux. Mol. Cell *76*, 163-176.e8.

Beier, D., Hau, P., Proescholdt, M., Lohmeier, A., Wischhusen, J., Oefner, P.J., Aigner, L., Brawanski, A., Bogdahn, U., and Beier, C.P. (2007). CD133(+) and CD133(-) glioblastoma-derived cancer stem cells show differential growth characteristics and molecular profiles. Cancer Res. *67*, 4010–4015.

Ben-David, U., Ha, G., Tseng, Y.-Y., Greenwald, N.F., Oh, C., Shih, J., McFarland, J.M., Wong, B., Boehm, J.S., Beroukhim, R., et al. (2017). Patient-derived xenografts undergo mouse-specific tumor evolution. Nat. Genet. *49*, 1567–1575.

Benes, P., Vetvicka, V., and Fusek, M. (2008). Cathepsin D--many functions of one aspartic protease. Crit. Rev. Oncol. Hematol. *68*, 12–28.

Ben-Porath, I., Thomson, M.W., Carey, V.J., Ge, R., Bell, G.W., Regev, A., and Weinberg, R.A. (2008). An embryonic stem cell-like gene expression signature in poorly differentiated aggressive human tumors. Nat. Genet. *40*, 499–507.

Ben-Sahra, I., Howell, J.J., Asara, J.M., and Manning, B.D. (2013). Stimulation of de novo pyrimidine synthesis by growth signaling through mTOR and S6K1. Science *339*, 1323–1328.

van den Bent, M.J., Gao, Y., Kerkhof, M., Kros, J.M., Gorlia, T., van Zwieten, K., Prince, J., van Duinen, S., Sillevis Smitt, P.A., Taphoorn, M., et al. (2015). Changes in the EGFR amplification and EGFRvIII expression between paired primary and recurrent glioblastomas. Neuro-Oncol. *17*, 935–941.

Bhat, K.P.L., Balasubramaniyan, V., Vaillant, B., Ezhilarasan, R., Hummelink, K., Hollingsworth, F., Wani, K., Heathcock, L., James, J.D., Goodman, L.D., et al. (2013). Mesenchymal Differentiation Mediated by NF-κB Promotes Radiation Resistance in Glioblastoma. Cancer Cell *24*.

Bissig, C., Hurbain, I., Raposo, G., and van Niel, G. (2017). PIKfyve activity regulates reformation of terminal storage lysosomes from endolysosomes. Traffic

Cph. Den. *18*, 747–757.

Blaho, V.A., Galvani, S., Engelbrecht, E., Liu, C., Swendeman, S.L., Kono, M., Proia, R.L., Steinman, L., Han, M.H., and Hla, T. (2015). HDL-bound sphingosine 1-phosphate restrains lymphopoiesis and neuroinflammation. Nature *523*, 342–346.

Bleau, A.-M., Hambardzumyan, D., Ozawa, T., Fomchenko, E.I., Huse, J.T., Brennan, C.W., and Holland, E.C. (2009). PTEN/PI3K/Akt Pathway Regulates the Side Population Phenotype and ABCG2 Activity in Glioma Tumor Stem-like Cells. Cell Stem Cell *4*, 226–235.

Bonaguidi, M.A., McGuire, T., Hu, M., Kan, L., Samanta, J., and Kessler, J.A. (2005). LIF and BMP signaling generate separate and discrete types of GFAP-expressing cells. Dev. Camb. Engl. *132*, 5503–5514.

Bond, A.M., Ming, G.-L., and Song, H. (2015). Adult Mammalian Neural Stem Cells and Neurogenesis: Five Decades Later. Cell Stem Cell *17*, 385–395.

Bonizzi, G., and Karin, M. (2004). The two NF-κB activation pathways and their role in innate and adaptive immunity. Trends Immunol. *25*, 280–288.

Bonnet, D., and Dick, J.E. (1997). Human acute myeloid leukemia is organized as a hierarchy that originates from a primitive hematopoietic cell. Nat. Med. *3*, 730–737.

Bornancin, F., Renner, F., Touil, R., Sic, H., Kolb, Y., Touil-Allaoui, I., Rush, J.S., Smith, P.A., Bigaud, M., Junker-Walker, U., et al. (2015). Deficiency of MALT1 paracaspase activity results in unbalanced regulatory and effector T and B cell responses leading to multiorgan inflammation. J. Immunol. Baltim. Md 1950 *194*, 3723–3734.

Boya, P., Andreau, K., Poncet, D., Zamzami, N., Perfettini, J.-L., Metivier, D., Ojcius, D.M., Jäättelä, M., and Kroemer, G. (2003). Lysosomal membrane permeabilization induces cell death in a mitochondrion-dependent fashion. J. Exp. Med. *197*, 1323–1334.

Brem, H., Piantadosi, S., Burger, P.C., Walker, M., Selker, R., Vick, N.A., Black, K., Sisti, M., Brem, S., Mohr, G., et al. (1995). Placebo-controlled trial of safety and efficacy of intraoperative controlled delivery by biodegradable polymers of chemotherapy for recurrent gliomas. The Lancet *345*, 1008–1012.

Brennan, C.W., Verhaak, R.G.W., McKenna, A., Campos, B., Noushmehr, H., Salama, S.R., Zheng, S., Chakravarty, D., Sanborn, J.Z., Berman, S.H., et al. (2013). The somatic genomic landscape of glioblastoma. Cell *155*, 462–477.

Bright, N.A., Davis, L.J., and Luzio, J.P. (2016). Endolysosomes Are the Principal Intracellular Sites of Acid Hydrolase Activity. Curr. Biol. CB *26*, 2233–2245.

Britten, C.D., Garrett-Mayer, E., Chin, S.H., Shirai, K., Ogretmen, B., Bentz, T.A., Brisendine, A., Anderton, K., Cusack, S.L., Maines, L.W., et al. (2017). A Phase I Study of ABC294640, a First-in-Class Sphingosine Kinase-2 Inhibitor, in Patients

with Advanced Solid Tumors. Clin. Cancer Res. Off. J. Am. Assoc. Cancer Res. *23*, 4642–4650.

Bronisz, A., Wang, Y., Nowicki, M.O., Peruzzi, P., Ansari, K., Ogawa, D., Balaj, L., De Rienzo, G., Mineo, M., Nakano, I., et al. (2014). Extracellular vesicles modulate the glioblastoma microenvironment via a tumor suppression signaling network directed by miR-1. Cancer Res. *74*, 738–750.

Brown, E.J., Albers, M.W., Shin, T.B., Ichikawa, K., Keith, C.T., Lane, W.S., and Schreiber, S.L. (1994). A mammalian protein targeted by G1-arresting rapamycin-receptor complex. Nature *369*, 756–758.

Brown, T.J., Brennan, M.C., Li, M., Church, E.W., Brandmeir, N.J., Rakszawski, K.L., Patel, A.S., Rizk, E.B., Suki, D., Sawaya, R., et al. (2016). Association of the Extent of Resection With Survival in Glioblastoma: A Systematic Review and Meta-analysis. JAMA Oncol. *2*, 1460–1469.

Brugarolas, J., Lei, K., Hurley, R.L., Manning, B.D., Reiling, J.H., Hafen, E., Witters, L.A., Ellisen, L.W., and Kaelin Jr., W.G. (2004). Regulation of mTOR function in response to hypoxia by REDD1 and the TSC1/TSC2 tumor suppressor complex. Genes Dev. *18*, 2893–2904.

Brunk, U.T., and Ericsson, J.L. (1972). Cytochemical evidence for the leakage of acid phosphatase through ultrastructurally intact lysosomal membranes. Histochem. J. *4*, 479–491.

Brunn, G.J., Hudson, C.C., Sekulić, A., Williams, J.M., Hosoi, H., Houghton, P.J., Lawrence, J.C., and Abraham, R.T. (1997). Phosphorylation of the translational repressor PHAS-I by the mammalian target of rapamycin. Science *277*, 99–101.

Brüstle, A., Brenner, D., Knobbe-Thomsen, C.B., Cox, M., Lang, P.A., Lang, K.S., and Mak, T.W. (2017). MALT1 is an intrinsic regulator of regulatory T cells. Cell Death Differ. *24*, 1214–1223.

Cafferkey, R., Young, P.R., McLaughlin, M.M., Bergsma, D.J., Koltin, Y., Sathe, G.M., Faucette, L., Eng, W.K., Johnson, R.K., and Livi, tia (1993). Dominant missense mutations in a novel yeast protein related to mammalian phosphatidylinositol 3-kinase and VPS34 abrogate rapamycin cytotoxicity. Mol. Cell. Biol. *13*, 6012–6023.

Calabrese, C., Poppleton, H., Kocak, M., Hogg, T.L., Fuller, C., Hamner, B., Oh, E.Y., Gaber, M.W., Finklestein, D., Allen, M., et al. (2007). A perivascular niche for brain tumor stem cells. Cancer Cell *11*, 69–82.

Cancer Genome Atlas Research Network (2008). Comprehensive genomic characterization defines human glioblastoma genes and core pathways. Nature *455*, 1061–1068.

Canuel, M., Korkidakis, A., Konnyu, K., and Morales, C.R. (2008). Sortilin mediates the lysosomal targeting of cathepsins D and H. Biochem. Biophys. Res. Commun.

373, 292–297.

Carlsson, S.R., and Fukuda, M. (1992). The lysosomal membrane glycoprotein lamp-1 is transported to lysosomes by two alternative pathways. Arch. Biochem. Biophys. *296*, 630–639.

Carpentier, A., Canney, M., Vignot, A., Reina, V., Beccaria, K., Horodyckid, C., Karachi, C., Leclercq, D., Lafon, C., Chapelon, J.-Y., et al. (2016). Clinical trial of blood-brain barrier disruption by pulsed ultrasound. Sci. Transl. Med. *8*, 343re2.

Carroll, S.L. (2012). Molecular mechanisms promoting the pathogenesis of Schwann cell neoplasms. Acta Neuropathol. (Berl.) *123*, 321–348.

Castino, R., Peracchio, C., Salini, A., Nicotra, G., Trincheri, N.F., Démoz, M., Valente, G., and Isidoro, C. (2009). Chemotherapy drug response in ovarian cancer cells strictly depends on a cathepsin D-Bax activation loop. J. Cell. Mol. Med. *13*, 1096–1109.

Chakravarti, A., Zhai, G., Suzuki, Y., Sarkesh, S., Black, P.M., Muzikansky, A., and Loeffler, J.S. (2004). The Prognostic Significance of Phosphatidylinositol 3-Kinase Pathway Activation in Human Gliomas. J. Clin. Oncol. *22*, 1926–1933.

Chan, E.Y.W., Kir, S., and Tooze, S.A. (2007). siRNA screening of the kinome identifies ULK1 as a multidomain modulator of autophagy. J. Biol. Chem. *282*, 25464–25474.

Chan, E.Y.W., Longatti, A., McKnight, N.C., and Tooze, S.A. (2009). Kinase-Inactivated ULK Proteins Inhibit Autophagy via Their Conserved C-Terminal Domains Using an Atg13-Independent Mechanism. Mol. Cell. Biol. *29*, 157–171.

Chantranupong, L., Wolfson, R.L., Orozco, J.M., Saxton, R.A., Scaria, S.M., Bar-Peled, L., Spooner, E., Isasa, M., Gygi, S.P., and Sabatini, D.M. (2014). The Sestrins Interact with GATOR2 to Negatively Regulate the Amino-Acid-Sensing Pathway Upstream of mTORC1. Cell Rep. *9*, 1–8.

Chantranupong, L., Scaria, S.M., Saxton, R.A., Gygi, M.P., Shen, K., Wyant, G.A., Wang, T., Harper, J.W., Gygi, S.P., and Sabatini, D.M. (2016). The CASTOR Proteins Are Arginine Sensors for the mTORC1 Pathway. Cell *165*, 153–164.

Charles, N., Ozawa, T., Squatrito, M., Bleau, A.-M., Brennan, C.W., Hambardzumyan, D., and Holland, E.C. (2010). Perivascular nitric oxide activates notch signaling and promotes stem-like character in PDGF-induced glioma cells. Cell Stem Cell *6*, 141–152.

Chauhan, S., Kumar, S., Jain, A., Ponpuak, M., Mudd, M.H., Kimura, T., Choi, S.W., Peters, R., Mandell, M., Bruun, J.-A., et al. (2016). TRIMs and Galectins Globally Cooperate and TRIM16 and Galectin-3 Co-direct Autophagy in Endomembrane Damage Homeostasis. Dev. Cell *39*, 13–27.

Chen, A.-J., Paik, J.-H., Zhang, H., Shukla, S.A., Mortensen, R., Hu, J., Ying, H., Hu,

B., Hurt, J., Farny, N., et al. (2012a). STAR RNA-binding protein Quaking suppresses cancer via stabilization of specific miRNA. Genes Dev. *26*, 1459–1472.

Chen, D.S., Irving, B.A., and Hodi, F.S. (2012b). Molecular Pathways: Next-Generation Immunotherapy—Inhibiting Programmed Death-Ligand 1 and Programmed Death-1. Clin. Cancer Res. *18*, 6580–6587.

Chen, J., Li, Y., Yu, T.-S., McKay, R.M., Burns, D.K., Kernie, S.G., and Parada, L.F. (2012c). A restricted cell population propagates glioblastoma growth after chemotherapy. Nature *488*, 522–526.

Chen, J., McKay, R.M., and Parada, L.F. (2012d). Malignant Glioma: Lessons from Genomics, Mouse Models, and Stem Cells. Cell *149*, 36–47.

Chen, Q., Wu, J., Ye, Q., Ma, F., Zhu, Q., Wu, Y., Shan, C., Xie, X., Li, D., Zhan, X., et al. (2018). Treatment of Human Glioblastoma with a Live Attenuated Zika Virus Vaccine Candidate. MBio *9*.

Chen, Q., Liu, Y., Jeong, H.-W., Stehling, M., Dinh, V.V., Zhou, B., and Adams, R.H. (2019a). Apelin+ Endothelial Niche Cells Control Hematopoiesis and Mediate Vascular Regeneration after Myeloablative Injury. Cell Stem Cell *0*.

Chen, Q., Liu, Y., Jeong, H.-W., Stehling, M., Dinh, V.V., Zhou, B., and Adams, R.H. (2019b). Apelin+ Endothelial Niche Cells Control Hematopoiesis and Mediate Vascular Regeneration after Myeloablative Injury. Cell Stem Cell *25*, 768-783.e6.

Cheng, L., Huang, Z., Zhou, W., Wu, Q., Donnola, S., Liu, J.K., Fang, X., Sloan, A.E., Mao, Y., Lathia, J.D., et al. (2013). Glioblastoma Stem Cells Generate Vascular Pericytes to Support Vessel Function and Tumor Growth. Cell *153*, 139–152.

Cheong, H., Lindsten, T., Wu, J., Lu, C., and Thompson, C.B. (2011). Ammonia-induced autophagy is independent of ULK1/ULK2 kinases. Proc. Natl. Acad. Sci. U. S. A. *108*, 11121–11126.

Chinot, O.L., Wick, W., Mason, W., Henriksson, R., Saran, F., Nishikawa, R., Carpentier, A.F., Hoang-Xuan, K., Kavan, P., Cernea, D., et al. (2014). Bevacizumab plus radiotherapy-temozolomide for newly diagnosed glioblastoma. N. Engl. J. Med. *370*, 709–722.

Chiu, M.I., Katz, H., and Berlin, V. (1994). RAPT1, a mammalian homolog of yeast Tor, interacts with the FKBP12/rapamycin complex. Proc. Natl. Acad. Sci. U. S. A. *91*, 12574–12578.

Choi, C., Gillespie, G.Y., Van Wagoner, N.J., and Benveniste, E.N. (2002). Fas engagement increases expression of interleukin-6 in human glioma cells. J. Neurooncol. *56*, 13–19.

Choi, Y.-J., Di Nardo, A., Kramvis, I., Meikle, L., Kwiatkowski, D.J., Sahin, M., and He, X. (2008). Tuberous sclerosis complex proteins control axon formation. Genes Dev. *22*, 2485–2495.

Choksi, S., Lin, Y., Pobezinskaya, Y., Chen, L., Park, C., Morgan, M., Li, T., Jitkaew, S., Cao, X., Kim, Y.-S., et al. (2011). A HIF-1 target, ATIA, protects cells from apoptosis by modulating the mitochondrial thioredoxin, TRX2. Mol. Cell *42*, 597–609.

Chongsathidkiet, P., Jackson, C., Koyama, S., Loebel, F., Cui, X., Farber, S.H., Woroniecka, K., Elsamadicy, A.A., Dechant, C.A., Kemeny, H.R., et al. (2018). Sequestration of T-cells in bone marrow in the setting of glioblastoma and other intracranial tumors. Nat. Med. *24*, 1459–1468.

Chu, B.-B., Liao, Y.-C., Qi, W., Xie, C., Du, X., Wang, J., Yang, H., Miao, H.-H., Li, B.-L., and Song, B.-L. (2015). Cholesterol transport through lysosome-peroxisome membrane contacts. Cell *161*, 291–306.

Clarke, K., Smith, K., Gullick, W.J., and Harris, A.L. (2001). Mutant epidermal growth factor receptor enhances induction of vascular endothelial growth factor by hypoxia and insulin-like growth factor-1 via a PI3 kinase dependent pathway. Br. J. Cancer *84*, 1322–1329.

Clement, V., Sanchez, P., de Tribolet, N., Radovanovic, I., and Ruiz i Altaba, A. (2007). HEDGEHOG-GLI1 signaling regulates human glioma growth, cancer stem cell self-renewal, and tumorigenicity. Curr. Biol. CB *17*, 165–172.

Cloughesy, T.F., Mochizuki, A.Y., Orpilla, J.R., Hugo, W., Lee, A.H., Davidson, T.B., Wang, A.C., Ellingson, B.M., Rytlewski, J.A., Sanders, C.M., et al. (2019). Neoadjuvant anti-PD-1 immunotherapy promotes a survival benefit with intratumoral and systemic immune responses in recurrent glioblastoma. Nat. Med. *25*, 477–486.

Cohen, M.H., Shen, Y.L., Keegan, P., and Pazdur, R. (2009). FDA drug approval summary: bevacizumab (Avastin) as treatment of recurrent glioblastoma multiforme. The Oncologist *14*, 1131–1138.

Conus, S., and Simon, H.-U. (2008). Cathepsins: key modulators of cell death and inflammatory responses. Biochem. Pharmacol. *76*, 1374–1382.

Coornaert, B., Baens, M., Heyninck, K., Bekaert, T., Haegman, M., Staal, J., Sun, L., Chen, Z.J., Marynen, P., and Beyaert, R. (2008a). T cell antigen receptor stimulation induces MALT1 paracaspase-mediated cleavage of the NF-kappaB inhibitor A20. Nat. Immunol. *9*, 263–271.

Coornaert, B., Baens, M., Heyninck, K., Bekaert, T., Haegman, M., Staal, J., Sun, L., Chen, Z.J., Marynen, P., and Beyaert, R. (2008b). T cell antigen receptor stimulation induces MALT1 paracaspase–mediated cleavage of the NF-κB inhibitor A20. Nat. Immunol. *9*, 263–271.

Dahms, N.M. (1996). Insulin-like growth factor II/cation-independent mannose 6-phosphate receptor and lysosomal enzyme recognition. Biochem. Soc. Trans. *24*, 136–141.

Darbelli, L., and Richard, S. (2016). Emerging functions of the Quaking RNA-binding proteins and link to human diseases. Wiley Interdiscip. Rev. RNA *7*, 399–412.

De Bonis, P., Anile, C., Pompucci, A., Fiorentino, A., Balducci, M., Chiesa, S., Maira, G., and Mangiola, A. (2012). Safety and efficacy of Gliadel wafers for newly diagnosed and recurrent glioblastoma. Acta Neurochir. (Wien) *154*, 1371–1378.

deCarvalho, A.C., Kim, H., Poisson, L.M., Winn, M.E., Mueller, C., Cherba, D., Koeman, J., Seth, S., Protopopov, A., Felicella, M., et al. (2018). Discordant inheritance of chromosomal and extrachromosomal DNA elements contributes to dynamic disease evolution in glioblastoma. Nat. Genet. *50*, 708–717.

Del Vecchio, C.A., Li, G., and Wong, A.J. (2012). Targeting EGF receptor variant III: tumor-specific peptide vaccination for malignant gliomas. Expert Rev. Vaccines *11*, 133–144.

Delgado, A.C., Ferrón, S.R., Vicente, D., Porlan, E., Perez-Villalba, A., Trujillo, C.M., D'Ocón, P., and Fariñas, I. (2014). Endothelial NT-3 delivered by vasculature and CSF promotes quiescence of subependymal neural stem cells through nitric oxide induction. Neuron *83*, 572–585.

Démoz, M., Castino, R., Dragonetti, A., Raiteri, E., Baccino, F.M., and Isidoro, C. (1999). Transformation by oncogenic ras-p21 alters the processing and subcellular localization of the lysosomal protease cathepsin D. J. Cell. Biochem. *73*, 370–378.

Desjardins, A., Gromeier, M., Herndon, J.E., Beaubier, N., Bolognesi, D.P., Friedman, A.H., Friedman, H.S., McSherry, F., Muscat, A.M., Nair, S., et al. (2018). Recurrent Glioblastoma Treated with Recombinant Poliovirus. N. Engl. J. Med. *379*, 150–161.

Di Malta, C., Siciliano, D., Calcagni, A., Monfregola, J., Punzi, S., Pastore, N., Eastes, A.N., Davis, O., De Cegli, R., Zampelli, A., et al. (2017). Transcriptional activation of RagD GTPase controls mTORC1 and promotes cancer growth. Science *356*, 1188–1192.

Diao, J., Liu, R., Rong, Y., Zhao, M., Zhang, J., Lai, Y., Zhou, Q., Wilz, L.M., Li, J., Vivona, S., et al. (2015). ATG14 promotes membrane tethering and fusion of autophagosomes to endolysosomes. Nature *520*, 563–566.

Dielschneider, R.F., Eisenstat, H., Mi, S., Curtis, J.M., Xiao, W., Johnston, J.B., and Gibson, S.B. (2016). Lysosomotropic agents selectively target chronic lymphocytic leukemia cells due to altered sphingolipid metabolism. Leukemia *30*, 1290–1300.

Dikic, I., and Elazar, Z. (2018). Mechanism and medical implications of mammalian autophagy. Nat. Rev. Mol. Cell Biol. *19*, 349–364.

Ding, X., Chaiteerakij, R., Moser, C.D., Shaleh, H., Boakye, J., Chen, G., Ndzengue, A., Li, Y., Zhou, Y., Huang, S., et al. (2016). Antitumor effect of the novel sphingosine kinase 2 inhibitor ABC294640 is enhanced by inhibition of autophagy and by sorafenib in human cholangiocarcinoma cells. Oncotarget *7*, 20080–20092.

Donatien, P.D., Diment, S.L., Boissy, R.E., and Orlow, S.J. (1996). Melanosomal and lysosomal alterations in murine melanocytes following transfection with the v-rasHa

oncogene. Int. J. Cancer *66*, 557–563.

Dooley, H.C., Razi, M., Polson, H.E.J., Girardin, S.E., Wilson, M.I., and Tooze, S.A. (2014). WIPI2 links LC3 conjugation with PI3P, autophagosome formation, and pathogen clearance by recruiting Atg12-5-16L1. Mol. Cell *55*, 238–252.

Dorrello, N.V., Peschiaroli, A., Guardavaccaro, D., Colburn, N.H., Sherman, N.E., and Pagano, M. (2006). S6K1- and betaTRCP-mediated degradation of PDCD4 promotes protein translation and cell growth. Science *314*, 467–471.

Douanne, T., Gavard, J., and Bidère, N. (2016). The paracaspase MALT1 cleaves the LUBAC subunit HOIL1 during antigen receptor signaling. J. Cell Sci.

Douros, J., and Suffness, M. (1981). New antitumor substances of natural origin. Cancer Treat. Rev. *8*, 63–87.

Dumont, F.J., Melino, M.R., Staruch, M.J., Koprak, S.L., Fischer, P.A., and Sigal, N.H. (1990). The immunosuppressive macrolides FK-506 and rapamycin act as reciprocal antagonists in murine T cells. J. Immunol. Baltim. Md 1950 *144*, 1418–1424.

de Duve, C. (2005). The lysosome turns fifty. Nat. Cell Biol. *7*, 847–849.

de Duve, C., Pressman, B.C., Gianetto, R., Wattiaux, R., and Appelmans, F. (1955). Tissue fractionation studies. 6. Intracellular distribution patterns of enzymes in rat-liver tissue. Biochem. J. *60*, 604–617.

Düvel, K., Yecies, J.L., Menon, S., Raman, P., Lipovsky, A.I., Souza, A.L., Triantafellow, E., Ma, Q., Gorski, R., Cleaver, S., et al. (2010). Activation of a metabolic gene regulatory network downstream of mTOR complex 1. Mol. Cell *39*, 171–183.

Ebner, M., Sinkovics, B., Szczygieł, M., Ribeiro, D.W., and Yudushkin, I. (2017). Localization of mTORC2 activity inside cells. J. Cell Biol. *216*, 343–353.

Ebner, P., Poetsch, I., Deszcz, L., Hoffmann, T., Zuber, J., and Ikeda, F. (2018). The IAP family member BRUCE regulates autophagosome–lysosome fusion. Nat. Commun. *9*, 599.

Egan, D.F., Shackelford, D.B., Mihaylova, M.M., Gelino, S.R., Kohnz, R.A., Mair, W., Vasquez, D.S., Joshi, A., Gwinn, D.M., Taylor, R., et al. (2011). Phosphorylation of ULK1 (hATG1) by AMP-activated protein kinase connects energy sensing to mitophagy. Science *331*, 456–461.

Egan, D.F., Chun, M.G.H., Vamos, M., Zou, H., Rong, J., Miller, C.J., Lou, H.J., Raveendra-Panickar, D., Yang, C.-C., Sheffler, D.J., et al. (2015). Small molecule inhibition of the autophagy kinase ULK1 and identification of ULK1 substrates. Mol. Cell *59*, 285–297.

Eitelhuber, A.C., Vosyka, O., Nagel, D., Bognar, M., Lenze, D., Lammens, K.,

Schlauderer, F., Hlahla, D., Hopfner, K.-P., Lenz, G., et al. (2015). Activity-based probes for detection of active MALT1 paracaspase in immune cells and lymphomas. Chem. Biol. *22*, 129–138.

Ellegaard, A.-M., Dehlendorff, C., Vind, A.C., Anand, A., Cederkvist, L., Petersen, N.H.T., Nylandsted, J., Stenvang, J., Mellemgaard, A., Østerlind, K., et al. (2016). Repurposing Cationic Amphiphilic Antihistamines for Cancer Treatment. EBioMedicine *9*, 130–139.

Elrick, M.J., and Lieberman, A.P. (2013). Autophagic dysfunction in a lysosomal storage disorder due to impaired proteolysis. Autophagy *9*, 234–235.

Elsamadicy, A.A., Babu, R., Kirkpatrick, J.P., and Adamson, D.C. (2015). Radiation-induced malignant gliomas: a current review. World Neurosurg. *83*, 530–542.

Elton, L., Carpentier, I., Staal, J., Driege, Y., Haegman, M., and Beyaert, R. (2016). MALT1 cleaves the E3 ubiquitin ligase HOIL-1 in activated T cells, generating a dominant negative inhibitor of LUBAC-induced NF-κB signaling. FEBS J. *283*, 403–412.

Eng, C.P., Sehgal, S.N., and Vézina, C. (1984). Activity of rapamycin (AY-22,989) against transplanted tumors. J. Antibiot. (Tokyo) *37*, 1231–1237.

Eskelinen, E.-L., Tanaka, Y., and Saftig, P. (2003). At the acidic edge: emerging functions for lysosomal membrane proteins. Trends Cell Biol. *13*, 137–145.

Ezashi, T., Das, P., and Roberts, R.M. (2005). Low O2 tensions and the prevention of differentiation of hES cells. Proc. Natl. Acad. Sci. U. S. A. *102*, 4783–4788.

Fabian, D., Guillermo Prieto Eibl, M. del P., Alnahhas, I., Sebastian, N., Giglio, P., Puduvalli, V., Gonzalez, J., and Palmer, J.D. (2019). Treatment of Glioblastoma (GBM) with the Addition of Tumor-Treating Fields (TTF): A Review. Cancers *11*, 174.

Fan, X., Khaki, L., Zhu, T.S., Soules, M.E., Talsma, C.E., Gul, N., Koh, C., Zhang, J., Li, Y.-M., Maciaczyk, J., et al. (2010). NOTCH pathway blockade depletes CD133-positive glioblastoma cells and inhibits growth of tumor neurospheres and xenografts. Stem Cells Dayt. Ohio *28*, 5–16.

Fehrenbacher, N., Gyrd-Hansen, M., Poulsen, B., Felbor, U., Kallunki, T., Boes, M., Weber, E., Leist, M., and Jäättelä, M. (2004). Sensitization to the lysosomal cell death pathway upon immortalization and transformation. Cancer Res. *64*, 5301–5310.

Fehrenbacher, N., Bastholm, L., Kirkegaard-Sørensen, T., Rafn, B., Bøttzauw, T., Nielsen, C., Weber, E., Shirasawa, S., Kallunki, T., and Jäättelä, M. (2008). Sensitization to the lysosomal cell death pathway by oncogene-induced down-regulation of lysosome-associated membrane proteins 1 and 2. Cancer Res. *68*, 6623–6633.

Feng, Z., Hu, W., De Stanchina, E., Teresky, A.K., Jin, S., Lowe, S., and Levine, A.J.

(2007). The regulation of AMPK β1, TSC2, and PTEN expression by p53: Stress, cell and tissue specificity, and the role of these gene products in modulating the IGF-1-AKT-mTOR pathways. Cancer Res. *67*, 3043–3053.

Ferch, U., Kloo, B., Gewies, A., Pfänder, V., Düwel, M., Peschel, C., Krappmann, D., and Ruland, J. (2009). Inhibition of MALT1 protease activity is selectively toxic for activated B cell-like diffuse large B cell lymphoma cells. J. Exp. Med. *206*, 2313–2320.

Figueroa, J., Phillips, L.M., Shahar, T., Hossain, A., Gumin, J., Kim, H., Bean, A.J., Calin, G.A., Fueyo, J., Walters, E.T., et al. (2017). Exosomes from Glioma-Associated Mesenchymal Stem Cells Increase the Tumorigenicity of Glioma Stem-like Cells via Transfer of miR-1587. Cancer Res. *77*, 5808–5819.

Filipek, P.A., de Araujo, M.E.G., Vogel, G.F., De Smet, C.H., Eberharter, D., Rebsamen, M., Rudashevskaya, E.L., Kremser, L., Yordanov, T., Tschaikner, P., et al. (2017). LAMTOR/Ragulator is a negative regulator of Arl8b- and BORC-dependent late endosomal positioning. J. Cell Biol. *216*, 4199–4215.

Fimia, G.M., Stoykova, A., Romagnoli, A., Giunta, L., Di Bartolomeo, S., Nardacci, R., Corazzari, M., Fuoco, C., Ucar, A., Schwartz, P., et al. (2007). Ambra1 regulates autophagy and development of the nervous system. Nature *447*, 1121–1125.

Fine, B., Hodakoski, C., Koujak, S., Su, T., Saal, L.H., Maurer, M., Hopkins, B., Keniry, M., Sulis, M.L., Mense, S., et al. (2009). Activation of the PI3K pathway in cancer through inhibition of PTEN by exchange factor P-REX2a. Science *325*, 1261–1265.

Firestone, R.A., Pisano, J.M., and Bonney, R.J. (1979). Lysosomotropic agents. 1. Synthesis and cytotoxic action of lysosomotropic detergents. J. Med. Chem. *22*, 1130–1133.

Fonseca, B.D., Zakaria, C., Jia, J.-J., Graber, T.E., Svitkin, Y., Tahmasebi, S., Healy, D., Hoang, H.-D., Jensen, J.M., Diao, I.T., et al. (2015). La-related Protein 1 (LARP1) Represses Terminal Oligopyrimidine (TOP) mRNA Translation Downstream of mTOR Complex 1 (mTORC1). J. Biol. Chem. *290*, 15996–16020.

Fontan, L., Yang, C., Kabaleeswaran, V., Volpon, L., Osborne, M.J., Beltran, E., Garcia, M., Cerchietti, L., Shaknovich, R., Yang, S.N., et al. (2012). MALT1 small molecule inhibitors specifically suppress ABC-DLBCL in vitro and in vivo. Cancer Cell *22*, 812–824.

Forgac, M. (2007). Vacuolar ATPases: rotary proton pumps in physiology and pathophysiology. Nat. Rev. Mol. Cell Biol. *8*, 917–929.

Frias, M.A., Thoreen, C.C., Jaffe, J.D., Schroder, W., Sculley, T., Carr, S.A., and Sabatini, D.M. (2006). mSin1 is necessary for Akt/PKB phosphorylation, and its isoforms define three distinct mTORC2s. Curr. Biol. CB *16*, 1865–1870.

Fueyo, J., Gomez-Manzano, C., Alemany, R., Lee, P.S., McDonnell, T.J., Mitlianga,

P., Shi, Y.-X., Levin, V.A., Yung, W.K.A., and Kyritsis, A.P. (2000). A mutant oncolytic adenovirus targeting the Rb pathway produces anti-glioma effect in vivo. Oncogene *19*, 2–12.

Fuh, B., Sobo, M., Cen, L., Josiah, D., Hutzen, B., Cisek, K., Bhasin, D., Regan, N., Lin, L., Chan, C., et al. (2009). LLL-3 inhibits STAT3 activity, suppresses glioblastoma cell growth and prolongs survival in a mouse glioblastoma model. Br. J. Cancer *100*, 106–112.

Fujioka, Y., Noda, N.N., Nakatogawa, H., Ohsumi, Y., and Inagaki, F. (2010). Dimeric coiled-coil structure of Saccharomyces cerevisiae Atg16 and its functional significance in autophagy. J. Biol. Chem. *285*, 1508–1515.

Gabandé-Rodríguez, E., Boya, P., Labrador, V., Dotti, C.G., and Ledesma, M.D. (2014). High sphingomyelin levels induce lysosomal damage and autophagy dysfunction in Niemann Pick disease type A. Cell Death Differ. *21*, 864–875.

Gabrusiewicz, K., Liu, D., Cortes-Santiago, N., Hossain, M.B., Conrad, C.A., Aldape, K.D., Fuller, G.N., Marini, F.C., Alonso, M.M., Idoate, M.A., et al. (2014). Anti-vascular endothelial growth factor therapy-induced glioma invasion is associated with accumulation of Tie2-expressing monocytes. Oncotarget *5*, 2208–2220.

Galan-Moya, E.M., Le Guelte, A., Lima Fernandes, E., Thirant, C., Dwyer, J., Bidere, N., Couraud, P.-O., Scott, M.G.H., Junier, M.-P., Chneiweiss, H., et al. (2011). Secreted factors from brain endothelial cells maintain glioblastoma stem-like cell expansion through the mTOR pathway. EMBO Rep. *12*, 470–476.

Galan-Moya, E.M., Treps, L., Oliver, L., Chneiweiss, H., Vallette, F.M., Bidère, N., and Gavard, J. (2014). Endothelial Secreted Factors Suppress Mitogen Deprivation-Induced Autophagy and Apoptosis in Glioblastoma Stem-Like Cells. PLOS ONE *9*, e93505.

Galli, R., Binda, E., Orfanelli, U., Cipelletti, B., Gritti, A., Vitis, S.D., Fiocco, R., Foroni, C., Dimeco, F., and Vescovi, A. (2004). Isolation and Characterization of Tumorigenic, Stem-like Neural Precursors from Human Glioblastoma. Cancer Res. *64*, 7011–7021.

Gamp, A.-C., Tanaka, Y., Lüllmann-Rauch, R., Wittke, D., D'Hooge, R., De Deyn, P.P., Moser, T., Maier, H., Hartmann, D., Reiss, K., et al. (2003). LIMP-2/LGP85 deficiency causes ureteric pelvic junction obstruction, deafness and peripheral neuropathy in mice. Hum. Mol. Genet. *12*, 631–646.

Gan, X., Wang, J., Wang, C., Sommer, E., Kozasa, T., Srinivasula, S., Alessi, D., Offermanns, S., Simon, M.I., and Wu, D. (2012). PRR5L degradation promotes mTORC2-mediated PKC-δ phosphorylation and cell migration downstream of Gα12. Nat. Cell Biol. *14*, 686–696.

Ganguly, D., Fan, M., Yang, C.H., Zbytek, B., Finkelstein, D., Roussel, M.F., and Pfeffer, L.M. (2018). The critical role that STAT3 plays in glioma-initiating cells: STAT3 addiction in glioma. Oncotarget *9*, 22095–22112.

Ganley, I.G., Lam, D.H., Wang, J., Ding, X., Chen, S., and Jiang, X. (2009). ULK1·ATG13·FIP200 Complex Mediates mTOR Signaling and Is Essential for Autophagy. J. Biol. Chem. *284*, 12297–12305.

Gao, L., Li, F., Dong, B., Zhang, J., Rao, Y., Cong, Y., Mao, B., and Chen, X. (2010). Inhibition of STAT3 and ErbB2 suppresses tumor growth, enhances radiosensitivity, and induces mitochondria-dependent apoptosis in glioma cells. Int. J. Radiat. Oncol. Biol. Phys. *77*, 1223–1231.

Garami, A., Zwartkruis, F.J.T., Nobukuni, T., Joaquin, M., Roccio, M., Stocker, H., Kozma, S.C., Hafen, E., Bos, J.L., and Thomas, G. (2003). Insulin Activation of Rheb, a Mediator of mTOR/S6K/4E-BP Signaling, Is Inhibited by TSC1 and 2. Mol. Cell *11*, 1457–1466.

García-Martínez, J.M., and Alessi, D.R. (2008). mTOR complex 2 (mTORC2) controls hydrophobic motif phosphorylation and activation of serum- and glucocorticoid-induced protein kinase 1 (SGK1). Biochem. J. *416*, 375–385.

Gary-Bobo, M., Nirdé, P., Jeanjean, A., Morère, A., and Garcia, M. (2007). Mannose 6-phosphate receptor targeting and its applications in human diseases. Curr. Med. Chem. *14*, 2945–2953.

Gaspar, L.E., Fisher, B.J., Macdonald, D.R., LeBer, D.V., Halperin, E.C., Schold, S.C., and Cairncross, J.G. (1992). Supratentorial malignant glioma: patterns of recurrence and implications for external beam local treatment. Int. J. Radiat. Oncol. Biol. Phys. *24*, 55–57.

Gearing, D.P., Thut, C.J., VandeBos, T., Gimpel, S.D., Delaney, P.B., King, J., Price, V., Cosman, D., and Beckmann, M.P. (1991). Leukemia inhibitory factor receptor is structurally related to the IL-6 signal transducer, gp130. EMBO J. *10*, 2839–2848.

Gewies, A., Gorka, O., Bergmann, H., Pechloff, K., Petermann, F., Jeltsch, K.M., Rudelius, M., Kriegsmann, M., Weichert, W., Horsch, M., et al. (2014). Uncoupling Malt1 threshold function from paracaspase activity results in destructive autoimmune inflammation. Cell Rep. *9*, 1292–1305.

Ghinda, C.D., and Duffau, H. (2017). Network Plasticity and Intraoperative Mapping for Personalized Multimodal Management of Diffuse Low-Grade Gliomas. Front. Surg. *4*.

Gilbert, M.R., Wang, M., Aldape, K.D., Stupp, R., Hegi, M.E., Jaeckle, K.A., Armstrong, T.S., Wefel, J.S., Won, M., Blumenthal, D.T., et al. (2013). Dose-dense temozolomide for newly diagnosed glioblastoma: a randomized phase III clinical trial. J. Clin. Oncol. Off. J. Am. Soc. Clin. Oncol. *31*, 4085–4091.

Gilbert, M.R., Dignam, J.J., Armstrong, T.S., Wefel, J.S., Blumenthal, D.T., Vogelbaum, M.A., Colman, H., Chakravarti, A., Pugh, S., Won, M., et al. (2014). A randomized trial of bevacizumab for newly diagnosed glioblastoma. N. Engl. J. Med. *370*, 699–708.

Gilbertson, R.J., and Rich, J.N. (2007). Making a tumour's bed: glioblastoma stem cells and the vascular niche. Nat. Rev. Cancer *7*, 733–736.

Gill, B.J., Pisapia, D.J., Malone, H.R., Goldstein, H., Lei, L., Sonabend, A., Yun, J., Samanamud, J., Sims, J.S., Banu, M., et al. (2014). MRI-localized biopsies reveal subtype-specific differences in molecular and cellular composition at the margins of glioblastoma. Proc. Natl. Acad. Sci. U. S. A. *111*, 12550–12555.

Gingras, A.C., Kennedy, S.G., O'Leary, M.A., Sonenberg, N., and Hay, N. (1998). 4E-BP1, a repressor of mRNA translation, is phosphorylated and inactivated by the Akt(PKB) signaling pathway. Genes Dev. *12*, 502–513.

Gini, B., Zanca, C., Guo, D., Matsutani, T., Masui, K., Ikegami, S., Yang, H., Nathanson, D., Villa, G.R., Shackelford, D., et al. (2013). The mTOR Kinase Inhibitors, CC214-1 and CC214-2, Preferentially Block the Growth of EGFRvIII-Activated Glioblastomas. Clin. Cancer Res. *19*, 5722–5732.

Giusti, I., Delle Monache, S., Di Francesco, M., Sanità, P., D'Ascenzo, S., Gravina, G.L., Festuccia, C., and Dolo, V. (2016). From glioblastoma to endothelial cells through extracellular vesicles: messages for angiogenesis. Tumour Biol. J. Int. Soc. Oncodevelopmental Biol. Med. *37*, 12743–12753.

Gómez Ravetti, M., Rosso, O.A., Berretta, R., and Moscato, P. (2010). Uncovering Molecular Biomarkers That Correlate Cognitive Decline with the Changes of Hippocampus' Gene Expression Profiles in Alzheimer's Disease. PLoS ONE *5*, e10153.

Gonzalez, A., Valeiras, M., Sidransky, E., and Tayebi, N. (2014). Lysosomal integral membrane protein-2: A new player in lysosome-related pathology. Mol. Genet. Metab. *111*, 84–91.

Grabiner, B.C., Nardi, V., Birsoy, K., Possemato, R., Shen, K., Sinha, S., Jordan, A., Beck, A.H., and Sabatini, D.M. (2014). A Diverse Array of Cancer-Associated MTOR Mutations Are Hyperactivating and Can Predict Rapamycin Sensitivity. Cancer Discov. *4*, 554–563.

Granato, M., Lacconi, V., Peddis, M., Lotti, L.V., Renzo, L.D., Gonnella, R., Santarelli, R., Trivedi, P., Frati, L., D'Orazi, G., et al. (2013). HSP70 inhibition by 2-phenylethynesulfonamide induces lysosomal cathepsin D release and immunogenic cell death in primary effusion lymphoma. Cell Death Dis. *4*, e730.

Griveau, A., Seano, G., Shelton, S.J., Kupp, R., Jahangiri, A., Obernier, K., Krishnan, S., Lindberg, O.R., Yuen, T.J., Tien, A.-C., et al. (2018). A Glial Signature and Wnt7 Signaling Regulate Glioma-Vascular Interactions and Tumor Microenvironment. Cancer Cell *33*, 874-889.e7.

Groth-Pedersen, L., Ostenfeld, M.S., Høyer-Hansen, M., Nylandsted, J., and Jäättelä, M. (2007). Vincristine Induces Dramatic Lysosomal Changes and Sensitizes Cancer Cells to Lysosome-Destabilizing Siramesine. Cancer Res. *67*, 2217–2225.

Groth-Pedersen, L., Aits, S., Corcelle-Termeau, E., Petersen, N.H.T., Nylandsted, J., and Jäättelä, M. (2012). Identification of Cytoskeleton-Associated Proteins Essential for Lysosomal Stability and Survival of Human Cancer Cells. PLOS ONE *7*, e45381.

Gu, X., Orozco, J.M., Saxton, R.A., Condon, K.J., Liu, G.Y., Krawczyk, P.A., Scaria, S.M., Harper, J.W., Gygi, S.P., and Sabatini, D.M. (2017). SAMTOR is an S-adenosylmethionine sensor for the mTORC1 pathway. Science *358*, 813–818.

Guertin, D.A., Stevens, D.M., Thoreen, C.C., Burds, A.A., Kalaany, N.Y., Moffat, J., Brown, M., Fitzgerald, K.J., and Sabatini, D.M. (2006). Ablation in mice of the mTORC components raptor, rictor, or mLST8 reveals that mTORC2 is required for signaling to Akt-FOXO and PKCalpha, but not S6K1. Dev. Cell *11*, 859–871.

Guertin, D.A., Stevens, D.M., Saitoh, M., Kinkel, S., Crosby, K., Sheen, J.-H., Mullholland, D.J., Magnuson, M.A., Wu, H., and Sabatini, D.M. (2009). mTOR complex 2 is required for the development of prostate cancer induced by Pten loss in mice. Cancer Cell *15*, 148–159.

Gulbins, E., and Kolesnick, R.N. (2013). It takes a CAD to kill a tumor cell with a LMP. Cancer Cell *24*, 279–281.

Gwinn, D.M., Shackelford, D.B., Egan, D.F., Mihaylova, M.M., Mery, A., Vasquez, D.S., Turk, B.E., and Shaw, R.J. (2008). AMPK Phosphorylation of Raptor Mediates a Metabolic Checkpoint. Mol. Cell *30*, 214–226.

Gyrd-Hansen, M., Nylandsted, J., and Jäättelä, M. (2004). Heat shock protein 70 promotes cancer cell viability by safeguarding lysosomal integrity. Cell Cycle Georget. Tex *3*, 1484–1485.

Hailfinger, S., Lenz, G., Ngo, V., Posvitz-Fejfar, A., Rebeaud, F., Guzzardi, M., Penas, E.-M.M., Dierlamm, J., Chan, W.C., Staudt, L.M., et al. (2009). Essential role of MALT1 protease activity in activated B cell-like diffuse large B-cell lymphoma. Proc. Natl. Acad. Sci. U. S. A. *106*, 19946–19951.

Hailfinger, S., Nogai, H., Pelzer, C., Jaworski, M., Cabalzar, K., Charton, J.-E., Guzzardi, M., Décaillet, C., Grau, M., Dörken, B., et al. (2011). Malt1-dependent RelB cleavage promotes canonical NF-kappaB activation in lymphocytes and lymphoma cell lines. Proc. Natl. Acad. Sci. U. S. A. *108*, 14596–14601.

Hait, W.N., Gesmonde, J.F., Murren, J.R., Jin-Ming, Y., Hong-Xing, C., and Reiss, M. (1993). Terfenadine (seldane®): A new drug for restoring sensitivity to multidrug resistant cancer cells. Biochem. Pharmacol. *45*, 401–406.

Halliday, J., Helmy, K., Pattwell, S.S., Pitter, K.L., LaPlant, Q., Ozawa, T., and Holland, E.C. (2014). In vivo radiation response of proneural glioma characterized by protective p53 transcriptional program and proneural-mesenchymal shift. Proc. Natl. Acad. Sci. U. S. A. *111*, 5248–5253.

Hamanaka, R.B., and Chandel, N.S. (2009). Mitochondrial reactive oxygen species regulate hypoxic signaling. Curr. Opin. Cell Biol. *21*, 894–899.

Hamasaki, M., Furuta, N., Matsuda, A., Nezu, A., Yamamoto, A., Fujita, N., Oomori, H., Noda, T., Haraguchi, T., Hiraoka, Y., et al. (2013). Autophagosomes form at ER-mitochondria contact sites. Nature *495*, 389–393.

Hamilton, K.S., Phong, B., Corey, C., Cheng, J., Gorentla, B., Zhong, X., Shiva, S., and Kane, L.P. (2014). T cell receptor-dependent activation of mTOR signaling in T cells is mediated by Carma1 and MALT1, but not Bcl10. Sci. Signal. *7*, ra55.

Han, S.J., Englot, D.J., Birk, H., Molinaro, A.M., Chang, S.M., Clarke, J.L., Prados, M.D., Taylor, J.W., Berger, M.S., and Butowski, N.A. (2015a). Impact of Timing of Concurrent Chemoradiation for Newly Diagnosed Glioblastoma: A Critical Review of Current Evidence. Neurosurgery *62 Suppl 1*, 160–165.

Han, S.J., Rutledge, W.C., Molinaro, A.M., Chang, S.M., Clarke, J.L., Prados, M.D., Taylor, J.W., Berger, M.S., and Butowski, N.A. (2015b). The Effect of Timing of Concurrent Chemoradiation in Patients With Newly Diagnosed Glioblastoma. Neurosurgery *77*, 248–253; discussion 253.

Hanif, F., Muzaffar, K., Perveen, K., Malhi, S.M., and Simjee, S.U. (2017). Glioblastoma Multiforme: A Review of its Epidemiology and Pathogenesis through Clinical Presentation and Treatment. Asian Pac. J. Cancer Prev. APJCP *18*, 3–9.

Hara, K., Maruki, Y., Long, X., Yoshino, K., Oshiro, N., Hidayat, S., Tokunaga, C., Avruch, J., and Yonezawa, K. (2002). Raptor, a binding partner of target of rapamycin (TOR), mediates TOR action. Cell *110*, 177–189.

Harford-Wright, E., Andre-Gregoire, G., Jacobs, K.A., Treps, L., Le Gonidec, S., Leclair, H.M., Gonzalez-Diest, S., Roux, Q., Guillonneau, F., Loussouarn, D., et al. (2017). Pharmacological targeting of apelin impairs glioblastoma growth. Brain J. Neurol. *140*, 2939–2954.

Harrabi, S.B., Bougatf, N., Mohr, A., Haberer, T., Herfarth, K., Combs, S.E., Debus, J., and Adeberg, S. (2016). Dosimetric advantages of proton therapy over conventional radiotherapy with photons in young patients and adults with low-grade glioma. Strahlenther. Onkol. *192*, 759–769.

Harrington, L.S., Findlay, G.M., Gray, A., Tolkacheva, T., Wigfield, S., Rebholz, H., Barnett, J., Leslie, N.R., Cheng, S., Shepherd, P.R., et al. (2004). The TSC1-2 tumor suppressor controls insulin-PI3K signaling via regulation of IRS proteins. J. Cell Biol. *166*, 213–223.

Harter, C., and Mellman, I. (1992). Transport of the lysosomal membrane glycoprotein lgp120 (lgp-A) to lysosomes does not require appearance on the plasma membrane. J. Cell Biol. *117*, 311–325.

Hay, N., and Sonenberg, N. (2004). Upstream and downstream of mTOR. Genes Dev. *18*, 1926–1945.

Heitman, J., Movva, N.R., and Hall, M.N. (1991). Targets for cell cycle arrest by the immunosuppressant rapamycin in yeast. Science *253*, 905–909.

Hemmati, H.D., Nakano, I., Lazareff, J.A., Masterman-Smith, M., Geschwind, D.H., Bronner-Fraser, M., and Kornblum, H.I. (2003). Cancerous stem cells can arise from pediatric brain tumors. Proc. Natl. Acad. Sci. U. S. A. *100*, 15178–15183.

Hentges, K.E., Sirry, B., Gingeras, A.-C., Sarbassov, D., Sonenberg, N., Sabatini, D., and Peterson, A.S. (2001). FRAP/mTOR is required for proliferation and patterning during embryonic development in the mouse. Proc. Natl. Acad. Sci. *98*, 13796–13801.

Heuser, J. (1989). Changes in lysosome shape and distribution correlated with changes in cytoplasmic pH. J. Cell Biol. *108*, 855–864.

Hirrlinger, J., and Dringen, R. (2010). The cytosolic redox state of astrocytes: Maintenance, regulation and functional implications for metabolite trafficking. Brain Res. Rev. *63*, 177–188.

Höglinger, D., Burgoyne, T., Sanchez-Heras, E., Hartwig, P., Colaco, A., Newton, J., Futter, C.E., Spiegel, S., Platt, F.M., and Eden, E.R. (2019). NPC1 regulates ER contacts with endocytic organelles to mediate cholesterol egress. Nat. Commun. *10*, 1–14.

Holland, E.C., Celestino, J., Dai, C., Schaefer, L., Sawaya, R.E., and Fuller, G.N. (2000). Combined activation of Ras and Akt in neural progenitors induces glioblastoma formation in mice. Nat. Genet. *25*, 55–57.

Holz, M.K., Ballif, B.A., Gygi, S.P., and Blenis, J. (2005). mTOR and S6K1 mediate assembly of the translation preinitiation complex through dynamic protein interchange and ordered phosphorylation events. Cell *123*, 569–580.

Hosokawa, N., Hara, T., Kaizuka, T., Kishi, C., Takamura, A., Miura, Y., Iemura, S., Natsume, T., Takehana, K., Yamada, N., et al. (2009). Nutrient-dependent mTORC1 Association with the ULK1–Atg13–FIP200 Complex Required for Autophagy. Mol. Biol. Cell *20*, 1981–1991.

Hossain, A., Gumin, J., Gao, F., Figueroa, J., Shinojima, N., Takezaki, T., Priebe, W., Villarreal, D., Kang, S.-G., Joyce, C., et al. (2015). Mesenchymal Stem Cells Isolated from Human Gliomas Increase Proliferation and Maintain Stemness of Glioma Stem Cells Through the IL-6/gp130/STAT3 pathway. Stem Cells Dayt. Ohio *33*, 2400–2415.

Hsu, P.P., Kang, S.A., Rameseder, J., Zhang, Y., Ottina, K.A., Lim, D., Peterson, T.R., Choi, Y., Gray, N.S., Yaffe, M.B., et al. (2011). The mTOR-Regulated Phosphoproteome Reveals a Mechanism of mTORC1-Mediated Inhibition of Growth Factor Signaling. Science *332*, 1317–1322.

Hubert, C.G., Rivera, M., Spangler, L.C., Wu, Q., Mack, S.C., Prager, B.C., Couce, M., McLendon, R.E., Sloan, A.E., and Rich, J.N. (2016). A Three-Dimensional Organoid Culture System Derived from Human Glioblastomas Recapitulates the Hypoxic Gradients and Cancer Stem Cell Heterogeneity of Tumors Found In Vivo. Cancer Res. *76*, 2465–2477.

Hung, Y.-H., Chen, L.M.-W., Yang, J.-Y., and Yang, W.Y. (2013). Spatiotemporally controlled induction of autophagy-mediated lysosome turnover. Nat. Commun. *4*, 2111.

Huynh, C., Roth, D., Ward, D.M., Kaplan, J., and Andrews, N.W. (2004). Defective lysosomal exocytosis and plasma membrane repair in Chediak-Higashi/beige cells. Proc. Natl. Acad. Sci. U. S. A. *101*, 16795–16800.

Idbaih, A., Canney, M., Belin, L., Desseaux, C., Vignot, A., Bouchoux, G., Asquier, N., Law-Ye, B., Leclercq, D., Bissery, A., et al. (2019). Safety and Feasibility of Repeated and Transient Blood-Brain Barrier Disruption by Pulsed Ultrasound in Patients with Recurrent Glioblastoma. Clin. Cancer Res. Off. J. Am. Assoc. Cancer Res. *25*, 3793–3801.

Ikeda, Y., Imai, Y., Kumagai, H., Nosaka, T., Morikawa, Y., Hisaoka, T., Manabe, I., Maemura, K., Nakaoka, T., Imamura, T., et al. (2004). Vasorin, a transforming growth factor beta-binding protein expressed in vascular smooth muscle cells, modulates the arterial response to injury in vivo. Proc. Natl. Acad. Sci. U. S. A. *101*, 10732–10737.

Inoki, K., Li, Y., Zhu, T., Wu, J., and Guan, K.-L. (2002). TSC2 is phosphorylated and inhibited by Akt and suppresses mTOR signalling. Nat. Cell Biol. *4*, 648–657.

Inoki, K., Li, Y., Xu, T., and Guan, K.-L. (2003a). Rheb GTPase is a direct target of TSC2 GAP activity and regulates mTOR signaling. Genes Dev. *17*, 1829–1834.

Inoki, K., Zhu, T., and Guan, K.-L. (2003b). TSC2 Mediates Cellular Energy Response to Control Cell Growth and Survival. Cell *115*, 577–590.

Inoki, K., Ouyang, H., Zhu, T., Lindvall, C., Wang, Y., Zhang, X., Yang, Q., Bennett, C., Harada, Y., Stankunas, K., et al. (2006). TSC2 Integrates Wnt and Energy Signals via a Coordinated Phosphorylation by AMPK and GSK3 to Regulate Cell Growth. Cell *126*, 955–968.

Inpanathan, S., and Botelho, R.J. (2019). The Lysosome Signaling Platform: Adapting With the Times. Front. Cell Dev. Biol. *7*.

Itakura, E., Kishi-Itakura, C., and Mizushima, N. (2012). The hairpin-type tail-anchored SNARE syntaxin 17 targets to autophagosomes for fusion with endosomes/lysosomes. Cell *151*, 1256–1269.

Ito, H., Aoki, H., Kühnel, F., Kondo, Y., Kubicka, S., Wirth, T., Iwado, E., Iwamaru, A., Fujiwara, K., Hess, K.R., et al. (2006). Autophagic Cell Death of Malignant Glioma Cells Induced by a Conditionally Replicating Adenovirus. JNCI J. Natl. Cancer Inst. *98*, 625–636.

Iwasaki, H., Takeuchi, O., Teraguchi, S., Matsushita, K., Uehata, T., Kuniyoshi, K., Satoh, T., Saitoh, T., Matsushita, M., Standley, D.M., et al. (2011). The IκB kinase complex regulates the stability of cytokine-encoding mRNA induced by TLR-IL-1R by controlling degradation of regnase-1. Nat. Immunol. *12*, 1167–1175.

Jacinto, E., Loewith, R., Schmidt, A., Lin, S., Rüegg, M.A., Hall, A., and Hall, M.N. (2004). Mammalian TOR complex 2 controls the actin cytoskeleton and is rapamycin insensitive. Nat. Cell Biol. *6*, 1122–1128.

Jacinto, E., Facchinetti, V., Liu, D., Soto, N., Wei, S., Jung, S.Y., Huang, Q., Qin, J., and Su, B. (2006). SIN1/MIP1 maintains rictor-mTOR complex integrity and regulates Akt phosphorylation and substrate specificity. Cell *127*, 125–137.

Jaffrézou, J.-P., Chen, G., Durán, G.E., Muller, C., Bordier, C., Laurent, G., Sikic, B.I., and Levade, T. (1995). Inhibition of lysosomal acid sphingomyelinase by agents which reverse multidrug resistance. Biochim. Biophys. Acta BBA - Mol. Cell Res. *1266*, 1–8.

Jaiswal, J.K., Andrews, N.W., and Simon, S.M. (2002). Membrane proximal lysosomes are the major vesicles responsible for calcium-dependent exocytosis in nonsecretory cells. J. Cell Biol. *159*, 625–635.

Janvier, K., and Bonifacino, J.S. (2005). Role of the Endocytic Machinery in the Sorting of Lysosome-associated Membrane Proteins. Mol. Biol. Cell *16*, 4231–4242.

Jaworski, M., Marsland, B.J., Gehrig, J., Held, W., Favre, S., Luther, S.A., Perroud, M., Golshayan, D., Gaide, O., and Thome, M. (2014). Malt1 protease inactivation efficiently dampens immune responses but causes spontaneous autoimmunity. EMBO J. *33*, 2765–2781.

Jeltsch, K.M., Hu, D., Brenner, S., Zöller, J., Heinz, G.A., Nagel, D., Vogel, K.U., Rehage, N., Warth, S.C., Edelmann, S.L., et al. (2014). Cleavage of roquin and regnase-1 by the paracaspase MALT1 releases their cooperatively repressed targets to promote T(H)17 differentiation. Nat. Immunol. *15*, 1079–1089.

Jespersen, S.N., and Østergaard, L. (2012). The roles of cerebral blood flow, capillary transit time heterogeneity, and oxygen tension in brain oxygenation and metabolism. J. Cereb. Blood Flow Metab. Off. J. Int. Soc. Cereb. Blood Flow Metab. *32*, 264–277.

Jewell, J.L., Kim, Y.C., Russell, R.C., Yu, F.-X., Park, H.W., Plouffe, S.W., Tagliabracci, V.S., and Guan, K.-L. (2015). Differential regulation of mTORC1 by leucine and glutamine. Science *347*, 194–198.

Jhaveri, J., Cheng, E., Tian, S., Buchwald, Z., Chowdhary, M., Liu, Y., Gillespie, T.W., Olson, J.J., Diaz, A.Z., Voloschin, A., et al. (2018). Proton vs. Photon Radiation Therapy for Primary Gliomas: An Analysis of the National Cancer Data Base. Front. Oncol. *8*.

Jin, X., Kim, L.J.Y., Wu, Q., Wallace, L.C., Prager, B.C., Sanvoranart, T., Gimple, R.C., Wang, X., Mack, S.C., Miller, T.E., et al. (2017). Targeting glioma stem cells through combined BMI1 and EZH2 inhibition. Nat. Med. *23*, 1352–1361.

Joachim, J., Jefferies, H.B.J., Razi, M., Frith, D., Snijders, A.P., Chakravarty, P., Judith, D., and Tooze, S.A. (2015). Activation of ULK Kinase and Autophagy by

GABARAP Trafficking from the Centrosome Is Regulated by WAC and GM130. Mol. Cell *60*, 899–913.

Joyce, J.A., and Hanahan, D. (2004). Multiple Roles for Cysteine Cathepsins in Cancer. Cell Cycle *3*, 1516–1519.

Jung, C.H., Jun, C.B., Ro, S.-H., Kim, Y.-M., Otto, N.M., Cao, J., Kundu, M., and Kim, D.-H. (2009). ULK-Atg13-FIP200 Complexes Mediate mTOR Signaling to the Autophagy Machinery. Mol. Biol. Cell *20*, 1992–2003.

Jung, J., Genau, H.M., and Behrends, C. (2015). Amino Acid-Dependent mTORC1 Regulation by the Lysosomal Membrane Protein SLC38A9. Mol. Cell. Biol. *35*, 2479–2494.

Kågedal, K., Zhao, M., Svensson, I., and Brunk, U.T. (2001). Sphingosine-induced apoptosis is dependent on lysosomal proteases. Biochem. J. *359*, 335–343.

Kakee, A., Terasaki, T., and Sugiyama, Y. (1996). Brain efflux index as a novel method of analyzing efflux transport at the blood-brain barrier. J. Pharmacol. Exp. Ther. *277*, 1550–1559.

Kalender, A., Selvaraj, A., Kim, S.Y., Gulati, P., Brûlé, S., Viollet, B., Kemp, B.E., Bardeesy, N., Dennis, P., Schlager, J.J., et al. (2010). Metformin, Independent of AMPK, Inhibits mTORC1 in a Rag GTPase-Dependent Manner. Cell Metab. *11*, 390–401.

Karanasios, E., Stapleton, E., Manifava, M., Kaizuka, T., Mizushima, N., Walker, S.A., and Ktistakis, N.T. (2013). Dynamic association of the ULK1 complex with omegasomes during autophagy induction. J. Cell Sci. *126*, 5224–5238.

Karanasios, E., Walker, S.A., Okkenhaug, H., Manifava, M., Hummel, E., Zimmermann, H., Ahmed, Q., Domart, M.-C., Collinson, L., and Ktistakis, N.T. (2016). Autophagy initiation by ULK complex assembly on ER tubulovesicular regions marked by ATG9 vesicles. Nat. Commun. *7*, 1–17.

Karlsson, K., and Carlsson, S.R. (1998). Sorting of lysosomal membrane glycoproteins lamp-1 and lamp-2 into vesicles distinct from mannose 6-phosphate receptor/gamma-adaptin vesicles at the trans-Golgi network. J. Biol. Chem. *273*, 18966–18973.

Kassai, H., Sugaya, Y., Noda, S., Nakao, K., Maeda, T., Kano, M., and Aiba, A. (2014). Selective Activation of mTORC1 Signaling Recapitulates Microcephaly, Tuberous Sclerosis, and Neurodegenerative Diseases. Cell Rep. *7*, 1626–1639.

Kidoya, H., Ueno, M., Yamada, Y., Mochizuki, N., Nakata, M., Yano, T., Fujii, R., and Takakura, N. (2008). Spatial and temporal role of the apelin/APJ system in the caliber size regulation of blood vessels during angiogenesis. EMBO J. *27*, 522–534.

Kim, D.-H., Sarbassov, D.D., Ali, S.M., King, J.E., Latek, R.R., Erdjument-Bromage, H., Tempst, P., and Sabatini, D.M. (2002). mTOR interacts with raptor to form a

nutrient-sensitive complex that signals to the cell growth machinery. Cell *110*, 163–175.

Kim, D.-H., Sarbassov, D.D., Ali, S.M., Latek, R.R., Guntur, K.V.P., Erdjument-Bromage, H., Tempst, P., and Sabatini, D.M. (2003). GbetaL, a positive regulator of the rapamycin-sensitive pathway required for the nutrient-sensitive interaction between raptor and mTOR. Mol. Cell *11*, 895–904.

Kim, E., Goraksha-Hicks, P., Li, L., Neufeld, T.P., and Guan, K.-L. (2008). Regulation of TORC1 by Rag GTPases in nutrient response. Nat. Cell Biol. *10*, 935–945.

Kim, J., Kundu, M., Viollet, B., and Guan, K.-L. (2011). AMPK and mTOR regulate autophagy through direct phosphorylation of Ulk1. Nat. Cell Biol. *13*, 132–141.

Kim, J.E., Patel, M., Ruzevick, J., Jackson, C.M., and Lim, M. (2014). STAT3 Activation in Glioblastoma: Biochemical and Therapeutic Implications. Cancers *6*, 376–395.

Kim, Y.-M., Jung, C.H., Seo, M., Kim, E.K., Park, J.-M., Bae, S.S., and Kim, D.-H. (2015). mTORC1 Phosphorylates UVRAG to Negatively Regulate Autophagosome and Endosome Maturation. Mol. Cell *57*, 207–218.

Kirchhausen, T., Owen, D., and Harrison, S.C. (2014). Molecular structure, function, and dynamics of clathrin-mediated membrane traffic. Cold Spring Harb. Perspect. Biol. *6*, a016725.

Kirkegaard, T., Roth, A.G., Petersen, N.H.T., Mahalka, A.K., Olsen, O.D., Moilanen, I., Zylicz, A., Knudsen, J., Sandhoff, K., Arenz, C., et al. (2010). Hsp70 stabilizes lysosomes and reverts Niemann-Pick disease-associated lysosomal pathology. Nature *463*, 549–553.

Kirkpatrick, J.P., Laack, N.N., Shih, H.A., and Gondi, V. (2017). Management of GBM: a problem of local recurrence. J. Neurooncol. *134*, 487–493.

Kirson, E.D., Gurvich, Z., Schneiderman, R., Dekel, E., Itzhaki, A., Wasserman, Y., Schatzberger, R., and Palti, Y. (2004). Disruption of Cancer Cell Replication by Alternating Electric Fields. Cancer Res. *64*, 3288–3295.

Klein, T., Fung, S.-Y., Renner, F., Blank, M.A., Dufour, A., Kang, S., Bolger-Munro, M., Scurll, J.M., Priatel, J.J., Schweigler, P., et al. (2015). The paracaspase MALT1 cleaves HOIL1 reducing linear ubiquitination by LUBAC to dampen lymphocyte NF-κB signalling. Nat. Commun. *6*, 8777.

Koehler, J.W., Miller, A.D., Miller, C.R., Porter, B., Aldape, K., Beck, J., Brat, D., Cornax, I., Corps, K., Frank, C., et al. (2018). A Revised Diagnostic Classification of Canine Glioma: Towards Validation of the Canine Glioma Patient as a Naturally Occurring Preclinical Model for Human Glioma. J. Neuropathol. Exp. Neurol. *77*, 1039–1054.

Kohsaka, S., Wang, L., Yachi, K., Mahabir, R., Narita, T., Itoh, T., Tanino, M., Kimura, T., Nishihara, H., and Tanaka, S. (2012). STAT3 inhibition overcomes temozolomide resistance in glioblastoma by downregulating MGMT expression. Mol. Cancer Ther. *11*, 1289–1299.

Konczalla, L., Perez, D.R., Wenzel, N., Wolters-Eisfeld, G., Klemp, C., Lüddeke, J., Wolski, A., Landschulze, D., Meier, C., Buchholz, A., et al. Biperiden and mepazine effectively inhibit MALT1 activity and tumor growth in pancreatic cancer. Int. J. Cancer *0*.

Kornfeld, S. (1992). Structure and function of the mannose 6-phosphate/insulinlike growth factor II receptors. Annu. Rev. Biochem. *61*, 307–330.

Kornfeld, S., and Mellman, I. (1989). The biogenesis of lysosomes. Annu. Rev. Cell Biol. *5*, 483–525.

Korolchuk, V.I., Saiki, S., Lichtenberg, M., Siddiqi, F.H., Roberts, E.A., Imarisio, S., Jahreiss, L., Sarkar, S., Futter, M., Menzies, F.M., et al. (2011). Lysosomal positioning coordinates cellular nutrient responses. Nat. Cell Biol. *13*, 453–460.

Korth, C., May, B.C., Cohen, F.E., and Prusiner, S.B. (2001). Acridine and phenothiazine derivatives as pharmacotherapeutics for prion disease. Proc. Natl. Acad. Sci. U. S. A. *98*, 9836–9841.

Kreuzaler, P.A., Staniszewska, A.D., Li, W., Omidvar, N., Kedjouar, B., Turkson, J., Poli, V., Flavell, R.A., Clarkson, R.W.E., and Watson, C.J. (2011). Stat3 controls lysosomal-mediated cell death in vivo. Nat. Cell Biol. *13*, 303–309.

Krusche, B., Ottone, C., Clements, M.P., Johnstone, E.R., Goetsch, K., Lieven, H., Mota, S.G., Singh, P., Khadayate, S., Ashraf, A., et al. (2016). EphrinB2 drives perivascular invasion and proliferation of glioblastoma stem-like cells. ELife *5*, e14845.

Kuma, A., Mizushima, N., Ishihara, N., and Ohsumi, Y. (2002). Formation of the approximately 350-kDa Apg12-Apg5.Apg16 multimeric complex, mediated by Apg16 oligomerization, is essential for autophagy in yeast. J. Biol. Chem. *277*, 18619–18625.

Kunz, J., Henriquez, R., Schneider, U., Deuter-Reinhard, M., Movva, N.R., and Hall, M.N. (1993). Target of rapamycin in yeast, TOR2, is an essential phosphatidylinositol kinase homolog required for G1 progression. Cell *73*, 585–596.

Kuronita, T., Hatano, T., Furuyama, A., Hirota, Y., Masuyama, N., Saftig, P., Himeno, M., Fujita, H., and Tanaka, Y. (2005). The NH2-Terminal Transmembrane and Lumenal Domains of LGP85 are Needed for the Formation of Enlarged Endosomes/Lysosomes. Traffic *6*, 895–906.

Kurz, T., Terman, A., Gustafsson, B., and Brunk, U.T. (2008a). Lysosomes and oxidative stress in aging and apoptosis. Biochim. Biophys. Acta *1780*, 1291–1303.

Kurz, T., Terman, A., Gustafsson, B., and Brunk, U.T. (2008b). Lysosomes in iron metabolism, ageing and apoptosis. Histochem. Cell Biol. *129*, 389–406.

Kwon, C.-H., Zhao, D., Chen, J., Alcantara, S., Li, Y., Burns, D.K., Mason, R.P., Lee, E.Y.-H.P., Wu, H., and Parada, L.F. (2008). Pten haploinsufficiency accelerates formation of high-grade astrocytomas. Cancer Res. *68*, 3286–3294.

Lahr, R.M., Fonseca, B.D., Ciotti, G.E., Al-Ashtal, H.A., Jia, J.-J., Niklaus, M.R., Blagden, S.P., Alain, T., and Berman, A.J. (2017). La-related protein 1 (LARP1) binds the mRNA cap, blocking eIF4F assembly on TOP mRNAs. ELife *6*.

Lal, S., La Du, J., Tanguay, R.L., and Greenwood, J.A. (2012). Calpain 2 is required for the invasion of glioblastoma cells in the zebrafish brain microenvironment. J. Neurosci. Res. *90*, 769–781.

Lancaster, M.A., Renner, M., Martin, C.-A., Wenzel, D., Bicknell, L.S., Hurles, M.E., Homfray, T., Penninger, J.M., Jackson, A.P., and Knoblich, J.A. (2013). Cerebral organoids model human brain development and microcephaly. Nature *501*, 373–379.

Lapidot, T., Sirard, C., Vormoor, J., Murdoch, B., Hoang, T., Caceres-Cortes, J., Minden, M., Paterson, B., Caligiuri, M.A., and Dick, J.E. (1994). A cell initiating human acute myeloid leukaemia after transplantation into SCID mice. Nature *367*, 645–648.

Lathia, J.D., Mack, S.C., Mulkearns-Hubert, E.E., Valentim, C.L.L., and Rich, J.N. (2015). Cancer stem cells in glioblastoma. Genes Dev. *29*, 1203–1217.

Lawrence, R.E., and Zoncu, R. (2019). The lysosome as a cellular centre for signalling, metabolism and quality control. Nat. Cell Biol. *21*, 133–142.

Lawrence, M.S., Stojanov, P., Mermel, C.H., Robinson, J.T., Garraway, L.A., Golub, T.R., Meyerson, M., Gabriel, S.B., Lander, E.S., and Getz, G. (2014). Discovery and saturation analysis of cancer genes across 21 tumour types. Nature *505*, 495–501.

Lazarus, M.B., Novotny, C.J., and Shokat, K.M. (2015). Structure of the human autophagy initiating kinase ULK1 in complex with potent inhibitors. ACS Chem. Biol. *10*, 257–261.

Le Joncour, V., Filppu, P., Hyvönen, M., Holopainen, M., Turunen, S.P., Sihto, H., Burghardt, I., Joensuu, H., Tynninen, O., Jääskeläinen, J., et al. (2019). Vulnerability of invasive glioblastoma cells to lysosomal membrane destabilization. EMBO Mol. Med. *11*.

Lee, D.-F., Kuo, H.-P., Chen, C.-T., Hsu, J.-M., Chou, C.-K., Wei, Y., Sun, H.-L., Li, L.-Y., Ping, B., Huang, W.-C., et al. (2007). IKKβ Suppression of TSC1 Links Inflammation and Tumor Angiogenesis via the mTOR Pathway. Cell *130*, 440–455.

Lee, J., Kotliarova, S., Kotliarov, Y., Li, A., Su, Q., Donin, N.M., Pastorino, S., Purow, B.W., Christopher, N., Zhang, W., et al. (2006). Tumor stem cells derived from glioblastomas cultured in bFGF and EGF more closely mirror the phenotype and

genotype of primary tumors than do serum-cultured cell lines. Cancer Cell *9*, 391–403.

Lee, J.H., Lee, J.E., Kahng, J.Y., Kim, S.H., Park, J.S., Yoon, S.J., Um, J.-Y., Kim, W.K., Lee, J.-K., Park, J., et al. (2018). Human glioblastoma arises from subventricular zone cells with low-level driver mutations. Nature *560*, 243–247.

Leeman, D.S., Hebestreit, K., Ruetz, T., Webb, A.E., McKay, A., Pollina, E.A., Dulken, B.W., Zhao, X., Yeo, R.W., Ho, T.T., et al. (2018). Lysosome activation clears aggregates and enhances quiescent neural stem cell activation during aging. Science *359*, 1277–1283.

Leto, G., Tumminello, F.M., Crescimanno, M., Flandina, C., and Gebbia, N. (2004). Cathepsin D expression levels in nongynecological solid tumors: clinical and therapeutic implications. Clin. Exp. Metastasis *21*, 91–106.

Lewis, C.S., Voelkel-Johnson, C., and Smith, C.D. (2016). Suppression of c-Myc and RRM2 expression in pancreatic cancer cells by the sphingosine kinase-2 inhibitor ABC294640. Oncotarget *7*, 60181–60192.

Li, X., and Gao, T. (2014). mTORC2 phosphorylates protein kinase Cζ to regulate its stability and activity. EMBO Rep. *15*, 191–198.

Li, G.-H., Wei, H., Lv, S.-Q., Ji, H., and Wang, D.-L. (2010). Knockdown of STAT3 expression by RNAi suppresses growth and induces apoptosis and differentiation in glioblastoma stem cells. Int. J. Oncol. *37*, 103–110.

Li, X., Alafuzoff, I., Soininen, H., Winblad, B., and Pei, J.-J. (2005). Levels of mTOR and its downstream targets 4E-BP1, eEF2, and eEF2 kinase in relationships with tau in Alzheimer's disease brain. FEBS J. *272*, 4211–4220.

Li, X., Rydzewski, N., Hider, A., Zhang, X., Yang, J., Wang, W., Gao, Q., Cheng, X., and Xu, H. (2016). A Molecular Mechanism to Regulate Lysosome Motility for Lysosome Positioning and Tubulation. Nat. Cell Biol. *18*, 404–417.

Li, Z., Bao, S., Wu, Q., Wang, H., Eyler, C., Sathornsumetee, S., Shi, Q., Cao, Y., Lathia, J., McLendon, R.E., et al. (2009). Hypoxia-inducible factors regulate tumorigenic capacity of glioma stem cells. Cancer Cell *15*, 501–513.

Liang, W., Guo, B., Ye, J., Liu, H., Deng, W., Lin, C., Zhong, X., and Wang, L. (2019). Vasorin stimulates malignant progression and angiogenesis in glioma. Cancer Sci. *110*, 2558–2572.

Ligon, K.L., Huillard, E., Mehta, S., Kesari, S., Liu, H., Alberta, J.A., Bachoo, R.M., Kane, M., Louis, D.N., DePinho, R.A., et al. (2007). Olig2-Regulated Lineage-Restricted Pathway Controls Replication Competence in Neural Stem Cells and Malignant Glioma. Neuron *53*, 503–517.

Lim, C.-Y., Davis, O.B., Shin, H.R., Zhang, J., Berdan, C.A., Jiang, X., Counihan, J.L., Ory, D.S., Nomura, D.K., and Zoncu, R. (2019). ER–lysosome contacts enable

cholesterol sensing by mTORC1 and drive aberrant growth signalling in Niemann–Pick type C. Nat. Cell Biol. *21*, 1206–1218.

Lin, F., Gooijer, M.C. de, Hanekamp, D., Chandrasekaran, G., Buil, L.C.M., Thota, N., Sparidans, R.W., Beijnen, J.H., Würdinger, T., and Tellingen, O. van (2017). PI3K–mTOR Pathway Inhibition Exhibits Efficacy Against High-grade Glioma in Clinically Relevant Mouse Models. Clin. Cancer Res. *23*, 1286–1298.

Linkous, A., Balamatsias, D., Snuderl, M., Edwards, L., Miyaguchi, K., Milner, T., Reich, B., Cohen-Gould, L., Storaska, A., Nakayama, Y., et al. (2019). Modeling Patient-Derived Glioblastoma with Cerebral Organoids. Cell Rep. *26*, 3203-3211.e5.

Lipton, J.O., and Sahin, M. (2014). The neurology of mTOR. Neuron *84*, 275–291.

Liu, D., Martin, V., Fueyo, J., Lee, O.-H., Xu, J., Cortes-Santiago, N., Alonso, M.M., Aldape, K., Colman, H., and Gomez-Manzano, C. (2010). Tie2/TEK modulates the interaction of glioma and brain tumor stem cells with endothelial cells and promotes an invasive phenotype. Oncotarget *1*, 700–709.

Liu, F., Hon, G.C., Villa, G.R., Turner, K.M., Ikegami, S., Yang, H., Ye, Z., Li, B., Kuan, S., Lee, A.Y., et al. (2015a). EGFR Mutation Promotes Glioblastoma through Epigenome and Transcription Factor Network Remodeling. Mol. Cell *60*, 307–318.

Liu, G., Yuan, X., Zeng, Z., Tunici, P., Ng, H., Abdulkadir, I.R., Lu, L., Irvin, D., Black, K.L., and Yu, J.S. (2006). Analysis of gene expression and chemoresistance of CD133+ cancer stem cells in glioblastoma. Mol. Cancer *5*, 67.

Liu, P., Gan, W., Chin, Y.R., Ogura, K., Guo, J., Zhang, J., Wang, B., Blenis, J., Cantley, L.C., Toker, A., et al. (2015b). PtdIns(3,4,5)P3-Dependent Activation of the mTORC2 Kinase Complex. Cancer Discov. *5*, 1194–1209.

Llaguno, S.A., Sun, D., Pedraza, A., Vera, E., Wang, Z., Burns, D.K., and Parada, L.F. (2019). Cell of Origin Susceptibility to Glioblastoma Formation Declines with Neural Lineage Restriction. Nat. Neurosci. *22*, 545–555.

Loewith, R., Jacinto, E., Wullschleger, S., Lorberg, A., Crespo, J.L., Bonenfant, D., Oppliger, W., Jenoe, P., and Hall, M.N. (2002). Two TOR complexes, only one of which is rapamycin sensitive, have distinct roles in cell growth control. Mol. Cell *10*, 457–468.

Lois, C., and Alvarez-Buylla, A. (1993). Proliferating subventricular zone cells in the adult mammalian forebrain can differentiate into neurons and glia. Proc. Natl. Acad. Sci. U. S. A. *90*, 2074–2077.

Loison, F., Zhu, H., Karatepe, K., Kasorn, A., Liu, P., Ye, K., Zhou, J., Cao, S., Gong, H., Jenne, D.E., et al. (2014). Proteinase 3–dependent caspase-3 cleavage modulates neutrophil death and inflammation. J. Clin. Invest. *124*, 4445–4458.

Long, X., Lin, Y., Ortiz-Vega, S., Yonezawa, K., and Avruch, J. (2005). Rheb binds and regulates the mTOR kinase. Curr. Biol. CB *15*, 702–713.

Loor, G., and Schumacker, P.T. (2008). Role of hypoxia-inducible factor in cell survival during myocardial ischemia-reperfusion. Cell Death Differ. *15*, 686–690.

Lorenzetti, D., Antalffy, B., Vogel, H., Noveroske, J., Armstrong, D., and Justice, M. (2004). The neurological mutant quaking(viable) is Parkin deficient. Mamm. Genome Off. J. Int. Mamm. Genome Soc. *15*, 210–217.

Louis, D.N., Perry, A., Reifenberger, G., von Deimling, A., Figarella-Branger, D., Cavenee, W.K., Ohgaki, H., Wiestler, O.D., Kleihues, P., and Ellison, D.W. (2016). The 2016 World Health Organization Classification of Tumors of the Central Nervous System: a summary. Acta Neuropathol. (Berl.) *131*, 803–820.

Ludwig, T., Le Borgne, R., and Hoflack, B. (1995). Roles for mannose-6-phosphate receptors in lysosomal enzyme sorting, IGF-II binding and clathrin-coat assembly. Trends Cell Biol. *5*, 202–206.

Luzio, J.P., Pryor, P.R., and Bright, N.A. (2007). Lysosomes: fusion and function. Nat. Rev. Mol. Cell Biol. *8*, 622–632.

Ma, D.K., Ming, G.-L., and Song, H. (2005a). Glial influences on neural stem cell development: cellular niches for adult neurogenesis. Curr. Opin. Neurobiol. *15*, 514–520.

Ma, L., Chen, Z., Erdjument-Bromage, H., Tempst, P., and Pandolfi, P.P. (2005b). Phosphorylation and Functional Inactivation of TSC2 by Erk. Cell *121*, 179–193.

Machado, E., White-Gilbertson, S., Vlekkert, D. van de, Janke, L., Moshiach, S., Campos, Y., Finkelstein, D., Gomero, E., Mosca, R., Qiu, X., et al. (2015). Regulated lysosomal exocytosis mediates cancer progression. Sci. Adv. *1*, e1500603.

Mai, T.T., Hamaï, A., Hienzsch, A., Cañeque, T., Müller, S., Wicinski, J., Cabaud, O., Leroy, C., David, A., Acevedo, V., et al. (2017). Salinomycin kills cancer stem cells by sequestering iron in lysosomes. Nat. Chem. *9*, 1025–1033.

Mammucari, C., Milan, G., Romanello, V., Masiero, E., Rudolf, R., Del Piccolo, P., Burden, S.J., Di Lisi, R., Sandri, C., Zhao, J., et al. (2007). FoxO3 controls autophagy in skeletal muscle in vivo. Cell Metab. *6*, 458–471.

Man, J., Yu, X., Huang, H., Zhou, W., Xiang, C., Huang, H., Miele, L., Liu, Z., Bebek, G., Bao, S., et al. (2018). Hypoxic Induction of Vasorin Regulates Notch1 Turnover to Maintain Glioma Stem-like Cells. Cell Stem Cell *22*, 104-118.e6.

Manning, B.D., Tee, A.R., Logsdon, M.N., Blenis, J., and Cantley, L.C. (2002). Identification of the tuberous sclerosis complex-2 tumor suppressor gene product tuberin as a target of the phosphoinositide 3-kinase/akt pathway. Mol. Cell *10*, 151–162.

Martina, J.A., Chen, Y., Gucek, M., and Puertollano, R. (2012). MTORC1 functions as a transcriptional regulator of autophagy by preventing nuclear transport of TFEB. Autophagy *8*, 903–914.

Martuza, R.L., Malick, A., Markert, J.M., Ruffner, K.L., and Coen, D.M. (1991). Experimental therapy of human glioma by means of a genetically engineered virus mutant. Science *252*, 854–856.

Marumoto, T., Tashiro, A., Friedmann-Morvinski, D., Scadeng, M., Soda, Y., Gage, F.H., and Verma, I.M. (2009). Development of a novel mouse glioma model using lentiviral vectors. Nat. Med. *15*, 110–116.

Maruyama, T., Araki, T., Kawarazaki, Y., Naguro, I., Heynen, S., Aza-Blanc, P., Ronai, Z., Matsuzawa, A., and Ichijo, H. (2014). Roquin-2 promotes ubiquitin-mediated degradation of ASK1 to regulate stress responses. Sci. Signal. *7*, ra8.

Masri, J., Bernath, A., Martin, J., Jo, O.D., Vartanian, R., Funk, A., and Gera, J. (2007). mTORC2 activity is elevated in gliomas and promotes growth and cell motility via overexpression of rictor. Cancer Res. *67*, 11712–11720.

Mastrella, G., Hou, M., Li, M., Stoecklein, V.M., Zdouc, N., Volmar, M.N.M., Miletic, H., Reinhard, S., Herold-Mende, C.C., Kleber, S., et al. (2019a). Targeting APLN/APLNR Improves Antiangiogenic Efficiency and Blunts Proinvasive Side Effects of VEGFA/VEGFR2 Blockade in Glioblastoma. Cancer Res. *79*, 2298–2313.

Mastrella, G., Hou, M., Li, M., Stoecklein, V.M., Zdouc, N., Volmar, M.N.M., Miletic, H., Reinhard, S., Herold-Mende, C.C., Kleber, S., et al. (2019b). Targeting APLN/APLNR Improves Antiangiogenic Efficiency and Blunts Proinvasive Side Effects of VEGFA/VEGFR2 Blockade in Glioblastoma. Cancer Res. *79*, 2298–2313.

McAuley, J.R., Bailey, K.M., Ekambaram, P., Klei, L.R., Kang, H., Hu, D., Freeman, T.J., Concel, V.J., Hubel, N.E., Lee, J.-Y. (Lloyd), et al. (2019). MALT1 is a critical mediator of PAR1-driven NF-κB activation and metastasis in multiple tumor types. Oncogene 1–15.

McEwan, D.G., Popovic, D., Gubas, A., Terawaki, S., Suzuki, H., Stadel, D., Coxon, F.P., Miranda de Stegmann, D., Bhogaraju, S., Maddi, K., et al. (2015). PLEKHM1 regulates autophagosome-lysosome fusion through HOPS complex and LC3/GABARAP proteins. Mol. Cell *57*, 39–54.

McKnight, N.C., Jefferies, H.B.J., Alemu, E.A., Saunders, R.E., Howell, M., Johansen, T., and Tooze, S.A. (2012). Genome-wide siRNA screen reveals amino acid starvation-induced autophagy requires SCOC and WAC. EMBO J. *31*, 1931–1946.

Meadows, K.L., and Hurwitz, H.I. (2012). Anti-VEGF Therapies in the Clinic. Cold Spring Harb. Perspect. Med. *2*.

Mecca, C., Giambanco, I., Donato, R., and Arcuri, C. (2018a). Targeting mTOR in Glioblastoma: Rationale and Preclinical/Clinical Evidence.

Mecca, C., Giambanco, I., Bruscoli, S., Bereshchenko, O., Fioretti, B., Riccardi, C., Donato, R., and Arcuri, C. (2018b). PP242 Counteracts Glioblastoma Cell Proliferation, Migration, Invasiveness and Stemness Properties by Inhibiting

mTORC2/AKT. Front. Cell. Neurosci. *12*.

Meikle, L., Talos, D.M., Onda, H., Pollizzi, K., Rotenberg, A., Sahin, M., Jensen, F.E., and Kwiatkowski, D.J. (2007). A mouse model of tuberous sclerosis: neuronal loss of Tsc1 causes dysplastic and ectopic neurons, reduced myelination, seizure activity, and limited survival. J. Neurosci. Off. J. Soc. Neurosci. *27*, 5546–5558.

Mellman, I. (1996). Endocytosis and molecular sorting. Annu. Rev. Cell Dev. Biol. *12*, 575–625.

Menon, S., Dibble, C.C., Talbott, G., Hoxhaj, G., Valvezan, A.J., Takahashi, H., Cantley, L.C., and Manning, B.D. (2014). Spatial control of the TSC complex integrates insulin and nutrient regulation of mTORC1 at the lysosome. Cell *156*, 771–785.

Meric-Bernstam, F., Akcakanat, A., Chen, H., Do, K.-A., Sangai, T., Adkins, F., Gonzalez-Angulo, A.M., Rashid, A., Crosby, K., Dong, M., et al. (2012). PIK3CA/PTEN Mutations and Akt Activation as Markers of Sensitivity to Allosteric mTOR inhibitors. Clin. Cancer Res. *18*, 1777–1789.

Meyer, C., Zizioli, D., Lausmann, S., Eskelinen, E.-L., Hamann, J., Saftig, P., von Figura, K., and Schu, P. (2000). µ1A-adaptin-deficient mice: lethality, loss of AP-1 binding and rerouting of mannose 6-phosphate receptors. EMBO J. *19*, 2193–2203.

Milkereit, R., Persaud, A., Vanoaica, L., Guetg, A., Verrey, F., and Rotin, D. (2015). LAPTM4b recruits the LAT1-4F2hc Leu transporter to lysosomes and promotes mTORC1 activation. Nat. Commun. *6*, 1–9.

Mirzadeh, Z., Merkle, F.T., Soriano-Navarro, M., Garcia-Verdugo, J.M., and Alvarez-Buylla, A. (2008). Neural stem cells confer unique pinwheel architecture to the ventricular surface in neurogenic regions of the adult brain. Cell Stem Cell *3*, 265–278.

Monteiro, A.R., Hill, R., Pilkington, G.J., and Madureira, P.A. (2017). The Role of Hypoxia in Glioblastoma Invasion. Cells *6*.

Moody, C.L., and Wheelhouse, R.T. (2014). The Medicinal Chemistry of Imidazotetrazine Prodrugs. Pharmaceuticals *7*, 797–838.

Mora, R., Dokic, I., Kees, T., Hüber, C.M., Keitel, D., Geibig, R., Brügge, B., Zentgraf, H., Brady, N.R., and Régnier-Vigouroux, A. (2010). Sphingolipid rheostat alterations related to transformation can be exploited for specific induction of lysosomal cell death in murine and human glioma. Glia *58*, 1364–1383.

Morrison, S.J., Perez, S.E., Qiao, Z., Verdi, J.M., Hicks, C., Weinmaster, G., and Anderson, D.J. (2000). Transient Notch activation initiates an irreversible switch from neurogenesis to gliogenesis by neural crest stem cells. Cell *101*, 499–510.

Mrakovic, A., Kay, J.G., Furuya, W., Brumell, J.H., and Botelho, R.J. (2012). Rab7 and Arl8 GTPases are necessary for lysosome tubulation in macrophages. Traffic

Cph. Den. *13*, 1667–1679.

Munier-Lehmann, H., Mauxion, F., and Hoflack, B. (1996). Function of the two mannose 6-phosphate receptors in lysosomal enzyme transport. Biochem. Soc. Trans. *24*, 133–136.

Nagel, D., Spranger, S., Vincendeau, M., Grau, M., Raffegerst, S., Kloo, B., Hlahla, D., Neuenschwander, M., Peter von Kries, J., Hadian, K., et al. (2012a). Pharmacologic inhibition of MALT1 protease by phenothiazines as a therapeutic approach for the treatment of aggressive ABC-DLBCL. Cancer Cell *22*, 825–837.

Nagel, D., Spranger, S., Vincendeau, M., Grau, M., Raffegerst, S., Kloo, B., Hlahla, D., Neuenschwander, M., Kries, J.P. von, Hadian, K., et al. (2012b). Pharmacologic Inhibition of MALT1 Protease by Phenothiazines as a Therapeutic Approach for the Treatment of Aggressive ABC-DLBCL. Cancer Cell *22*, 825–837.

Nagpal, S., Harsh, G., and Recht, L. (2011). Bevacizumab Improves Quality of Life in Patients with Recurrent Glioblastoma. Chemother. Res. Pract. *2011*.

Nakada, M., Kita, D., Watanabe, T., Hayashi, Y., Teng, L., Pyko, I.V., and Hamada, J.-I. (2011). Aberrant signaling pathways in glioma. Cancers *3*, 3242–3278.

Nakano, I. (2015). Stem cell signature in glioblastoma: therapeutic development for a moving target. J. Neurosurg. *122*, 324–330.

Nakaya, M., Xiao, Y., Zhou, X., Chang, J.-H., Chang, M., Cheng, X., Blonska, M., Lin, X., and Sun, S.-C. (2014). Inflammatory T cell responses rely on amino acid transporter ASCT2 facilitation of glutamine uptake and mTORC1 kinase activation. Immunity *40*, 692–705.

Nakayama, K. (2009). Cellular signal transduction of the hypoxia response. J. Biochem. (Tokyo) *146*, 757–765.

Nanegrungsunk, D., Onchan, W., Chattipakorn, N., and Chattipakorn, S.C. (2015). Current evidence of temozolomide and bevacizumab in treatment of gliomas. Neurol. Res. *37*, 167–183.

Napolitano, G., and Ballabio, A. (2016a). TFEB at a glance. J. Cell Sci. *129*, 2475–2481.

Napolitano, G., and Ballabio, A. (2016b). TFEB at a glance. J. Cell Sci. *129*, 2475–2481.

Neshat, M.S., Mellinghoff, I.K., Tran, C., Stiles, B., Thomas, G., Petersen, R., Frost, P., Gibbons, J.J., Wu, H., and Sawyers, C.L. (2001). Enhanced sensitivity of PTEN-deficient tumors to inhibition of FRAP/mTOR. Proc. Natl. Acad. Sci. *98*, 10314.

Nguyen, T.N., Padman, B.S., Usher, J., Oorschot, V., Ramm, G., and Lazarou, M. (2016). Atg8 family LC3/GABARAP proteins are crucial for autophagosome-lysosome fusion but not autophagosome formation during PINK1/Parkin mitophagy

and starvation. J. Cell Biol. *215*, 857–874.

Ni, X., and Morales, C.R. (2006). The lysosomal trafficking of acid sphingomyelinase is mediated by sortilin and mannose 6-phosphate receptor. Traffic Cph. Den. *7*, 889–902.

Nishimura, T., Tamura, N., Kono, N., Shimanaka, Y., Arai, H., Yamamoto, H., and Mizushima, N. (2017). Autophagosome formation is initiated at phosphatidylinositol synthase-enriched ER subdomains. EMBO J. *36*, 1719–1735.

Nishimura, Y., Sameni, M., and Sloane, B.F. (1998). Malignant transformation alters intracellular trafficking of lysosomal cathepsin D in human breast epithelial cells. Pathol. Oncol. Res. *4*, 283.

Niu, G., Wright, K.L., Huang, M., Song, L., Haura, E., Turkson, J., Zhang, S., Wang, T., Sinibaldi, D., Coppola, D., et al. (2002). Constitutive Stat3 activity up-regulates VEGF expression and tumor angiogenesis. Oncogene *21*, 2000–2008.

Nixon, R.A. (2013). The role of autophagy in neurodegenerative disease. Nat. Med. *19*, 983–997.

Noack, J., Choi, J., Richter, K., Kopp-Schneider, A., and Régnier-Vigouroux, A. (2014). A sphingosine kinase inhibitor combined with temozolomide induces glioblastoma cell death through accumulation of dihydrosphingosine and dihydroceramide, endoplasmic reticulum stress and autophagy. Cell Death Dis. *5*, e1425.

Nojima, H., Tokunaga, C., Eguchi, S., Oshiro, N., Hidayat, S., Yoshino, K., Hara, K., Tanaka, N., Avruch, J., and Yonezawa, K. (2003). The mammalian target of rapamycin (mTOR) partner, raptor, binds the mTOR substrates p70 S6 kinase and 4E-BP1 through their TOR signaling (TOS) motif. J. Biol. Chem. *278*, 15461–15464.

Novikoff, A.B., Beaufay, H., and de Duve, C. (1956). ELECTRON MICROSCOPY OF LYSOSOME-RICH FRACTIONS FROM RAT LIVER. J. Biophys. Biochem. Cytol. *2*, 179–184.

Nylandsted, J., Wick, W., Hirt, U.A., Brand, K., Rohde, M., Leist, M., Weller, M., and Jäättelä, M. (2002). Eradication of glioblastoma, and breast and colon carcinoma xenografts by Hsp70 depletion. Cancer Res. *62*, 7139–7142.

Obermeier, B., Daneman, R., and Ransohoff, R.M. (2013). Development, maintenance and disruption of the blood-brain barrier. Nat. Med. *19*, 1584–1596.

Ohgaki, H., and Kleihues, P. (2013). The definition of primary and secondary glioblastoma. Clin. Cancer Res. Off. J. Am. Assoc. Cancer Res. *19*, 764–772.

Olsvik, H.L., Lamark, T., Takagi, K., Larsen, K.B., Evjen, G., Øvervatn, A., Mizushima, T., and Johansen, T. (2015). FYCO1 Contains a C-terminally Extended, LC3A/B-preferring LC3-interacting Region (LIR) Motif Required for Efficient Maturation of Autophagosomes during Basal Autophagy. J. Biol. Chem. *290*, 29361–

29374.

Ono, K., Kim, S.O., and Han, J. (2003). Susceptibility of lysosomes to rupture is a determinant for plasma membrane disruption in tumor necrosis factor alpha-induced cell death. Mol. Cell. Biol. *23*, 665–676.

Orsi, A., Razi, M., Dooley, H.C., Robinson, D., Weston, A.E., Collinson, L.M., and Tooze, S.A. (2012). Dynamic and transient interactions of Atg9 with autophagosomes, but not membrane integration, are required for autophagy. Mol. Biol. Cell *23*, 1860–1873.

Ostenfeld, M.S., Fehrenbacher, N., Høyer-Hansen, M., Thomsen, C., Farkas, T., and Jäättelä, M. (2005). Effective Tumor Cell Death by σ-2 Receptor Ligand Siramesine Involves Lysosomal Leakage and Oxidative Stress. Cancer Res. *65*, 8975–8983.

Ostenfeld, M.S., Høyer-Hansen, M., Bastholm, L., Fehrenbacher, N., Olsen, O.D., Groth-Pedersen, L., Puustinen, P., Kirkegaard-Sørensen, T., Nylandsted, J., Farkas, T., et al. (2008). Anti-cancer agent siramesine is a lysosomotropic detergent that induces cytoprotective autophagosome accumulation. Autophagy *4*, 487–499.

Ostrom, Q.T., Bauchet, L., Davis, F.G., Deltour, I., Fisher, J.L., Langer, C.E., Pekmezci, M., Schwartzbaum, J.A., Turner, M.C., Walsh, K.M., et al. (2014). The epidemiology of glioma in adults: a “state of the science” review. Neuro-Oncol. *16*, 896–913.

Pak, Y., Glowacka, W.K., Bruce, M.C., Pham, N., and Rotin, D. (2006). Transport of LAPTM5 to lysosomes requires association with the ubiquitin ligase Nedd4, but not LAPTM5 ubiquitination. J. Cell Biol. *175*, 631–645.

Palmer, T.D., Willhoite, A.R., and Gage, F.H. (2000). Vascular niche for adult hippocampal neurogenesis. J. Comp. Neurol. *425*, 479–494.

Pan, D., Jiang, C., Ma, Z., Blonska, M., You, M.J., and Lin, X. (2016). MALT1 is required for EGFR-induced NF-κB activation and contributes to EGFR-driven lung cancer progression. Oncogene *35*, 919–928.

Papadopoulos, C., and Meyer, H. (2017). Detection and Clearance of Damaged Lysosomes by the Endo-Lysosomal Damage Response and Lysophagy. Curr. Biol. CB *27*, R1330–R1341.

Papinski, D., Schuschnig, M., Reiter, W., Wilhelm, L., Barnes, C.A., Maiolica, A., Hansmann, I., Pfaffenwimmer, T., Kijanska, M., Stoffel, I., et al. (2014). Early steps in autophagy depend on direct phosphorylation of Atg9 by the Atg1 kinase. Mol. Cell *53*, 471–483.

Pardal, R., Clarke, M.F., and Morrison, S.J. (2003). Applying the principles of stem-cell biology to cancer. Nat. Rev. Cancer *3*, 895–902.

Park, J.-M., Jung, C.H., Seo, M., Otto, N.M., Grunwald, D., Kim, K.H., Moriarity, B., Kim, Y.-M., Starker, C., Nho, R.S., et al. (2016). The ULK1 complex mediates

MTORC1 signaling to the autophagy initiation machinery via binding and phosphorylating ATG14. Autophagy *12*, 547–564.

Parmigiani, A., Nourbakhsh, A., Ding, B., Wang, W., Kim, Y.C., Akopiants, K., Guan, K.-L., Karin, M., and Budanov, A.V. (2014). Sestrins Inhibit mTORC1 Kinase Activation through the GATOR Complex. Cell Rep. *9*, 1281–1291.

Patel, A.P., Tirosh, I., Trombetta, J.J., Shalek, A.K., Gillespie, S.M., Wakimoto, H., Cahill, D.P., Nahed, B.V., Curry, W.T., Martuza, R.L., et al. (2014). Single-cell RNA-seq highlights intratumoral heterogeneity in primary glioblastoma. Science *344*, 1396–1401.

Pattingre, S., Tassa, A., Qu, X., Garuti, R., Liang, X.H., Mizushima, N., Packer, M., Schneider, M.D., and Levine, B. (2005). Bcl-2 antiapoptotic proteins inhibit Beclin 1-dependent autophagy. Cell *122*, 927–939.

Pearce, L.R., Huang, X., Boudeau, J., Pawłowski, R., Wullschleger, S., Deak, M., Ibrahim, A.F.M., Gourlay, R., Magnuson, M.A., and Alessi, D.R. (2007). Identification of Protor as a novel Rictor-binding component of mTOR complex-2. Biochem. J. *405*, 513–522.

Peng, M., Yin, N., and Li, M.O. (2017). SZT2 dictates GATOR control of mTORC1 signalling. Nature *543*, 433–437.

Perera, R.M., and Zoncu, R. (2016). The Lysosome as a Regulatory Hub. Annu. Rev. Cell Dev. Biol. *32*, 223–253.

Petersen, C.M., Nielsen, M.S., Nykjaer, A., Jacobsen, L., Tommerup, N., Rasmussen, H.H., Roigaard, H., Gliemann, J., Madsen, P., and Moestrup, S.K. (1997). Molecular identification of a novel candidate sorting receptor purified from human brain by receptor-associated protein affinity chromatography. J. Biol. Chem. *272*, 3599–3605.

Petersen, N.H.T., Olsen, O.D., Groth-Pedersen, L., Ellegaard, A.-M., Bilgin, M., Redmer, S., Ostenfeld, M.S., Ulanet, D., Dovmark, T.H., Lønborg, A., et al. (2013). Transformation-associated changes in sphingolipid metabolism sensitize cells to lysosomal cell death induced by inhibitors of acid sphingomyelinase. Cancer Cell *24*, 379–393.

Peterson, T.R., Laplante, M., Thoreen, C.C., Sancak, Y., Kang, S.A., Kuehl, W.M., Gray, N.S., and Sabatini, D.M. (2009). DEPTOR is an mTOR inhibitor frequently overexpressed in multiple myeloma cells and required for their survival. Cell *137*, 873–886.

Peterson, T.R., Sengupta, S.S., Harris, T.E., Carmack, A.E., Kang, S.A., Balderas, E., Guertin, D.A., Madden, K.L., Carpenter, A.E., Finck, B.N., et al. (2011). mTOR complex 1 regulates lipin 1 localization to control the SREBP pathway. Cell *146*, 408–420.

Petherick, K.J., Conway, O.J.L., Mpamhanga, C., Osborne, S.A., Kamal, A., Saxty,

B., and Ganley, I.G. (2015). Pharmacological inhibition of ULK1 kinase blocks mammalian target of rapamycin (mTOR)-dependent autophagy. J. Biol. Chem. *290*, 28726.

Petit, C.S., Roczniak-Ferguson, A., and Ferguson, S.M. (2013). Recruitment of folliculin to lysosomes supports the amino acid–dependent activation of Rag GTPases. J. Cell Biol. *202*, 1107–1122.

Philippe, L., Vasseur, J.-J., Debart, F., and Thoreen, C.C. (2018). La-related protein 1 (LARP1) repression of TOP mRNA translation is mediated through its cap-binding domain and controlled by an adjacent regulatory region. Nucleic Acids Res. *46*, 1457–1469.

Piao, Y., Liang, J., Holmes, L., Henry, V., Sulman, E., and de Groot, J.F. (2013). Acquired resistance to anti-VEGF therapy in glioblastoma is associated with a mesenchymal transition. Clin. Cancer Res. Off. J. Am. Assoc. Cancer Res. *19*, 4392–4403.

Piccirillo, S.G.M., Reynolds, B.A., Zanetti, N., Lamorte, G., Binda, E., Broggi, G., Brem, H., Olivi, A., Dimeco, F., and Vescovi, A.L. (2006). Bone morphogenetic proteins inhibit the tumorigenic potential of human brain tumour-initiating cells. Nature *444*, 761–765.

Plate, K.H., and Mennel, H.D. (1995). Vascular morphology and angiogenesis in glial tumors. Exp. Toxicol. Pathol. Off. J. Ges. Toxikol. Pathol. *47*, 89–94.

Platet, N., Liu, S.Y., Atifi, M.E., Oliver, L., Vallette, F.M., Berger, F., and Wion, D. (2007). Influence of oxygen tension on CD133 phenotype in human glioma cell cultures. Cancer Lett. *258*, 286–290.

Pontén, J., and Macintyre, E.H. (1968). Long Term Culture of Normal and Neoplastic Human Glia. Acta Pathol. Microbiol. Scand. *74*, 465–486.

Porstmann, T., Santos, C.R., Griffiths, B., Cully, M., Wu, M., Leevers, S., Griffiths, J.R., Chung, Y.-L., and Schulze, A. (2008). SREBP activity is regulated by mTORC1 and contributes to Akt-dependent cell growth. Cell Metab. *8*, 224–236.

Pu, J., Schindler, C., Jia, R., Jarnik, M., Backlund, P., and Bonifacino, J.S. (2015). BORC, a multisubunit complex that regulates lysosome positioning. Dev. Cell *33*, 176–188.

Pudelko, L., Edwards, S., Balan, M., Nyqvist, D., Al-Saadi, J., Dittmer, J., Almlöf, I., Helleday, T., and Bräutigam, L. (2018). An orthotopic glioblastoma animal model suitable for high-throughput screenings. Neuro-Oncol. *20*, 1475–1484.

Puente, C., Hendrickson, R.C., and Jiang, X. (2016). Nutrient-regulated Phosphorylation of ATG13 Inhibits Starvation-induced Autophagy. J. Biol. Chem. *291*, 6026–6035.

Pyonteck, S.M., Akkari, L., Schuhmacher, A.J., Bowman, R.L., Sevenich, L., Quail,

D.F., Olson, O.C., Quick, M.L., Huse, J.T., Teijeiro, V., et al. (2013). CSF-1R inhibition alters macrophage polarization and blocks glioma progression. Nat. Med. *19*, 1264–1272.

Qiao, Q., Yang, C., Zheng, C., Fontán, L., David, L., Yu, X., Bracken, C., Rosen, M., Melnick, A., Egelman, E.H., et al. (2013). Structural architecture of the CARMA1/Bcl10/MALT1 signalosome: nucleation-induced filamentous assembly. Mol. Cell *51*, 766–779.

Quail, D.F., Bowman, R.L., Akkari, L., Quick, M.L., Schuhmacher, A.J., Huse, J.T., Holland, E.C., Sutton, J.C., and Joyce, J.A. (2016). The tumor microenvironment underlies acquired resistance to CSF1R inhibition in gliomas. Science *352*, aad3018.

Quistgaard, E.M., Madsen, P., Grøftehauge, M.K., Nissen, P., Petersen, C.M., and Thirup, S.S. (2009). Ligands bind to Sortilin in the tunnel of a ten-bladed beta-propeller domain. Nat. Struct. Mol. Biol. *16*, 96–98.

Raben, N., and Puertollano, R. (2016). TFEB and TFE3: Linking Lysosomes to Cellular Adaptation to Stress. Annu. Rev. Cell Dev. Biol. *32*, 255–278.

Radulovic, M., Schink, K.O., Wenzel, E.M., Nähse, V., Bongiovanni, A., Lafont, F., and Stenmark, H. (2018). ESCRT-mediated lysosome repair precedes lysophagy and promotes cell survival. EMBO J. *37*.

Raiborg, C., Wenzel, E.M., Pedersen, N.M., Olsvik, H., Schink, K.O., Schultz, S.W., Vietri, M., Nisi, V., Bucci, C., Brech, A., et al. (2015). Repeated ER-endosome contacts promote endosome translocation and neurite outgrowth. Nature *520*, 234–238.

Ravi, R., Mookerjee, B., Bhujwalla, Z.M., Sutter, C.H., Artemov, D., Zeng, Q., Dillehay, L.E., Madan, A., Semenza, G.L., and Bedi, A. (2000). Regulation of tumor angiogenesis by p53-induced degradation of hypoxia-inducible factor 1α. Genes Dev. *14*, 34–44.

Ravikumar, B., Vacher, C., Berger, Z., Davies, J.E., Luo, S., Oroz, L.G., Scaravilli, F., Easton, D.F., Duden, R., O'Kane, C.J., et al. (2004). Inhibition of mTOR induces autophagy and reduces toxicity of polyglutamine expansions in fly and mouse models of Huntington disease. Nat. Genet. *36*, 585–595.

Read, R.D., Cavenee, W.K., Furnari, F.B., and Thomas, J.B. (2009). A Drosophila Model for EGFR-Ras and PI3K-Dependent Human Glioma. PLOS Genet. *5*, e1000374.

Rebeaud, F., Hailfinger, S., Posevitz-Fejfar, A., Tapernoux, M., Moser, R., Rueda, D., Gaide, O., Guzzardi, M., Iancu, E.M., Rufer, N., et al. (2008). The proteolytic activity of the paracaspase MALT1 is key in T cell activation. Nat. Immunol. *9*, 272–281.

Rebsamen, M., Pochini, L., Stasyk, T., de Araújo, M.E.G., Galluccio, M., Kandasamy, R.K., Snijder, B., Fauster, A., Rudashevskaya, E.L., Bruckner, M., et al.

(2015). SLC38A9 is a component of the lysosomal amino acid sensing machinery that controls mTORC1. Nature *519*, 477–481.

Reczek, D., Schwake, M., Schröder, J., Hughes, H., Blanz, J., Jin, X., Brondyk, W., Van Patten, S., Edmunds, T., and Saftig, P. (2007). LIMP-2 is a receptor for lysosomal mannose-6-phosphate-independent targeting of beta-glucocerebrosidase. Cell *131*, 770–783.

Reddy, A., Caler, E.V., and Andrews, N.W. (2001). Plasma membrane repair is mediated by Ca(2+)-regulated exocytosis of lysosomes. Cell *106*, 157–169.

Reitman, M.L., and Kornfeld, S. (1981a). Lysosomal enzyme targeting. N-Acetylglucosaminylphosphotransferase selectively phosphorylates native lysosomal enzymes. J. Biol. Chem. *256*, 11977–11980.

Reitman, M.L., and Kornfeld, S. (1981b). UDP-N-acetylglucosamine:glycoprotein N-acetylglucosamine-1-phosphotransferase. Proposed enzyme for the phosphorylation of the high mannose oligosaccharide units of lysosomal enzymes. J. Biol. Chem. *256*, 4275–4281.

Repnik, U., Hafner Česen, M., and Turk, B. (2014). Lysosomal membrane permeabilization in cell death: concepts and challenges. Mitochondrion *19 Pt A*, 49–57.

Reya, T., Morrison, S.J., Clarke, M.F., and Weissman, I.L. (2001). Stem cells, cancer, and cancer stem cells. Nature *414*, 105–111.

Reynolds, B.A., and Weiss, S. (1992). Generation of neurons and astrocytes from isolated cells of the adult mammalian central nervous system. Science *255*, 1707–1710.

Ricci-Vitiani, L., Pallini, R., Biffoni, M., Todaro, M., Invernici, G., Cenci, T., Maira, G., Parati, E.A., Stassi, G., Larocca, L.M., et al. (2010). Tumour vascularization via endothelial differentiation of glioblastoma stem-like cells. Nature *468*, 824–828.

Ricklefs, F., Mineo, M., Rooj, A.K., Nakano, I., Charest, A., Weissleder, R., Breakefield, X.O., Chiocca, E.A., Godlewski, J., and Bronisz, A. (2016). Extracellular vesicles from high grade glioma exchange diverse pro-oncogenic signals that maintain intratumoral heterogeneity. Cancer Res. *76*, 2876–2881.

Ricos, M.G., Hodgson, B.L., Pippucci, T., Saidin, A., Ong, Y.S., Heron, S.E., Licchetta, L., Bisulli, F., Bayly, M.A., Hughes, J., et al. (2016). Mutations in the mammalian target of rapamycin pathway regulators NPRL2 and NPRL3 cause focal epilepsy. Ann. Neurol. *79*, 120–131.

Riquelme, P.A., Drapeau, E., and Doetsch, F. (2008). Brain micro-ecologies: neural stem cell niches in the adult mammalian brain. Philos. Trans. R. Soc. Lond. B. Biol. Sci. *363*, 123–137.

Rivera, L.B., Meyronet, D., Hervieu, V., Frederick, M.J., Bergsland, E., and Bergers,

G. (2015). Intratumoral myeloid cells regulate responsiveness and resistance to antiangiogenic therapy. Cell Rep. *11*, 577–591.

Roa, W., Brasher, P.M.A., Bauman, G., Anthes, M., Bruera, E., Chan, A., Fisher, B., Fulton, D., Gulavita, S., Hao, C., et al. (2004). Abbreviated course of radiation therapy in older patients with glioblastoma multiforme: a prospective randomized clinical trial. J. Clin. Oncol. Off. J. Am. Soc. Clin. Oncol. *22*, 1583–1588.

Robertson, F.L., Marqués-Torrejón, M.-A., Morrison, G.M., and Pollard, S.M. (2019). Experimental models and tools to tackle glioblastoma. Dis. Model. Mech. *12*, dmm040386.

Rocha, N., Kuijl, C., van der Kant, R., Janssen, L., Houben, D., Janssen, H., Zwart, W., and Neefjes, J. (2009). Cholesterol sensor ORP1L contacts the ER protein VAP to control Rab7-RILP-p150 Glued and late endosome positioning. J. Cell Biol. *185*, 1209–1225.

Rochefort, H., Garcia, M., Glondu, M., Laurent, V., Liaudet, E., Rey, J.-M., and Roger, P. (2000). Cathepsin D in breast cancer: mechanisms and clinical applications, a 1999 overview. Clin. Chim. Acta *291*, 157–170.

Roczniak-Ferguson, A., Petit, C.S., Froehlich, F., Qian, S., Ky, J., Angarola, B., Walther, T.C., and Ferguson, S.M. (2012). The Transcription Factor TFEB Links mTORC1 Signaling to Transcriptional Control of Lysosome Homeostasis. Sci. Signal. *5*, ra42–ra42.

Ross, E., Ata, R., Thavarajah, T., Medvedev, S., Bowden, P., Marshall, J.G., and Antonescu, C.N. (2015). AMP-Activated Protein Kinase Regulates the Cell Surface Proteome and Integrin Membrane Traffic. PLOS ONE *10*, e0128013.

Rousseau, A., and Bertolotti, A. (2016). An evolutionarily conserved pathway controls proteasome homeostasis. Nature *536*, 184–189.

Roux, P.P., Ballif, B.A., Anjum, R., Gygi, S.P., and Blenis, J. (2004). Tumor-promoting phorbol esters and activated Ras inactivate the tuberous sclerosis tumor suppressor complex via p90 ribosomal S6 kinase. Proc. Natl. Acad. Sci. U. S. A. *101*, 13489–13494.

Roy, D., Liston, D.R., Idone, V.J., Di, A., Nelson, D.J., Pujol, C., Bliska, J.B., Chakrabarti, S., and Andrews, N.W. (2004). A process for controlling intracellular bacterial infections induced by membrane injury. Science *304*, 1515–1518.

Ruefli-Brasse, A.A., French, D.M., and Dixit, V.M. (2003). Regulation of NF-kappaB-dependent lymphocyte activation and development by paracaspase. Science *302*, 1581–1584.

Ruland, J., and Hartjes, L. (2019). CARD–BCL-10–MALT1 signalling in protective and pathological immunity. Nat. Rev. Immunol. *19*, 118–134.

Ruland, J., Duncan, G.S., Wakeham, A., and Mak, T.W. (2003). Differential

Requirement for Malt1 in T and B Cell Antigen Receptor Signaling. Immunity *19*, 749–758.

Sabatini, D.M., Erdjument-Bromage, H., Lui, M., Tempst, P., and Snyder, S.H. (1994). RAFT1: a mammalian protein that binds to FKBP12 in a rapamycin-dependent fashion and is homologous to yeast TORs. Cell *78*, 35–43.

Sabers, C.J., Martin, M.M., Brunn, G.J., Williams, J.M., Dumont, F.J., Wiederrecht, G., and Abraham, R.T. (1995). Isolation of a protein target of the FKBP12-rapamycin complex in mammalian cells. J. Biol. Chem. *270*, 815–822.

Saftig, P., and Klumperman, J. (2009). Lysosome biogenesis and lysosomal membrane proteins: trafficking meets function. Nat. Rev. Mol. Cell Biol. *10*, 623–635.

Sahagian, G.G., and Steer, C.J. (1985). Transmembrane orientation of the mannose 6-phosphate receptor in isolated clathrin-coated vesicles. J. Biol. Chem. *260*, 9838–9842.

Sahara, S., and Yamashima, T. (2010). Calpain-mediated Hsp70.1 cleavage in hippocampal CA1 neuronal death. Biochem. Biophys. Res. Commun. *393*, 806–811.

Sakamaki, J., Wilkinson, S., Hahn, M., Tasdemir, N., O'Prey, J., Clark, W., Hedley, A., Nixon, C., Long, J.S., New, M., et al. (2017). Bromodomain Protein BRD4 Is a Transcriptional Repressor of Autophagy and Lysosomal Function. Mol. Cell *66*, 517-532.e9.

Sampson, J.H., Gunn, M.D., Fecci, P.E., and Ashley, D.M. (2020). Brain immunology and immunotherapy in brain tumours. Nat. Rev. Cancer *20*, 12–25.

Sancak, Y., Thoreen, C.C., Peterson, T.R., Lindquist, R.A., Kang, S.A., Spooner, E., Carr, S.A., and Sabatini, D.M. (2007). PRAS40 is an insulin-regulated inhibitor of the mTORC1 protein kinase. Mol. Cell *25*, 903–915.

Sancak, Y., Peterson, T.R., Shaul, Y.D., Lindquist, R.A., Thoreen, C.C., Bar-Peled, L., and Sabatini, D.M. (2008). The Rag GTPases bind raptor and mediate amino acid signaling to mTORC1. Science *320*, 1496–1501.

Sancak, Y., Bar-Peled, L., Zoncu, R., Markhard, A.L., Nada, S., and Sabatini, D.M. (2010). Ragulator-Rag Complex Targets mTORC1 to the Lysosomal Surface and Is Necessary for Its Activation by Amino Acids. Cell *141*, 290–303.

Sansal, I., and Sellers, W.R. (2004). The biology and clinical relevance of the PTEN tumor suppressor pathway. J. Clin. Oncol. Off. J. Am. Soc. Clin. Oncol. *22*, 2954–2963.

Sarbassov, D.D., Ali, S.M., Kim, D.-H., Guertin, D.A., Latek, R.R., Erdjument-Bromage, H., Tempst, P., and Sabatini, D.M. (2004). Rictor, a novel binding partner of mTOR, defines a rapamycin-insensitive and raptor-independent pathway that regulates the cytoskeleton. Curr. Biol. CB *14*, 1296–1302.

Sarbassov, D.D., Guertin, D.A., Ali, S.M., and Sabatini, D.M. (2005). Phosphorylation and regulation of Akt/PKB by the rictor-mTOR complex. Science *307*, 1098–1101.

Sarbassov, D.D., Ali, S.M., Sengupta, S., Sheen, J.-H., Hsu, P.P., Bagley, A.F., Markhard, A.L., and Sabatini, D.M. (2006). Prolonged rapamycin treatment inhibits mTORC2 assembly and Akt/PKB. Mol. Cell *22*, 159–168.

Sardiello, M., Palmieri, M., di Ronza, A., Medina, D.L., Valenza, M., Gennarino, V.A., Di Malta, C., Donaudy, F., Embrione, V., Polishchuk, R.S., et al. (2009). A gene network regulating lysosomal biogenesis and function. Science *325*, 473–477.

Saxton, R.A., and Sabatini, D.M. (2017). mTOR Signaling in Growth, Metabolism, and Disease. Cell *168*, 960–976.

Saxton, R.A., Chantranupong, L., Knockenhauer, K.E., Schwartz, T.U., and Sabatini, D.M. (2016). Mechanism of arginine sensing by CASTOR1 upstream of mTORC1. Nature *536*, 229–233.

Schaefer, J.S., and Klein, J.R. (2016). Roquin – a multifunctional regulator of immune homeostasis. Genes Immun. *17*, 79–84.

Schalm, S.S., Fingar, D.C., Sabatini, D.M., and Blenis, J. (2003). TOS motif-mediated raptor binding regulates 4E-BP1 multisite phosphorylation and function. Curr. Biol. CB *13*, 797–806.

Schlauderer, F., Lammens, K., Nagel, D., Vincendeau, M., Eitelhuber, A.C., Verhelst, S.H.L., Kling, D., Chrusciel, A., Ruland, J., Krappmann, D., et al. (2013). Structural Analysis of Phenothiazine Derivatives as Allosteric Inhibitors of the MALT1 Paracaspase. Angew. Chem. Int. Ed. *52*, 10384–10387.

Schreiber, S.L. (1991). Chemistry and biology of the immunophilins and their immunosuppressive ligands. Science *251*, 283–287.

Semenza, G.L. (2010). HIF-1: upstream and downstream of cancer metabolism. Curr. Opin. Genet. Dev. *20*, 51–56.

Settembre, C., and Ballabio, A. (2011). TFEB regulates autophagy: an integrated coordination of cellular degradation and recycling processes. Autophagy *7*, 1379–1381.

Settembre, C., Zoncu, R., Medina, D.L., Vetrini, F., Erdin, S., Erdin, S., Huynh, T., Ferron, M., Karsenty, G., Vellard, M.C., et al. (2012). A lysosome-to-nucleus signalling mechanism senses and regulates the lysosome via mTOR and TFEB. EMBO J. *31*, 1095–1108.

Settembre, C., Fraldi, A., Medina, D.L., and Ballabio, A. (2013). Signals from the lysosome: a control centre for cellular clearance and energy metabolism. Nat. Rev. Mol. Cell Biol. *14*, 283–296.

Shalem, O., Sanjana, N.E., Hartenian, E., Shi, X., Scott, D.A., Mikkelson, T., Heckl,

D., Ebert, B.L., Root, D.E., Doench, J.G., et al. (2014). Genome-scale CRISPR-Cas9 knockout screening in human cells. Science *343*, 84–87.

Shaw, R.J., Bardeesy, N., Manning, B.D., Lopez, L., Kosmatka, M., DePinho, R.A., and Cantley, L.C. (2004). The LKB1 tumor suppressor negatively regulates mTOR signaling. Cancer Cell *6*, 91–99.

Shen, Q., Goderie, S.K., Jin, L., Karanth, N., Sun, Y., Abramova, N., Vincent, P., Pumiglia, K., and Temple, S. (2004). Endothelial cells stimulate self-renewal and expand neurogenesis of neural stem cells. Science *304*, 1338–1340.

Shi, Y., Zhou, W., Cheng, L., Chen, C., Huang, Z., Fang, X., Wu, Q., He, Z., Xu, S., Lathia, J.D., et al. (2017). Tetraspanin CD9 stabilizes gp130 by preventing its ubiquitin-dependent lysosomal degradation to promote STAT3 activation in glioma stem cells. Cell Death Differ. *24*, 167–180.

Shi, Y., Guryanova, O.A., Zhou, W., Liu, C., Huang, Z., Fang, X., Wang, X., Chen, C., Wu, Q., He, Z., et al. (2018). Ibrutinib inactivates BMX-STAT3 in glioma stem cells to impair malignant growth and radioresistance. Sci. Transl. Med. *10*.

Shida, D., Takabe, K., Kapitonov, D., Milstien, S., and Spiegel, S. (2008). Targeting SphK1 as a new strategy against cancer. Curr. Drug Targets *9*, 662–673.

Shin, H.-J.R., Kim, H., Oh, S., Lee, J.-G., Kee, M., Ko, H.-J., Kweon, M.-N., Won, K.-J., and Baek, S.H. (2016). AMPK–SKP2–CARM1 signalling cascade in transcriptional regulation of autophagy. Nature *534*, 553–557.

Shingu, T., Ho, A.L., Yuan, L., Zhou, X., Dai, C., Zheng, S., Wang, Q., Zhong, Y., Chang, Q., Horner, J.W., et al. (2016). Qki deficiency maintains stemness of glioma stem cells in suboptimal environment by downregulating endolysosomal degradation. Nat. Genet. *49*, 75.

Singh, S.K., Clarke, I.D., Terasaki, M., Bonn, V.E., Hawkins, C., Squire, J., and Dirks, P.B. (2003). Identification of a Cancer Stem Cell in Human Brain Tumors. Cancer Res. *63*, 5821–5828.

Singh, S.K., Hawkins, C., Clarke, I.D., Squire, J.A., Bayani, J., Hide, T., Henkelman, R.M., Cusimano, M.D., and Dirks, P.B. (2004). Identification of human brain tumour initiating cells. Nature *432*, 396–401.

Skog, J., Würdinger, T., van Rijn, S., Meijer, D.H., Gainche, L., Sena-Esteves, M., Curry, W.T., Carter, B.S., Krichevsky, A.M., and Breakefield, X.O. (2008). Glioblastoma microvesicles transport RNA and proteins that promote tumour growth and provide diagnostic biomarkers. Nat. Cell Biol. *10*, 1470–1476.

Skowyra, M.L., Schlesinger, P.H., Naismith, T.V., and Hanson, P.I. (2018). Triggered recruitment of ESCRT machinery promotes endolysosomal repair. Science *360*.

Sloane, B.F., Moin, K., Sameni, M., Tait, L.R., Rozhin, J., and Ziegler, G. (1994). Membrane association of cathepsin B can be induced by transfection of human

breast epithelial cells with c-Ha-ras oncogene. J. Cell Sci. *107*, 373–384.

Slobodkin, M.R., and Elazar, Z. (2013). The Atg8 family: multifunctional ubiquitin-like key regulators of autophagy. Essays Biochem. *55*, 51–64.

Solomon, M., and Muro, S. (2017). Lysosomal Enzyme Replacement Therapies: Historical Development, Clinical Outcomes, and Future Perspectives. Adv. Drug Deliv. Rev. *118*, 109–134.

Spampanato, C., Feeney, E., Li, L., Cardone, M., Lim, J.-A., Annunziata, F., Zare, H., Polishchuk, R., Puertollano, R., Parenti, G., et al. (2013). Transcription factor EB (TFEB) is a new therapeutic target for Pompe disease. EMBO Mol. Med. *5*, 691–706.

Staal, J., Driege, Y., Bekaert, T., Demeyer, A., Muyllaert, D., Van Damme, P., Gevaert, K., and Beyaert, R. (2011). T-cell receptor-induced JNK activation requires proteolytic inactivation of CYLD by MALT1. EMBO J. *30*, 1742–1752.

Stein, G.H. (1979). T98G: An anchorage-independent human tumor cell line that exhibits stationary phase G1 arrest in vitro. J. Cell. Physiol. *99*, 43–54.

Stinchcombe, J.C., and Griffiths, G.M. (1999). Regulated Secretion from Hemopoietic Cells. J. Cell Biol. *147*, 1–5.

Stummer, W., Pichlmeier, U., Meinel, T., Wiestler, O.D., Zanella, F., Reulen, H.-J., and ALA-Glioma Study Group (2006). Fluorescence-guided surgery with 5-aminolevulinic acid for resection of malignant glioma: a randomised controlled multicentre phase III trial. Lancet Oncol. *7*, 392–401.

Stupp, R., Mason, W.P., van den Bent, M.J., Weller, M., Fisher, B., Taphoorn, M.J.B., Belanger, K., Brandes, A.A., Marosi, C., Bogdahn, U., et al. (2005). Radiotherapy plus concomitant and adjuvant temozolomide for glioblastoma. N. Engl. J. Med. *352*, 987–996.

Stupp, R., Hegi, M.E., Mason, W.P., van den Bent, M.J., Taphoorn, M.J.B., Janzer, R.C., Ludwin, S.K., Allgeier, A., Fisher, B., Belanger, K., et al. (2009). Effects of radiotherapy with concomitant and adjuvant temozolomide versus radiotherapy alone on survival in glioblastoma in a randomised phase III study: 5-year analysis of the EORTC-NCIC trial. Lancet Oncol. *10*, 459–466.

Stupp, R., Wong, E.T., Kanner, A.A., Steinberg, D., Engelhard, H., Heidecke, V., Kirson, E.D., Taillibert, S., Liebermann, F., Dbalý, V., et al. (2012). NovoTTF-100A versus physician's choice chemotherapy in recurrent glioblastoma: a randomised phase III trial of a novel treatment modality. Eur. J. Cancer Oxf. Engl. 1990 *48*, 2192–2202.

Stupp, R., Taillibert, S., Kanner, A.A., Kesari, S., Steinberg, D.M., Toms, S.A., Taylor, L.P., Lieberman, F., Silvani, A., Fink, K.L., et al. (2015). Maintenance Therapy With Tumor-Treating Fields Plus Temozolomide vs Temozolomide Alone for Glioblastoma: A Randomized Clinical Trial. JAMA *314*, 2535–2543.

Stupp, R., Taillibert, S., Kanner, A., Read, W., Steinberg, D., Lhermitte, B., Toms, S., Idbaih, A., Ahluwalia, M.S., Fink, K., et al. (2017). Effect of Tumor-Treating Fields Plus Maintenance Temozolomide vs Maintenance Temozolomide Alone on Survival in Patients With Glioblastoma: A Randomized Clinical Trial. JAMA *318*, 2306–2316.

Su, H., Yang, F., Wang, Q., Shen, Q., Huang, J., Peng, C., Zhang, Y., Wan, W., Wong, C.C.L., Sun, Q., et al. (2017). VPS34 Acetylation Controls Its Lipid Kinase Activity and the Initiation of Canonical and Non-canonical Autophagy. Mol. Cell *67*, 907-921.e7.

Suh, H., Consiglio, A., Ray, J., Sawai, T., D'Amour, K.A., and Gage, F.H. (2007). In vivo fate analysis reveals the multipotent and self-renewal capacities of Sox2+ neural stem cells in the adult hippocampus. Cell Stem Cell *1*, 515–528.

Sumoza-Toledo, A., and Penner, R. (2011). TRPM2: a multifunctional ion channel for calcium signalling. J. Physiol. *589*, 1515–1525.

Sun, Y., Kong, W., Falk, A., Hu, J., Zhou, L., Pollard, S., and Smith, A. (2009). CD133 (Prominin) negative human neural stem cells are clonogenic and tripotent. PloS One *4*, e5498.

Swartz, A., Li, Q., and Sampson, J. (2014). Rindopepimut®: A promising immunotherapeutic for the treatment of glioblastoma multiforme. Immunotherapy *6*, 679–690.

Szatmári, T., Lumniczky, K., Désaknai, S., Trajcevski, S., Hídvégi, E.J., Hamada, H., and Sáfrány, G. (2006). Detailed characterization of the mouse glioma 261 tumor model for experimental glioblastoma therapy. Cancer Sci. *97*, 546–553.

Taha, T.A., Kitatani, K., Bielawski, J., Cho, W., Hannun, Y.A., and Obeid, L.M. (2005). Tumor necrosis factor induces the loss of sphingosine kinase-1 by a cathepsin B-dependent mechanism. J. Biol. Chem. *280*, 17196–17202.

Takahashi, K., and Yamanaka, S. (2006). Induction of pluripotent stem cells from mouse embryonic and adult fibroblast cultures by defined factors. Cell *126*, 663–676.

Takahashi, T., Hara, K., Inoue, H., Kawa, Y., Tokunaga, C., Hidayat, S., Yoshino, K., Kuroda, Y., and Yonezawa, K. (2000). Carboxyl-terminal region conserved among phosphoinositide-kinase-related kinases is indispensable for mTOR function in vivo and in vitro. Genes Cells *5*, 765–775.

Takei, N., Inamura, N., Kawamura, M., Namba, H., Hara, K., Yonezawa, K., and Nawa, H. (2004). Brain-Derived Neurotrophic Factor Induces Mammalian Target of Rapamycin-Dependent Local Activation of Translation Machinery and Protein Synthesis in Neuronal Dendrites. J. Neurosci. *24*, 9760–9769.

Tanaka, K., Babic, I., Nathanson, D., Akhavan, D., Guo, D., Gini, B., Dang, J., Zhu, S., Yang, H., de Jesus, J., et al. (2011). Oncogenic EGFR signaling activates an mTORC2-NF-κB pathway that promotes chemotherapy resistance. Cancer Discov. *1*, 524–538.

Tanimoto, K., Makino, Y., Pereira, T., and Poellinger, L. (2000). Mechanism of regulation of the hypoxia-inducible factor-1α by the von Hippel-Lindau tumor suppressor protein. EMBO J. *19*, 4298–4309.

Tanjore, H., and Kalluri, R. (2006). The Role of Type IV Collagen and Basement Membranes in Cancer Progression and Metastasis. Am. J. Pathol. *168*, 715–717.

Tanti, J.-F., and Jager, J. (2009). Cellular mechanisms of insulin resistance: role of stress-regulated serine kinases and insulin receptor substrates (IRS) serine phosphorylation. Curr. Opin. Pharmacol. *9*, 753–762.

Tavazoie, M., Van der Veken, L., Silva-Vargas, V., Louissaint, M., Colonna, L., Zaidi, B., Garcia-Verdugo, J.M., and Doetsch, F. (2008). A Specialized Vascular Niche for Adult Neural Stem Cells. Cell Stem Cell *3*, 279–288.

Tavazoie, S.F., Alvarez, V.A., Ridenour, D.A., Kwiatkowski, D.J., and Sabatini, B.L. (2005). Regulation of neuronal morphology and function by the tumor suppressors Tsc1 and Tsc2. Nat. Neurosci. *8*, 1727–1734.

Taylor, A.J., Little, M.P., Winter, D.L., Sugden, E., Ellison, D.W., Stiller, C.A., Stovall, M., Frobisher, C., Lancashire, E.R., Reulen, R.C., et al. (2010). Population-based risks of CNS tumors in survivors of childhood cancer: the British Childhood Cancer Survivor Study. J. Clin. Oncol. Off. J. Am. Soc. Clin. Oncol. *28*, 5287–5293.

Tchirkov, A., Khalil, T., Chautard, E., Mokhtari, K., Véronèse, L., Irthum, B., Vago, P., Kémény, J.-L., and Verrelle, P. (2007). Interleukin-6 gene amplification and shortened survival in glioblastoma patients. Br. J. Cancer *96*, 474–476.

Tee, A.R., Manning, B.D., Roux, P.P., Cantley, L.C., and Blenis, J. (2003). Tuberous sclerosis complex gene products, Tuberin and Hamartin, control mTOR signaling by acting as a GTPase-activating protein complex toward Rheb. Curr. Biol. CB *13*, 1259–1268.

van Tellingen, O., Yetkin-Arik, B., de Gooijer, M.C., Wesseling, P., Wurdinger, T., and de Vries, H.E. (2015). Overcoming the blood-brain tumor barrier for effective glioblastoma treatment. Drug Resist. Updat. Rev. Comment. Antimicrob. Anticancer Chemother. *19*, 1–12.

Thedieck, K., Holzwarth, B., Prentzell, M.T., Boehlke, C., Kläsener, K., Ruf, S., Sonntag, A.G., Maerz, L., Grellscheid, S.-N., Kremmer, E., et al. (2013). Inhibition of mTORC1 by Astrin and Stress Granules Prevents Apoptosis in Cancer Cells. Cell *154*, 859–874.

Thomanetz, V., Angliker, N., Cloëtta, D., Lustenberger, R.M., Schweighauser, M., Oliveri, F., Suzuki, N., and Rüegg, M.A. (2013). Ablation of the mTORC2 component rictor in brain or Purkinje cells affects size and neuron morphology. J. Cell Biol. *201*, 293–308.

Thoreen, C.C., Chantranupong, L., Keys, H.R., Wang, T., Gray, N.S., and Sabatini, D.M. (2012). A unifying model for mTORC1-mediated regulation of mRNA

translation. Nature *485*, 109–113.

Thurston, T.L.M., Wandel, M.P., von Muhlinen, N., Foeglein, A., and Randow, F. (2012). Galectin 8 targets damaged vesicles for autophagy to defend cells against bacterial invasion. Nature *482*, 414–418.

Tian, T., Li, X., and Zhang, J. (2019). mTOR Signaling in Cancer and mTOR Inhibitors in Solid Tumor Targeting Therapy. Int. J. Mol. Sci. *20*, 755.

Tremblay, F., and Marette, A. (2001). Amino acids and insulin signaling via the mTOR/p70 S6 kinase pathway: A negative feedback mechanism leading to insulin resistance in skeletal muscle cells. J. Biol. Chem.

Treps, L., Edmond, S., Harford-Wright, E., Galan-Moya, E.M., Schmitt, A., Azzi, S., Citerne, A., Bidère, N., Ricard, D., and Gavard, J. (2016). Extracellular vesicle-transported Semaphorin3A promotes vascular permeability in glioblastoma. Oncogene *35*, 2615–2623.

Treps, L., Perret, R., Edmond, S., Ricard, D., and Gavard, J. (2017). Glioblastoma stem-like cells secrete the pro-angiogenic VEGF-A factor in extracellular vesicles. J. Extracell. Vesicles *6*.

Tsuboyama, K., Koyama-Honda, I., Sakamaki, Y., Koike, M., Morishita, H., and Mizushima, N. (2016). The ATG conjugation systems are important for degradation of the inner autophagosomal membrane. Science *354*, 1036–1041.

Tsun, Z.-Y., Bar-Peled, L., Chantranupong, L., Zoncu, R., Wang, T., Kim, C., Spooner, E., and Sabatini, D.M. (2013). The Folliculin Tumor Suppressor Is a GAP for the RagC/D GTPases That Signal Amino Acid Levels to mTORC1. Mol. Cell *52*, 495–505.

Tu, Y., Zhong, Y., Fu, J., Cao, Y., Fu, G., Tian, X., and Wang, B. (2011). Activation of JAK/STAT signal pathway predicts poor prognosis of patients with gliomas. Med. Oncol. Northwood Lond. Engl. *28*, 15–23.

Tunici, P., Bissola, L., Lualdi, E., Pollo, B., Cajola, L., Broggi, G., Sozzi, G., and Finocchiaro, G. (2004). Genetic alterations and in vivo tumorigenicity of neurospheres derived from an adult glioblastoma. Mol. Cancer *3*, 25.

Uehata, T., Iwasaki, H., Vandenbon, A., Matsushita, K., Hernandez-Cuellar, E., Kuniyoshi, K., Satoh, T., Mino, T., Suzuki, Y., Standley, D.M., et al. (2013). Malt1-induced cleavage of regnase-1 in CD4(+) helper T cells regulates immune activation. Cell *153*, 1036–1049.

Uren, A.G., O'Rourke, K., Aravind, L.A., Pisabarro, M.T., Seshagiri, S., Koonin, E.V., and Dixit, V.M. (2000). Identification of paracaspases and metacaspases: two ancient families of caspase-like proteins, one of which plays a key role in MALT lymphoma. Mol. Cell *6*, 961–967.

Uribesalgo, I., Hoffmann, D., Zhang, Y., Kavirayani, A., Lazovic, J., Berta, J.,

Novatchkova, M., Pai, T.-P., Wimmer, R.A., László, V., et al. (2019). Apelin inhibition prevents resistance and metastasis associated with anti-angiogenic therapy. EMBO Mol. Med. *11*, e9266.

Van Der Sanden, B., Appaix, F., Berger, F., Selek, L., Issartel, J.-P., and Wion, D. (2013). Translation of the ecological trap concept to glioma therapy: the cancer cell trap concept. Future Oncol. Lond. Engl. 817–824.

Vander Haar, E., Lee, S.-I., Bandhakavi, S., Griffin, T.J., and Kim, D.-H. (2007). Insulin signalling to mTOR mediated by the Akt/PKB substrate PRAS40. Nat. Cell Biol. *9*, 316–323.

Vasiljeva, O., Papazoglou, A., Krüger, A., Brodoefel, H., Korovin, M., Deussing, J., Augustin, N., Nielsen, B.S., Almholt, K., Bogyo, M., et al. (2006). Tumor cell-derived and macrophage-derived cathepsin B promotes progression and lung metastasis of mammary cancer. Cancer Res. *66*, 5242–5250.

Vergarajauregui, S., and Puertollano, R. (2006). Two di-leucine motifs regulate trafficking of mucolipin-1 to lysosomes. Traffic Cph. Den. *7*, 337–353.

Verhaak, R.G.W., Hoadley, K.A., Purdom, E., Wang, V., Qi, Y., Wilkerson, M.D., Miller, C.R., Ding, L., Golub, T., Mesirov, J.P., et al. (2010). Integrated genomic analysis identifies clinically relevant subtypes of glioblastoma characterized by abnormalities in PDGFRA, IDH1, EGFR, and NF1. Cancer Cell *17*, 98–110.

Vézina, C., Kudelski, A., and Sehgal, S.N. (1975). Rapamycin (AY-22,989), a new antifungal antibiotic. I. Taxonomy of the producing streptomycete and isolation of the active principle. J. Antibiot. (Tokyo) *28*, 721–726.

Villegas, F., Lehalle, D., Mayer, D., Rittirsch, M., Stadler, M.B., Zinner, M., Olivieri, D., Vabres, P., Duplomb-Jego, L., Bont, E.S.J.M.D., et al. (2019). Lysosomal Signaling Licenses Embryonic Stem Cell Differentiation via Inactivation of Tfe3. Cell Stem Cell *24*, 257-270.e8.

van der Vos, K.E., Abels, E.R., Zhang, X., Lai, C., Carrizosa, E., Oakley, D., Prabhakar, S., Mardini, O., Crommentuijn, M.H.W., Skog, J., et al. (2016). Directly visualized glioblastoma-derived extracellular vesicles transfer RNA to microglia/macrophages in the brain. Neuro-Oncol. *18*, 58–69.

Waheed, A., Hasilik, A., and von Figura, K. (1981). Processing of the phosphorylated recognition marker in lysosomal enzymes. Characterization and partial purification of a microsomal alpha-N-acetylglucosaminyl phosphodiesterase. J. Biol. Chem. *256*, 5717–5721.

Wang, T., and Hong, W. (2002). Interorganellar regulation of lysosome positioning by the Golgi apparatus through Rab34 interaction with Rab-interacting lysosomal protein. Mol. Biol. Cell *13*, 4317–4332.

Wang, F., Yu, L., Monopoli, M.P., Sandin, P., Mahon, E., Salvati, A., and Dawson, K.A. (2013). The biomolecular corona is retained during nanoparticle uptake and

protects the cells from the damage induced by cationic nanoparticles until degraded in the lysosomes. Nanomedicine Nanotechnol. Biol. Med. *9*, 1159–1168.

Wang, F., Salvati, A., and Boya, P. (2018). Lysosome-dependent cell death and deregulated autophagy induced by amine-modified polystyrene nanoparticles. Open Biol. *8*.

Wang, H., Lathia, J.D., Wu, Q., Wang, J., Li, Z., Heddleston, J.M., Eyler, C.E., Elderbroom, J., Gallagher, J., Schuschu, J., et al. (2009). Targeting Interleukin 6 Signaling Suppresses Glioma Stem Cell Survival and Tumor Growth. Stem Cells Dayt. Ohio *27*, 2393–2404.

Wang, H., Deng, J., Ren, H.-Y., Jia, P., Zhang, W., Li, M.-Q., Li, S.-W., and Zhou, Q.-H. (2017a). STAT3 influences the characteristics of stem cells in cervical carcinoma. Oncol. Lett. *14*, 2131–2136.

Wang, L., Harris, T.E., Roth, R.A., and Lawrence, J.C. (2007). PRAS40 regulates mTORC1 kinase activity by functioning as a direct inhibitor of substrate binding. J. Biol. Chem. *282*, 20036–20044.

Wang, Q., Hu, B., Hu, X., Kim, H., Squatrito, M., Scarpace, L., deCarvalho, A.C., Lyu, S., Li, P., Li, Y., et al. (2017b). Tumor evolution of glioma intrinsic gene expression subtype associates with immunological changes in the microenvironment. Cancer Cell *32*, 42-56.e6.

Wang, S., Tsun, Z.-Y., Wolfson, R.L., Shen, K., Wyant, G.A., Plovanich, M.E., Yuan, E.D., Jones, T.D., Chantranupong, L., Comb, W., et al. (2015). Lysosomal amino acid transporter SLC38A9 signals arginine sufficiency to mTORC1. Science *347*, 188–194.

Wang, W.-T., Chen, Y.-H., Hsu, J.-L., Leu, W.-J., Yu, C.-C., Chan, S.-H., Ho, Y.-F., Hsu, L.-C., and Guh, J.-H. (2014). Terfenadine induces anti-proliferative and apoptotic activities in human hormone-refractory prostate cancer through histamine receptor-independent Mcl-1 cleavage and Bak up-regulation. Naunyn. Schmiedebergs Arch. Pharmacol. *387*, 33–45.

Welker, A.M., Jaros, B.D., Puduvalli, V.K., Imitola, J., Kaur, B., and Beattie, C.E. (2016). Standardized orthotopic xenografts in zebrafish reveal glioma cell-line-specific characteristics and tumor cell heterogeneity. Dis. Model. Mech. *9*, 199–210.

Westermark, B., Pontén, J., and Hugosson, R. (1973). Determinants for the Establishment of Permanent Tissue Culture Lines from Human Gliomas. Acta Pathol. Microbiol. Scand. [A] *81A*, 791–805.

Westphal, M., and Lamszus, K. (2011). The neurobiology of gliomas: from cell biology to the development of therapeutic approaches. Nat. Rev. Neurosci. *12*, 495–508.

Westphal, M., Hilt, D.C., Bortey, E., Delavault, P., Olivares, R., Warnke, P.C., Whittle, I.R., Jääskeläinen, J., and Ram, Z. (2003). A phase 3 trial of local

chemotherapy with biodegradable carmustine (BCNU) wafers (Gliadel wafers) in patients with primary malignant glioma. Neuro-Oncol. *5*, 79–88.

White, U.A., and Stephens, J.M. (2011). The gp130 Receptor Cytokine Family: Regulators of Adipocyte Development and Function. Curr. Pharm. Des. *17*, 340–346.

White, J.H., Wise, A., Main, M.J., Green, A., Fraser, N.J., Disney, G.H., Barnes, A.A., Emson, P., Foord, S.M., and Marshall, F.H. (1998). Heterodimerization is required for the formation of a functional GABA(B) receptor. Nature *396*, 679–682.

Wick, W., Gorlia, T., Bendszus, M., Taphoorn, M., Sahm, F., Harting, I., Brandes, A.A., Taal, W., Domont, J., Idbaih, A., et al. (2017). Lomustine and Bevacizumab in Progressive Glioblastoma. N. Engl. J. Med. *377*, 1954–1963.

Wiesmann, C., Leder, L., Blank, J., Bernardi, A., Melkko, S., Decock, A., D'Arcy, A., Villard, F., Erbel, P., Hughes, N., et al. (2012). Structural determinants of MALT1 protease activity. J. Mol. Biol. *419*, 4–21.

Wippich, F., Bodenmiller, B., Trajkovska, M.G., Wanka, S., Aebersold, R., and Pelkmans, L. (2013). Dual Specificity Kinase DYRK3 Couples Stress Granule Condensation/Dissolution to mTORC1 Signaling. Cell *152*, 791–805.

Withana, N.P., Blum, G., Sameni, M., Slaney, C., Anbalagan, A., Olive, M.B., Bidwell, B.N., Edgington, L., Wang, L., Moin, K., et al. (2012). Cathepsin B inhibition limits bone metastasis in breast cancer. Cancer Res. *72*, 1199–1209.

Witte, H.T., Jeibmann, A., Klämbt, C., and Paulus, W. (2009). Modeling Glioma Growth and Invasion in Drosophila melanogaster. Neoplasia N. Y. N *11*, 882–888.

Wolfson, R.L., Chantranupong, L., Saxton, R.A., Shen, K., Scaria, S.M., Cantor, J.R., and Sabatini, D.M. (2016). Sestrin2 is a leucine sensor for the mTORC1 pathway. Science *351*, 43–48.

Wolfson, R.L., Chantranupong, L., Wyant, G.A., Gu, X., Orozco, J.M., Shen, K., Condon, K.J., Petri, S., Kedir, J., Scaria, S.M., et al. (2017). KICSTOR recruits GATOR1 to the lysosome and is necessary for nutrients to regulate mTORC1. Nature *543*, 438–442.

Wu, C.-H., Yang, Y.-H., Chen, M.-R., Tsai, C.-H., Cheng, A.-L., and Doong, S.-L. (2018). Autocleavage of the paracaspase MALT1 at Arg-781 attenuates NF-κB signaling and regulates the growth of activated B-cell like diffuse large B-cell lymphoma cells. PloS One *13*, e0199779.

Wyant, G.A., Abu-Remaileh, M., Wolfson, R.L., Chen, W.W., Freinkman, E., Danai, L.V., Vander Heiden, M.G., and Sabatini, D.M. (2017). mTORC1 Activator SLC38A9 Is Required to Efflux Essential Amino Acids from Lysosomes and Use Protein as a Nutrient. Cell *171*, 642-654.e12.

Xu, J., Fu, S., Peng, W., and Rao, Z. (2012a). MCP-1-induced protein-1, an immune regulator. Protein Cell *3*, 903–910.

Xu, J., Peng, W., Sun, Y., Wang, X., Xu, Y., Li, X., Gao, G., and Rao, Z. (2012b). Structural study of MCPIP1 N-terminal conserved domain reveals a PIN-like RNase. Nucleic Acids Res. *40*, 6957–6965.

Yadav, L., Puri, N., Rastogi, V., Satpute, P., and Sharma, V. (2015). Tumour Angiogenesis and Angiogenic Inhibitors: A Review. J. Clin. Diagn. Res. JCDR *9*, XE01–XE05.

Yamamoto, H., Kakuta, S., Watanabe, T.M., Kitamura, A., Sekito, T., Kondo-Kakuta, C., Ichikawa, R., Kinjo, M., and Ohsumi, Y. (2012). Atg9 vesicles are an important membrane source during early steps of autophagosome formation. J. Cell Biol. *198*, 219–233.

Yan, K., Yang, K., and Rich, J.N. (2013). The evolving landscape of glioblastoma stem cells. Curr. Opin. Neurol. *26*, 701–707.

Yang, F., Liu, X., Liu, Y., Liu, Y., Zhang, C., Wang, Z., Jiang, T., and Wang, Y. (2017). miR-181d/MALT1 regulatory axis attenuates mesenchymal phenotype through NF-κB pathways in glioblastoma. Cancer Lett. *396*, 1–9.

Yang, G., Murashige, D.S., Humphrey, S.J., and James, D.E. (2015). A Positive Feedback Loop between Akt and mTORC2 via SIN1 Phosphorylation. Cell Rep. *12*, 937–943.

Yang, H., Rudge, D.G., Koos, J.D., Vaidialingam, B., Yang, H.J., and Pavletich, N.P. (2013). mTOR kinase structure, mechanism and regulation. Nature *497*, 217–223.

Yang, Q., Inoki, K., Ikenoue, T., and Guan, K.-L. (2006). Identification of Sin1 as an essential TORC2 component required for complex formation and kinase activity. Genes Dev. *20*, 2820–2832.

Yang, Y.-P., Chang, Y.-L., Huang, P.-I., Chiou, G.-Y., Tseng, L.-M., Chiou, S.-H., Chen, M.-H., Chen, M.-T., Shih, Y.-H., Chang, C.-H., et al. (2012). Resveratrol suppresses tumorigenicity and enhances radiosensitivity in primary glioblastoma tumor initiating cells by inhibiting the STAT3 axis. J. Cell. Physiol. *227*, 976–993.

Ye, J., Palm, W., Peng, M., King, B., Lindsten, T., Li, M.O., Koumenis, C., and Thompson, C.B. (2015). GCN2 sustains mTORC1 suppression upon amino acid deprivation by inducing Sestrin2. Genes Dev. *29*, 2331–2336.

Yogalingam, G., Bonten, E.J., van de Vlekkert, D., Hu, H., Moshiach, S., Connell, S.A., and d'Azzo, A. (2008). Neuraminidase 1 is a Negative Regulator of Lysosomal Exocytosis. Dev. Cell *15*, 74–86.

Yu, J.W., Hoffman, S., Beal, A.M., Dykon, A., Ringenberg, M.A., Hughes, A.C., Dare, L., Anderson, A.D., Finger, J., Kasparcova, V., et al. (2015). MALT1 Protease Activity Is Required for Innate and Adaptive Immune Responses. PloS One *10*, e0127083.

Yu, Y., Yoon, S.-O., Poulogiannis, G., Yang, Q., Ma, X.M., Villén, J., Kubica, N.,

Hoffman, G.R., Cantley, L.C., Gygi, S.P., et al. (2011). Phosphoproteomic Analysis Identifies Grb10 as an mTORC1 Substrate That Negatively Regulates Insulin Signaling. Science *332*, 1322–1326.

Yuan, F., Salehi, H.A., Boucher, Y., Vasthare, U.S., Tuma, R.F., and Jain, R.K. (1994). Vascular permeability and microcirculation of gliomas and mammary carcinomas transplanted in rat and mouse cranial windows. Cancer Res. *54*, 4564–4568.

Yuan, H.-X., Russell, R.C., and Guan, K.-L. (2013). Regulation of PIK3C3/VPS34 complexes by MTOR in nutrient stress-induced autophagy. Autophagy *9*, 1983–1995.

Zaarur, N., Meriin, A.B., Bejarano, E., Xu, X., Gabai, V.L., Cuervo, A.M., and Sherman, M.Y. (2014). Proteasome Failure Promotes Positioning of Lysosomes around the Aggresome via Local Block of Microtubule-Dependent Transport. Mol. Cell. Biol. *34*, 1336–1348.

Zeng, L.-H., Xu, L., Gutmann, D.H., and Wong, M. (2008). Rapamycin prevents epilepsy in a mouse model of tuberous sclerosis complex. Ann. Neurol. *63*, 444–453.

Zhang, J., Stevens, M.F.G., and Bradshaw, T.D. (2012). Temozolomide: mechanisms of action, repair and resistance. Curr. Mol. Pharmacol. *5*, 102–114.

Zhao, J., Brault, J.J., Schild, A., Cao, P., Sandri, M., Schiaffino, S., Lecker, S.H., and Goldberg, A.L. (2007). FoxO3 coordinately activates protein degradation by the autophagic/lysosomal and proteasomal pathways in atrophying muscle cells. Cell Metab. *6*, 472–483.

Zhao, J., Zhai, B., Gygi, S.P., and Goldberg, A.L. (2015). mTOR inhibition activates overall protein degradation by the ubiquitin proteasome system as well as by autophagy. Proc. Natl. Acad. Sci. U. S. A. *112*, 15790–15797.

Zhao, K., Zhao, X., Tu, Y., Miao, Q., Cao, D., Duan, W., Sun, Y., Wang, J., Wei, T., and Yang, F. (2010). Lysosomal chymotrypsin B potentiates apoptosis via cleavage of Bid. Cell. Mol. Life Sci. *67*, 2665–2678.

Zhitomirsky, B., and Assaraf, Y.G. (2014). Lysosomal sequestration of hydrophobic weak base chemotherapeutics triggers lysosomal biogenesis and lysosome-dependent cancer multidrug resistance. Oncotarget *6*, 1143–1156.

Zhitomirsky, B., and Assaraf, Y.G. (2017). Lysosomal accumulation of anticancer drugs triggers lysosomal exocytosis. Oncotarget *8*, 45117–45132.

Zhou, Y., Peng, Z., Seven, E.S., and Leblanc, R.M. (2018). Crossing the blood-brain barrier with nanoparticles. J. Control. Release Off. J. Control. Release Soc. *270*, 290–303.

Zhu, T.S., Costello, M.A., Talsma, C.E., Flack, C.G., Crowley, J.G., Hamm, L.L., He, X., Hervey-J umper, S.L., Heth, J.A., Muraszko, K.M., et al. (2011). Endothelial cells

create a stem cell niche in glioblastoma by providing Notch ligands that nurture self-renewal of cancer stem-like cells. Cancer Res. *71*, 6061–6072.

Zhu, Y., Li, X., Kyazike, J., Zhou, Q., Thurberg, B.L., Raben, N., Mattaliano, R.J., and Cheng, S.H. (2004). Conjugation of mannose 6-phosphate-containing oligosaccharides to acid alpha-glucosidase improves the clearance of glycogen in pompe mice. J. Biol. Chem. *279*, 50336–50341.

Zhu, Y., Guignard, F., Zhao, D., Liu, L., Burns, D.K., Mason, R.P., Messing, A., and Parada, L.F. (2005). Early inactivation of p53 tumor suppressor gene cooperating with NF1 loss induces malignant astrocytoma. Cancer Cell *8*, 119–130.

Zhu, Z., Gorman, M.J., McKenzie, L.D., Chai, J.N., Hubert, C.G., Prager, B.C., Fernandez, E., Richner, J.M., Zhang, R., Shan, C., et al. (2017). Zika virus has oncolytic activity against glioblastoma stem cells. J. Exp. Med. *214*, 2843–2857.

Zoncu, R., Bar-Peled, L., Efeyan, A., Wang, S., Sancak, Y., and Sabatini, D.M. (2011). mTORC1 senses lysosomal amino acids through an inside-out mechanism that requires the Vacuolar H+-ATPase. Science *334*, 678–683.

Zouaoui, S., Rigau, V., Mathieu-Daudé, H., Darlix, A., Bessaoud, F., Fabbro-Peray, P., Bauchet, F., Kerr, C., Fabbro, M., Figarella-Branger, D., et al. (2012). [French brain tumor database: general results on 40,000 cases, main current applications and future prospects]. Neurochirurgie. *58*, 4–13.

UNIVERSITE BIOLOGIE BRETAGNE SANTE LOIRE

UNIVERSITÉ DE NANTES

Title: Exploring the Role of Intercellular and Intracellular Signaling in the Sustenance of Glioblastoma Stem-like Cells

Keywords: Signaling, Cancer Stem-like Cells, GBM, Lysosome, mTOR, Niche

Abstract: Glioblastoma multiforme, GBM, is the deadliest adult primary brain tumor with a median survival time of approximately 12 to 15 months. Within these heterogeneous tumors exists a subpopulation of cells with stem-like properties termed glioblastoma stem-like cells, GSCs. As they are suspected to be involved in initiation, expansion, and relapse, they represent a promising strategy for treating these tumors. *In situ*, GSCs reside in part in a protective vascular niche in close interaction with endothelial cells, however these cells have also been found in more hostile areas of the tumor, away from their privileged microenvironment. Therefore, uncovering intrinsic cell signaling regulating autocrine and paracrine survival mechanisms can produce novel targets for therapy.
Here, we approach the analysis of signaling mechanisms employed by GSCs in their survival, in order to identify potential targets for therapy.
On one hand, we report that the glycoprotein gp130 has an important role in endothelial cell communication with GSCs. In fact, the endothelial secretome is able to sustain GSC stemness in the absence of other mitogens. However, pharmacological blockade of gp130 abrogates this effect. On the other hand, in the absence of signals emanating from endothelial cells, we uncover that the paracaspase MALT1 is important to maintain GSC survival and expansion, as knockdown or inhibition of this protease is lethal to these cells. From a molecular standpoint, we found that inhibition of MALT1 disrupts endo-lysosomal homeostasis, resulting in a lysosomal cell death concomitant with mTOR inactivation. Therefore, we identified two signaling axes within GSCs with the potential for therapeutic targeting.

Titre : Exploration du rôle de la signalisation intercellulaire et intracellulaire dans le maintien des cellules de type souche de glioblastome

Mots clés : signalisation, cellules souches cancéreuses, GBM, lysosome, mTOR, niche

Résumé : Le Glioblastome Multiforme, GBM, est une tumeur cérébrale parmi les plus agressives de l'adulte, avec une médiane de survie s'échelonnant autour de 12 à 15 mois. Au sein de ces tumeurs hétérogènes réside une sous-population de cellules aux propriétés souches appelées GSC pour cellules de type souche du glioblastome, Une stratégie potentielle pour le traitement de ces tumeurs consisterait à cibler ces GSCs. Les GSCs résident à la fois dans une niche vasculaire protectrice en interaction étroite avec les cellules endothéliales et dans des zones non vascularisées, plus hostiles. Dans ce contexte, il est crucial de mieux caractériser la signalisation cellulaire intrinsèque régulant les mécanismes de survie autocrine et paracrine des GSCs.
Ma thèse s'est concentrée sur l'analyse des mécanismes de signalisation régissant les décisions de vie/mort des GSCs, dans le but d'offrir de nouvelles perspectives thérapeutiques
D'une part, mes résultats montrent que la glycoprotéine gp130 joue un rôle important dans la communication entre les GSCs et les cellules endothéliales. Le sécrétome endothélial est en effet capable de maintenir le caractère souche des GSCs, en l'absence d'autres mitogènes externes. Le blocage pharmacologique de gp130 annule cet effet. Par ailleurs, en l'absence de signaux émanant des cellules endothéliales, j'ai mis en évidence le rôle instrumental de la paracaspase MALT1 dans la survie et l'expansion des GSCs. La suppression ou l'inhibition de cette protéase s'avère toxique pour ces cellules. D'un point de vue mécanistique, j'ai trouvé que l'inhibition de MALT1 perturbe l'homéostasie endo-lysosomale, entraînant une mort cellulaire lysosomale concomitante à l'inactivation de mTOR. J'ai donc identifié deux axes de signalisation au sein des GSCs avec un potentiel de ciblage thérapeutique.